



Non compact conformal field theories in statistical mechanics

Eric Vernier

► To cite this version:

Eric Vernier. Non compact conformal field theories in statistical mechanics. Physics [physics]. Ecole normale supérieure - ENS PARIS, 2015. English. NNT : 2015ENSU0005 . tel-01199078v2

HAL Id: tel-01199078

<https://theses.hal.science/tel-01199078v2>

Submitted on 4 Oct 2017

HAL is a multi-disciplinary open access archive for the deposit and dissemination of scientific research documents, whether they are published or not. The documents may come from teaching and research institutions in France or abroad, or from public or private research centers.

L'archive ouverte pluridisciplinaire **HAL**, est destinée au dépôt et à la diffusion de documents scientifiques de niveau recherche, publiés ou non, émanant des établissements d'enseignement et de recherche français ou étrangers, des laboratoires publics ou privés.

Non compact conformal field theories in statistical mechanics

Éric Vernier

March 2, 2015

Abstract

The critical points of statistical mechanical systems in 2 dimensions or quantum mechanical systems in 1+1 dimensions (this also includes non interacting systems in 2+1 dimensions) are efficiently tackled by the exact methods of conformal field theory (CFT) and integrability, which have witnessed a spectacular progress during the past 40 years. Several problems have however escaped an exact understanding so far, among which the plateau transition in the Integer Quantum Hall Effect, the main reason for this being that such problems are usually associated with non unitary, logarithmic conformal field theories, the tentative classification of which leading to formidable mathematical difficulties. Turning to a lattice approach, and in particular to the quest for integrable, exactly solvable representatives of these problems, one hits the second difficulty that the associated CFTs are usually of the *non compact* type, or in other terms that they involve a continuum of critical exponents. The connection between non compact field theories and lattice models or spin chains is indeed not very clear, and in particular it has long been believed that the former could not arise as the continuum limit of discrete models built out of a compact set of degrees of freedom, which are the only ones allowing for a systematic construction of exact solutions.

In this thesis, we show that the world of compact lattice models/spin chains with a non compact continuum limit is much bigger than what could be expected from the few particular examples known up to this date. More precisely we propose an exact Bethe ansatz solution of an infinite family of models (the so-called $a_n^{(2)}$ models, as well as some results on the $b_n^{(1)}$ models), and show that all of these models allow for a regime described by a non compact CFT. Such models include cases of great physical relevance, among which a model for two-dimensional polymers with attractive interactions and loop models involved in the description of coupled Potts models or in a tentative description of the quantum Hall plateau transition by some compact geometrical truncation. We show that the existence of an unsuspected non compact continuum limit for such models can have dramatic practical effects, for instance on the output of numerical determination of the critical exponents or of Monte-Carlo simulations. We put our results to use for a better understanding of the controversial *theta transition* describing the collapse of polymers in two dimensions, and draw perspectives on a possible understanding of the quantum Hall plateau transition by the lattice approach.

Key words : Non compact conformal field theories, Lattice models, Loop models, Bethe ansatz, Black hole, Polymer collapse, Integer Quantum Hall Effect.

Résumé

Théories conformes non compactes en mécanique statistique

Les systèmes de mécanique statistique en 2 dimensions ou de mécanique quantique en 1+1 dimensions (ainsi que les systèmes sans interactions en 2+1 dimensions) à leurs points critiques sont sujets à résolution exacte par les méthodes de la théorie conforme des champs et de l'intégrabilité, qui ont connu développement spectaculaire au cours des 40 dernières années. Plusieurs problèmes résistent cependant toujours à une compréhension exacte, parmi lesquels celui de la transition entre plateaux dans l'Effet Hall Quantique Entier. La raison principale en est que de tels problèmes sont généralement associés à des théories non unitaires, ou théories conformes logarithmiques, dont la classification se révèle être d'une grande difficulté mathématique. Se tournant vers la recherche de modèles discrets (chaînes de spins, modèles sur réseau), dans l'espoir en particulier d'en trouver des représentations en termes de modèles exactement solubles (intégrables), on se heurte à la deuxième difficulté représentée par le fait que les théories associées sont la plupart du temps *non compactes*, ou en d'autres termes qu'elles donnent lieu à un continuum d'exposants critiques. En effet, le lien entre modèles discrets et théories des champs non compactes est à ce jour loin d'être compris, en particulier il a longtemps été cru que de telles théories ne pouvaient pas émerger comme limites continues de modèles discrets construits à partir d'un ensemble compact de degrés de libertés, par ailleurs les seuls qui donnent accès à une construction systématique de solutions exactes.

Dans cette thèse, on montre que le monde des modèles discrets compacts ayant une limite continue non compacte est en fait beaucoup plus grand que ce que les quelques exemples connus jusqu'ici auraient pu laisser suspecter. Plus précisément, on y présente une solution exacte par ansatz de Bethe d'une famille infinie de modèles (les modèles $a_n^{(2)}$, ainsi que quelques résultats sur les modèles $b_n^{(1)}$), où il est observé que tous ces modèles sont décrits dans un certain régime par des théories conformes non compactes. Parmi ces modèles, certains jouent un rôle important dans la description de phénomènes physiques, parmi lesquels la description de polymères en deux dimensions avec des interactions attractives et des modèles de boucles impliqués dans l'étude de modèles de Potts couplés ou dans une tentative de description de la transition entre plateaux dans l'Effet Hall par un modèle géométrique compact. On montre que l'existence insoupçonnée de limite continues non compacts pour de tels modèles peut avoir d'importantes conséquences pratiques, par exemple dans l'estimation numérique d'exposants critiques ou dans les résultats de simulations de Monte Carlo. Nos résultats sont appliqués à une meilleure compréhension de la transition θ décrivant l'effondrement des polymères en deux dimensions, et des perspectives pour une potentielle compréhension de la transition entre plateaux en termes de modèles sur réseaux sont présentées.

Mots clés : Théories conformes des champs non compactes, Modèles sur réseaux, Modèles de boucles, Ansatz de Bethe, Trou noir, Effondrement des polymères, Effet Hall Quantique Entier.

Remerciements

Contents

1	Introduction to critical phenomena, polymer collapse and the Integer Quantum Hall Effect	3
1.1	Universality in macroscopic systems, and conformal field theory	3
1.2	Polymer chains	7
1.3	The Integer Quantum Hall Effect	10
1.4	A step towards exact solutions : lattice models	14
1.5	Non-compactness	21
1.6	Plan of the rest of the manuscript	23
2	Exactly solvable models for polymers and the IQHE plateau transition	25
2.1	Introduction to integrability and exactly solvable models	25
2.1.1	Vertex models, integrability, and the Yang–Baxter equation	25
2.1.2	The quantum group $U_q(sl_2)$	32
2.1.3	General framework	34
2.2	Loop models and algebraic aspects	36
2.2.1	Loop formulation of the six-vertex model and the Temperley–Lieb algebra	36
2.2.2	Representation theory of the TL algebra	39
2.2.3	Periodic loop and vertex models	40
2.2.4	Schur–Weyl duality	42
2.3	From polymers to the $O(n)$ model, to the $a_2^{(2)}$ model	44
2.4	From the IQHE to the $b_2^{(1)}$ integrable model	47
2.4.1	The Chalker–Coddington model	47
2.4.2	A loop model for transport observables	50
2.4.3	The truncation procedure	54
2.4.4	Dense and dilute two-colour loop models	57
2.4.5	The $a_3^{(2)}$ and $b_2^{(1)}$ integrable chains	59
3	From exactly solvable models to non-compact CFTs	61
3.1	The algebraic Bethe Ansatz	61
3.1.1	Algebraic Bethe Ansatz for the six-vertex model	62
3.1.2	Algebraic Bethe ansatz for higher rank models	64
3.2	Continuum limit of the $a_2^{(2)}$ model	65
3.2.1	Continuum limit in regimes I and II	67
3.2.2	First observations in regime III	72
3.2.3	The black hole CFT	76
3.2.4	The density $\rho(s)$ and the discrete states	78
3.2.5	The parafermions	80

3.2.6	Conclusion: the continuum limit of the $a_2^{(2)}$ model	82
3.3	Continuum limit of the $a_3^{(2)}$ model	85
3.3.1	Continuum limit in regimes I and II	87
3.3.2	Continuum limit in regime III	88
3.4	General solution of the $a_n^{(2)}$ chains	90
3.4.1	Duality arguments for a non compact regime	92
3.4.2	The regimes I and II	95
3.4.3	The regimes III	96
3.5	The non compact world	98
3.5.1	A look at the Bethe ansatz kernels	98
3.5.2	The search for non compact degrees of freedom	99
3.5.3	Non compact theories in practice	102
4	Polymer collapse and non compact degrees of freedom	105
4.1	The VISAW phase diagram	106
4.2	Physical properties at the non compact point	110
4.2.1	Grand-canonical Monte-Carlo simulations	110
4.2.2	The ν and γ exponents	113
4.2.3	Discrete states and polymer attraction	114
4.3	Probing the non compact degrees of freedom	115
4.3.1	Relationship between the black hole and dense phase	115
4.3.2	Probing degrees of freedom	116
4.3.3	A model for $K \approx K_{\text{BN}}$	117
4.4	The collapse transition	119
5	Application to the Integer Quantum Hall Effect	123
5.1	Review of the results by Ikhlef <i>et. al.</i>	123
5.2	Continuum limit of the $b_n^{(1)}$ model	125
5.2.1	Bethe ansatz solution in regime IV	125
5.2.2	$b_2^{(1)}$, $a_3^{(2)}$, and Pohlmeyer reduction	128
5.2.3	Critical exponents of the truncated model	129
5.3	Continuous exponents at the IQHE transitions	131
5.3.1	$GL(2 2)$ interpretation of point-contact conductances	131
5.3.2	Loop interpretation	132
5.3.3	Pure scaling observables	133
	Conclusion	137
	Bibliography	139

Chapter 1

Introduction to critical phenomena, polymer collapse and the Integer Quantum Hall Effect

1.1 Universality in macroscopic systems, and conformal field theory

This thesis deals with systems having in common a large number of degrees of freedom, which it would be both vain and not too useful to treat exactly as one would typically do in few-body systems. Take for instance substances as different as water, oil, or mercury close to their boiling temperature T_b . While microscopically, raising the temperature from slightly below to slightly above T_b does not show any appreciable qualitative difference – only does it increase slightly the average velocity of the composing atoms or molecules –, a dramatic change is observed on macroscopic scales, namely the *transition* between two *phases* of very different properties. Following the transition line the as the pressure is increased, one reaches a *critical point* where the two phases merge, and around which the physical properties of the fluid are described by a set of *critical exponents*. Remarkably, these exponents are the same for all fluids under consideration, irrespectively of their microscopic details or chemical composition. How such *universal* phenomena come about has been successfully investigated in the framework of the *renormalization* procedure, which shows that changing the length scale of a system amounts to moving in the space of the various couplings constants (microscopic parameters), and that therefore the large scale, macroscopic properties, of infinitely many microscopically different systems can be described by a few *fixed points* of the *renormalization group* (RG) *flow*. Let us illustrate this by a look at the Ising model, where magnets (*spins*) pointing in either the up or down direction are placed at the sites of some lattice with a ferromagnetic interaction between pairs of neighbouring spins. Increasing the length scale at which the system is observed can be implemented by various types of block-decimation procedures, where blocks of spins are averaged and taken as the new unit cells, with renormalized interaction parameters. In the process all microscopic details about the interaction (whether it couples between nearest neighbours only or has a wider range, etc...) or the geometry of the lattice turn out to vanish, and the large scale properties essentially depend on the *dimension* of the space and one single *relevant* coupling parameter, which we can tune through the temperature T . The renormalization group flow in $d \geq 2$ is shown in figure

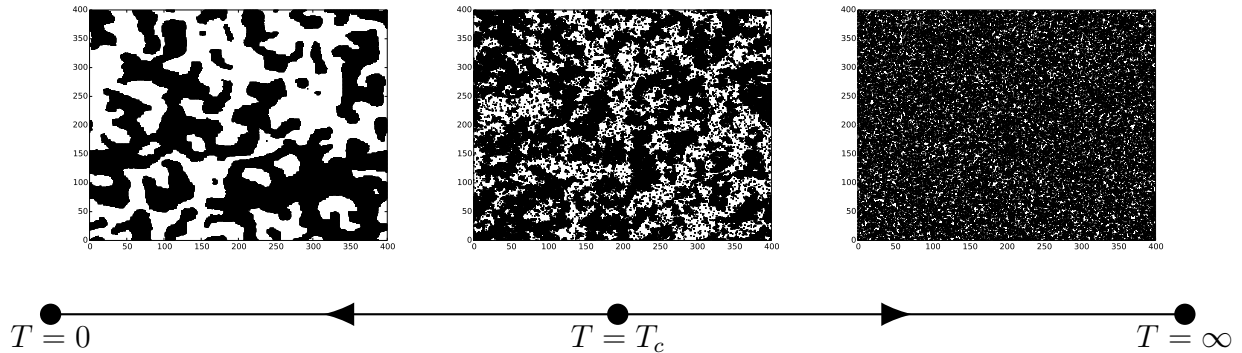


Figure 1.1: Renormalization group flow of the two-dimensional Ising model, whose typical configurations at various temperatures are represented on a square lattice of 400×400 sites. The critical point $T = T_c$ is characterized by the absence of a length scale (infinite correlation length).

1.1 and is characterized by a critical temperature T_c separating two phases, where the characteristic length ξ of spin correlations is observed to diverge following an universal law

$$\xi \propto |T - T_c|^{-\nu}. \quad (1.1)$$

Once again the exponent ν as well as other exponents describing the physical properties of Ising models at or around T_c are universal. Even more strikingly, they match exactly those of the liquid-gas critical point mentioned above.

An central task is therefore, rather than studying the details of every possible microscopic model, to classify and understand the various *universality classes*, or fixed points of the RG flow. As was realized by Polyakov in [1], where the scale invariant RG fixed points were further assumed to be preserved under *local* scale transformations, this amounts to classify and solve the possible *conformally invariant quantum field theories* (or Conformal Field Theories, or CFTs) in $(d - 1) + 1$ dimensions. This is achieved by finding in each case a family of local fields $\{\Phi_n(x)\}$ which are eigenvalues of the dilatation operator, namely $\Phi_n(\lambda x) \rightarrow \lambda^{-\Delta_n} \Phi_n(x)$, and over which any operator $O(x)$ can be decomposed as a linear sum. Provided that the *scaling dimensions* Δ_n and operator product expansions $\Phi_n(x)\Phi_m(y) = \sum_p \frac{C_{m,n}^p}{|x-y|^{\Delta_m+\Delta_n-\Delta_p}} \Phi_p(y)$ are known, any correlation function in the theory can be computed. In particular, the critical exponents are obtained from the dimensions Δ_n through various *scaling relations*. Whereas for d larger than the *upper critical dimension* these match their mean-field expectations, lower-dimensional systems usually exhibit a much richer physics. Of particular importance is the two-dimensional case, where the group of conformal transformations can be extended to the infinite-dimensional algebra of *local* conformal transformations, which viewed in the complex plane coincide with analytical mappings $z \rightarrow w(z), \bar{z} \rightarrow \bar{w}(\bar{z})$. Although these are not proper symmetries of the theory (rather, they relate theories defined on different geometries), it turns out to be of fundamental importance to consider the *primary fields* $\Phi_{\Delta,\bar{\Delta}}$, which are tensors under these transformations,

$$\Phi_{\Delta,\bar{\Delta}}(w, \bar{w}) = \left(\frac{dw}{dz}\right)^{-\Delta} \left(\frac{d\bar{w}}{d\bar{z}}\right)^{-\bar{\Delta}} \Phi_{\Delta,\bar{\Delta}}(z, \bar{z}), \quad (1.2)$$

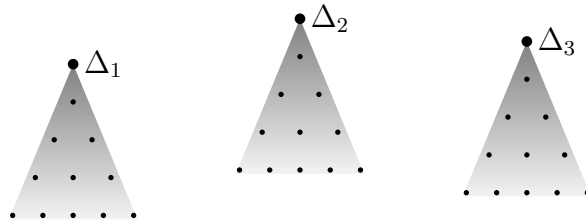


Figure 1.2: The simplest CFTs such as the minimal models $\mathcal{M}(p, q)$ are described by a set of highest-weight modules, each composed of one primary field (thick dots on the picture) and its conformal descendants (smaller dots) obtained by action of the Virasoro generators $\{L_n\}_{n<0}$ on the latter.

and from which all scaling (or *quasi-primary*) fields can be obtained by acting with the Virasoro generators $\{L_n\}_{n \in \mathbb{Z}}$ (as well as their antiholomorphic counterparts $\{\bar{L}_n\}$), subject to the commutation relations

$$[L_n, L_m] = (n - m)L_{m+n} + \frac{c}{12}n(n^2 - 1)\delta_{n+m,0}, \quad (1.3)$$

where the parameter c is called the *central charge*. From there, the classification of two-dimensional CFTs can be achieved as the classification of Virasoro representations, namely, in the *radial quantization* scheme, as a Hilbert space structure characterized by a vacuum state $|0\rangle$ invariant under global conformal transformations as well as *highest-weight states*

$$|\Delta, \bar{\Delta}\rangle \equiv \lim_{z, \bar{z} \rightarrow 0} \Phi_{\Delta, \bar{\Delta}}(z, \bar{z})|0\rangle \quad (1.4)$$

and the corresponding descendants, obtained by repeated actions of the Virasoro generators.

Whereas many exact results have been obtained from this construction since the seminal paper of [2], recovering in particular [3] the two-dimensional Ising, tricritical Ising and 3-state Potts model as the first three representatives of the series of *unitary minimal models* corresponding to unitary *irreducible* representations of the Virasoro algebra built from a finite number of primary fields (see figure 1.2), several important physical problems have escaped so far a complete classification. These include for instance geometrical models of self-avoiding walks or percolation [4] and the study of classical [5] or quantum [6] systems with quenched disorder. The latter have important applications in condensed matter theory, as they encompass the study of quantum critical points in disordered systems of non-interacting fermions, among which lies the transition between plateaus in the Integer Quantum Hall Effect (IQHE) ([7], see section 1.3). The reason for this is that such problems are associated with much more complicated representations of the Virasoro algebra, namely which may be (the two cases are not exclusive)

- *indecomposable*, which means that they cannot be decomposed as sums of irreducible representations. We are then dealing with *Logarithmic CFTs* (LCFTs), whose investigation has become over the recent years one of the most active branches of the field but whose classification, despite important progress (for a review see [8, 9], and references therein), is believed in mathematical terms to be *wild*, namely, it can lead to arbitrarily complicated algebraic structures (see figure 1.3),

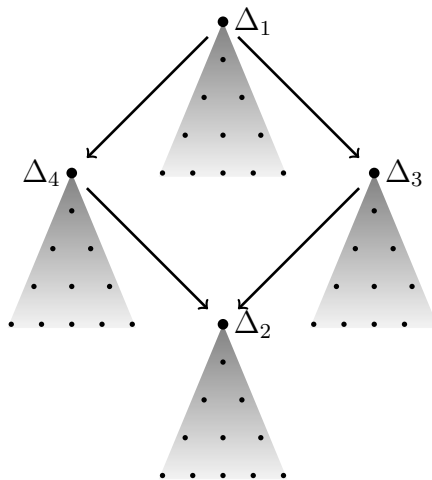


Figure 1.3: Logarithmic CFTs involve *indecomposable Virasoro modules* such as the *diamond* module represented on this figure. The arrows indicate the action of Viraroso generators relating between the different highest-weight modules. That the representation theory of LCFTs is said to be *wild* means that this can get infinitely more complicated.

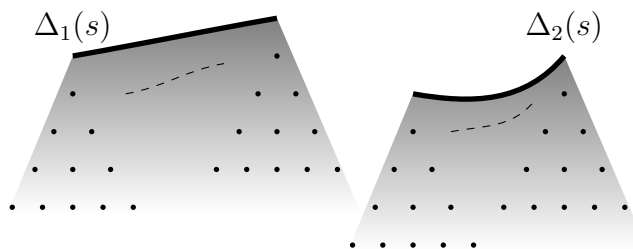


Figure 1.4: Non compact CFTs involve a continuous set of primary fields. In the case of non compact LCFTs such as the theory of the quantum Hall plateau transition, this gets coupled to indecomposability.

- *irrational*, namely which involve an infinite number of primaries. A highly irrational case is that of theories with a *non compact target space*, where the set of primary fields is not even discrete (see figure 1.4). This fact can be seen for instance in the *mini-superspace approximation* [10], where the theory is put on a narrow cylinder whose axis is the time direction and the spatial dependence of the fields is neglected. At any time these become simply a parametrization of the target space, the Hamiltonian becomes the Laplacian, and any non compact direction in the target therefore naturally results in a continuum of conformal weights just as, in usual quantum mechanics, the discrete eigen momenta or energies of a particle in a box become continuous when the size of the box is sent to infinity.

Whereas the study of logarithmic CFTs and their applications in statistical mechanics and condensed matter has witnessed steady progress during the course of the past few years [8], non compact conformal field theories have been until recently essentially studied in the context of string theory or in disordered condensed matter systems through a rather formal approach [11], and a clear understanding of *whether*, *where* and *how* these might show up in simple statistical mechanics model has so far been lacking. This thesis is an

attempt to start filling this lack, and the rest of this chapter one to show how crucial such an understanding shall be for further progress in the direction towards cornerstone problems such as that of the IQHE plateau transition. Before introducing the latter, we now take a detour through some aspects of two-dimensional polymer physics which, as strange as it may seem at this stage, will serve us as a guideline throughout all this presentation and which will show some aspects arguably interesting enough for their own sake.

1.2 Polymer chains

Polymers are long, flexible macromolecules composed of many chemical subunits. Whereas many of their properties depend on the details of these subunits (obviously plastic polymers such as polystyrene or biopolymers such as DNA or proteins are not expected to behave quite exactly the same), several global, large scale properties can be studied in a general setting. For polymers in a dilute solution, consider for instance the radius of gyration R_G , namely the mean squared distance from a given polymer's building blocks to its center of mass. As was checked from light-scattering experiments, the latter follows an universal scaling law as a function of the number of monomer units N , namely,

$$R_G \propto N^\nu, \quad (1.5)$$

with a proportionality factor that depends on the details of the considered polymer, whereas the exponent ν is, in the case of linear polymers and a *good* solvent (see below), always approximately equal to $\frac{3}{5}$ in three spatial dimensions, $\frac{3}{4}$ in $d = 2$ and obviously $\nu = 1$ in $d = 1$, following the conjecture of Flory [12]. The entropy of a polymer chain of length N can also be studied, and is observed to have the form

$$S_N = \text{extensive part} + (\gamma - 1) \log N + \dots, \quad (1.6)$$

where the exponent γ is once again universal, namely in good solvents $\gamma \simeq 7/6$ in $d = 3$ and $\gamma \simeq 4/3$ in $d = 2$. Other exponents can be defined, for instance relating to the response of a polymer to end-to-end stretching, and turn out to be all expressible in terms of the exponents γ and ν through some simple set of scaling relations [13]. For future reference we introduce among these the correlation length exponent η , defined by the large distance scaling of the correlation function $G(r, r')$ counting the probability that a polymer with one end at point r has its other end at point r' , namely

$$G(r, r') \propto |r - r'|^{-\eta}. \quad (1.7)$$

This exponent is related to γ and ν through the usual scaling relation (see for instance [13])

$$\gamma = (2 - \eta)\nu. \quad (1.8)$$

Long polymers as critical systems

The presence of universal scaling laws and critical exponents in polymer chains is very reminiscent of the universality of critical points presented earlier. Comparing more specifically equation (1.5) with (1.1) suggests a correspondence between the degree of polymerization N and the inverse distance $|T - T_c|^{-1}$ to the critical point in magnetic systems.

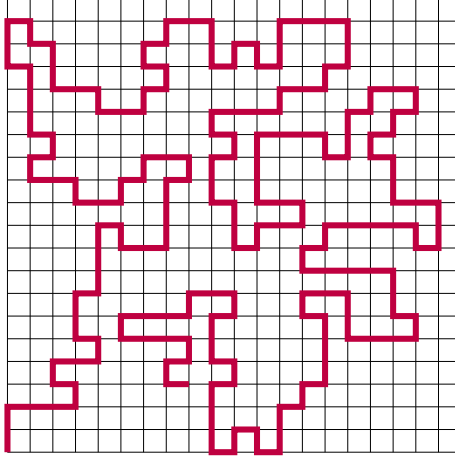


Figure 1.5: Self-avoiding walk (SAW) on the two-dimensional square lattice.

In order to make this correspondence precise, let us anticipate slightly on the lattice descriptions of polymers, which we will use extensively throughout this thesis. One of the simplest of such descriptions is that of the *ideal chain*, which is a walk consisting of N random steps on (say) the d -dimensional square lattice. The latter however yields an exponent $\nu = \frac{1}{2}$ in any dimension, and real chains in good solvents are rather described as self-avoiding walks (SAW), which differ from the classical random walks in that they cannot interstect themselves (see figure 1.5) and recover indeed the values of the critical exponents introduced in the beginning of this section. Turning back to magnetic systems, let us consider in particular the so-called $O(n)$ vector model [14], where magnets represented by n -dimensional vectors of \vec{S}_i fixed length live on the sites of the square lattice and interact through a ferromagnetic nearest-neighbour coupling $-K \vec{S}_i \cdot \vec{S}_j$. Just as the Ising model, the $O(n)$ model shows a transition between a high temperature phase where the average magnetization is zero, and a low-temperature, broken symmetry phase where the average magnetization acquires some non zero expectation value. The two are separated by a critical temperature T_c , which can be described in field-theoretical terms by the non trivial fixed-point (namely, other from the gaussian fixed point $g = m = 0$) of a Landau-Ginzburg Lagrangian of the form [15, 16]

$$\mathcal{L} = \frac{1}{2} (\nabla \varphi)^2 + m^2 \varphi^2 + \frac{g}{4!} \varphi^4 \quad (1.9)$$

for some n -component vector field $\varphi(x)$, and where the usual set of exponents can be defined. On the square lattice model we consider the correlation function $\langle \vec{S}_i \cdot \vec{S}_j \rangle$ between the orientation of two spins on sites i, j , namely

$$\langle \vec{S}_i \cdot \vec{S}_j \rangle = \frac{\int \prod_k d\vec{S}_k \vec{S}_i \cdot \vec{S}_j \prod_{\langle k,l \rangle} e^{\beta K \vec{S}_k \cdot \vec{S}_l}}{\int \prod_k d\vec{S}_k \prod_{\langle k,l \rangle} e^{\beta K \vec{S}_k \cdot \vec{S}_l}}. \quad (1.10)$$

Series expanding the $e^{\beta K \vec{S}_k \cdot \vec{S}_l}$ terms and integrating over the spin orientations, the denominator (partition function) can be reexpressed [13] as a sum over configurations of closed loops running over the edges of the square lattice, with a weight n for each closed loop and a weight βK for each loop segment, whereas in the numerator one has in addition one open path going from site i to site j . Taking the limit $n \rightarrow 0$ all configurations



Figure 1.6: Coil (left) and globule (right) configurations of a polymer chain, obtained by varying the solvent temperature across the so-called *theta temperature* Θ .

with closed loops vanish, therefore the only configuration contributing to the partition function is the empty one with weight 1, and the spin-spin correlation function simply reads

$$\langle \vec{S}_i \cdot \vec{S}_j \rangle \Big|_{n \rightarrow 0} = \sum_{\substack{\text{SAW: } i \rightarrow j \\ \text{length } N}} (\beta K)^N = \sum_N \Omega_N(i, j) (\beta K)^N, \quad (1.11)$$

where $\Omega_N(i, j)$ is the number of SAW of length N joining sites i and j . We therefore start to see how the properties of polymer chains described by self-avoiding walks can be related to those of the magnetic $O(n)$ model in the limit $n \rightarrow 0$. In particular, slightly above the critical temperature in the $O(n)$ model we have $\beta K \propto T^{-1} \simeq T_c^{-1} e^{-\frac{T-T_c}{T_c}}$, so the relation between magnetic correlations and SAW is of the Laplace transform type, and the distance to the critical point $\frac{T-T_c}{T_c}$ is conjugate to the degree of polymerization N . Universal scaling laws for polymer chains are obtained in the limit $N \rightarrow \infty$, for instance recovering the correspondence mentioned earlier between equations (1.5) and (1.1).

The collapse transition

The equilibrium conformations of dilute polymer chains in a solvent are governed by the competition between hydrophobic monomer-solvent interactions and entropic, excluded volume effects. Whereas the latter dominate at high enough temperatures (which we take as a definition of a *good solvent*), leading to the *coil* configuration described previously with exponent $\nu = \frac{3}{5}$ in three dimensions, the former usually take on at low temperatures, leading to a collapsed phase where the polymer is in a *globule*-like, compact configuration characterized by a smaller value of the exponent $\nu = \frac{1}{3}$ (see figure 1.6). The transition between the two regimes occurs at the so-called *theta temperature* and is characterized by an intermediate value of the exponent ν , namely $\nu = \frac{1}{2}$ in three dimensions. The coil-globule transition, or *theta transition*, has been observed experimentally for many polymer-solvent systems, for instance in the case of polystyrene in a cyclohexane solvent where the theta temperature is found to be $\Theta \simeq 35^\circ$. It also plays a role of great importance in biophysics, where it is believed to describe the folding of proteins from a swollen configuration to their collapsed, *native* conformation [17].

The theta transition was identified by De Gennes [18] to be described by a *tricritical point*, which is rather natural in the sense that, long polymers being themselves mapped

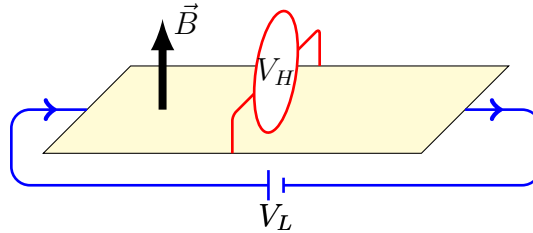


Figure 1.7: Experimental setup for the observation of the Integer Quantum Hall Effect. A current $V_{xx} \equiv V_L$ is imposed throughout the sample. Because of the transverse magnetic field \vec{B} , a transverse 'Hall' voltage $V_{xy} \equiv V_H$ is measured.

onto critical systems, the existence of phase transitions within the latter should be associated with the introduction of one additional relevant parameter in the RG sense, and therefore to a tricritical point. From the field-theoretical point of view this amounts [18] to replace the Lagrangian (1.12) by

$$\mathcal{L} = \frac{1}{2} (\nabla\varphi)^2 + m^2\varphi^2 + \frac{g}{4!}\varphi^4 + \frac{g'}{6!}\varphi^6, \quad (1.12)$$

which for a certain value of the coupling constants gives rise to a tricritical point. The corresponding set of (tri)critical exponents can be described by its mean-field predictions for space dimensions larger than the upper critical dimension $d = 3$ ¹, but differs from these in $d = 2$. Despite a considerable amount of work during the three past decades, the exact determination of these exponents has still remained an open question. Some progress towards a solution of this long standing puzzle will be the object of our discussion in chapter 4.

1.3 The Integer Quantum Hall Effect

The Integer Quantum Hall Effect (IQHE) is observed in a two-dimensional sample of electrons subject to a strong transverse magnetic field, as described in figure 1.7. It is easily shown classically that the magnetic field originates for a nonzero transverse Hall current. More precisely the longitudinal (Ohmic) and transverse (Hall) components of the resistivity, ρ_{xx} and ρ_{xy} are expected to behave as

$$\rho_{xx} = 0, \quad \rho_{xy} = \frac{B}{en}, \quad (1.13)$$

where e and n are the electric charge and density of electrons, respectively. The experimental observations of Von Klitzing ([7], Nobel Prize 1985), see figure 1.8, go against these expectations, as for large enough magnetic fields the Hall resistivity shows well defined plateaus at integer fractions of the ratio $\frac{h}{e^2}$.

Explaining this quantification clearly requires taking account of the quantum nature of the electron system, and we introduce the following Hamiltonian for a single spinless electron in two spatial dimensions with a perpendicular magnetic field [21]

$$H_0 = \frac{1}{2m} \left(\vec{p} + e\vec{A} \right)^2. \quad (1.14)$$

¹It is easily checked that for Lagrangian theories of the type $\mathcal{L} = \frac{1}{2}(\nabla\varphi)^2 + g_1\varphi + \dots \frac{g_p}{p!}\varphi^p$, the upper critical dimension is $d_u = \frac{2p}{p-1}$ (see for instance [19]).

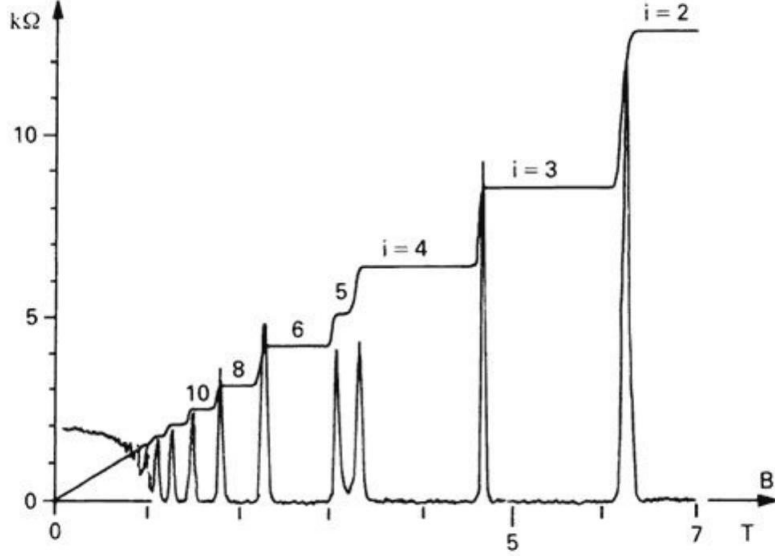


Figure 1.8: Plateaus for the Hall resistance R_{xy} and peaks of the Ohmic resistance R_{xx} measured as a function of the magnetic field B in the Integer Quantum Hall Effect (figure taken from [20]).

Here the vector potential has been taken in the Landau gauge $\vec{A} = (0, Bx, 0)$ and the effects of lattice atoms and interactions (which as we will see are not essential to the description of the IQHE) are taken in account by the effective mass m . As for the absence of spin in this description, it stems from the fact that the electronic spins are aligned with the strong magnetic field, and thereby do not contribute to the dynamics. The problem is translationally invariant along the direction y , and reduces in the x direction to that of a quantum harmonic oscillator. The corresponding energy levels, the so-called Landau levels, are quantized as

$$E_n = \left(n + \frac{1}{2}\right) \hbar \omega_c, \quad n = 0, 1, \dots, \quad (1.15)$$

where $\omega_c = \frac{eB}{m}$ the so called *cyclotron frequency*. They are moreover hugely degenerate with respect to the y -direction wave number k , with a degree of degeneracy per unit area $n_B = \frac{eB}{h} = \frac{B}{\Phi_0}$, where $\Phi_0 = \frac{h}{e}$ is the density of flux quanta. The number of occupied Landau level is given by the so-called *filling fraction*

$$\nu = \frac{n}{n_B} = \frac{n \phi_0}{B}. \quad (1.16)$$

Owing to this description, all states are delocalized, and therefore current-carrying in the y direction. Upon varying the density n , or equivalently the magnetic field B at fixed ν , the Fermi level jumps between Landau levels and the Hall conductivity varies as the number of occupied states, that is, continuously. We see from there that more ingredients are needed to take account of the emergence of plateaus, and it turns out that a crucial role is played by the impurity-induced disorder, which we can model as a random potential $V(x, y)$ in the Hamiltonian

$$H = H_0 + V(x, y). \quad (1.17)$$

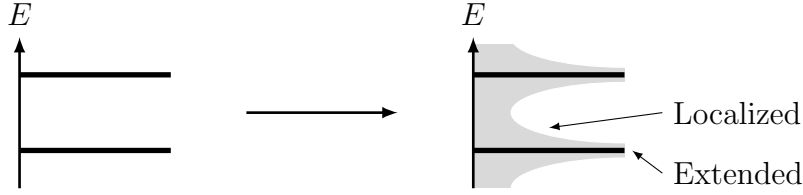


Figure 1.9: Broadening of the Landau levels into Landau bands.

The effect of this random potential is a broadening of the Landau levels into Landau bands, with localized eigenstates occurring in the band tails (see figure 1.9). These have wavefunctions exponentially localized around a small region of space (whose size we call the localization length ξ), forbidding them to contribute to dc-transport at low temperature. The states at the center of the bands are however still delocalized, in other words they have an infinite localization length, and spread randomly across the entire system. We now see how the IQHE originates : increasing the filling fraction between two half odd integer values, that is increasing the Fermi energy between two Landau bands, results in populating localized levels, under which the conductivity remains constant. Crossing a half-integer value of the filling fraction populates the extended states at the center of the corresponding band, originating for both a peak in the longitudinal conductivity and a jump of the Hall conductivity. The accurate description of the latter actually requires taking in account the finite size of the sample and the so-called *edge states* along its boundary, and we refer to [22] for more details about this mechanism.

The plateau transitions

Whereas the physics inside plateaus is well understood, this is not the case of the transitions between one plateau to the next, the so called IQHE plateau transitions. All analytical and numerical results so far [23] are consistent with the picture that at zero temperature the localization length diverges only at specific energies E_n close to the center of the Landau bands with the following power law

$$\xi \propto |E - E_n|^{-\nu}, \quad (1.18)$$

where the *localization length exponent* ν is independent of the Landau band index and of the microscopic details of the disorder. The conjectured value of this exponent from experiments on GaAs-AlGaAs heterostructures [24] or from the numerical simulations on various models (see for instance Table V in [25] for a review) has been widely discussed over the years, yielding estimations ranging between 2.3 and 2.7 , with most recent results close to 2.62 [25].

Once again, this is reminiscent of the scaling laws presented earlier for critical systems in statistical mechanics, in particular of (1.1). Indeed, the plateau transitions correspond to critical points, which are now of a *quantum critical nature* (the transition is not driven by varying the temperature, rather it can be observed at $T = 0$). As induced by the localization of electrons due to disorder, these are one example of the so called *Anderson localization-delocalization transitions*, which were shown in the seminal work of Altland and Zirnbauer to fall into 10 symmetry classes of universal behaviour [26] (the IQHE plateau transition, on which we will mostly focus, corresponds to the so-called ‘class A’).

As any second order phase transition, the plateau transitions are expected to be described by a CFT, whose knowledge should enable us to yield exact predictions for the critical exponents and correlation functions. Let us pause here for two remarks. First, the powerful machinery of CFT presented in the introduction holds only in the two-dimensional case, and therefore in the description of the critical points of classical systems in 2 dimensions or of quantum systems in 1+1 dimensions. That the field theory of the IQHE, which is originally a problem in 2+1 dimensions, can be reduced to one of those owes to its non interacting nature : since electrons do not interact with one another and evolve in a static potential their one-body energy is preserved, so the frequency which enters Green's functions becomes simply a parameter of the action and one may consider each frequency separately, thus reducing the problem to some 2-dimensional Euclidean field theory. Second, we have been leaving aside the presence of disorder, which manifestly breaks translational invariance. Conformal invariance is actually expected to be restored at large scales by averaging over disorder, which brings us to the issue of computing the disorder average of physical quantities such as correlation functions

$$\langle \mathcal{O} \rangle = \frac{\int d\phi \mathcal{O} e^{-\mathcal{S}[\phi, V]}}{\int d\phi e^{-\mathcal{S}[\phi, V]}} . \quad (1.19)$$

The main difficulty in computing (1.19) is the presence of the random potential V in the denominator. There are essentially two known techniques used to overcome this :

- The *replica trick* consists in considering $n \in \mathbb{N}$ copies (replicas) of the system, and then taking a formal $n \rightarrow 0$ limit. The free energy (whose derivatives yield the different correlation functions of interest) is obtained from the identity

$$\ln Z = \lim_{n \rightarrow 0} \frac{Z^n - 1}{n} , \quad (1.20)$$

and in the right-hand side Z^n can be disordered averaged, yielding an effective field theory in the replicated space.

- The *supersymmetry trick* (SUSY) consists in introducing Grassmann (anticommuting) variables ψ such that

$$\frac{1}{\int d\phi e^{-\mathcal{S}[\phi, V]}} = \int d\psi e^{-\mathcal{S}[\psi, V]} , \quad (1.21)$$

yielding an effective field theory in the supersymmetric space of fields ϕ, ψ .

Both of these techniques were applied to the IQHE case respectively by Pruisken [27] and Weidenmüller [28]. The averaging over disorder was proceeded with a Hubbard-Stratonovitch transformation onto matrix-valued fields, yielding an effective field theory whose low-energy modes (the ones of interest for the large scale, critical point physics) are described by a sigma model with action

$$S[Q] = \frac{1}{8} \int d^2r \text{Str} \left[-\sigma_{xx} (\nabla Q)^2 + 2\sigma_{xy} Q \partial_x Q \partial_y Q \right] , \quad (1.22)$$

where σ_{xx} and σ_{xy} are the dimensionless conductivities, and the matrix field Q lives in some symmetric target (super)space, namely $\frac{U(n,n)}{U(n) \times U(n)}$ ($n \rightarrow 0$) in the replica approach

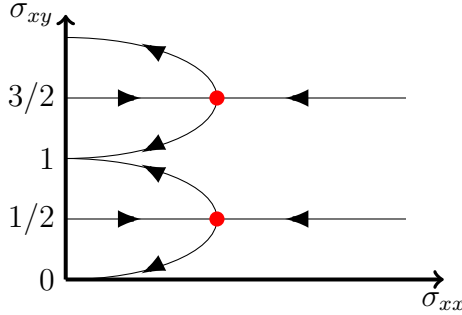


Figure 1.10: Two-parameter flow diagram of the sigma model (1.22) for the Integer Quantum Hall Effect. The strong coupling fixed points at $\sigma_{xy} = n + \frac{1}{2}$ (in red) are critical and correspond to the transitions between plateaus.

and $\frac{U(1,1|2)}{U(1|1) \times U(1|1)}$ in the SUSY one. Crucially the action (1.22) carries a so-called *topological term* (the one proportional to σ_{xy}), of a strongly non perturbative nature. Whereas the usual scaling theory of localization [29] predicts that in two dimensions all single-particle electronic states are localized by arbitrarily weak disorder, the presence of a topological term in the sigma model action is one of the few mechanisms responsible for exceptions to this rule (for a general review of the possible mechanisms see for instance [30]). It is actually believed that the corresponding two-parameter RG flow diagram is the one given in figure 1.10, where the fixed points at $\theta = 2\pi\sigma_{xy} = (2n+1)\pi$ describe the plateau transitions.

Turning to the CFT of the critical points, the fact it has escaped the range of manageable CFTs so far can be explained by two aspects, directly read off the sigma model target space : it is *non unitary*, which can be related to general supergroup properties or, in the replica approach, to the $n \rightarrow 0$ limit, and it is *non compact* due to the non positive-definiteness of the target space metrics. Non-unitarity, though unphysical in field theory and particle physics, emerges naturally in condensed matter theory as soon as one considers disorder averages, or in geometrical problems such as percolation or self-avoiding walks as soon as one consider non local observables. One consequence is that the theory of the plateau transitions in the IQHE is expected to be *logarithmic*, as introduced in section 1.1.

1.4 A step towards exact solutions : lattice models

From crystallography to quantum chromodynamics, through condensed matter physics and network models, *lattice models* (that is, physical models with an underlying discrete spatial structure) have played a central role in several areas of modern physics. In some cases, such as the study of ferromagnetic solids which lead to the Ising model, the underlying lattice structure is dictated by nature. In other cases, however, it is ‘artificial’. The models we will be using in this thesis to describe the collapse of two-dimensional polymers and the quantum Hall plateau transition fall into this second category, and it is legitimate to ask whether the introduction of a lattice structure in these cases may spoil the physics under study, and if not, what we may actually gain from it.

The answer to the first question traces back to universality. Considering that the large scale physics of critical systems should not depend on their microscopic details,

describing a continuous material by its lattice analog should not affect its large scale behaviour provided that the essential symmetries are respected. In practice, we will get to introduce *loop*, *vertex*, *face* models (all to be defined shortly), whose different control parameters (the strength of an interaction, the anisotropy of the lattice, all of which enter the model through the Boltzmann weights of its various configurations) will need to be fine-tuned to possibly recover the critical points of interest.

The second question, “why do that ?”, allows for several levels of answer. First, it is likely that the field theories of polymer collapse and quantum Hall plateau transitions may not be understood in the same way as for simpler, unitary CFTs, namely by the classification of Virasoro representations. The representation theory of the Virasoro algebra is actually believed to be *wild* in the sense that it is as complicated as it can be, and for this reason the indecomposable modules corresponding to logarithmic CFTs, which both theories of the polymer collapse and the plateau transitions are believed to be, may very well escape the most sophisticated, though, to their own extent, successful [31], attempts of classification. The use of lattice models as a possible alternative can be traced back to the works of Pasquier and Saleur [32], and later Read and Saleur [33] as well as Pearce, Rasmussen and Zuber [34], where it was observed that many of the algebraic features that make logarithmic CFTs so complicated are already present in the corresponding lattice models. The corresponding *lattice algebras* and their various representations have been the object of extensive study during the past decades, and powerful methods have been developed to tackle all kinds of models on the same footing. For instance, various vertex or loop models can be mapped onto height models, whose critical behaviour can be understood from the *Coulomb gas formalism* [35] as that of bosonic fields dressed with electric or magnetic excitations. More generally, lattice models are well suited for numerical experiments, and we will see shortly how the whole operator content of the continuum CFTs can be obtained by diagonalization of the corresponding finite size *transfer matrix*. What shall however be the key point in this thesis is that many of these models allow for an exact solution, at the price of yet another fine-tuning of the Boltzmann weights so that these obey well-known constraints, gathered under the name of the *Yang-Baxter equation* [36]. It turns out that most common critical systems were found to have such an *exactly solvable*, or (*quantum*) *integrable* lattice model in their universality class ², and the corresponding solutions can be found by the *inverse scattering method*, or (*algebraic*) *Bethe ansatz* [37], reducing the diagonalization of a one-dimensional transfer matrix or the corresponding quantum Hamiltonian, which usually involves a set of equations exponentially growing with the size of the system, to the resolution of the so-called *Bethe equations*, whose number is instead proportional to the system size and which allow for powerful analytic developments in the continuum limit.

The rest of this section is devoted to a first and yet very evocative encounter with some of the essential notions brought up in this short introduction, namely some of the various forms of two-dimensional lattice models and the mappings that exist between them, the transfer matrix and the associated technique of finite-size scaling for critical systems, as well as the Bethe ansatz procedure for exactly solvable models.

²Note in that two-dimensional conformal field theories are, by essence, integrable, in the sense that the decoupling between holomorphic and anti-holomorphic sectors allows for an infinite number of conserved quantities. Considering indeed the spin- s current $\mathcal{J}_s = (J, \bar{J})$ where J and \bar{J} are descendent of the identity at level $(s+1)$ in the holomorphic (resp. antiholomorphic) sector, one has $\partial_{\bar{z}} J = \partial_z \bar{J} = 0$, hence $\partial_\mu \mathcal{J}_s^\mu = 0$, and therefore the conservation of the charge $\mathcal{Q}_s = \int dx \mathcal{J}_s^0 = \oint dz J + d\bar{z} \bar{J}$.



Figure 1.11: Loop configurations arising from the lattice description of a two-dimensional polymer (left) and the supersymmetric path integral formulation of the point-contact conductance at the IQHE plateau transition (right). Both these constructions will be detailed in chapter 2.

Loop models, vertex models, face models and the equivalence between them

As we will detail in the next chapter, models for the collapse of a polymer in two dimensions and for the computation of transport observables at the Integer Quantum Hall Effect plateau transition can be formulated in terms of geometrical paths propagating on the square lattice and interacting at its vertices. In the former case, the emergence of such a geometrical interpretation is quite straightforward, as the propagating path is just a representation of the polymer itself on a discretized space, already discussed in section 1.2. The latter case requires a more indirect way [38, 39], where the computation of a transport observable such as the point-contact conductance (see section 2.4.2) is written in its supersymmetric path integral formulation as a sum over advanced and retarded paths going from one edge e_1 to another edge e_2 of the square lattice, yielding another *classical* geometrical model with two different colours of paths.

Both of the resulting models, for which representations of typical configurations are shown in figure 1.11, belong to the class of *loop models*, which is a term generically used to describe models for loop gases on the lattice. See [40] for a review, and [41] for a variety of new models and results; such models are also encountered in the field of topological quantum computation, namely the ground state and worldlines of quasiparticles excitations of $2 + 1$ -dimensional quantum mechanical models are projected onto the 2-dimensional plane, where they can be considered as the configurations of a classical loop gas, hence furnishing a natural geometrical interpretation for the non trivial braiding of quasiparticles [42, 43]. Loop models are in general specified by a variety of parameters, namely the number of loop colours involved [44], the fugacity n attributed to each closed loop (in the model built at the IQHE transition every closed loop has to be traced over a supersymmetric space, and therefore has a weight $n = 0$; in particular, the configuration depicted on the right panel of figure 1.11 is associated with a weight zero; $n = 0$ also holds true in the polymer model as long as the polymer under consideration cannot close on itself), the way loops interact with themselves or one another (via, for instance, the Boltzmann weight attributed to configurations where two loops come close to each other at a given vertex), if they can cross [45], etc...

Investigating the various aspects of a given model, it is generally useful, if not crucial, to switch between this model's different formulations. All the loop models of interest for us can be mapped onto *vertex models*, which are statistical models where the degrees of freedom are carried by the edges of a given lattice and the interactions are encoded by the Boltzmann weights associated with the various configurations at vertices. Alternatively,

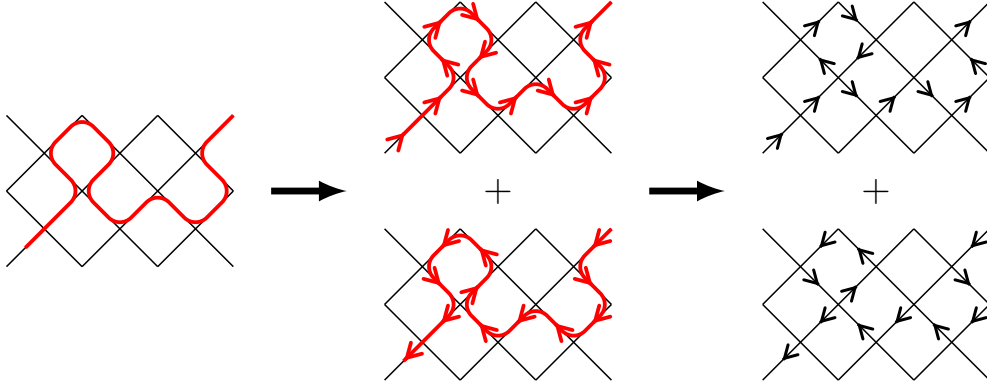


Figure 1.12: Mapping from a dilute loop configuration on the square lattice to a sum over the configurations of a ‘spin one’ vertex model, where each edge carries either an orientation ± 1 , or no orientation at all (0).

these can sometimes also be written as *face models*, where the degrees of freedom are attached to the sites of the lattice and interact through ‘*interactions-round-a-face*’ (IRF) around each plaquette (see for instance [41]). Details of such mappings in the particular cases of interest will be given in Chapter 2, and we shall here simply sketch the idea on how a simple loop model such as that originating from the description of polymers can be turned into a vertex formulation [40]. This is summed up in figure 1.12, where loops are first given an orientation destined to be summed over, each configuration of oriented loops being thereby translated into a configuration of edges either oriented, or empty. Importantly, the orientation of edges allows to translate the weight of closed loops in terms of local angular contributions, which allows to decompose the Boltzmann weight of each configuration of edges as a product over the configurations at each vertex, hence the resulting vertex model. We note in passing that the non-locality intrinsic to the problem of counting closed loops has thereby been traded against a problem of *local*, albeit *complex* weights, which is an example on how non-unitarity naturally emerges from physical statistical mechanics problems.

The transfer matrix formalism

We now move on to introduce the *transfer matrix* formalism, whose role will be of central importance throughout this thesis and which is more generally nothing less than the discrete formulation of the well-known equivalence between classical statistical systems with short-ranged interactions in d dimensions and relativistic quantum field theories in $d - 1$ space dimensions³.

Let a model defined on a square lattice of dimensions $L \times M$ sites, with specified boundary conditions (if these are periodic in the horizontal direction, our lattice amounts

³Close enough to its critical point such that its correlation length is larger than any of its microscopic scales, a given statistical mechanics model with local interactions can be rewritten in terms of (say) one continuous function $\varphi(x)$ on the d -dimensional euclidian space and the corresponding local Hamiltonian $\mathcal{H}[\varphi] = \int d^d x H(\varphi(x), \partial\varphi(x), \dots)$, such that the expectation value of any operator may be written as $\langle \dots \rangle = \int D\varphi(x) \dots \exp(-\int d^d x H)$. Interpreting one particular space dimension as an imaginary time, say $x^0 = -it$, the above expectation value can be rewritten as $\int D\varphi(\vec{x}, t) \dots \exp(\int dt \int d^{d-1} \vec{x} \mathcal{L})$, namely as the Feynman path integral formulation of a quantum-mechanical expectation value over a set of fields evolving in $d - 1$ dimensions of space and one dimension of time.

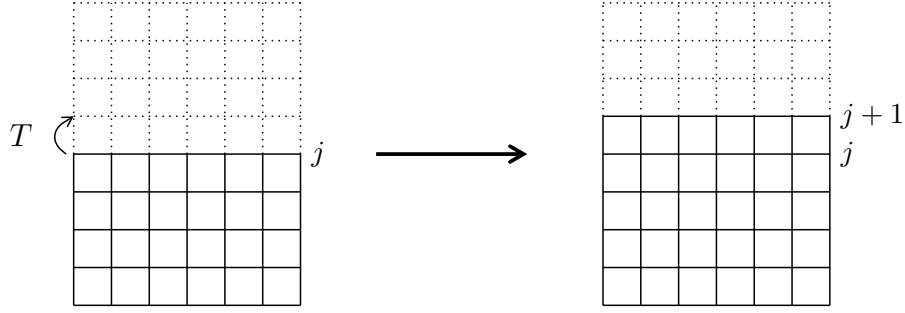


Figure 1.13: The configurations of a d -dimensional statistical mechanics model can be built up by repeated actions of the transfer matrix T , which can be interpreted as the discrete imaginary time evolution operator of a $d - 1$ -dimensional quantum system.

to a cylinder; if these are periodic in both directions, our lattice amounts to a torus, etc...). For simplicity we assume that the degrees of freedom are ‘spins’ $s_\mu \equiv s_{i,j}$ living on the sites of the lattice ($i = 1, \dots, L$, $j = 1, \dots, M$) and that the interactions are between nearest-neighbouring spins only. The partition function at inverse temperature β is a sum over the possible spin configurations

$$Z = \sum_{\{s_\mu\}} e^{-\beta H} = \sum_{\{s_\mu\}} e^{-\beta \sum_{\langle \mu, \nu \rangle} h(s_\mu, s_\nu)}, \quad (1.23)$$

and can be decomposed into horizontal slices as

$$Z = \prod_j \sum_{\{s_{i,j}\}} e^{-\beta \tilde{H}_{j,j+1}} \equiv \prod_j T_{j,j+1}, \quad (1.24)$$

where $\tilde{H}_{j,j+1}$ encodes all interactions $h(s_{i,j}, s_{i\pm 1,j})$ within row j , as well as interactions between the spins in row j and those of row $j + 1$. The matrix T with elements $T_{j,j+1}$, acting on the configurations of row j , is the so-called *transfer matrix*, which can be interpreted geometrically as adding one row to the system, see figure 1.13

Interpreting the vertical direction as an imaginary time $\tau = it$, the transfer matrix is therefore seen to play the role of the discrete time evolution operator for a one-dimensional quantum system with Hamiltonian $H_{1D} = H_{j,j+1}$. We emphasise that this construction can be generalized to any type of lattice model with local interactions. In particular, we have remained purposely loose on the treatment of boundary conditions in the vertical direction : for spin models with periodic boundary conditions in the vertical direction, the product T^M of transfer matrices has to be traced over in order to recover the partition function. For loop models with periodic boundary conditions, some care has to be taken to give the correct weight to loops winding around the vertical direction of the torus, hence the so-called *Markov trace* [40], on which we will not give any more detail here.

As we shall now see progressively, the transfer matrix formalism makes quite natural the access to the large-scale behaviour of the model of interest. Consider for instance the calculation of the partition function for a system of size $L \times M$ with specified boundary conditions, where L is kept finite and M is arbitrarily large. Expanding the product (1.24) over a basis of eigenvectors of T with eigenvalues $\Lambda_0^{(L)} > \Lambda_1^{(L)} > \dots$, we see that it is dominated for M large enough by a term proportional to $(\Lambda_0^{(L)})^M$, hence the corresponding free energy per site in the $M \rightarrow \infty$ limit, $f_{L,\infty} = -\frac{1}{LM} \log Z = -\frac{1}{L} \log \Lambda_0^{(L)}$.

Further, we can choose to compute in the same way, say, a spin-spin correlation function between one spin on row j and one spin on row $j + y$. The result in the y large, M large limit is easily seen to involve the two largest transfer matrix eigenvalues, more precisely the connected correlation function is seen to have the following exponential decay,

$$\langle s_{i,j} s_{i,j+y} \rangle \propto e^{-y/\xi} \quad (1.25)$$

where the correlation length ξ is obtained as

$$\xi = \frac{1}{\ln \Lambda_0^{(L)} / \Lambda_1^{(L)}}. \quad (1.26)$$

We now start to see how criticality may show up in the transfer matrix analysis as the thermodynamic limit $L, M \rightarrow \infty$ is taken : for a non critical system, that is, with a finite correlation length, we expect the ratio $\Lambda_0^{(L)} / \Lambda_1^{(L)}$ to have a finite limit as $L \rightarrow \infty$, or in other terms, we expect the corresponding one-dimensional quantum system to be *gapped*, or *massive*. On the contrary, for a critical system, an infinite correlation length implies that the ratio $\Lambda_0^{(L)} / \Lambda_1^{(L)}$ should go to 1 as $L \rightarrow \infty$, or in other terms, that the corresponding one-dimensional quantum system is *gapless*.

The asymptotic behaviour of the gap $f_1^{(L)} - f_0^{(L)} \equiv \ln \Lambda_0^{(L)} / \Lambda_1^{(L)}$ at criticality is actually well-determined from conformal field theory, as will be the object of the next paragraph. As we shall see more generally, the study of the transfer matrix's dominant eigenvalues (the *low-lying levels* of the 1d quantum Hamiltonian) can inform us about the whole set of critical exponents of the corresponding CFT.

From transfer matrices to critical exponents: finite-size scaling on the cylinder

Consider a quasi-primary field ϕ with conformal weight Δ (we restrict for simplicity to the holomorphic sector), whose two-point function on the plane is known from conformal invariance to be of the form

$$\langle \phi(z) \phi(0) \rangle = \frac{1}{z^{2\Delta}}. \quad (1.27)$$

Mapping the plane onto a cylinder of width L by means of the transformation

$$w = \frac{iL}{\pi} \ln z, \quad (1.28)$$

yields on the latter

$$\langle \phi(iy) \phi(0) \rangle \propto e^{-\frac{\pi\Delta}{L}y}. \quad (1.29)$$

Comparing with the scaling of lattice correlation functions as studied above (where periodic boundary conditions need to be taken for comparison with the cylinder; for other types of boundary conditions, one should need to consider CFT two-point functions on other geometries such as the half-infinite complex plane, leading to analog results) suggests that there is a correspondence between the operators of the CFT under investigation and the dominant eigenvalues of the corresponding lattice transfer matrix, or, equivalently, with the low-lying levels of the corresponding quantum Hamiltonian. More precisely, the transfer matrix's largest eigenvalue is shown [46] to scale as

$$f_0^{(L)} \equiv -\ln \Lambda_0^{(L)} = Lf_\infty - \frac{\pi c}{6L} + \dots \quad (1.30)$$

⁴, whereas the eigenvalue $\Lambda_\phi^{(L)}$ related to the field ϕ yields the corresponding conformal weights $(\Delta, \bar{\Delta})$ as

$$f_\phi^{(L)} - f_0^{(L)} \equiv \ln \frac{\Lambda_0^{(L)}}{\Lambda_\phi^{(L)}} = \frac{2\pi(\Delta + \bar{\Delta})}{L} + \dots \quad (1.31)$$

Let us now look back on the way we have taken so far. From a given classical or quantum critical problem, namely that of polymer collapse in two dimensions or the plateau transition in the Integer Quantum Hall Effect, we have claimed that one may derive classical two-dimensional geometrical models on the square lattice, hoping that a fine-tuning of the corresponding Boltzmann weights should recover the universal behaviour of interest in each case. Once the corresponding transfer matrix or quantum Hamiltonian clearly defined in either its loop, vertex, or any of its representations, criticality can be investigated and the associated set of critical exponents *in principle* extracted from the finite-size scaling of the corresponding eigenvalues. Additionally, peculiar algebraic features of the continuum limit such as indecomposability in the case of a logarithmic conformal field theory can be dug out from algebraic features of the finite size transfer matrix itself, or its associated quantum Hamiltonian [8]. What remains hidden behind our use of the term ‘*in principle*’ is that the finite-size scaling analysis can turn out to be very difficult in practice. The dimension of the transfer matrix usually grows up exponentially with the system size L , limiting the range of sizes tractable by usual numerical methods to, at best, $L \sim 10$ or 20 for usual systems. Adding to this the fact that in some cases (namely, whenever marginal operators are present, or, more fundamentally, in the case of the *non compact CFTs* which are of central interest for us) the corrections to the conformal charges in (1.30) and (1.31) may show a really slow convergence of the order of $\log L$, we cannot escape as a conclusion that the critical exponents can sometimes simply turn out to be untractable from straight numerics. What is left for us to rely on is the possibility to turn the corresponding models into exactly-solvable ones, a procedure whose main lines we shall depict now.

Exactly solvable models and Bethe Ansatz

Assume, as announced, that we are able to obtain an integrable lattice model for each of the universality classes of interest. Namely, and as will be explained at length in section 2.1, that we have been able to tune the Boltzmann weights of the corresponding (say) vertex models so that these obey the so-called *Yang-Baxter equation*, without spoiling the original critical behaviour.

For a given integrable vertex model whose degrees of freedom live in some finite dimensional vector space (such as, for instance, the assumed integrable version of the ‘spin one’ vertex model inherited from the loop description of polymers), the eigenvalues of the transfer matrix or its equivalent quantum Hamiltonian at a given size L can be obtained by the *algebraic Bethe ansatz* [37], which consists in building eigenstates from a reference, trivial one called the *pseudovacuum*. These eigenstates and the corresponding eigenvalues are parametrized by a set of $\propto L$ complex *Bethe roots* subject to a set of non linear equations, hence reducing the problem of diagonalizing matrices of sizes $\sim \exp L$

⁴Equation (1.30) is analog to the *Casimir effect* in quantum electrodynamics, where the boundary conditions imposed on the wavefunction by two metallic plates induce a force between them, varying as a function of the distance L between the two plates and interpreted as resulting from an *energy of the vacuum*.

to the resolution of $\propto L$ *Bethe ansatz equations* (BAE). There are in general two ways to proceed from there

- Solve numerically the BAE for large values of L (typically of order 100 or 1000), compute the corresponding transfer matrix eigenvalues and infer the conformal spectrum from finite size scaling.
- Use analytical techniques to infer the conformal spectrum directly from the $L \rightarrow \infty$ limit of the BAE.

These two ways are actually quite complementary: indeed, it will in practice sometimes turn too complicated to obtain the whole conformal content from purely analytical methods; conversely, numerical data for systems of a few thousands of sites should sometimes not be enough to fix completely the logarithmic finite-size corrections mentioned earlier. Understanding the continuum limit of a given integrable model can therefore end up being a very complicated task, which will for us involve a substantial combination of numerical and analytical techniques.

1.5 Non-compactness

As might not have escaped the reader's attention, we have insisted on the fact that only *compact* lattice models, namely models with a finite number of degrees of freedom per lattice site or edge, qualify for a Bethe ansatz solution. Progress in the non compact case has been made recently [47], but leaves the problem of exact solutions still largely open.

Whereas the lattice model for polymer collapse clearly enters the first category (as it can be reformulated in terms of a vertex model with three possible states per edge), this is not the case of that describing the IQHE transition. This fact can be seen straightforwardly from the loop language, as the blue and red loops corresponding to the Feynman paths in figure 1.11 are allowed to pass through any edge an arbitrary number of times. In order to reach any exact result, the procedure we follow in this thesis is that introduced by Ikhlef, Cardy and Fendley [39] of *truncating* the infinite loop model to a finite one, hoping that the universal behaviour might be left unaffected in the process. The original results of [39] obtained from direct transfer matrix diagonalization are in this sense rather disappointing, as the critical exponents found in the truncated case differ significantly from those expected at the plateau transition. In particular, the correlation length exponent for the truncated model is measured as

$$\nu \simeq 1.1, \quad (1.32)$$

which definitely lies out of the range $2.3 \leq \nu \leq 2.7$ of common expectations (see section 1.3). This apparent failure raises the general question of whether *compact* spin chains or lattice models might at all give rise, in the continuum limit, to *non compact* field theories such as that of the IQHE. As an illustration, we can consider the simplest of such theories, namely that of the two-dimensional euclidean free field with action

$$S = \int d^2x (\partial_\mu \varphi)^2, \quad (1.33)$$

which is a theory of a real bosonic field taking its values on the (non compact) real line

⁵. This theory is well-known [48] to describe the properties of a two-dimensional Brownian motion, and recovers in particular the constant value of the propagator $G_1(r, r') = \langle \varphi(0)\varphi(r) \rangle$ and therefore the corresponding trivial critical exponent $x_1 = 0$ [49], in agreement with the fact that a Brownian motion starting from a point r should visit any point r' with probability one. From there the *fuseau*, or *watermelon* exponents x_ℓ (to be defined in more detail later in this manuscript) associated with the scaling of the probability that ℓ independent Brownian motions starting from a point r meet at some point r' are readily deduced to be identically equal to zero. As it is well-known, Brownian motions allow for a discrete representation as random walks on the (say) square lattice, which are, from the fact that they can visit any lattice site or edge an arbitrary number of times, a manifest example of model with a non compact set of degrees of freedom. In contrast, the self-avoiding walks introduced in section 1.2 (see figure 1.5), which are a compact lattice model, will be argued later in this thesis to be described by a *compact* CFT, resulting in particular in a non trivial set of exponents x_ℓ .

A significant breakthrough was brought in by the 2002 paper of Jacobsen, Read and Saleur [50], where it was shown that introducing the possibility for loop crossings in the low-temperature (*dense*) phase of the self-avoiding walks leads the latter to a different critical point described by a set of *non compact bosonic fields*, and reproducing precisely the zero fuseau exponents of the Brownian motion as could also be seen from an equivalent exactly solvable model [51] (recently, [52], the particular $Osp(3|2)$ case was studied by mean of Bethe ansatz, and shown explicitly to give rise to a continuum spectrum of exponents). More precisely, the formulation introduced in section 1.2 in terms of a $O(n)$ -invariant vector model was there traded for a $Osp(2m+n|2m)$ -invariant supersymmetric model, whose low-temperature phase identifies as a broken symmetry, Goldstone phase with target space $Osp(2m+n|2m)/Osp(2m+n-1|2m) \simeq S^{2m+n-1|2m}$, allowed from the fact that for $n < 2$ the supergroup action cannot be implemented in terms of unitary vector transformations, hence rendering ineffective the use of the Mermin–Wagner theorem. In the original $O(n)$ -invariant model (1.10) this phase is absent, but it was argued in [50] to indeed be restored in the dense phase of the latter by the introduction of more general interactions of the type $(\vec{S}_k \cdot \vec{S}_l)^2$, associated geometrically with the crossing of loops. One of the conclusions of this analysis, pushed further in [53], was that several properties of the non compact CFT for Brownian walks can be recovered in, for instance, a *compact* model of dense loops allowed to cross on the bidimensional square lattice. Over the years, several further examples of such a phenomenon were then discovered :

- In 2005, the integrable vertex model built out of the product of the (three dimensional) fundamental and dual representations of the superalgebra $sl(2|1)$ was shown [54] to be described in the continuum limit by the $SU(2|1)$ Wess-Zumino-Witten model at level $k = 1$, which can be equivalently be defined on some *non compact* target space by trading the indefinite metric to a positive definite one.
- The following year, the antiferromagnetic Potts model [55] and related staggered six-vertex model [56, 57] were shown to be described in the continuum limit by a theory involving a non compact boson, which was later identified [58] as the $SL(2, \mathbb{R})/U(1)$ black hole sigma model, introduced by Witten in the context of string theory [59] (see section 3.2.3 for more details). Recently, this model as well

⁵We note in passing that from the CFT point of view this is a trivial theory, in the sense that all its primary fields have conformal dimension zero. To construct a non trivial CFT from the bosonic field φ , one should consider instead the *Liouville theory* with action $S = \int d^2x (\partial_\mu \varphi)^2 + \mu e^{\beta\varphi}$ [11]

as the $sl(2|1)$ one mentioned above were also identified as some particular points in the phase diagram of the $U_q(sl((2|1)))$ model [60], which has been shown to allow for a whole critical phase described by the black hole theory [61] .

Due to their very peculiar setup, for instance a supergroup symmetry or delicate staggering of the spectral parameter, these few counterexamples have however for long been considered to be quite exotic, and it did remain widely believed that non compact continuum limits (other than the somewhat trivial free euclidean boson -related theories) could not emerge from ‘ordinary’ compact spin chains or lattice models, for instance related to statistical mechanics problems with local interactions and positive Boltzmann weights. The results we present in this thesis go quite against the latter argument. In [62, 63], we first observed that the integrable $a_2^{(2)}$ model, candidating for the description of polymer collapse and in particular involving a loop representation with physical, positive Boltzmann weights, has a non compact continuum limit with a continuous spectrum of critical exponents which identifies precisely as the $SL(2, \mathbb{R})/U(1)$ black hole. A similar observation was made in the case of a dense two-colours loop model [64], which can be seen as a representation of two coupled Potts models or as a dense counterpart of the truncated IQHE model of interest here. This raises immediately several questions : how frequent are in fact such non compact limits ? How can we know a priori whether a given model will or will not give rise to a non compact limit, which interpretation can we give to the non compact degrees of freedom, and what will these change in practice ? Might the truncated model for the IQHE actually be itself of a non compact nature, and if so, what can we gain from it in the understanding of the plateau transition ?

1.6 Plan of the rest of the manuscript

The rest of this manuscript is organized as follows. In chapter 2, we introduce the notion of integrable lattice models and show that those related to a tentative description of the collapse of two-dimensional polymers and the (truncated) IQHE transition can be identified as the so-called $a_2^{(2)}$ and $b_2^{(1)}$ vertex models, respectively. The algebraic Bethe ansatz is introduced in the beginning of chapter 3, and used to understand the continuum limit of the whole $a_n^{(2)}$ hierarchy of integrable models. In all cases the continuum limit is observed to be non-compact, some of the dramatic consequences of which are presented in chapters 4 and 5. In the former, we use our results on $a_2^{(2)}$ and Monte-Carlo checks to draw conclusions on the phase diagram of two-dimensional polymers, and in particular on the controversial Θ point critical exponents. The detailed analysis of the two-dimensional polymers phase diagram meanwhile serves us as a guide to investigate the nature of non-compact degrees of freedom emerging from the corresponding lattice model. In chapter 5, which can be considered largely open, we give an exact solution of the $b_2^{(1)}$ (as well as hints on the whole $b_n^{(1)}$ hierarchy) and conclude on the non-compact nature of the truncated model of [39]. This allows to explain several puzzling observations initially made in [39], and present conjecture on how the corresponding critical properties might be related to those of the IQHE transition.

Chapter 2

Exactly solvable models for polymers and the IQHE plateau transition

As announced in the previous chapter, both the problems of calculating correlation functions of two-dimensional polymers and studying transport observables at the Quantum Hall plateau transitions, as well as many other two-dimensional statistical mechanics or one-dimensional quantum mechanics problems, can be reformulated in the framework of *loop* or *vertex* models on a bidimensional lattice.

The first section of the present chapter aims at introducing the tools and concepts related to the physics of integrable, exactly solvable lattice models. For pedagogical reasons the presentation is mostly based on the well-known six-vertex model, from which we introduce the notions of quantum integrability, Yang–Baxter equation and quantum groups. In section 2.2, we introduce in detail the notion of loop model as well as the related algebraic concepts, and work out the precise relationship between the six-vertex model and the related fully packed loop model on the square lattice. The mappings from the problem of polymer collapse and the computation of transport observables at the IQHE transition to integrable loop and vertex models are then detailed in sections 2.3 and 2.4 respectively.

2.1 Introduction to integrability and exactly solvable models

This presentation is very much inspired from the lectures of H. Saleur and J-B. Zuber [66], which we recommend for more details and references on the subject. We also discuss the connection with integrable quantum field theories and factorizable S -matrices, and refer for this matter to the original work of Zamolodchikov and Zamolodchikov [67] and the more recent review [68].

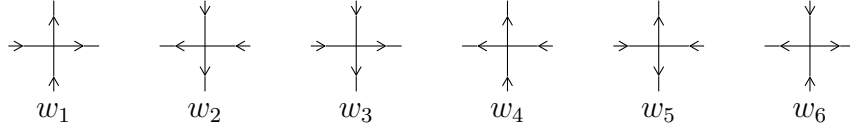
2.1.1 Vertex models, integrability, and the Yang–Baxter equation

Let us first give a proper definition of what a vertex model is: the degrees of freedom are attached to the links of a given lattice, which for us will always be the two-dimensional square lattice, and interactions take place at the vertices as each configuration of four links incident to a vertex is assigned a Boltzmann weight

$$w(\alpha, \beta, \gamma, \delta) = \alpha \begin{array}{c} \delta \\ | \\ \hline | \\ \beta \end{array} \gamma$$

A configuration of the system living on a lattice of size $L \times M$ with some given prescription on the boundary conditions is specified by the corresponding values of the degrees of freedom $\{\alpha_i\}$ on every edge, and the associated Boltzmann weight is the product of all corresponding vertex contributions. The degrees of freedom α_i may be of a rather general nature: in the cases we will be dealing with, they will be vectors in some given complex vector space (more precisely, in representations of some q -deformed (super)algebras, a notion which will be introduced further).

The toy-model we will be using throughout this section is Lieb's six-vertex model (1967), in which the degrees of freedom live in the vector space \mathbb{C}^2 whose basis $\{|\uparrow\rangle, |\downarrow\rangle\}$ can be represented as arrows on the links of the square lattice. The possible configurations of arrows are restricted by demanding that at each vertex the number of incoming arrows equals the number of outgoing ones (*ice rule*), restricting to 6 the number of admissible vertex configurations,



Moreover requiring that these weights be invariant under a global reversal of all arrows restricts to 3 the number of independent weights, $w_1 = w_2 \equiv a$, $w_3 = w_4 \equiv b$ and $w_5 = w_6 \equiv c$. Such a model was first introduced for describing crystal lattices with hydrogen bonds such as ice (the position of the hydrogen atom on each bond, closer to one or the other of the lattice atoms, is indicated by the corresponding arrow, and the ice rules indicates that each of the lattice atoms has a valence number equal to two), but is of central importance in the world of spin chains, loop models and quantum integrability.

Going back to the general case, it will turn convenient to temporarily assume that the degrees of freedom on horizontal and vertical edges can be of different nature, and we therefore call V and V_a the finite-dimensional vector space of degrees of freedom living on each vertical (resp. horizontal) link. A lattice of horizontal width L sites can be viewed in the Hamiltonian picture as a one-dimensional quantum system of Hilbert space $\mathcal{H} = V^{\otimes L}$ evolving in discrete imaginary time. The discrete time evolution corresponds to the addition of one horizontal row, and the corresponding matrix elements between the state $\{\alpha_1, \alpha_2, \dots, \alpha_L\}$ at time t and the state $\{\alpha'_1, \alpha'_2, \dots, \alpha'_L\}$ at time $t+1$ is encoded by the so-called *row-to-row transfer matrix*

$$\langle \alpha'_1, \alpha'_2, \dots, \alpha'_L | T | \alpha_1, \alpha_2, \dots, \alpha_L \rangle \equiv T_{\alpha_1, \alpha_2, \dots, \alpha_L}^{\alpha'_1, \alpha'_2, \dots, \alpha'_L} = \begin{array}{c} \alpha'_1 \quad \alpha'_2 \quad \dots \quad \alpha'_L \\ \hline a_0 \mid a_1 \mid a_2 \mid \dots \mid a_{L-1} \mid a_L \\ \hline \alpha_1 \quad \alpha_2 \quad \dots \quad \alpha_L \end{array},$$

where the labels a_j denote the states on the horizontal links, and must accordingly be traced over in accordance with the boundary conditions. In the graphical representation we have pictured the space V_a by a double line, to insist on its a priori different nature

than that of V . The horizontal $\mathcal{A} \equiv V_a$ space is referred to as the *auxilliary space*, whereas $\mathcal{H} \equiv V^{\otimes L}$ is referred to as the *quantum space*. Choosing for instance periodic boundary conditions in the horizontal direction imposes $a_0 = a_L$, and we have

$$T_{\alpha_1, \alpha_2, \dots, \alpha_L}^{\alpha'_1, \alpha'_2, \dots, \alpha'_L} = \sum_{a_0, \dots, a_{L-1}} w(a_0, \alpha_1, \alpha'_1, a_1) w(a_1, \alpha_2, \alpha'_2, a_2) \dots w(a_{L-1}, \alpha_L, \alpha'_L, a_0) \quad (2.1)$$

$$= \sum_{a_0} \begin{array}{c} a_0 \\ \hline | \quad | \quad \dots \quad | \\ \hline \end{array} \quad (2.2)$$

$$= \text{Tr}_{V_a} \begin{array}{c} | \quad | \quad \dots \quad | \\ \hline \end{array} \equiv \text{Tr}_{V_a} \mathcal{T}, \quad (2.3)$$

where the sums are over some basis of V_a . The matrix \mathcal{T} in (2.3), which acts on $V_a \otimes V^{\otimes L}$, is called the *monodromy matrix*, and we can for instance express the partition function of the $L \times M$ system with periodic boundary conditions in both directions as

$$Z_{L \times M} = \text{Tr}_{V^{\otimes L}} (\mathcal{T}^M). \quad (2.4)$$

Integrable vertex models, the R -matrix and the Yang–Baxter equation

We are now ready to turn to the definition of integrability for such a system. Quite naturally, we associate it with the existence of an infinite set of conserved quantities (although in practice only $\dim \mathcal{H}$ independent of them are needed; we note however that this definition actually allows for some loopholes, and alternative definitions can be proposed, see [69]), or in other terms, of quantities commuting with the transfer matrix. This can be realized quite easily if we actually seek for a one-parameter family of Boltzmann weights $w(a, \alpha, \alpha', a' | u)$, hence a one-parameter family of transfer matrices $T(u)$, such that

$$[T(u), T(v)] = 0, \quad (2.5)$$

for any u and v . Indeed, if this is the case, each coefficient in the Laurent expansion of $T(u)$ furnishes one observable commuting with $T(u)$ for any u , moreover these observables are mutually commuting. The physical interpretation of the parameter u , which is called the *spectral parameter*, will be discussed shortly. One sufficient condition for (2.5) to hold is the existence of a $V_a \otimes V_a \rightarrow V_a \otimes V_a$ two-parameter dependent matrix $\check{R}(u, v)$ such that the following ‘RTT relation’ holds :

$$\check{R}(u, v) \cdot (\mathcal{T}(u) \otimes \mathcal{T}(v)) = (\mathcal{T}(v) \otimes \mathcal{T}(u)) \cdot \check{R}(u, v), \quad (2.6)$$

where the tensor product denotes a matrix multiplication over the quantum space, and the dot denotes a matrix multiplication over the product of the two auxilliary spaces. Defining the *braiding matrix* $R = \mathcal{P} \check{R}$, where \mathcal{P} is the permutation operator of the two auxilliary spaces in $V_a \otimes V_a$, we have the following graphical representation of (2.6) :

$$\begin{array}{c} u \\ \swarrow \quad \searrow \\ v \end{array} \begin{array}{c} | \quad | \quad \dots \quad | \\ \hline \end{array} = \begin{array}{c} | \quad | \quad \dots \quad | \\ \hline \end{array} \begin{array}{c} \swarrow \quad \searrow \\ v \end{array} \begin{array}{c} u \end{array},$$

where we have adopted the notations

$$R(u, v) = \begin{array}{c} u \\ \swarrow \quad \searrow \\ v \end{array}, \quad R(u, v)^{-1} = \begin{array}{c} u \\ \searrow \quad \swarrow \\ v \end{array}. \quad (2.7)$$

It can be shown that the R -matrix satisfying this ‘RTT’ requirement is subject to a consistency condition, which is fulfilled if we take R to satisfy the *Yang–Baxter equation*,

$$R_{23}(v, w)R_{13}(u, w)R_{12}(u, v) = R_{12}(u, v)R_{13}(u, w)R_{23}(v, w). \quad (2.8)$$

This equation, which of course holds in a similar form for \check{R} , is defined in the tensor product $V_a \otimes V_a \otimes V_a$, and for instance the notation R_{23} indicates the product of the identity operator acting on the first space times the braiding of the second and third spaces. It allows for the following simple pictorial representation

In most cases of physical interest, the dependence of $\check{R}(u, v)$ in the spectral parameters will be through the difference $u - v$. It is usual to require the *unitarity condition* on the R -matrix,

$$R(u)R(-u) \propto \mathbf{1}, \quad (2.9)$$

in particular all the solutions we will get to consider are *regular solutions*, in the sense that they satisfy $\check{R}(0) = \mathbf{1}$, $R(0) = \mathcal{P}$.

We can now go back to the case where the vertical and horizontal spaces are of the same nature, $V = V_a$: assuming that a solution of the Yang Baxter has been found, the RTT relation is readily solved provided the Boltzmann weights are taken to be

$$w(\alpha, \beta, \gamma, \delta|u) = R_{\alpha, \beta}^{\gamma, \delta}(u) = \check{R}_{\alpha, \beta}^{\delta, \gamma}(u). \quad (2.10)$$

In particular, $w(\alpha, \beta, \gamma, \delta|0) = \delta_\alpha^\delta \delta_\beta^\gamma$, which can be represented pictorially as

and from which follows that the transfer matrix $T(0)$ is nothing but the discrete translation operator in the horizontal direction. More generally, we can consider the operators

$$H_n = \left. \frac{d^n \log T(u)}{du^n} \right|_{u=0}, \quad (2.11)$$

which form the family of mutually commuting operators we were in quest for. Interpreting $H \equiv -H_1$ as the Hamiltonian of the quantum system, we therefore indeed have for this system an infinite number of conserved quantities.

We now go back to the six-vertex model, and investigate the solutions of the Yang–Baxter equation in this case, which will allow us to make contact with a general geometrical interpretation of the spectral parameter. The corresponding R -matrix acts on $\mathbb{C}^2 \otimes \mathbb{C}^2$ and reads

$$R = \begin{pmatrix} a & 0 & 0 & 0 \\ 0 & b & c & 0 \\ 0 & c & b & 0 \\ 0 & 0 & 0 & a \end{pmatrix} \quad (2.12)$$

in the basis $\{\uparrow\uparrow, \uparrow\downarrow, \downarrow\uparrow, \downarrow\downarrow\}$. A family of solutions is found, parametrized by a complex number γ , as

$$a = \frac{\sin(\gamma - u)}{\sin \gamma} \quad b = \frac{\sin u}{\sin \gamma} \quad c = 1. \quad (2.13)$$

For $u = \frac{\gamma}{2}$ one has $a = b$, and more generally the weights of the model are in this case isotropic, namely, invariant under discrete rotations of the lattice. The spectral parameter u is thus understood as introducing an anisotropy, which can be thought of as a spatial anisotropy of the lattice and as such is not supposed to affect the critical behaviour of the model, if any. This statement should however be made more precise, since for instance at a real value of γ the geometrical interpretation does not hold anymore for complex values of u . It turns out that for the six-vertex model the phase structure can be described in terms of the parameter $\Delta = \frac{a^2+b^2-c^2}{2ab} = \cos \gamma$: for $\Delta \geq 1$ or $\Delta < -1$, that is for imaginary γ the system is in a non-critical, massive phase, whereas for $-1 \leq \Delta < 1$, that is for real non zero γ the system is in a critical, massless phase. In the latter case, the critical behaviour does not depend on the spectral parameter if real, whereas complex values of u perturb the system to a massive phase.

These observations can be related to the more general statement : there are, in general (and forgetting about some higher-genus solutions in some cases), three types of regular solutions of the Yang–Baxter equation. These are said to be *rational*, *trigonometric* (or *hyperbolic*) or *elliptic* according to their dependence in the spectral parameter, and all the trigonometric solutions found to this date have turned out to be critical. The solution (2.13) for the six-vertex model is trigonometric for generic real γ , rational for $\gamma \rightarrow 0$ and $\gamma \rightarrow \pi$, and hyperbolic for imaginary γ . The eight-vertex model [36] gives in turn an example of elliptic solution of the Yang–Baxter equation. From now on, and unless specified, we will therefore restrict to real values of the spectral parameters, keep in mind the geometrical interpretation and use indistinctly the following graphical notations

$$w(\alpha, \beta, \gamma, \delta | u - v) = \check{R}_{\alpha, \beta}^{\delta, \gamma}(u - v) = \alpha \begin{array}{c} \delta \\ | \\ \hline u - v \\ | \\ \beta \end{array} \gamma = \alpha \begin{array}{c} \delta \\ | \\ \hline u \\ | \\ v \\ | \\ \beta \end{array} \gamma.$$

We close this paragraph by deriving the quantum Hamiltonian related to the integrable six-vertex model. For a system of horizontal size L with periodic boundary conditions, it is given by

$$H = \frac{1}{2 \sin \gamma} \sum_{i=1}^L h_{i, i+1}, \quad (2.14)$$

where we set $L + 1 \equiv 1$, and the Hamiltonian density $h_{i, i+1}$ acts on sites $i, i + 1$ as

$$h_{i, i+1} = \sigma_i^x \sigma_{i+1}^x + \sigma_i^y \sigma_{i+1}^y + \cos \gamma (\mathbf{1}_i \mathbf{1}_{i+1} + \sigma_i^z \sigma_{i+1}^z) \quad (2.15)$$

and as the identity on the other sites. Up to an irrelevant additive constant and proportionality factor, we therefore have

$$H = \frac{1}{2} \sum_{i=1}^L (\sigma_i^x \sigma_{i+1}^x + \sigma_i^y \sigma_{i+1}^y + \Delta \sigma_i^z \sigma_{i+1}^z), \quad (2.16)$$

which is the Hamiltonian of the so-called periodic *XXZ chain*. This denomination is transparent, as the coupling is anisotropic in the spin space (this anisotropy must not

be confused with the lattice anisotropy introduced by u), and the parameter $\Delta = \cos \gamma$, sometimes even γ , is often called the *anisotropy* of the model. At $\gamma = 0$ ($\Delta = 1$), H reduces to the Hamiltonian of the Heisenberg antiferromagnetic spin- $\frac{1}{2}$ chain, or *XXX chain*.

For later reference, we introduce generators

$$\begin{aligned} e_{i,i+1} &= \frac{q + q^{-1}}{4} - \frac{1}{2} (\sigma_i^x \sigma_{i+1}^x + \sigma_i^y \sigma_{i+1}^y + \Delta \sigma_i^z \sigma_{i+1}^z) - \frac{q - q^{-1}}{4} (\sigma_i^z - \sigma_{i+1}^z) \\ &= \mathbf{1}_1 \otimes \mathbf{1}_2 \otimes \dots \otimes \begin{pmatrix} 0 & 0 & 0 & 0 \\ 0 & q^{-1} & -1 & 0 \\ 0 & -1 & q & 0 \\ 0 & 0 & 0 & 0 \end{pmatrix}_{i,i+1} \otimes \dots \otimes \mathbf{1}_L, \end{aligned} \quad (2.17)$$

in terms of which we can rewrite the XXZ Hamiltonian (2.16) as

$$H = -\frac{1}{2} \sum_{i=1}^L e_{i,i+1}, \quad (2.18)$$

up to some immaterial additive constant.

Relation with integrable field theories in 1+1 dimensions

We close this section with a word on 1+1-dimensional integrable quantum field theories (IQFTs), and how their study is related to the notions we have just encountered, namely the Yang–Baxter equation, and ultimately, quantum spin chains. As announced in the beginning of the section, this follows the approach of Zamolodchikov and Zamolodchikov in [67].

Consider a 1+1-dimensional quantum theory of relativistic particles of masses m_{a_1}, \dots, m_{a_N} ¹, whose on-shell light-cone momenta are parametrized by

$$p_a = p_a^0 + p_a^1 = m_a e^{\theta_a}, \quad \bar{p}_a = p_a^0 - p_a^1 = m_a e^{-\theta_a}. \quad (2.19)$$

The real parameters θ_a are the so-called *rapidities*, and we assume that these actually denote narrow momenta wavepackets such that each particle can be assigned an approximate position at any time. Assuming for simplicity that the theory is massive (in the case of a CFT we consider an infinitesimal massive deformation) and therefore that the interactions are finite-ranged, one can view the N -particle states as a collection of free particles when these do not overlap. In particular, one can define the *in*- and *out*-asymptotic states

$$|A_{a_1}(\theta_1) \dots A_{a_N}(\theta_N)\rangle_{in,out}, \quad (2.20)$$

characterized respectively by there being no further interactions at $t \rightarrow -\infty$ and $+\infty$ (the symbol $A_{a_i}(\theta_i)$ denotes a particle of type a_i with rapidity θ_i). In the former case the particles' rapidities must be increasing from left to right, whereas in the latter case they must be decreasing, so both states can be represented by thinking of the symbols $A_{a_i}(\theta_i)$ as non-commuting operators written in the same order as the corresponding particles, namely

$$|A_{a_1}(\theta_1) \dots A_{a_N}(\theta_N)\rangle_{in} = A_{a_1}(\theta_1) \dots A_{a_N}(\theta_N) \quad \theta_1 > \dots > \theta_N \quad (2.21)$$

$$|A_{b_1}(\theta_1) \dots A_{b_N}(\theta_N)\rangle_{out} = A_{b_1}(\theta_1) \dots A_{b_N}(\theta_N) \quad \theta_1 < \dots < \theta_N. \quad (2.22)$$

¹In such a relativistic theory the number N of particles can vary. We will see however that integrability in 1+1 dimensions forbids particle production and annihilation, and that therefore N is fixed.

The assumption of *asymptotic completeness* translates into the fact that any state at intermediate time can be expanded over the basis of *in* or *out* states equivalently. Considering for instance a two-particle *in* state, we can write

$$A_{a_1}(\theta_1)A_{a_2}(\theta_2) = \sum_{N=0}^{\infty} \sum_{\theta'_1 < \dots < \theta'_N} S_{a_1, a_2}^{b_1, \dots, b_N}(\theta_1, \theta_2; \theta'_1, \dots, \theta'_N) A_{b_1}(\theta'_1) \dots A_{b_N}(\theta'_N), \quad (2.23)$$

where the sum over momenta is actually an integral constrained by the conservation of the total momentum, and the object $S_{a_1, a_2}^{b_1, \dots, b_N}$ is the so-called $2 \rightarrow N$ *S-matrix*.

Quite naturally once again, we define an *integrable quantum field theory* by the existence of an infinite set of conserved charges. We consider to this end operators of Lorentz spin s ,

$$Q_s A_a(\theta) = q_a^{(s)} e^{s\theta} A_a(\theta), \quad (2.24)$$

(the energy-momentum operator (P, \bar{P}) , is one of these, with Lorentz spin 1: $P(\bar{P})A_a(\theta) = m_a e^{\pm\theta} A_a(\theta)$), which can be written as integrals over particle densities and therefore act additively on N -particle states,

$$Q_s A_{a_1}(\theta_1) \dots A_{a_N}(\theta_N) = (q_{a_1}^{(s)} + \dots + q_{a_N}^{(s)}) e^{s\theta} A_{a_1}(\theta_1) \dots A_{a_N}(\theta_N). \quad (2.25)$$

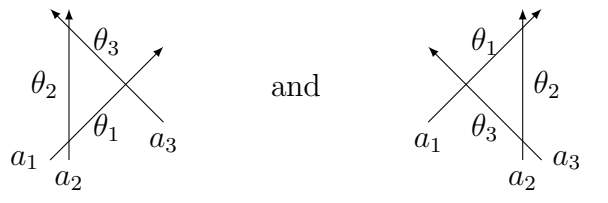
Such operators are mutually commuting, and we will now see that imposing an infinite set of such conserved charges (the so-called *conserved local charges*) puts severe constraints on the *S-matrix*, and how these constraints are so particular in 1+1-dimensional theories.

The first constraint imposed by the existence of local charges for arbitrarily large values of s is an infinite number of conservation laws of the form

$$q_{a_1}^{(s)} e^{\theta_1} + \dots + q_{a_M}^{(s)} e^{\theta_M} = q_{b_1}^{(s)} e^{\theta'_1} + \dots + q_{b_N}^{(s)} e^{\theta'_N} \quad (2.26)$$

between the *in* and *out* momenta of any scattering process, implying the equality between the initial and final sets of momenta, and in particular, forbidding particle production or annihilation.

The second constraint comes from the fact that for any scattering process we can use the conserved charges to reorder the incoming or outgoing particles at will. Assume indeed, for a sketchy demonstration [68], that the set of charges $P_s \equiv (P_1)^s$ are conserved, where P_1 is the spatial part of the energy-momentum. Acting with $e^{i\alpha P_s}$ on a particle of momentum p_a yields a phase factor αp^s , and so amounts to shift the position of this particle by $s\alpha p^{s-1}$. In more than one spatial dimensions the particles of any scattering process can therefore be translated so that they simply avoid each other without changing the corresponding scattering amplitude, which forces the *S-matrix* to be trivial, or, in other terms, the theory to be non interacting (this is a very unrigorous justification of the Coleman-Mandula theorem in three spatial dimensions). This however does not apply to 1+1 dimensions where obviously interactions cannot be avoided, yet these are severely constrained: consider for instance the $3 \rightarrow 3$ scattering process between the *in* state $A_{a_1}(\theta_1)A_{a_2}(\theta_2)A_{a_3}(\theta_3)$ ($\theta_1 > \theta_2 > \theta_3$) and the *out* state $A_{a_3}(\theta_3)A_{a_2}(\theta_2)A_{a_1}(\theta_1)$. Shifting the *in* particles as described above shows that the two following processes are equivalent,



from which we can deduce that the $3 \rightarrow 3$ S -matrix, and similarly any $N \rightarrow N$, can be factorized as the product of $2 \rightarrow 2$ scattering processes. Even once factorizability of the S -matrix is assumed, the equality between the two above diagrams is not trivial as soon as the $2 \rightarrow 2$ S -matrix is not entirely diagonal in the space of different possible kinds of particles (or if these particles have, say, a non zero spin). Assuming (as imposed from Lorentz invariance) that the latter depends on the rapidities only through their difference, this equality translates into the following matrix equation

$$S_{23}(\theta_3 - \theta_2)S_{13}(\theta_3 - \theta_1)S_{12}(\theta_2 - \theta_1) = S_{12}(\theta_2 - \theta_1)S_{13}(\theta_3 - \theta_1)S_{23}(\theta_3 - \theta_2), \quad (2.27)$$

which is nothing but the Yang–Baxter equation (2.8) for the $2 \rightarrow 2$ S -matrix, where the rapidities θ_i play the role of the spectral parameters. The connection with integrable vertex models is now quite clear, for instance the integrable \check{R} matrix found for the six-vertex model (or, equivalently, for the XXZ Hamiltonian) has its equivalent in quantum field theory as the S -matrix of the *deformed $SU(2)$ Nambu–Jona-Lasinio model* (also called *deformed chiral Gross–Neveu model*), which is a 1+1 dimensional relativistic theory of Dirac fermions with action

$$\mathcal{S}_{\text{NJL}} = \int dx \left(i\bar{\psi}^a \not{\partial} \psi^a - g j_\mu^3 j^{3\mu} - f(j_\mu^1 j^{1\mu} + j_\mu^2 j^{2\mu}) \right), \quad (2.28)$$

where \vec{j}^μ is the $SU(2)$ current ($j^{\mu x,y,z} = \frac{1}{2}\bar{\psi}_a \sigma_{ab}^{x,y,z} \gamma^\mu \psi_b$), and the correspondence with XXZ is $\cos \gamma \leftrightarrow \frac{\cos g}{\cos f}$ (for a review see [70], and references therein). For future reference, we point out that this model can (up to some subtleties [70]) be related to the *Sine-Gordon* model, which is a theory of a free bosonic field Φ with action

$$\mathcal{S}_{SG} = \int dx \left((\partial_\mu \Phi)^2 + g \cos(\beta \Phi) \right), \quad (2.29)$$

In summary, the task of finding the eigenstates of an integrable quantum field theory has been reduced to that of finding the corresponding $2 \rightarrow 2$ S -matrix solution of the Yang–Baxter equation, which then allows for an exact resolution by the method of algebraic Bethe ansatz to be presented in detail in the next chapter.

2.1.2 The quantum group $U_q(sl_2)$

The integrable R -matrix found for the six-vertex model belongs to the class of *quasi-classical* solutions of the Yang–Baxter equation, in the sense that it can be expanded in terms of some \hbar ($= \gamma$ here) parameter as follows

$$R(\hbar, u) \propto \mathbf{1} + \hbar r(u) + \mathcal{O}(\hbar^2). \quad (2.30)$$

The matrix $r(u)$ is called the classical limit of $R(\gamma, u)$ and satisfies the so-called *classical Yang–Baxter equation*

$$[r_{12}(u), r_{13}(u+v)] + [r_{12}(u), r_{23}(v)] + [r_{13}(u+v), r_{23}(v)] = 0, \quad (2.31)$$

which appears in the context of classical integrable systems, and has for characteristic feature that it involves only commutation relations. As a consequence, if $r(u)$ can be decomposed as

$$r(u) = \sum_{\mu, \nu} r^{\mu\nu}(u) X_\mu \otimes X_\nu \quad (2.32)$$

where $q = e^{i\gamma}$ and we have introduced the q -deformed numbers

$$[x] \equiv \frac{q^x - q^{-x}}{q - q^{-1}} = \frac{\sin \gamma x}{\sin \gamma}. \quad (2.39)$$

These commutation relations define the *quantum group* $U_q(sl_2)$ which can be viewed as a deformation of the universal enveloping algebra $U(sl_2)$ of sl_2 and should therefore be more appropriately called a quantum algebra. In particular the usual sl_2 commutation relations are recovered in the limit $q \rightarrow 1$ ($\gamma \rightarrow 0$). We also note that in the spin $\frac{1}{2}$ representation (for the moment we can have in mind the simple picture, valid for q not a root of unity, in which the representation theory of $U_q(sl_2)$ is similar to that of sl_2), the commutation relations (2.37, 2.38) reduce to those of sl_2 , and the monodromy matrix (2.36) recovers its original six-vertex model form. Let us now put these findings in a more general perspective.

2.1.3 General framework

Dealing with integrable systems, one encounters generically quantum groups $U_q(\mathfrak{g})$ associated with various Lie algebras \mathfrak{g} . What we call a quantum group in general is essentially a *quasitriangular Hopf algebra*, that is an associative algebra \mathcal{A} equipped with a *coproduct* $\Delta : \mathcal{A} \rightarrow \mathcal{A} \otimes \mathcal{A}$, a *co-unit* $\epsilon : \mathcal{A} \rightarrow \mathbb{C}$ and an *antipode* $\eta : \mathcal{A} \rightarrow \mathcal{A}$ subject to some conditions. In particular, the coproduct is an algebra homomorphism, and its expression in the $U_q(sl_2)$ case is ²

$$\Delta(S^z) = \mathbf{1} \otimes S^z + S^z \otimes \mathbf{1} \quad (2.41)$$

$$\Delta(S^\pm) = q^{S^z} \otimes S^\pm + S^\pm \otimes q^{-S^z}. \quad (2.42)$$

As we can see in this particular case, the coproduct treats the two copies of \mathcal{A} in $\mathcal{A} \otimes \mathcal{A}$ in an asymmetric way, and another coproduct can be defined as $\Delta' = \tau \circ \Delta$, where τ is the permutation operator between the two copies. This construction is general, and quantum groups are also equipped with a so-called *universal \mathcal{R} matrix* that intertwines the two coproducts

$$\mathcal{R} \Delta = \Delta' \mathcal{R}. \quad (2.43)$$

The name ‘universal’ stems from the fact that \mathcal{R} is defined algebraically, independently of any particular representation. In the $U_q(sl_2)$ case in particular, the explicit expression of \mathcal{R} in terms of the S^\pm, S^z generators is known. One essential property of the universal \mathcal{R} matrix is that it satisfies the following equation

$$\mathcal{R}_{23} \mathcal{R}_{13} \mathcal{R}_{12} = \mathcal{R}_{12} \mathcal{R}_{13} \mathcal{R}_{23}, \quad (2.44)$$

which is nothing but the Yang–Baxter equation without spectral parameter. Remembering about the six-vertex model, this brings along two conclusions :

² Note that the coproduct is *not* the usual tensor product. As a consequence the tensor product $S_i \otimes S_i$ of two $U_q(sl_2)$ generators is not itself a $U_q(sl_2)$ generator, and the idea of extending (2.33) to higher-dimensional solutions of the Yang–Baxter equation of the form

$$R(u) = \sum_{i=0, \dots, 3} \rho_i(u) S^i \otimes S^i, \quad (2.40)$$

does not work.

- Specializing to the spin $\frac{1}{2}$ representation of $U_q(sl_2)$, the \mathcal{R} matrix $\mathcal{R}^{\frac{1}{2}\frac{1}{2}}$ in this representation should relate to the original integrable R -matrix of the six-vertex model $R(u)$. This is indeed the case, as $\mathcal{R}^{\frac{1}{2}\frac{1}{2}}$ is obtained as the $u \rightarrow i\infty$ (*braiding limit*) of a gauged transformed version of $R(u)$.
- Reciprocally for any spin j, j' representations, we expect the $\mathcal{R}^{jj'}$ matrix to be the braiding limit of some solution $R(u)$ of the Yang–Baxter equation acting on $\mathbb{C}^{2j+1} \otimes \mathbb{C}^{2j'+1}$. The general task of promoting the universal \mathcal{R} matrix of some quantum group in its different representations to spectral parameter-dependent R -matrices (*‘baxterisation’*) has a well-defined algebraic meaning, which requires promoting the notion of quantum group to a spectral parameter-dependent algebraic object. This is what we want to describe now.

To each simple Lie algebra \mathfrak{g} can be associated an *affine Lie algebra* $\widehat{\mathfrak{g}}$, which can be understood as a central extension of the loop algebra $\widehat{\mathfrak{g}}_0 \simeq \mathfrak{g} \otimes \mathbb{C}[x, x^{-1}]$, and whose Dynkin diagram is obtained from that of \mathfrak{g} by the addition of a node corresponding to an imaginary root. Similarly, for a quantum group $U_q(\mathfrak{g})$ one can define the corresponding *affine quantum group* $U_q(\widehat{\mathfrak{g}})$. The complex parameter x is intimately related to the notion of spectral parameter, more precisely we set $x \equiv q^u$ and will be interested in the so-called *evaluation representations* of $U_q(\widehat{\mathfrak{g}})$, which can be built as *affinizations* of the quantum group representations and are therefore characterized by some $U_q(\mathfrak{g})$ spin j and a spectral parameter u . For two such representations $V_{j_1}(u_1), V_{j_2}(u_2)$, we can define as for the finite-dimensional case a matrix $R_{12}(u_1 - u_2)$ intertwining $V_{j_1}(u_1) \otimes V_{j_2}(u_2)$ and $V_{j_2}(u_2) \otimes V_{j_1}(u_1)$ ³, which satisfies the Yang–Baxter equation (2.8) and can therefore be used as a building block for constructing the associated integrable model. For instance, we see that the six-vertex model studied previously can be defined as the integrable model associated with the affine algebra $U_q(\widehat{sl_2})$ in products of its fundamental (spin- $\frac{1}{2}$) evaluation representations. More generally we can consider transfer matrices acting on the product $V_1 \otimes \dots \otimes V_L$ of evaluation representations for any affine quantum algebra. Whereas for usual, finite dimensional Lie algebras the products or irreducible representations are usually fully reducible, this is not the case anymore in the affine case and products of the form $V_1 \otimes \dots \otimes V_L$ are themselves irreducible. Note that all this persists in the $q \rightarrow 1$ limit, where instead of recovering the algebra $\widehat{\mathfrak{g}}$ the affine quantum group $U_q(\widehat{\mathfrak{g}})$ degenerates into the so-called *Yangian*, $\mathcal{Y}(\mathfrak{g})$, with similar properties as the affine quantum group itself.

This construction can be further extended in the case where the Dynkin diagram of $\widehat{\mathfrak{g}}$ allows for a rank k group of automorphisms (in practice $k = 1, 2$, or exceptionally $k = 3$). We can then consider the *twisted* algebra $\widehat{\mathfrak{g}}^{(k)}$ obtained as a folding of the original Dynkin diagram with respect to these automorphisms, and similarly we can construct the corresponding *twisted affine quantum algebras* $U_q(\widehat{\mathfrak{g}}^{(k)})$, which can in turn be used to construct integrable lattice models.

The baxterized trigonometric R -matrices associated with various evaluation representations of the (un)twisted quantum groups are given in references [71] and [72] respectively. In all the following, we will use the notations $\mathfrak{g}^{(1)} \equiv \widehat{\mathfrak{g}}$, $\mathfrak{g}^{(k)} \equiv \widehat{\mathfrak{g}}^{(k)}$, and will refer to models associated with the quantum algebra $U_q(\mathfrak{g}^{(k)})$ as simply the ‘ $\mathfrak{g}^{(k)}$ models’.

³From now on we will commonly use the shorthand notation \otimes to refer to the quantum group coproduct, when appropriate.

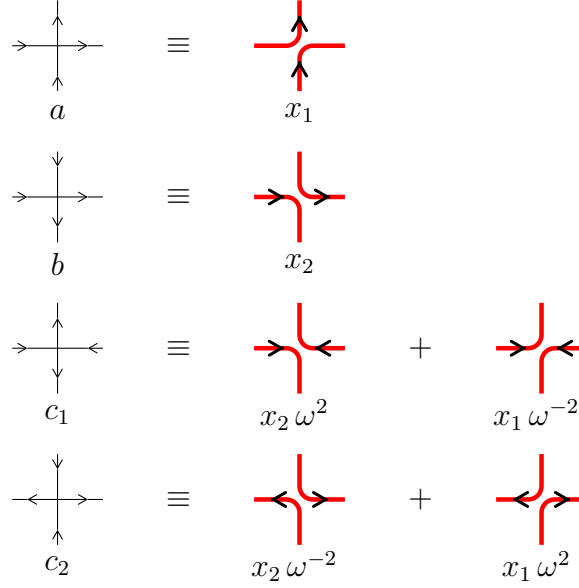
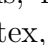
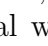


Figure 2.1: Mapping from the six-vertex model on the square lattice to a model of completely packed oriented loops. Similar relations hold when reverting all the arrows.

2.2 Loop models and algebraic aspects

Whereas we have been dealing so far with (integrable) *vertex* models, we will now see, focusing on the example of the six-vertex model, that some of these can be reformulated in a geometric fashion, namely as (integrable) statistical mechanics models whose degrees of freedom can be represented by *loops*. This reformulation is a natural step towards the study of physical problems such as those related with polymers or transport observables at the IQHE transition, and will give us the chance for a first encounter with a few important algebraic objects, among which the Temperley–Lieb algebra.

2.2.1 Loop formulation of the six-vertex model and the Temperley–Lieb algebra

The configurations of the six-vertex model map to those of a model of completely packed, oriented loops living on the edges of the square lattice, as described in figure 2.1 (see also, for instance, [40]). As indicated in the figure, we can then parametrize the Boltzmann weights as a product of two contributions, namely $x\Omega$ where x depends only on the geometrical loop configuration at the vertex, $x = x_1$ for , $x = x_2$ for , and Ω is an angular contribution counting the total winding angle of the oriented loops at the vertex, ω, ω^{-1} for each left and right turn respectively. Note that this parametrization gives a different weight c_1 and c_2 to vertices which were attributed the same weight c so far. This apparent paradox can actually be resolved by the following argument : taking, say, periodic boundary conditions in the horizontal direction and following this direction around the cylinder, the vertices with weight c_1 and those with weight c_2 act respectively as sources and sinks of vertical arrow flux, as in the second two vertical arrows leave the vertex, whereas in the first case two vertical arrows enter it. Due to conservation of the net arrow flux inside the region encompassing the row under consideration, the number of vertices of the first and second kind must be the same on each horizontal line,

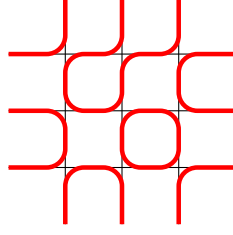


Figure 2.2: Configuration of the completely packed loop model emerging from the six-vertex model. Each closed loop goes with a weight $n = \omega^4 + \omega^{-4}$. To yield back the six-vertex arrow configurations, one has to sum over the two possible orientations of each loop and reformulate the local weight n as local, angular contributions to the Boltzmann weights.

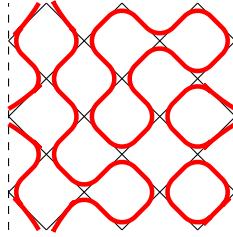


Figure 2.3: Configuration of the completely packed loop model on the rotated square lattice. Time flows in the upward direction, and periodic boundary conditions in the horizontal direction are indicated by dashed lines.

which allows to replace the weights c_1 and c_2 by $c \equiv \sqrt{c_1 c_2}$. This parametrization of the weights a, b, c in terms of x_1, x_2 and ω allows for a reformulation of the six-vertex model in terms of a model of pure, unoriented loops, where the weights at the vertices are simply x_1 and x_2 and each closed loop corresponds to a sum over its two possible orientations, with a weight $n = \omega^4 + \omega^{-4}$ coming from the corresponding angular contributions. A configuration of the corresponding loop model is given in figure 2.2.

To study this model further, we temporarily choose to rotate the lattice by 45° , or equivalently, to consider the time direction to be along a diagonal of the square lattice, as depicted in figure 2.3. The evolution along this diagonal time is encoded by the so-called *diagonal transfer matrix*, which we can represent as

$$T_D = \begin{array}{|c|} \hline \text{Diagram 1: A square lattice with a diagonal path highlighted by dashed lines.} \\ \hline \end{array} \equiv \begin{array}{|c|} \hline \text{Diagram 2: A square lattice with a diagonal path highlighted by dashed lines, showing a different configuration.} \\ \hline \end{array} \equiv \begin{array}{|c|} \hline \text{Diagram 3: A square lattice with a diagonal path highlighted by dashed lines, showing a third configuration.} \\ \hline \end{array},$$

where from left to right we have shifted from the original square lattice to a representation in terms of square plaquettes, each plaquette being associated with a vertex of the original lattice. This yields for the diagonal transfer matrix a natural decomposition, as it is obtained by summing independently every plaquette over the two possible configurations

$$\diamond = x_1 \begin{array}{|c|} \hline \text{Diagram 4: A square plaquette with a red loop on the left side.} \\ \hline \end{array} + x_2 \begin{array}{|c|} \hline \text{Diagram 5: A square plaquette with a red loop on the right side.} \\ \hline \end{array}. \quad (2.45)$$

The transfer matrix acts on states which can be represented as the sets of connectivities between L strands. We assume (for simplicity) that $L \equiv 2N$ is even, and rewrite the

transfer matrix as a product over its building blocks, namely

$$T_D = (\check{R}_{L-2,L-1} \dots \check{R}_{2,3} \check{R}_{L,1}) (\check{R}_{L-1,L} \dots \check{R}_{3,4} \check{R}_{1,2}) , \quad (2.46)$$

where $\check{R}_{i,i+1}$ corresponds to the plaquette where strands i and $i+1$ meet. The notation is not a coincidence, as \check{R} is formally the same object as the \check{R} matrix building up the row-to-row transfer matrix. We can further write

$$\check{R}_{i,i+1} = x_1 I + x_2 e_{i,i+1} , \quad (2.47)$$

where I is the identity operator whereas $e_{i,i+1}$ concatenates strands i and $i+1$ and acts as the identity on the other strands. Pictorially,

$$I = \begin{array}{c} \text{|||} \quad \dots \quad \text{||} \\ 123 \quad \quad \quad L \end{array} \quad (2.48)$$

$$e_{i,i+1} = \begin{array}{c} \text{|||} \dots \text{||} \text{ } \text{ } \text{||} \text{ } \text{||} \\ 123 \quad \quad i \quad \quad L \end{array} \quad (2.49)$$

The composition rules of the operators $e_{i,i+1}$ can readily be deduced from their pictorial representation, bearing in mind that strands can be stretched and that each closed loop corresponds to a weight n . For instance,

$$(e_{i,i+1})^2 = \begin{array}{c} \text{|||} \dots \text{||} \text{ } \text{ } \text{||} \text{ } \text{||} \\ 123 \quad \quad i \quad \quad L \end{array} = n \begin{array}{c} \text{|||} \dots \text{||} \text{ } \text{ } \text{||} \text{ } \text{||} \\ 123 \quad \quad i \quad \quad L \end{array} = n e_{i,i+1} , \quad (2.50)$$

and similarly,

$$e_{i,i+1} e_{j,j+1} = e_{j,j+1} e_{i,i+1} \quad \text{for } |i-j| > 1 \quad (2.51)$$

$$e_{i,i+1} e_{i+1,i+2} e_{i,i+1} = e_{i,i+1} e_{i-1,i} e_{i,i+1} = e_{i,i+1} \quad (2.52)$$

Equations (2.50), (2.51) and (2.52) define the so-called *Temperley–Lieb* (TL) algebra $TL_L(q)$. This is an example of a *lattice algebra*, which plays a role of great importance in the context of loop models and beyond. Other such algebras can be defined for instance by allowing crossings between loops (*Brauer algebra*), braiding (*braid-monoid algebras*), vacant sites carrying no loops (*dilute TL*), several species or colours of loops (*multi-coloured TL algebras*), etc. . . , several of which will be encountered in the following sections of this manuscript.

The TL algebra has many different representations, each of which is related to a particular statistical mechanics model, such as the Potts and Ising models as well as height models for rough interfaces. Since it has here been introduced from the loop formulation of the six-vertex model, it is now natural to look for vertex formulation of its generators. This is achieved by taking the weights a, b, c to be the integrable weights (2.13), which determines the parameters x_1, x_2, ω as

$$a = x_1 = \frac{\sin(\gamma - u)}{\sin \gamma} \quad (2.53)$$

$$b = x_2 = \frac{\sin u}{\sin \gamma} \quad (2.54)$$

$$c = \sqrt{c_1 c_2} = \sqrt{x_1 e^{i\frac{\gamma}{2}} + x_2 e^{-i\frac{\gamma}{2}}} \sqrt{x_1 e^{-i\frac{\gamma}{2}} + x_2 e^{i\frac{\gamma}{2}}} = 1 , \quad (2.55)$$

that is, $n = 2 \cos \gamma = q + q^{-1}$ (we point out, however, that unlike the row-to-row transfer matrices, the diagonal transfer matrices $T_D(u)$ do not form a commuting family). As it turns out, not exactly the integrable \check{R} matrix

$$\check{R}(u) = \mathcal{P}R = \begin{pmatrix} a & 0 & 0 & 0 \\ 0 & c & b & 0 \\ 0 & b & c & 0 \\ 0 & 0 & 0 & a \end{pmatrix} \quad (2.56)$$

can be decomposed as (2.47), rather we use the gauge transformation

$$\check{R}(u) \simeq \begin{pmatrix} a & 0 & 0 & 0 \\ 0 & e^{iu}c & -b & 0 \\ 0 & -b & e^{-iu}c & 0 \\ 0 & 0 & 0 & a \end{pmatrix} = \frac{\sin(\gamma - u)}{\sin \gamma} \mathbf{1} + \frac{\sin u}{\sin \gamma} e, \quad (2.57)$$

where we indeed recognize the decomposition (2.13), and the Temperley–Lieb generator e has the same expression as that introduced in equation (2.17). Note that the latter can further be written in terms of the projectors of the product $V_{\frac{1}{2}} \otimes V_{\frac{1}{2}}$ of $U_q(sl_2)$ spin $\frac{1}{2}$ representations over irreducible spin 0 and 1 representations,

$$P_0 = \frac{1}{[2]} \begin{pmatrix} 0 & 0 & 0 & 0 \\ 0 & q^{-1} & -1 & 0 \\ 0 & -1 & q & 0 \\ 0 & 0 & 0 & 0 \end{pmatrix}, \quad P_1 = \mathbf{1} - P_0 = \frac{1}{[2]} \begin{pmatrix} [2] & 0 & 0 & 0 \\ 0 & q & 1 & 0 \\ 0 & 1 & q^{-1} & 0 \\ 0 & 0 & 0 & [2] \end{pmatrix}, \quad (2.58)$$

namely

$$e = [2]P_0 = (q + q^{-1})P_0 = 2 \cos \gamma P_0 = nP_0. \quad (2.59)$$

2.2.2 Representation theory of the TL algebra

As was mentioned earlier, the Temperley–Lieb algebra allows for different kinds of representations. In this section we shall restrict to the loop representation, which is known to be faithful, and restrict to the case where q is generic *i.e.* not a root of unity. Even though this rules out most cases of physical interest (for instance the cases $q = e^{i\frac{\pi}{2}}$, $q = e^{i\frac{\pi}{3}}$ and $q = e^{i\frac{\pi}{4}}$ describe respectively problems of dense polymers, percolation and Ising model), this is enough for our purpose and will allow us to derive general conclusions. In this case the TL algebra is known to be semi-simple, namely all reducible representations are fully reducible [73]. These representations are called *standard modules*, and we will introduce them by looking first at the case of open boundary conditions.

Open boundary conditions

The loop Hilbert space $\mathcal{H}_{\text{loop}}$ on which the TL generators act can be viewed as the set of connectivities between L strands, allowing for an even (if L even, to which we will restrict for now on) number j of *through-lines*, also called *strings*, or *legs*, propagating from the infinite bottom of the cylinder. Taking as an example $L = 4$, the space of states reads

$$\begin{array}{ccc} 2j = 0 & 2j = 2 & 2j = 4 \\ \text{⋈} & \text{⋈} & \text{⋈} \\ \text{⋈} & \text{⋈} & \text{⋈} \\ \text{⋈} & \text{⋈} & \text{⋈} \\ \text{⋈} & \text{⋈} & \text{⋈} \end{array}.$$

Since through-lines can be contracted with one another under the action of the TL generators but cannot inversely be formed back, any transfer matrix built out of the latter clearly has a block-diagonal structure and we can, as long as the corresponding eigenvalue problem is concerned, focus on the diagonal part and therefore forbid through-lines to be connected with one another. We therefore decompose the loop space of states as a direct sum of spaces $\mathcal{S}_j[L]$ with $2j = 0, 2, \dots, L$ through lines, which are now thought as propagating from the infinite bottom to the infinite top of the cylinder. These have dimension

$$d_j(L) = \dim \mathcal{S}_j[L] = \binom{L}{L/2 - j} - \binom{L}{L/2 - j - 1}, \quad (2.60)$$

which indeed recovers for instance $d_1(4) = 3$.

Periodic boundary conditions

We now move on to the case where the L strands lie on the surface of a cylinder. Strictly speaking, the Temperley–Lieb algebra is the set of all the words written with the generators $e_{i,i+1}$, $i = 1, \dots, L$ (with $L + 1 \equiv 1$), and is therefore easily seen to be infinite dimensional from the existence of diagrams consisting of loops winding around the periodic boundary conditions an arbitrary number of times. To cure this we rather consider a quotient of the latter, the so-called *Jones–Temperley–Lieb* algebra $JTL_L(q)$ [74], which specifies that non contractible loops winding around the cylinder are given the same weight n as contractible ones and that isotopic diagrams connecting the same sites are to be identified (in particular this allows to unwind through-lines around the periodic condition). The representation theories of $TL_L(q)$ and $JTL_L(q)$ slightly differ only in a way that will not alter our understanding of their correspondence with $U_q(sl_2)$, so in the following we will restrict to the periodic version which we will nevertheless call $TL_L(q)$.

In this case the standard modules are labeled as $\mathcal{W}_j[L]$. For $L = 4$ we represent them as follows

$$\begin{array}{ccc} 2j = 0 & 2j = 2 & 2j = 4 \\ \text{⌒} \text{⌒} & \text{⌒} \text{⌒} \text{⌒} & \text{⌒} \text{⌒} \text{⌒} \text{⌒} \\ \text{⌒} & \text{⌒} \text{⌒} & \\ & \text{⌒} \text{⌒} & \\ & \text{⌒} \text{⌒} \text{⌒} & \end{array} .$$

For $j = 0$ the corresponding dimension is the same as in the open case, whereas for $2j > 0$

$$\check{d}_j(L) = \dim \mathcal{W}_j[L] = \binom{L}{L/2 - j}. \quad (2.61)$$

2.2.3 Periodic loop and vertex models

We now discuss the mapping between loop and vertex periodic transfer matrices and the corresponding spaces of states. Once again we shall focus essentially on the example of the six-vertex model, but our results will adapt easily to the various cases of interest throughout the rest of this manuscript. As a matter of fact most of the discussion also applies to the case of models with open boundary conditions, where it is actually slightly simpler.

Our goal here is to compare precisely the loop row-to-row transfer matrix,

$$\begin{aligned}
T &= \text{Tr } \check{R}_{a1} \dots \check{R}_{aL} \\
&= \text{Diagram: A horizontal chain of square plaquettes. The first and last plaquettes are connected by a red loop that goes above and below the chain. Each plaquette has four red lines extending from its corners.} \quad , \quad (2.62)
\end{aligned}$$

where each plaquette is the rotated version of (2.45) and can therefore be written in terms of the Temperley-Lieb generators $e_{a,i}$ and the geometric trace over the auxilliary space has to be taken with some care such as to give non contractible loops the same weight n as contractible ones, and the vertex transfer matrix

$$\begin{aligned}
T(u) &= \text{Tr}_{V_a} \left[\text{Diagram: A horizontal chain of vertical lines connected by horizontal lines. The chain is closed by a vertical line on the right.} \right] \\
&= \text{Tr}_{V_a} \check{R}_{a,1}(u) \dots \check{R}_{a,L}(u) , \quad (2.63)
\end{aligned}$$

acting on the Hilbert space $\mathcal{H} = (\mathbb{C}^2)^{\otimes L}$. The latter commutes with the total magnetization

$$m = \sum_{i=1}^L S_i^{(z)} = -\frac{L}{2}, \frac{L}{2} + 1, \dots, \frac{L}{2} , \quad (2.64)$$

so it is tempting to give a vertex interpretation to the spaces $\mathcal{W}_j[L]$ by associating them with sectors of fixed magnetization. Consider once again as an example the system of size $L = 4$. Whereas in the loop model the sector $2j = 0$ has the 2 states represented above, namely $\cup \cup$ and \smile , the vertex model in the sector $m = 0$ has obviously $\binom{L}{\frac{L}{2}-m} = 6$ states. The difference is that the loop model gives the same weight n to any loop, contractible or not, whereas in the vertex model *non contractible loops* that circle around the horizontal direction of the cylinder are easily seen to be given a different weight, namely $\tilde{n} = 2$. To endow the loop model with the capability of distinguishing between contractible and non contractible loops, we must enlarge its space of states with another 4 states, which can be represented graphically as $\cup \cup$, $\cup \smile$, $\smile \cup$, and $\smile \smile$, where a mark on an arc now means that it has traversed the periodic boundary condition, and the number of marks add up modulo 2 upon multiple traversals and concatenation. Shifting to the sectors with $2j \neq 0$, it is clear that non contractible loops cannot exist, so the corresponding loop states do not need to be augmented. In general, it is easy to prove that the extended modules $\widetilde{\mathcal{W}}_j$, which coincide with the \mathcal{W}_j for $2j > 0$, have a dimension given by (2.61) for all j .

Let us now prove rigorously that the enlarged spaces $\widetilde{\mathcal{W}}_j[L]$ of loop states are isomorphic to the sectors of, say, magnetizations $m = j$ (equivalently one could have chosen $m = -j$) of the vertex model. Starting from the loop model and reading the states from left to right, replace each opening of an unmarked (resp. a marked) loop by an up-spin (resp. a down-spin), each closing by a down-spin (resp. an up-spin), and each through-line by an up-spin. In this way, the first two states given above in the sector $2j = 0$ become $\uparrow\downarrow\uparrow\downarrow$ and $\uparrow\uparrow\downarrow\downarrow$, while the latter four states become $\downarrow\uparrow\uparrow\downarrow$, $\uparrow\downarrow\downarrow\uparrow$, $\downarrow\uparrow\downarrow\uparrow$, and $\downarrow\downarrow\uparrow\uparrow$. Reversely considering any initial spin configuration and starting from a given site, compute the accumulated magnetization upon moving rightwards (crossing the periodic boundary condition if necessary) until it becomes zero, or until the same spin is reached again. In the former case, the spin where the magnetization becomes zero is linked by an arc to

the initial spin. The corresponding spins are obviously opposite, and if the down-spin is to the left of the up-spin (and only if we are in the $j = 0$ sector) the arc is marked. In the latter case, there is no corresponding spin and the initial spin is a through-line.

Having studied in detail the space of states, we need in order to make the two transfer matrices (2.62, 2.63) equivalent to take proper account of the weight of non contractible (or marked) loops. For this sake, we replace the vertex transfer matrix (2.63) by a *twisted* version,

$$\begin{aligned} T(u, e^{i\varphi}) &= \text{Tr}_{V_a} \left[\begin{array}{c} | \\ \hline | \end{array} \begin{array}{c} | \\ \hline | \end{array} \cdots \begin{array}{c} | \\ \hline | \end{array} e^{2i\varphi S^{(z)}} \right] \\ &= \text{Tr}_{V_a} \check{R}_{a,1}(u) \cdots \check{R}_{a,L}(u) e^{2i\varphi S_a^{(z)}}, \end{aligned} \quad (2.65)$$

which results in tuning the weight of non contractible loops to

$$\tilde{n} = 2 \cos \varphi. \quad (2.66)$$

The twist parameter φ is chosen in a way depending on the magnetization sector, namely

- In the sector $m = 0$, we choose $\varphi = \gamma$ so that $\tilde{n} = n$. Non contractible loops are then treated on the same footing as contractible ones, and the spectrum of the original loop transfer matrix in the sector $\mathcal{W}_0[L]$ is therefore recovered up to enlarged multiplicities (those of $\widetilde{\mathcal{W}}_0[L]$).
- In sectors $m \neq 0$, non contractible loops are absent, and we choose instead $\varphi = 0$ so that through-lines do not accumulate extra phase factors while winding around the periodic direction of the cylinder.

Note that compared to the usual periodic XXZ Hamiltonian (2.16) the quantum Hamiltonian obtained from the twisted transfer matrix (2.65) is modified as follows

$$H = \frac{1}{2} \sum_{i=1}^{L-1} (\sigma_i^x \sigma_{i+1}^x + \sigma_i^y \sigma_{i+1}^y + \Delta \sigma_i^z \sigma_{i+1}^z) + \frac{e^{i\varphi}}{4} \sigma_L^+ \sigma_1^- + \frac{e^{-i\varphi}}{4} \sigma_L^- \sigma_1^+. \quad (2.67)$$

2.2.4 Schur-Weyl duality

We will now discuss an important feature of the relationship between the TL algebra and the quantum group $U_q(sl_2)$. For simplicity, we will restrict ourselves to the open chain of L strands, and refer to [33] for a complete discussion.

As we have seen in detail in the periodic case, but as can similarly be reviewed in the open case, the Hilbert space $\mathcal{H} = (\mathbb{C}^2)^{\otimes L}$ can be considered as acted on by two different algebras :

- The Temperley–Lieb algebra $TL_L(q)$, which can be decomposed in the open case in terms of the standard modules $\mathcal{S}_j[L]$.
- The quantum group $U_q(sl_2)$, for which the space \mathcal{H} is a product of spin $\frac{1}{2}$ modules, and therefore a (reducible) module itself. Similarly to the sl_2 case, we expect it to be decomposed in the case of generic q as a sum over irreducible modules V_j with dimensions $D_j = 2j + 1$.

In this sense, the space \mathcal{H} enjoys the structure of a $(TL_L(q), U_q(sl_2))$ *bimodule*. Moreover, the TL generator $e_{i,i+1}$ acting on strands i and $i+1$ was seen in equation (2.59) to be nothing but (up to some proportionality factor) the projector P_0 over the trivial, spin 0 representation of the corresponding product of $U_q(sl_2)$ spin $\frac{1}{2}$ representations. As a direct consequence $e_{i,i+1}$ commutes with the action of $U_q(sl_2)$ on the product $V_{\frac{1}{2}}^{(i)} \otimes V_{\frac{1}{2}}^{(i+1)}$, and this result is straightforwardly extended to its commutation with the $U_q(sl_2)$ action on the full chain. This sums up as

$$[TL_L(q), U_q(sl_2)] = 0, \quad (2.68)$$

and we are now ready to use the *double-commutant theorem*: let A a semisimple algebra with a fully reducible representation on some finite-dimensional space V . Let $B = Z(A)$, the centralizer of A in V (the algebra of V endomorphisms commuting with A). The following results hold :

1. B also acts semisimply on V
2. $Z(B) = A$
3. The irreducible representations R_j^A and R_j^B on V are in one-to-one correspondence, and V has the multiplicity-free decomposition $V = \bigoplus_j R_j^A \otimes R_j^B$.

Part of these results when applying the double-commutant theorem to $V = \mathcal{H}$, $A = U_q(sl_2)$ and $B = TL_L(q)$ (which is clearly the centralizer of $U_q(sl_2)$ in \mathcal{H}) were already known, as we have taken for granted that the action of $TL_L(q)$ is semisimple for q generic and that the corresponding modules \mathcal{S}_j are irreducible. The fundamentally new result here, known as a variant of the *Schur-Weyl duality*, is the decomposition

$$\mathcal{H} = \bigoplus_{j=0}^{L/2} V_j \otimes \mathcal{S}_j, \quad (2.69)$$

from which follow the decompositions of \mathcal{H} over $U_q(sl_2)$ or $TL_L(q)$ irreducibles:

$$\mathcal{H}|_{U_q(sl_2)} = \bigoplus_{j=0}^{L/2} d_j V_j \quad (2.70)$$

$$\mathcal{H}|_{TL_L(q)} = \bigoplus_{j=0}^{L/2} D_j \mathcal{S}_j, \quad (2.71)$$

where we see that the dimension of irreducible modules for one algebra play the role of multiplicities for the second.

‘Quantum group symmetry’ of integrable vertex models

It is readily deduced from (2.68) that the whole \check{R} matrix (2.57) commutes with $U_q(sl_2)$. However, one must keep in mind that this \check{R} matrix was obtained from the original one (2.55) through some gauge transformation, and therefore that the latter does itself commute with $U_q(sl_2)$. Turning to, say, the original row-to-row transfer matrix $T(u)$ built out of (2.55), transforming the gauge-transformed weights $a, b, c_1 = e^{iu}c, c_2 = e^{-iu}c$ back to

the original weights a, b, c amounts to the unescapable introduction of imaginary boundary terms. Therefore, the quantum group $U_q(sl_2)$ is *not* a symmetry of the integrable six-vertex model, only does it become the case in the infinite-size limit, or for some particular choice of *open* boundary conditions [32]. In the open case, one indeed sees that whereas the usual XXZ Hamiltonian

$$H_{XXZ} = -\frac{1}{2} \sum_{i=1}^{L-1} (\sigma_i^x \sigma_{i+1}^x + \sigma_i^y \sigma_{i+1}^y + \Delta \sigma_i^z \sigma_{i+1}^z) \quad (2.72)$$

does not commute with $U_q(sl_2)$, the $U_q(sl_2)$ invariance is restored when considering the following Hamiltonian with a particular choice of boundary terms [32]

$$H = -\frac{1}{2} \sum_{i=1}^{L-1} e_{i,i+1} \quad (2.73)$$

$$= -\frac{1}{2} \sum_{i=1}^{L-1} (\sigma_i^x \sigma_{i+1}^x + \sigma_i^y \sigma_{i+1}^y + \Delta \sigma_i^z \sigma_{i+1}^z) + \frac{q - q^{-1}}{4} (\sigma_1^z - \sigma_L^z) . \quad (2.74)$$

These observations can essentially be generalized to any other integrable model. Remember from the previous sections that the R -matrix associated with the (twisted) affine quantum $U_q(\mathfrak{g}^{(k)})$ intertwines between two evaluation representations V_1 and V_2 of $U_q(\mathfrak{g}^{(k)})$. Similarly, the monodromy matrix $\mathcal{T}(u)$ acting on the product $V_a(u) \otimes \mathcal{H}$ of an auxilliary space V_a and a quantum space $\mathcal{H} = V_1 \otimes \dots \otimes V_L$ intertwines between the corresponding affine quantum group actions,

$$\mathcal{T}(u) U_q(\mathfrak{g}^{(k)})|_{V_a \otimes \mathcal{H}} = U_q(\mathfrak{g}^{(k)})|_{\mathcal{H} \otimes V_a} \mathcal{T}(u) . \quad (2.75)$$

Therefore, the action of $U_q(\mathfrak{g}^{(k)})$ or any of its finite-dimensional quantum subalgebras on \mathcal{H} can be considered as commuting with $\mathcal{T}(u)$ only ‘modulo boundary terms’, in the sense that it does so provided one forgets abouts the auxilliary space V_a . In particular, the periodic transfer matrix obtained by tracing over V_a does not restore any of these symmetries whatsoever.

2.3 From polymers to the $O(n)$ model, to the $a_2^{(2)}$ model

Let us sum up what we have found so far : for a vertex model with a definite set of degrees of freedom, the condition of integrability can be re-expressed as a set of equations for the spectral parameter-dependent Boltzmann weights. These take the form of a matrix equation, the Yang–Baxter equation, for the \check{R} -matrix encoding these weights.

Now, given some physical two-dimensional statistical model or some one-dimensional quantum spin chain, there is no reason a priori that the physical Boltzmann weights obey these equations, more precisely that they correspond to one of the solutions of the Yang–Baxter equation taken at some fixed, isotropic value of the spectral parameter. However, most critical models turn out to have an integrable model in the same universality class. Facing to, say, the problems of polymers and IQHE formulated in terms of some critical lattice models, the first part of our program (to which this chapter is devoted) will

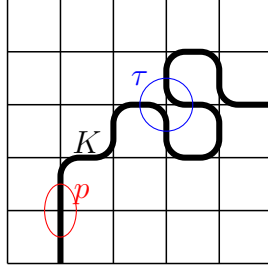


Figure 2.4: Configuration of the two-dimensional vertex interacting self-avoiding walk (VISAW). The Boltzmann weights K , p and τ are associated to each edge, each straight segment and each doubly visited site respectively.

therefore be to seek for integrable trigonometric deformations of these models' Boltzmann weights while leaving their universality class unchanged.

As described in the introductory chapter (section 1.2), the large scale properties of polymer chains in a good solvent are successfully described by self-avoiding walks (SAW). In order to describe the collapse transition, we however need to improve this model further and consider the so-called *vertex interacting self-avoiding walks* (VISAW), where short range-interactions are taken in account by an energy $-\epsilon_t$ for each site of the lattice where two pieces of the polymers meet and nearly collide, see figure 2.4. Additionally, it is convenient to also allow for some stiffness, and thus associate with two parallel consecutive monomers an energy $-\epsilon_s$.⁴ Introducing the corresponding Boltzmann weights $\tau \equiv e^{\beta\epsilon_t}$ and $p \equiv e^{\beta\epsilon_s}$, the partition function of a polymer made of N edges is thus given by

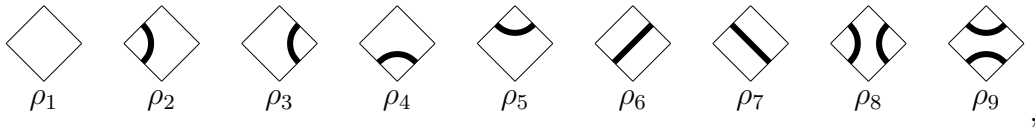
$$Z_N(\tau, p) = \sum_{\text{VISAW}} \tau^{\# \text{ doubly visited sites}} p^{\# \text{ straight segments}}, \quad (2.76)$$

however we will more commonly deal with the grand canonical partition function

$$G(K, \tau, p) = \sum_{N=0}^{\infty} K^N Z_N(\tau, p), \quad (2.77)$$

which is a sum over VISAWs of arbitrary lengths.

In order to work further the connection with lattice models as formulated in the previous section, we reformulate the model in terms of elementary plaquettes around each vertex. The allowed local configurations and corresponding Boltzmann weights are



where

$$\rho_1 = 1 \quad (2.78)$$

$$\rho_2 = \rho_3 = \rho_4 = \rho_5 = K \quad (2.79)$$

$$\rho_6 = \rho_7 = K p \quad (2.80)$$

$$\rho_8 = \rho_9 = K^2 \tau. \quad (2.81)$$

⁴In the lattice description we will commonly use the term ‘monomer’ for each elementary step of the self-avoiding-walk, namely for each bit of polymer covering one lattice edge, even though these may have not much to do with the chemical units of the original problem.

This model can be considered as the particular $n = 0$ case of a more general one, where closed loops are allowed and each results in a fugacity n . This corresponds precisely to the geometrical formulation of some square lattice $O(n)$ vector model, with a more general spin-spin interaction than that considered in section 1.2. The corresponding phase diagram of this model will be studied in detail in chapter 4, and we focus for the moment on integrable solutions, namely spectral parameter-dependent weights $\rho_1(u), \dots, \rho_9(u)$ solution of the Yang–Baxter equation.

As found by Nienhuis and collaborators in [75, 76], two types of solutions have to be distinguished :

- In the $p = 0$ plane, an integrable solution (which we give directly for isotropic values of the weights) is found at $K = \frac{1}{2}$, $\tau = 2$, namely

$$\rho_1 = 1, \quad \rho_2 = \rho_3 = \rho_4 = \rho_5 = \rho_8 = \rho_9 = \frac{1}{2}, \quad \rho_6 = \rho_7 = 0. \quad (2.82)$$

This solution, is usually labeled ‘branch 0’, can be obtained from the integrable completely packed loop model (2.45) at loop fugacity $n + 1$ by coloring each loop either in black (with fugacity n) or in white, as ‘empty’ (with fugacity 1).

- Another solution is found by parametrizing the loop fugacity as $n = -2 \cos 2\gamma$, and reads

$$\begin{aligned} \rho_1(u) &= 1 + \frac{2 \cos(u + \frac{3\gamma}{2}) \sin u \sin \frac{\gamma}{2}}{(2 \cos \gamma - 1) \sin^2 \gamma} \\ \rho_2(u) = \rho_3(u) &= \frac{\cos(u + \frac{3\gamma}{2})}{\cos \frac{3\gamma}{2}} \\ \rho_4(u) = \rho_5(u) &= -\frac{\sin u}{\cos \frac{3\gamma}{2}} \\ \rho_6(u) = \rho_7(u) &= \frac{2 \cos(u + \frac{3\gamma}{2}) \sin u \sin \frac{\gamma}{2}}{(2 \cos \gamma - 1) \sin^2 \gamma} \\ \rho_8(u) &= \frac{\sin(2u + \frac{5\gamma}{2}) - \sin \frac{\gamma}{2}}{2(\cos \gamma + \cos 2\gamma)} \\ \rho_9(u) &= \frac{\cos(u + \frac{\gamma}{2}) \sin u}{2 \cos^2 \frac{\gamma}{2} \sin \frac{\gamma}{2} (2 \cos \gamma - 1)}. \end{aligned} \quad (2.83)$$

For each value of n , there are four different integrable points corresponding to values of γ in the intervals $[0, \frac{\pi}{2}]$, $[\frac{\pi}{2}, \pi]$, $[\pi, \frac{3\pi}{2}]$ and $[\frac{3\pi}{2}, 2\pi]$ respectively, traditionally labeled as ‘branch 1’, ‘branch 2’, ‘branch 3’ and ‘branch 4’. In this thesis, we will take a slightly different convention where γ only runs between 0 and π and one has to consider the two signs of the quantum Hamiltonian, or equivalently two different isotropic value of the spectral parameter u .

Whereas the nature of the first solution is well understood from its mapping onto a completely dense model (ultimately it can be rewritten in terms of the integrable six-vertex model [77]), it is yet not as clear how the second fits into the classification of integrable models sketched in the previous sections. To proceed further, we reformulate the loop model as a vertex one, in a very similar fashion as what was done for the six-vertex model in section 2.2.4 (see figure 1.12, and [63] for details). Oriented loops and

empty sites give rise to three possible states, which we label as $-1, 0, 1$, and 19 possible vertex configurations. In the corresponding $\mathbb{C}^3 \otimes \mathbb{C}^3$ basis, the $R \equiv P\check{R}$ matrix can be written after some immaterial gauge changes as

$$R = \left(\begin{array}{ccc|ccc|ccc} c & 0 & 0 & 0 & 0 & 0 & 0 & 0 & 0 \\ 0 & b & 0 & e & 0 & 0 & 0 & 0 & 0 \\ 0 & 0 & d & 0 & g & 0 & f & 0 & 0 \\ \hline 0 & \bar{e} & 0 & b & 0 & 0 & 0 & 0 & 0 \\ 0 & 0 & \bar{g} & 0 & a & 0 & g & 0 & 0 \\ 0 & 0 & 0 & 0 & 0 & b & 0 & e & 0 \\ \hline 0 & 0 & f & 0 & \bar{g} & 0 & d & 0 & 0 \\ 0 & 0 & 0 & 0 & 0 & \bar{e} & 0 & b & 0 \\ 0 & 0 & 0 & 0 & 0 & 0 & 0 & 0 & c \end{array} \right), \quad (2.84)$$

where

$$\begin{aligned} a &= \sin\left(u - \frac{3\gamma}{2}\right) - \sin\frac{5\gamma}{2} + \sin\frac{3\gamma}{2} + \sin\frac{\gamma}{2} \\ b &= \sin\left(u - \frac{3\gamma}{2}\right) + \sin\frac{3\gamma}{2} \\ c &= \sin\left(u - \frac{5\gamma}{2}\right) + \sin\frac{\gamma}{2} \\ d &= \sin\left(u - \frac{\gamma}{2}\right) + \sin\frac{\gamma}{2} \\ e &= -2e^{-iu/2} \sin\gamma \cos\left(\frac{u}{2} - \frac{3\gamma}{2}\right) \\ \bar{e} &= -2e^{iu/2} \sin\gamma \cos\left(\frac{u}{2} - \frac{3\gamma}{2}\right) \\ f &= -2e^{-iu+i\gamma} \sin\frac{\gamma}{2} \sin\gamma - e^{-i\frac{\gamma}{2}} \sin 2\gamma \\ \bar{f} &= 2e^{iu-i\gamma} \sin\frac{\gamma}{2} \sin\gamma - e^{i\frac{\gamma}{2}} \sin 2\gamma \\ g &= 2e^{-i\frac{u}{2}+i\gamma} \sin\frac{u}{2} \sin\gamma \\ \bar{g} &= -2e^{i\frac{u}{2}-2\frac{\gamma}{2}} \sin\frac{u}{2} \sin\gamma. \end{aligned} \quad (2.85)$$

These are exactly the weights of the Izergin–Korepin model [79], which in the classification of integrable models sketched in the earlier sections corresponds to that associated with the algebra $a_2^{(2)} \equiv U_q(sl_3^{(2)})$ in the product of its fundamental, three dimensional representations.

2.4 From the IQHE to the $b_2^{(1)}$ integrable model

2.4.1 The Chalker–Coddington model

The construction of a network model which recovers the universality class of the IQHE plateau transition makes use of the following semi-classical picture, valid at very strong magnetic field: when this is the case, namely when the magnetic length $\ell_B = \sqrt{\frac{\hbar}{eB}}$

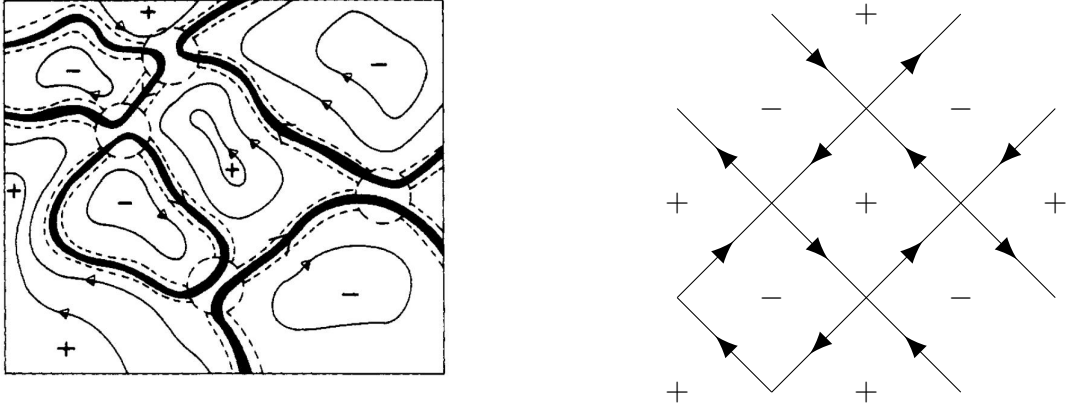


Figure 2.5: (Left) Disordered potential landscape whose thick level lines denote for a critical energy corresponding to the IQHE plateau transition (figure taken from [81]). The electrons flow clockwise (resp. counterclockwise) around the potential minima (resp. maxima). (Right) Description as an oriented network by Chalker and Coddington [81], whose vertices correspond to the saddle points of the disordered potential.

is much smaller than the characteristic length scale ℓ_c of the random potential V , the electrons in the disordered Landau levels can be seen as following a cyclotron motion of radius ℓ_B , with their center of motion drifting along the equipotential lines of V . More precisely, the eigenfunctions associated to a given equipotential line can be considered as the superposition of the Landau states with the same energy. Looking at a typical potential landscape, see figure 2.5, we see that the levels at low (resp. high) energy are localized around the minima (resp. maxima) of the potential, whereas at intermediate energies the corresponding levels can meander through the whole system, giving rise to the delocalized states responsible for the plateau transition.

This very simple view reduces the problem of localization-delocalization transitions in the Integer Quantum Hall Effect to the problem of finding the equipotential lines in a random potential landscape, or, in other terms, to a percolation picture. Owing to this formulation, we expect that only at a certain critical energy E_c corresponding to the percolation threshold will the semiclassical wavefunctions percolate through the whole, infinite system. From the theory of critical percolation [80], we expect the localization length, which can here be associated to the typical spatial extent of the wavefunction, to diverge as

$$\xi \sim |E - E_c|^{-\nu}, \quad (2.86)$$

where $\nu = \frac{4}{3}$. That this value is quite far from the usually expected values for the IQHE (see section 1.3) indicates that this percolation model misses one crucial ingredient, namely the quantum tunneling process that occurs between equipotential lines that get close to each other near the saddle points of the potential landscape.

The lattice model introduced by Chalker and Coddington (CC) in 1988 [81] aims at gathering all these ingredients. It models the discrete-time dynamics of a single electron along the equipotential lines, incorporating tunneling at the potential saddle points. Choose to model the potential landscape by an oriented square network, where the edges are the equipotential lines at a given energy and the nodes are the saddle points where two equipotential lines meet, see figure 2.5. A single electronic wavefunction is defined by its amplitude $\psi(e)$ over each edge e of the CC lattice, and its dynamics under an

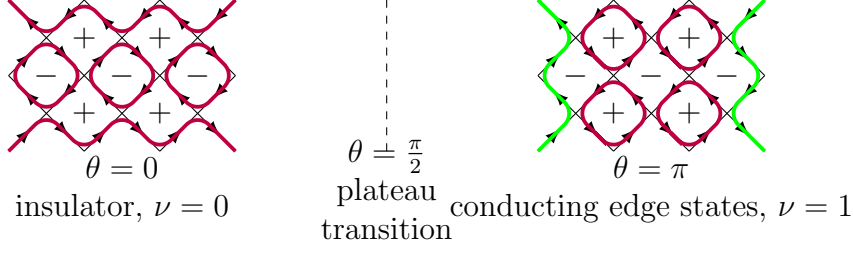


Figure 2.6: Limits $\theta \rightarrow 0$ and $\theta \rightarrow \pi$ of the CC eigenwavefunctions. At $\theta = 0$, the system is in an insulating phase corresponding to the $\nu = 0$ Hall plateau. At $\theta = \pi$, edge states have appeared carrying current in the y direction, the system is in a phase corresponding to the $\nu = 1$ Hall plateau. In between the two, at $\theta = \frac{\pi}{2}$, the plateau transition occurs.

elementary time increment Δt is described by an unitary evolution operator \mathcal{U} ,

$$\psi_{t+\Delta t}(e') = \mathcal{U}(e', e)\psi_t(e). \quad (2.87)$$

\mathcal{U} encodes both the effect of disorder, which we can model as random Bohm-Aharonov phases φ_e over each edge, and the tunneling at nodes, namely we can write

$$\mathcal{U}(e', e) = e^{i\varphi_e} S_{e', e}, \quad (2.88)$$

where the random phases φ_e are chosen to be independent and uniformly distributed over $[0, 2\pi]$ and S is a scattering matrix whose nonzero elements are associated with pairs of edges respectively incoming and outgoing to a common vertex, with matrix elements given by

$$\begin{array}{c} \begin{array}{ccc} & r & \\ t \swarrow & & \searrow -t \\ & r & \end{array} & , & \begin{array}{ccc} & -t & \\ r \swarrow & & \searrow r \\ & t & \end{array} \end{array}$$

where $r^2 + t^2 = 1$, so we parametrize $t = \sin \frac{\theta}{2}$, $r = \cos \frac{\theta}{2}$, $\theta \in [0, \pi]$. It is now instructive to look at the wavefunction dynamics in the $\theta \rightarrow 0$ and $\theta \rightarrow \pi$ limits, see figure 2.6. When $\theta \rightarrow 0$, left turns are suppressed and the electron trajectories are closed loops around the potential minima. This corresponds to the low energies in the percolation picture addressed in the beginning of this paragraph, and no current is carried. When $\theta \rightarrow \pi$, right turns are suppressed, and the electron trajectories in the bulk of the system are closed loops around the potential maxima, corresponding to the high energies in the percolation picture. At the intermediate, symmetric value $\theta = \frac{\pi}{2}$ (that is $t = r = \frac{1}{\sqrt{2}}$), we expect the electron trajectories to cover the whole sample, corresponding to the plateau transition. The fact that the Hall conductivity has increased by one unit across the transition is due to the fact that on the $\theta \rightarrow \pi$ side, the edge states close to the boundary are now running from one end of the sample to the other [22].

Several numerical tests of the Chalker–Coddington dynamics have comforted the idea that the latter indeed reproduces the exponents of the IQHE plateau transition [23]. It is therefore a good starting point for analytical or more numerical studies, or, as will be the object of the rest of this paragraph, for the reformulation of the IQHE transition as a classical statistical mechanics lattice model. We point out that it is also a starting point for generalization to other classes of lattices and/or of disorder, leading to various random network models aimed at describing other symmetry classes of Anderson transitions. This aspect will be come back over in the conclusion of this thesis.

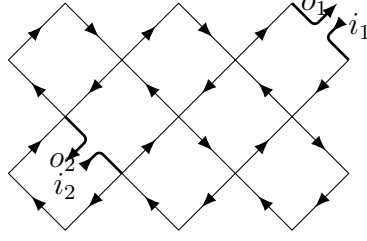


Figure 2.7: Setup of the contacts for the definition of the point-contact conductance in the CC model.

2.4.2 A loop model for transport observables

In [82], a set of transport observables suitable for analytical developments and numerical investigations was introduced, and defined rigorously on the CC lattice. These are the so-called *point-contact conductances* (PCC), namely the conductances between two small interior probes separated by a distance r .

On the (closed) CC lattice, these are constructed by selecting two distant links e_1 and e_2 and cutting them in halves, which defines two incoming links i_1 and i_2 entering the system and two outgoing links o_1 and o_2 exiting the system (see figure 2.7). The current injection through i_1 is modeled as follows : at each time step, inject one unit of probability flux through i_1 , and apply the time evolution operator \mathcal{U} once. After a sufficient amount of time, the system will have reached a stationary state where the equivalent amount of current exits through the drains o_1 and o_2 , and it can be shown that the dimensionless conductance $g(i_1, o_2)$ is obtained by the Landauer-Büttiker formula as

$$g = |t_{o_2, i_1}|^2, \quad (2.89)$$

where t_{o_2, i_1} is the transmission amplitude between i_1 and o_2 , obtained as

$$t_{o_2, i_1} = \langle o_2 | (1 - \mathcal{U})^{-1} | i_1 \rangle = \mathcal{G}(o_2, i_1, 1), \quad (2.90)$$

and the boundary conditions at the contacts are fixed by $\mathcal{U}|o_1\rangle = \mathcal{U}|o_2\rangle = \mathcal{U}^\dagger|i_1\rangle = \mathcal{U}^\dagger|i_2\rangle = 0$. These have for consequence a unitarity deficit, ensuring the definiteness of the operator $(1 - \mathcal{U})^{-1}$. In (2.90) we have also used the definition of the Green's function,

$$\mathcal{G}(e_2, e_1, z) = \left\langle e_2 \left| \frac{1}{1 - z\mathcal{U}} \right| e_1 \right\rangle, \quad (2.91)$$

which is the discrete time analog of the usual Green's function $(E - \mathcal{H})^{-1}$, where $z \sim e^{iE}$ and E is measured from the center of the Landau band.

Path integral formulation and disorder averaging

The Green's function $\mathcal{G}(o_2, i_1, z)$ can be written [39] as a Gaussian path integral over a set of bosonic fields $\phi(e)$, as

$$\mathcal{G}(o_2, i_1, z) = \frac{\int [\mathcal{D}\phi] \phi(o_2) \phi^*(i_1) e^{-\mathcal{S}[\phi]}}{\int [\mathcal{D}\phi] e^{-\mathcal{S}[\phi]}}, \quad (2.92)$$

where $[D\phi]$ denotes a Gaussian measure over the fields $\phi(e)$, and the action \mathcal{S} is written as a sum over the lattice nodes ,

$$\mathcal{S}[\phi] = \sum_{e,e'} z \phi^*(e') \mathcal{U}(e', e) \phi(e) = \sum_{e,e'} e^{i\varphi_e} z \phi^*(e') S_{e',e} \phi(e). \quad (2.93)$$

Similarly, the conjugate $\mathcal{G}^*(o_2, i_1, z)$ is written as a Gaussian path integral over another set of bosonic fields $\bar{\phi}(e)$. It is customary to call the fields ϕ and $\bar{\phi}$ *retarded* and *advanced* fields respectively, and we will stick to this denomination whenever necessary. In order to perform disorder averaging, we now use the supersymmetry trick introduced in section 1.3 : introduce a set of retarded and advanced fermionic (anticommuting) variables $\psi(e)$ and $\bar{\psi}(e)$, and a corresponding Gaussian integration measure. We use the following property of Gaussian integration over fermionic variables,

$$\frac{1}{\int [D\phi] e^{-\mathcal{S}[\phi]}} = \int [D\psi] e^{-\mathcal{S}[\psi]}, \quad (2.94)$$

which enables us to rewrite

$$|\mathcal{G}(o_2, i_1, z)|^2 = \int [D\phi][D\psi][D\bar{\phi}][D\bar{\psi}] \phi(o_2) \phi^*(i_1) \bar{\phi}(i_1) \bar{\phi}^*(o_2) e^{-\mathcal{S}[\phi] - \mathcal{S}[\psi] - \mathcal{S}^*[\bar{\phi}] - \mathcal{S}^*[\bar{\psi}]}, \quad (2.95)$$

or, in terms of the superfields $\Psi = \begin{pmatrix} \phi \\ \psi \end{pmatrix}$, $\bar{\Psi} = \begin{pmatrix} \bar{\phi} \\ \bar{\psi} \end{pmatrix}$,

$$|\mathcal{G}(o_2, i_1, z)|^2 = \int [D\Psi][D\bar{\Psi}] \Psi(o_2) \Psi^*(i_1) \bar{\Psi}(i_1) \bar{\Psi}^*(o_2) e^{-\mathcal{S}[\Psi] - \mathcal{S}^*[\bar{\Psi}]}. \quad (2.96)$$

The quantity of interest is ultimately the disorder-averaged

$$\bar{g} = \overline{|\mathcal{G}(o_2, i_1, 1)|^2}, \quad (2.97)$$

where, we denote by overbars quenched averages over the disorder variables φ_e . As for the two open contacts, we fix the random phases on the two halves of one same edge to be equal, that is, $\varphi_{i_1} = \varphi_{o_1} \equiv \varphi_{e_1}$ and $\varphi_{i_2} = \varphi_{o_2} \equiv \varphi_{e_2}$.

From (2.96), averaging over disorder now reduces to the following integration

$$\begin{aligned} \overline{e^{-\mathcal{S}[\Psi] - \mathcal{S}^*[\bar{\Psi}]}} &= \int \prod_e \frac{d\varphi_e}{2\pi} \exp \sum_{e,e'} (z e^{i\varphi_e} \Psi^\dagger(e') S_{e',e} \Psi(e) + z^* e^{-i\varphi_e} \bar{\Psi}^\dagger(e) S_{e',e} \bar{\Psi}(e')) \\ &= \prod_e \sum_{m_e=0}^{\infty} \frac{(z^* z)^{m_e}}{(m_e!)^2} \sum_{e',\bar{e}'} (\Psi^\dagger(e') S_{e',e} \Psi(e)) (\bar{\Psi}^\dagger(e) S_{\bar{e}',e} \bar{\Psi}(\bar{e}')) , \end{aligned} \quad (2.98)$$

where the scattering matrix S has been endowed with a matrix action in the boson/fermion superspace in a natural way. The disorder-averaged point-contact conductance $\bar{g}(z)$, whose definition has been extended on the lattice to generic values of z , has therefore the following expression

$$\bar{g}(z) = \overline{|\mathcal{G}(o_2, i_1, z)|^2} \quad (2.99)$$

$$\begin{aligned} &= \int [D\Psi][D\bar{\Psi}] \Psi(o_2) \Psi^*(i_1) \bar{\Psi}(i_1) \bar{\Psi}^*(o_2) \\ &\quad \prod_e \sum_{m_e=0}^{\infty} \frac{(z^* z)^{m_e}}{(m_e!)^2} \sum_{e',\bar{e}'} (\Psi^\dagger(e') S_{e',e} \Psi(e)) (\bar{\Psi}^\dagger(e) S_{\bar{e}',e} \bar{\Psi}(\bar{e}')) . \end{aligned} \quad (2.100)$$

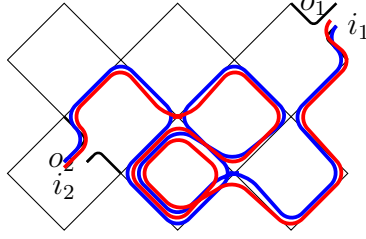


Figure 2.8: Term contributing to the loop representation of the disorder-averaged point-contact conductance.

The first line in equation (2.98) is the basis for a reformulation of the point-contact conductance as a correlation function of a vertex model with $GL(2|2)$ symmetry, a point on which we shall come back shortly. Instead, we here follow [39] and use the expansion given by the second line of (2.98) as starting point for a diagrammatic interpretation.

Reformulation as a loop model

As explained in [39], each term in the product (2.98) can be interpreted as a sum over a pair of paths γ and $\bar{\gamma}$, where γ and $\bar{\gamma}$ follow respectively the orientation of the CC lattice and the reverse orientation, and must use each edge e the same number of times m_e (a precise mathematical signification will be associated to this constraint later). Paths configurations are weighted by the elements of the scattering matrix S , and an additional factor $(zz^*)^{m_e}$, which can be interpreted geometrically as a *fugacity per monomer*, namely a weight $|z|$ associated to each path segment. The weight of closed loops is obtained by a supertrace over the boson/fermion superspace, and is accordingly equal to zero for both types of paths. Turning to the expression (2.100) for the conductance $\bar{g}(z)$, we can now interpret the latter as the sum over paths configurations obtained after inserting two γ path ends starting and ending at i_1 and o_2 respectively, and two $\bar{\gamma}$ path ends starting and ending at o_2 and i_1 respectively. From now on we assign the colours red and blue to the γ and $\bar{\gamma}$ paths respectively. The point-contact conductances on the CC lattice have therefore been reformulated exactly, that is, with no approximation, as two-point correlation functions of a *classical* two-colour loop model on the square lattice, see figure 2.8.

Let us contemplate this model and pause for a few remarks :

- Since closed loops vanish, the partition function is made of only one term, that is, the one with no paths at all. We therefore have the trivial identity $Z = 1$, as expected for systems with quenched disorder.
- The matrix elements of S are not necessarily positive, as resulting from quantum mechanical amplitudes. The resulting classical loop model is therefore not unitary, and does not bear as such a probabilistic interpretation in terms of classical Boltzmann weights. In [83], in contrast, Bettelheim, Gruzberg and Ludwig were able to partly resum paths configurations and obtain a geometrical formulation in terms of ‘pictures’ with positive definite Boltzmann weights. This allowed these authors to identify the *boundary* point-contact conductances with primary CFT operators and to deduce conjectures about the corresponding conformal weights. The way

we follow here, aiming at the description of the IQHE transition by an integrable model, does not make use of such an approach.

Another yet crucial aspect is the possibility for arbitrarily many loop segments covering each edge. In other terms, the model has infinitely many degrees of freedom, in contrast to the models we have been dealing with so far. In particular, the methods of exactly solvable models and most of the numerical techniques at hand cannot apply here. To hopefully make some progress with our usual statistical mechanics tools, we will here follow the truncation procedure of [39]. Before doing so, we however wish to convince the reader that the construction we have presented has a very rich and general algebraic underlying. This will be our object until the end of this section.

Algebraic structure of the IQHE transition

In [84], the Chalker–Coddington dynamics was reformulated in terms of a transfer matrix acting in the vertical direction on a Fock space of advanced and retarded bosons and fermions. On even (odd) sites the infinite Fock space \mathcal{F} ($\bar{\mathcal{F}}$) is spanned by monomials of bosonic and fermionic, advanced or retarded oscillators $b_{\pm}(e), f_{\pm}(e)$ ($\bar{b}_{\pm}(e), \bar{f}_{\pm}(e)$), which corresponds mathematically to the symmetric algebra $\mathcal{S}(\mathbb{C} \otimes \mathbb{C}^{2|2})$. There are two algebras (or the corresponding Lie groups) acting naturally on this Fock space :

- the algebra $u(1, 1|2)$, whose generators can be written as quadratic monomials of the advanced and retarded oscillators and can be shown to commute with the transfer matrix. The algebra $u(1, 1|2)$ is a non compact real form of the superalgebra $gl(2|2)$, and from now on we will not distinguish between the two.
- the algebra $u(1)$ associated with the random phases, whose exponentiated action is $b_{\pm}(e) \rightarrow e^{\pm i\varphi_e} b_{\pm}(e), f_{\pm}(e) \rightarrow e^{\pm i\varphi_e} f_{\pm}(e)$.

These act respectively on the \mathbb{C} and $\mathbb{C}^{2|2}$ parts of the product $\mathcal{S}(\mathbb{C} \otimes \mathbb{C}^{2|2})$, and are therefore mutually commuting. A stronger statement is that this property is maximal, namely $u(1)$ and $gl(2|2)$ are each other's centralizers, making $(u(1), gl(2|2))$ a dual pair in the sense of Howe [85]. This is very similar to the Schur–Weyl duality introduced in section 2.2.4, in particular an important consequence of this property is that each of the Fock spaces \mathcal{F} and $\bar{\mathcal{F}}$ admits a multiplicity-free decomposition into irreducible representations as a $(u(1), gl(2|2))$ bimodule :

$$\mathcal{F} = \bigoplus_{\lambda \in \mathbb{Z}} v_{\lambda} \otimes V_{\lambda} \quad (2.101)$$

$$\bar{\mathcal{F}} = \bigoplus_{\lambda \in \mathbb{Z}} \bar{v}_{\lambda} \otimes \bar{V}_{\lambda}, \quad (2.102)$$

where v_{λ} and V_{λ} (\bar{v}_{λ} and \bar{V}_{λ}) are respectively the irreducible representations of $u(1)$ and the corresponding infinite-dimensional representations of $gl(2|2)$, labeled by the value of the $u(1)$ charge $\lambda = b_+^{\dagger} b_+ + f_+^{\dagger} f_+ - b_-^{\dagger} b_- - f_-^{\dagger} f_-$ or $\lambda = \bar{b}_+^{\dagger} \bar{b}_+ - \bar{f}_+^{\dagger} \bar{f}_+ - \bar{b}_-^{\dagger} \bar{b}_- + \bar{f}_-^{\dagger} \bar{f}_-$ on even (resp. odd) sites.

We can now understand in a simple way the effect of disorder averaging: integrating over each random phase φ_e corresponds to projecting the corresponding Fock space onto the $u(1)$ singlet, that is the $v_0 \otimes V_0$ ($\bar{v}_0 \otimes \bar{V}_0$) bimodule of zero $u(1)$ charge. Since the corresponding $u(1)$ modules are trivial, we simply rename these bimodules $V \equiv V_0$ and

$V^* \equiv \bar{V}_0$. These are known from Howe duality to be irreducible, and are spanned by all the states with the same number of advanced and retarded particles (in the second quantization language). We recover here the constraint formulated previously in the loop language after disorder averaging. Another consequence is that the modules V and V^* can be used as the building blocks of a superspin chain describing the IQHE. The latter acts on the alternate tensor product $\dots V \otimes V^* \otimes V \otimes V^* \dots$, and the corresponding Hamiltonian can be shown directly from the transfer matrix of [84] to be the quadratic Casimir invariant of $gl(2|2)$. In a more physical language, the spin chain is a Heisenberg antiferromagnet with $gl(2|2)$ symmetry. Note that its space of states is, as that of the loop model derived earlier, infinite dimensional on each edge.

We close this section by reviewing, as in [86], that this spin chain or the corresponding vertex model can be obtained by several other ways :

- Starting from the first line in (2.98), [82] used the so-called *colour-flavour transformation* to trade the $U(1)$ random phases φ_e for a set of supermatrix fields Z and \bar{Z} , in terms of which the supersymmetric action can be decomposed as a sum over vertices, and is therefore that of a supersymmetric vertex model. The symmetries of this model are investigated by defining in a natural way an action of the Lie supergroup $GL(2|2)$ on the fields Z and \bar{Z} , under which the action is shown to be invariant. This result is used [82] for decomposing the average PCC and its moments as integrals over $GL(2|2)$ irreducibles, hence conjectures on the form of the corresponding correlators. We will come back to these conjectures in chapter 5.
- Another way [87] was to start directly from Pruisken's non linear sigma model (1.22) and to discretize the spatial direction under the form of a one-dimensional quantum lattice Hamiltonian. The strong-coupling limit of this Hamiltonian, which is believed to describe the plateau transition, was shown to be that of the antiferromagnetic superspin chain described above.
- Less abstractly, the route taken by [88] (see [89] for an earlier analog using replicas) consists in deriving a quantum one-dimensional Hamiltonian directly from a spatially anisotropic version of the Chalker–Coddington model, which is a sequence of counterpropagating ‘edges’ coupled by random complex tunneling amplitudes. With no surprise, the resulting Hamiltonian is once again the antiferromagnetic $g(2|2)$ quadratic Casimir.

2.4.3 The truncation procedure

In order to introduce the idea behind the truncation procedure, we make a short detour via the physics of the $O(n)$ models on the honeycomb lattice, following the approach presented by Nienhuis in [90] (see also [91] for a review). As introduced in the context of polymers (section 1.2), the n -component Heisenberg model is defined by assigning n -dimensional spin variables \vec{S}_i of unit length to each site of a given lattice, subject to the following interaction Hamiltonian with $O(n)$ symmetry,

$$\mathcal{H} = -J \sum_{\langle i,j \rangle} \vec{S}_i \cdot \vec{S}_j, \quad (2.103)$$

where $\sum_{\langle i,j \rangle}$ denotes a sum over pairs of neighbouring sites. The partition function is written as

$$Z = \int \mathcal{D}S e^{\beta J \sum_{\langle i,j \rangle} \vec{S}_i \cdot \vec{S}_j} = \int \mathcal{D}S \prod_{\langle i,j \rangle} e^{\beta J \vec{S}_i \cdot \vec{S}_j}, \quad (2.104)$$

(where the integration measure is normalized such that $\int \mathcal{D}S = 1$ and $\int \mathcal{D}S \vec{S}_i \cdot \vec{S}_i = n$) and can in the case of the honeycomb lattice be formally mapped to a sum over polygon configurations by series expanding the exponentials in the last formula and assigning a polygon segment between sites $\langle i,j \rangle$ to every factor $\vec{S}_i \cdot \vec{S}_j$ present in the expansion. The partition function corresponds to the sum over all configurations of closed polygons, with weight n for each of them (thus enabling the analytical continuation to non integer values of n), and spin-spin correlation functions between two sites can be written as polygon correlation functions, namely sum over the configurations with polygons starting and ending at the corresponding sites (the square lattice analog of this construction has been used earlier in the context of polymer models, see section 1.2). The resulting loop model is however infinite, as each edge can be covered by an arbitrary number of loop segments. To overcome this difficulty, the proposition of Nienhuis was to restrict the exponentials' series expansions to their two first terms, namely

$$Z = \int \mathcal{D}S \prod_{\langle i,j \rangle} (1 + \beta J \vec{S}_i \cdot \vec{S}_j), \quad (2.105)$$

leading to a polygon model where each edge can be visited only once and intersections are absent, while preserving the original model's $O(n)$ symmetry. For $n \leq 2$ this model has a low-temperature phase and a high-temperature phase (for $n > 2$ only the latter exists), and the transition between the two is of second order, hence shows universal behaviour, for $-2 \leq n \leq 2$ [90] (that the model is not critical for too large $|n|$ can be easily understood geometrically, as it is then dominated by configurations with many short loops, hence with a finite correlation length). From the universality principles and the fact that the large scale behaviour of (2.104) and (2.105) should essentially depend on the lattice dimensionality and their $O(n)$ symmetry, it is legitimate to hope that both models may have the same critical behaviour provided that the multiple occupancy of edges and the presence of intersections, considered as perturbations of the latter, are irrelevant. The irrelevance of multiply occupied edges can be deduced from the heuristic argument that looking at the system from far away these cannot be distinguished from singly occupied parallel bonds. The irrelevance of loop intersections, interpreted in the continuum limit as resulting from a perturbation by the four-leg operator, is in contrast only guaranteed in the *dilute*, high-temperature phase, where it follows from the value of the corresponding scaling dimension $x_4 = \frac{35}{12} > 2$ (see the results of chapter 4). As a conclusion of this analysis, the universal critical behaviour of the Heisenberg $O(n)$ model in its high-temperature phase has been left intact by the symmetry-preserving truncation (2.105).

Similarly, we follow the attempt of [39] for a similar construction in the case of the two-colour model derived for the IQHE transport observables. As was discussed earlier, what appears to be the fundamental symmetry of this model is a $U(1)$ symmetry, as averaging the first line in (2.98) over the random phases on each edge corresponds to a projection over the corresponding $U(1)$ singlets. In the geometrical formulation this corresponds to the fact that we constrain the number of advanced and retarded paths to be the same on each edge, or, equivalently, that each edge carries the same number

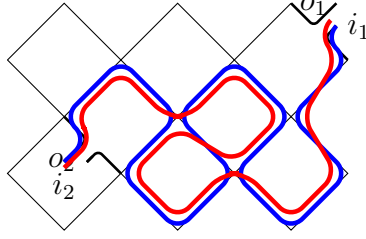


Figure 2.9: Term contributing to the loop representation of the truncated disorder-averaged point-contact conductance $\bar{g}_1(z)$.

of red and blue loop segments. The truncation introduced in [39] is the first non trivial truncation respecting this symmetry, namely, we restrict the numbers m_e on each edge in (2.98) to be either 0 or 1. Obviously this truncation also preserves the boson/fermion supersymmetry, and the closed loops of any colour still carry a weight 0. We denote by $\bar{g}_1(z)$ the truncated analog of (2.100), namely where the sums $\sum_{m_e=0}^{\infty}$ on each edge have been replaced by $\sum_{m_e=0}^1$. More generally, this can be extended to truncations of higher order, which we will not consider for the moment. A loop configuration contributing to the expansion of $\bar{g}_1(z)$ is shown in figure 2.9.

We are therefore left with a model of dilute, two-colours loops on the square lattice. As was introduced in section 2.2.1 in the case of the completely packed single-coloured loops, we can encode the corresponding (non positive) ‘Boltzmann’ weights in the geometrical \check{R} matrix, which at the isotropic point $\theta = \frac{\pi}{2}$ reads

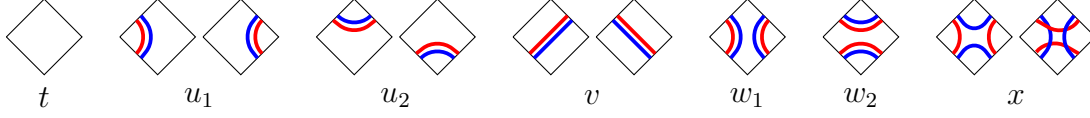
$$\check{R} = \text{diamond} + \frac{z^2}{2} \left(\text{diamond with red arc} + \text{diamond with blue arc} + \text{diamond with red and blue arcs} + \text{diamond with red and blue arcs} \right) + \frac{z^4}{4} \left(\text{diamond with two red arcs} + \text{diamond with two blue arcs} - \text{diamond with two red and blue arcs} - \text{diamond with two red and blue arcs} \right). \quad (2.106)$$

Of course, hoping that the brutal truncation we just performed might recover the original model’s critical point does not go without a fine-tuning of the corresponding weights. In [39], it is indeed found by varying the parameter z and studying numerically the ratio between the two largest eigenvalues of the transfer matrix, $\Lambda_0^{(L)}$ and $\Lambda_1^{(L)}$, for different system sizes L (away from criticality, the corresponding free energies $f_i^{(L)} = -\log \Lambda_i^{(L)}$ are separated by a finite gap, so the ratio $L \log(\Lambda_1^{(L)}/\Lambda_0^{(L)})$ is expected to vary linearly with L , whereas at a critical point conformal invariance predicts $L \log(\Lambda_1^{(L)}/\Lambda_0^{(L)}) \simeq 2\pi x_t$, where x_t is the so-called *thermal exponent*) that the truncated model is not critical at $z = 1$, but rather at some slightly larger value $z_c \simeq 1.03$ which can be understood from the fact that restricting the number of loop segments on each edge is compensated by augmenting the fugacity of each of these segments.

A few critical exponents were estimated in [39] from direct diagonalization of the transfer matrix and will be reviewed in chapter 5, however these present many unexplained features and any substantial progress requires looking for integrable deformations in the universality class of the critical truncation (2.106). In the next section we present such a construction, following essentially [39] but extending our scope to both the families of *dilute* and *completely packed* two-colour loop models on the square lattice. In section 2.4.5, we will reformulate the resulting models in a vertex language, allowing for their identification as the integrable models associated with (twisted) affine quantum algebras.

2.4.4 Dense and dilute two-colour loop models

The truncated model introduced in the previous section can be further augmented by allowing straight-line vertices, so that the set of possible configurations at each vertex is now



Whereas this manifestly breaks the oriented structure of the original CC lattice, we will argue, following [39] that this does not prevent from recovering the original truncated universality class, or in other terms that the introduction of straight vertices is an irrelevant perturbation in the RG sense. Moreover, we now take the more general point of view where the weight n of closed loops is left as a free parameter, and set for the following $n = q + q^{-1} = 2 \cos \gamma$, $q = e^{i\gamma}$.

The integrable fully packed two-colour model

It will turn out instructive to study at first stage the *completely packed* counterpart of this model, where no edges of the square lattice are left empty, namely $t = u_1 = u_2 = v = 0$. In the same way as a model of single-coloured fully packed loops with weight n per closed loop can be related to the Fortuin-Kasteleyn expansion of a $Q = n^2$ -states Potts model [40], this model can be related [64, 92] to a problem of two Potts models coupled by the product of their energy operators. In the latter case, we are left with the vertices

$$\begin{array}{c} \text{diamond with two red strands} \end{array} \equiv \text{id}_1 \otimes \text{id}_2, \quad \begin{array}{c} \text{diamond with two blue strands} \end{array} \equiv e_1 \otimes e_2, \quad \begin{array}{c} \text{diamond with one red and one blue strand} \end{array} \equiv e_1 \otimes \text{id}_2, \quad \begin{array}{c} \text{diamond with one red and one blue strand} \end{array} \equiv \text{id}_1 \otimes e_2, \quad (2.107)$$

where e_1 (resp. e_2) are Temperley–Lieb generators similar to those introduced in section 2.2.4, acting on the red (resp. blue) strands, with $(e_i)^2 = ne_i$. Setting now for each pair of strands

$$\text{Id} \equiv \text{id}_1 \otimes \text{id}_2 \quad (2.108)$$

$$E \equiv e_1 \otimes e_2 \quad (2.109)$$

$$B \equiv \left(q^{-\frac{1}{2}} \text{id}_1 - q^{\frac{1}{2}} e_1 \right) \otimes \left(q^{-\frac{1}{2}} \text{id}_2 - q^{\frac{1}{2}} e_2 \right), \quad (2.110)$$

it is easy [93, 92] to recognize these as the generators of the so-called $SO(4)$ *Birman–Wenzl–Murakami* (BWM) algebra. For general integer N the $SO(N)$ BWM algebra [94, 95] is built from the generators I, B_i, B_i^{-1} and E_i ($i = 1, \dots, L$) subject to the relations

$$\begin{aligned} B_i B_{i+1} B_i &= B_{i+1} B_i B_{i+1}, & B_j B_i &= B_i B_j \text{ for } |i - j| > 1 \\ E_i B_i &= B_i E_i = q^{1-N} E_i \\ E_i B_{i+1}^{\pm 1} E_i &= q^{\mp(1-N)} E_i \\ B_i - B_i^{-1} &= (q - q^{-1})(1 - E_i), \end{aligned} \quad (2.111)$$

from which it stems in particular that the $E_i \equiv E_{i,i+1}$ generate a Temperley–Lieb algebra, with

$$(E_i)^2 = (1 + [N - 1])E_i, \quad [N - 1] = \frac{q^{1-N} - q^{N-1}}{q^{-1} - q}. \quad (2.112)$$

Acting on L strands, the BWM algebra has a geometrical interpretation generalizing that of TL (2.49),

$$I = \begin{array}{c} \text{||||} \quad \dots \quad \text{||} \\ 123 \quad \quad L \end{array} \quad (2.113)$$

$$E_i = \begin{array}{c} \text{||||} \dots \text{||} \text{ } \text{ } \text{||} \dots \text{||} \\ 123 \quad \quad i \quad \quad L \end{array} \quad (2.114)$$

$$B_i = \begin{array}{c} \text{||||} \dots \text{||} \text{ } \text{ } \text{||} \dots \text{||} \\ 123 \quad \quad i \quad \quad L \end{array} \quad (2.115)$$

$$B_i^{-1} = \begin{array}{c} \text{||||} \dots \text{||} \text{ } \text{ } \text{||} \dots \text{||} \\ 123 \quad \quad i \quad \quad L \end{array}, \quad (2.116)$$

where, pictorially,

$$\bigcirc = 1 + [N + 1], \quad \text{ } \text{ } \text{ } = q^{1-N} \text{ } \text{ } , \quad \text{ } \text{ } = q^{N-1} \text{ } \text{ } . \quad (2.117)$$

Interestingly for our purpose, the construction of integrable trigonometric \check{R} matrices built out of the $SO(N)$ BWM generators is well known [96]. Using the parametrization $q = e^{i\frac{\pi}{N+k-2}}$, these can be written as

$$\check{R}^{(N,k)}(u) = I^{(N,k)} + \frac{[u] \left[2 - \frac{N}{2} + u\right]}{\left[\frac{N}{2} - 1 - u\right] [1 - u]} E^{(N,k)} + \frac{[u]}{[1 - u]} X^{(N,k)}, \quad (2.118)$$

where $X^{(N,k)} = q^{-1} I^{(N,k)} + q E^{(N,k)} - B^{(N,k)}$.

Following [92], we observe that taking $N = 4$ in (2.118) yields a completely factorizable \check{R} matrix, and hence a model where the two colours of loops are fully decoupled. This fact could have been expected from the factorizability of $SO(4)$ as a product of two $SU(2)$ algebras. More precisely one can think of the strands in $SO(N)$ BWM as behaving in the vector representation of the quantum-group algebra $U_q(so_N)$, which in the case $N = 4$ decomposes as in the case of ordinary Lie algebras into two copies of $U_q(sl_2)$ (see for instance [93]). In order to find an integrable model which couples the two colours non trivially, we follow the idea of [92], namely we use an interesting property of the BWM algebras that is the so-called *level-rank duality* [97], relating for $q = e^{i\frac{\pi}{N+k+2}}$, k integer, the generators of $SO(N)$ to those of $SO(k)$ (more precisely, one checks from the simple fact that $q^{N-1}q^{k-1} = -1$ that if the B_i satisfy the $SO(N)$ algebra, then the $-B_i^{-1}$ satisfy the $SO(k)$ algebra). One can therefore consider the $\check{R}^{(k,N=4)}$ matrix in equation (2.118), and transform back the $SO(k)$ generators into $SO(4)$ generators to obtain, up to some normalization, the following \check{R} matrix.

$$\check{R}(u) = \text{ } + \frac{\sin\left(\frac{\pi u}{2+k}\right)}{\sin\left(\pi \frac{1+u}{2+k}\right)} \left[\left(2 \cos\left(\frac{\pi}{2+k}\right) + \frac{\cos\left(\pi \frac{1+u-k}{k+2}\right)}{\cos\left(\pi \frac{2+u}{2+k}\right)} \right) \text{ } - \left(\text{ } + \text{ } \right) \right]. \quad (2.119)$$

The integrable dilute two-colours model

Back to the dilute case, we can follow a similar route, still along the lines of [39]. The two-colours generators are now written in terms of the *dilute* BWM algebra (dBWM), which is a version of the BWM algebra augmented by the presence of empty edges. In [98]

trigonometric integrable \check{R} matrices based on this algebra were found, among which the one relevant to our interests (the only one which might capture the original universality class of the truncated critical point) has weights given by [39]

$$\begin{aligned}
t(u) &= -\cos(2u - 3\theta) - \cos 5\theta + \cos 3\theta + \cos \theta \\
u_1(u) &= -2 \sin 2\theta \sin(u - 3\theta) \\
u_2(u) &= 2 \sin 2\theta \sin u \\
v(u) &= -2 \sin u \sin(u - 3\theta) \\
w_1(u) &= 2 \sin(u - 2\theta) \sin(u - 3\theta) \\
w_2(u) &= 2 \sin u \sin(u - \theta) \\
x(u) &= 2 \sin u \sin(u - 3\theta) ,
\end{aligned} \tag{2.120}$$

where θ parametrizes the loop weight as $n = -2 \cos 2\theta$ (this change of notation compared to the completely packed case will become clear in the following).

2.4.5 The $a_3^{(2)}$ and $b_2^{(1)}$ integrable chains

Having found two integrable set of weights for both the completely packed and dilute two-colours loop models, the next step towards an exact solution of these models is to express them in a vertex formulation.

In both cases the procedure follows from the results in [100], where the \check{R} matrices based on the generators of (d)BWM algebras are rewritten as those associated with certain affine quantum (super)algebras. From this reference it is straightforwardly seen that the fully packed solution (2.119) is algebraically equivalent to the integrable \check{R} matrix associated with the quantum superalgebras $U_q(sl(4 + r|r)^{(2)})$. We will focus on the $r = 0$ (purely bosonic) case, namely the $U_q(sl_4^{(2)}) = a_3^{(2)}$ model in its fundamental, four-dimensional representation. As was explained in the case of the single-coloured loop model in section 2.2.3 the corresponding (twisted) transfer matrix and space of states can be shown to be exactly isomorphic to those of the loop model augmented by the possibility of giving independent weights to contractible and non contractible loops. Details about the $a_3^{(2)}$ \check{R} matrix and an explicit mapping back to the two-colours model can be found in [64]. Similarly in the dilute case, we find that the integrable \check{R} matrix (2.120) corresponds to those associated with the $U_q(osp(2m + 5|2m)^{(1)})$ superalgebras, where $q = e^{-2i\theta}$. Once again we will focus on the purely bosonic case, namely the $U_q(so_5^{(1)})$ model in its fundamental, five-dimensional representation, which can be exactly mapped onto the loop model in its augmented formulation.

Let us recapitulate : for both the dilute two-colours loop model and its fully packed counterpart, we have found integrable \check{R} matrices leading to a possibly interesting physics, in the sense that these couple the two colours in a non trivial way, and, in the dilute case, that the corresponding model might recover the universality class of the critical truncation (2.106) (the question of whether this critical truncation itself might recover the universality class of the IQHE plateau transition is of course of utmost importance, and will be the object of the chapter 5).

- The integrable solution for the fully packed model with loop weight $n = q + q^{-1}$ is associated with the $U_q(sl_4^{(2)})$ ($a_3^{(2)}$) model in its fundamental representation.

- The integrable solution for the dilute model with loop weight $n = -2 \cos 2\theta$ is associated with the $U_q(so_5^{(1)})$ ($b_2^{(1)}$) model in its fundamental representation, where the quantum group parameter is given by $q = e^{-i\theta}$.

As will be reviewed in chapters 3 and 5, the physics governing the continuum limit of these models have quite a few features in common. For the moment let us simply advertise, without any further comment, that in general the algebras $a_{2n-1}^{(2)}$ and $b_n^{(1)}$ are dual to each other, in the sense that the dual roots system of one identifies with the root system of the other (for algebraic notions about the classification of simple or affine Lie algebras, we refer to the chapters 13 and 14 of [101]). This can be seen directly from the corresponding Dynkin diagrams, namely

$$\alpha_1 \Longrightarrow \alpha_2 \text{ --- } \text{-----} \text{ --- } \alpha_{n-1} \begin{cases} \nearrow \alpha_n \\ \searrow \alpha_{n+1} \end{cases},$$

for $a_{2n-1}^{(2)}$, and

$$\alpha_1 \Longleftarrow \alpha_2 \text{ --- } \text{-----} \text{ --- } \alpha_{n-1} \begin{cases} \nearrow \alpha_n \\ \searrow \alpha_{n+1} \end{cases}$$

for $b_n^{(1)}$, which are obtained from each other by an arrow reversal (we recall that the Dynkin diagram of a simple or affine Lie algebra associates a node to each simple root, non-mutually orthogonal roots are joined by one or several links according to their respective angle in the root lattice and links between roots of unequal length are oriented from the longer to the shorter).

From exactly solvable models to non-compact CFTs

$$T^{(L)}(u) = \text{diagram of an ellipse with 10 vertical lines passing through it, labeled } u \text{ at the bottom left}, \quad (3.1)$$

3.1 The algebraic Bethe Ansatz

61

attached to a different, *a priori* complex, spectral parameter. Namely,

$$T(u|\{v_l\}_{l=1,\dots,L}) = \text{Tr}_{V_a} \check{R}_{a1}(u - v_1) \dots \check{R}_{aL}(u - v_L) \quad (3.2)$$

$$= \text{Tr}_{V_a} \begin{array}{c} u \\ \diagdown \quad \diagup \quad \cdots \quad \diagdown \\ v_1 \quad v_2 \quad \quad \quad v_L \end{array} \quad (3.3)$$

(we focus here on the purely periodic case, but the discussion can easily be adapted to the various twisted transfer matrices we will be interested in). The homogeneous case is recovered for $v_1 = \dots = v_L = 0$, and the Hamiltonian of the corresponding quantum spin chain is defined as

$$H = - \left. \frac{d \log T(u|\{0\}_{l=1,\dots,L})}{du} \right|_{u=0}, \quad (3.4)$$

see section 2.1. To make notations lighter we will rewrite the transfer matrix $T(u|\{v_l\}_{l=1,\dots,L})$ as $T(u)$ (keeping in mind the values of the spectral parameters v_l in each specific case) and the corresponding eigenvalues as $\Lambda(u)$, and will use the notation E for the eigenvalues of the quantum Hamiltonian.

3.1.1 Algebraic Bethe Ansatz for the six-vertex model

We start with the case of the (inhomogeneous) six-vertex model, that is the model built from the spin- $\frac{1}{2}$ representation of the algebra $a_1^{(1)} \equiv U_q(\widehat{sl_2})$. A basis of the quantum space $(\mathbb{C}^2)^{\otimes L}$ is obtained by specifying the orientation of arrows on each site, which we will note as, for instance, $|\uparrow\uparrow\downarrow\uparrow \dots \downarrow\rangle$.

The monodromy matrix $\mathcal{T}(u)$ acting on the auxilliary space $(\mathbb{C}^2)_a$ is a 2×2 matrix which we can write in the basis $\{\uparrow_a, \downarrow_a\}$ under the following form

$$\mathcal{T}(u) = \begin{pmatrix} A(u) & B(u) \\ C(u) & D(u) \end{pmatrix}, \quad (3.5)$$

where each of the entries $A(u), B(u), C(u), D(u)$ is a linear operator acting on the quantum space. Due to the commutation of each $\check{R}_{a,i}$ matrix with the magnetization $S_a^{(z)} + S_i^{(z)}$, non-diagonal elements of the monodromy matrix corresponding to a change of $S_a^{(z)}$ are associated with an opposite change in the quantum space magnetization $S^{(z)} = \sum_{i=1}^L S_i^{(z)}$: $A(u)$ and $D(u)$ are therefore spin-conserving operators in the quantum space, whereas $B(u)$ and $C(u)$ are spin-lowering and spin-raising, respectively.

The essence of the Bethe Ansatz construction is the existence of a *pseudovacuum*, namely an eigenstate of both $A(u)$ and $D(u)$ which is annihilated by $C(u)$. These requirements are readily seen to be fulfilled by the state $|\Phi_0\rangle \equiv |\uparrow\rangle^{\otimes L} \equiv |\uparrow\uparrow \dots \uparrow\rangle$, as we have

$$A(u)|\Phi_0\rangle = \left(\prod_{l=1}^L a(u - v_l) \right) |\Phi_0\rangle, \quad D(u)|\Phi_0\rangle = \left(\prod_{l=1}^L b(u - v_l) \right) |\Phi_0\rangle, \quad C(u)|\Phi_0\rangle = 0, \quad (3.6)$$

where we recall that $a(u)$, $b(u)$ and $c(u)$ are given by (2.13). $|\Phi_0\rangle$ is an eigenstate of the transfer matrix $T(u) = \text{Tr}_a \mathcal{T}(u) = A(u) + D(u)$ with magnetization $S^{(z)} = \frac{1}{2}L$, and can be used to build other eigenstates by repeated action of the spin-lowering operators. In a more algebraic language, the algebraic Bethe Ansatz construction relies on the fact

that the quantum space $(\mathbb{C}^2)^{\otimes L}$ is a *highest-weight representation* of the algebra $U_q(\widehat{sl_2})$, namely all states in this representation can be obtained by repeated actions of the *creation operators* $B(\cdot)$ on the highest-weight state $|\Phi_0\rangle$.

We therefore look for eigenstates in the sector of magnetization $S^{(z)} = \frac{1}{2}L - m$ of the form

$$|\Phi_m\rangle = \prod_{i=1}^m B(u_i) |\Phi_0\rangle. \quad (3.7)$$

The complex parameters u_1, \dots, u_m are the so-called *Bethe roots*, and we will now see how these are constrained by the requirement that $|\Phi_m\rangle$ be an eigenvector of the transfer matrix, which we write as

$$[A(u) + D(u)] |\Phi_m\rangle = \Lambda(u) |\Phi_m\rangle. \quad (3.8)$$

Since the action of $A(u) + D(u)$ on $|\Phi_0\rangle$ is well known, all one has to do in order to compute the left-hand side of (3.8) is to commute $A(u)$ and $D(u)$ with the successive $B(u_i)$ factors. This is achieved using the commutation relations between the operators A, B, C, D , which are straightforwardly read off the RTT relation (2.6). The result bears the following form

$$A(u) |\Phi_m\rangle = \left(\prod_{l=1}^L a(u - v_l) \right) \prod_{i=1}^m \frac{a(u - u_i)}{b(u - u_i)} |\Phi_m\rangle + \sum_{i=1}^m \Lambda_i |\Phi_m^j(u)\rangle \quad (3.9)$$

$$D(u) |\Phi_m\rangle = \left(\prod_{l=1}^L b(u - v_l) \right) \prod_{i=1}^m \frac{a(u_i - u)}{b(u_i - u)} |\Phi_m\rangle + \sum_{i=1}^m \tilde{\Lambda}_i |\Phi_m^j(u)\rangle, \quad (3.10)$$

where $|\Phi_m^j(u)\rangle$ is obtained from the expression (3.7) of $|\Phi_m\rangle$ by replacing $B(u_j)$ by $B(u)$, and

$$\Lambda_i = \left(\prod_{l=1}^L a(u_i - v_l) \right) \frac{c(u_i - u)}{b(u_i - u)} \prod_{j(\neq i)} \frac{a(u_i - u_j)}{b(u_i - u_j)} \quad (3.11)$$

$$\tilde{\Lambda}_i = \left(\prod_{l=1}^L b(u_i - v_l) \right) \frac{c(u - u_i)}{b(u - u_i)} \prod_{j(\neq i)} \frac{a(u_j - u_i)}{b(u_j - u_i)}. \quad (3.12)$$

The right-hand sides of both (3.9) and (3.10) are the sum of one wanted term proportional to $|\Phi_m\rangle$ and one unwanted term not proportional to $|\Phi_m\rangle$. The cancellation of the unwanted terms in $[A(u) + D(u)] |\Phi_m\rangle$ is ensured by requiring $\Lambda_i + \tilde{\Lambda}_i = 0$, which leads to the *Bethe equations*

$$\prod_{l=1}^L \frac{\sin(u_i - v_l + \gamma)}{\sin(u_i - v_l)} = \prod_{j(\neq i)} \frac{\sin(u_j - u_i + \gamma)}{\sin(u_j - u_i - \gamma)}, \quad i = 1, \dots, m. \quad (3.13)$$

The corresponding transfer matrix eigenvalue reads

$$\Lambda(u) = \left(\prod_{l=1}^L a(u - v_l) \right) \prod_{i=1}^m \frac{a(u - u_i)}{b(u - u_i)} + \left(\prod_{l=1}^L b(u - v_l) \right) \prod_{i=1}^m \frac{a(u_i - u)}{b(u_i - u)} \quad (3.14)$$

$$= \left(\prod_{l=1}^L \frac{\sin(\gamma + u - v_l)}{\sin \gamma} \right) \prod_{i=1}^m \frac{\sin(u - u_i + \gamma)}{\sin(u - u_i)} + \left(\prod_{l=1}^L \frac{\sin(u - v_l)}{\sin \gamma} \right) \prod_{i=1}^m \frac{\sin(u - u_i - \gamma)}{\sin(u - u_i)}, \quad (3.15)$$

and the associated energy is

$$E = - \left. \frac{d \log \Lambda(u)}{du} \right|_{u=0} = - \sum_{i=1}^m \frac{2 \sin \gamma}{\cos(2u_i - \gamma) - \cos \gamma}. \quad (3.16)$$

3.1.2 Algebraic Bethe ansatz for higher rank models

For models of higher rank, namely in cases where the representations $V_l(v_l)$ are of dimension n larger than two, the method described above cannot be directly applied. Instead, one has to use the so-called *nested Bethe ansatz*, which we now want to describe in its main lines. We will keep the presentation generic (and very much inspired from [102]), and therefore will not go into the details of any particular model. Specifically, the case of models built on twisted affine algebras requires slight adaptations which will not be discussed.

The monodromy matrix, now acting on the auxilliary space $(\mathbb{C}^n)_a$ is a $n \times n$ matrix which we block-decompose as

$$\mathcal{T}(u) = \begin{pmatrix} \tau_{11}(u) & B^{(1)}(u) \\ C^{(1)}(u) & \mathcal{T}^{(2)}(u) \end{pmatrix}, \quad (3.17)$$

where $\tau_{11}(u)$ is the first row, first column matrix element of \mathcal{T} , while $B^{(1)}(u)$, $C^{(1)}(u)$ and $\mathcal{T}^{(2)}(u)$ are respectively a $(n-1)$ -row, column vector and a $(n-1) \times (n-1)$ matrix of operators acting on the quantum space.

As in the six-vertex case, the Bethe ansatz solution relies on the existence of a *highest weight vector* $|\Omega^{(1)}\rangle$ for the affine algebra under study in the space $V_1(v_1) \otimes \dots \otimes V_L(v_L) \simeq (\mathbb{C}^n)^{\otimes L}$. More precisely, unlike in the case of finite-dimensional simple Lie algebras, the tensor product $V_1 \otimes \dots \otimes V_L$ of irreducible representations is itself irreducible (see the discussion in section 2.1.3), and we can then use the near to general theorem presented in [103], stating that any such finite-dimensional irreducible representation is highest-weight, and contains an unique highest weight vector. The action of the monodromy matrix elements τ_{ij} on $|\Omega^{(1)}\rangle$ reads, by definition,

$$\tau_{ii}(u)|\Omega^{(1)}\rangle = \Lambda_i(u)|\Omega^{(1)}\rangle, \quad \tau_{ij}(u)|\Omega^{(1)}\rangle = 0 \quad \text{if } i > j. \quad (3.18)$$

In particular $C^{(1)}(u)|\Omega\rangle = 0$, and we can use $B^{(1)}()$ as a creation operator to build the transfer matrix eigenstates. Because of the $(n-1)$ -dimensional nature of B_1 , we now have to set

$$|\Phi_{m_1}\rangle = B_{a_1}^{(1)}(u_1^{(1)}) \dots B_{a_{m_1}}^{(1)}(u_{m_1}^{(1)}) F^{(1)a_1 \dots a_{m_1}}, \quad (3.19)$$

where Einstein's summation convention is used over the indices a_1, \dots, a_{m_1} , and $F^{(1)}$ is now a vector of $(\mathbb{C}^{n-1})^{\otimes m_1}$ built up from operators $\tau_{i,j}(u)$, $2 \leq i \leq j \leq n$. As in the six-vertex case studied previously the complex numbers $u_1^{(1)}, \dots, u_{m_1}^{(1)}$ are the so-called Bethe roots. Acting on $|\Phi_{m_1}\rangle$ with the diagonal elements of $\mathcal{T}(u)$, one finds a result of the form

$$\tau_{11}(u)|\Phi_{m_1}\rangle = \Lambda_1(u) \prod_{i=1}^{m_1} f_1(u - u_i^{(1)})|\Phi_{m_1}\rangle + \sum_{j=1}^{m_1} \Lambda'_i |\Phi_{m_1}^j(u)\rangle \quad (3.20)$$

$$\mathcal{T}^{(2)}(u)|\Phi_{m_1}\rangle = \prod_{i=1}^{m_1} f_2(u - u_i^{(1)})|\tilde{\Phi}_{m_1}\rangle + \sum_{j=1}^{m_1} \tilde{\Lambda}'_i |\tilde{\Phi}_{m_1}^j(u)\rangle \quad (3.21)$$

where $|\Phi_{m_1}^j(u)\rangle$ is obtained from $|\Phi_{m_1}\rangle$ by replacing $B^{(1)}(u_j^{(1)})$ by $B^{(1)}(u)$ and $|\tilde{\Phi}_{m_1}\rangle$, $|\tilde{\Phi}_{m_1}^j(u)\rangle$ are defined as

$$|\tilde{\Phi}_{m_1}\rangle = B_{a_1}^{(1)}(u_1^{(1)}) \dots B_{a_{m_1}}^{(1)}(u_{m_1}^{(1)}) \tilde{T}^{(2)}(u) F^{(1) a_1 \dots a_{m_1}} \quad (3.22)$$

$$|\tilde{\Phi}_{m_1}^j(u)\rangle = B_{a_1}^{(1)}(u_1^{(1)}) \dots B_{a_j}^{(1)}(u) \dots B_{a_{m_1}}^{(1)}(u_{m_1}^{(1)}) \tilde{T}^{(2)}(u_j) F^{(1) a_1 \dots a_{m_1}}, \quad (3.23)$$

where the *auxilliary transfer matrix* $\tilde{T}^{(2)}(u)$ acts on the space $(\mathbb{C}^{n-1})^{\otimes m_1}$ and the associated monodromy matrix obeys a relation of the RTT type, with an R -matrix $R^{(2)} : \mathbb{C}^{n-1} \otimes \mathbb{C}^{n-1} \rightarrow \mathbb{C}^{n-1} \otimes \mathbb{C}^{n-1}$ obtained from the original one by keeping only the indices ≥ 2 . In this sense $\tilde{T}^{(2)}$ can be viewed as the integrable transfer matrix associated with an affine algebra of lesser rank, for a chain of size m_1 with inhomogeneous spectral parameters $u_1^{(1)}, \dots, u_{m_1}^{(1)}$. To proceed further, one assumes that $F^{(1)}$ is an eigenvector of $\tilde{T}^{(2)}(u)$, namely $\tilde{T}^{(2)}(u) F^{(1)} = \Lambda^{(2)}(u) F^{(1)}$, such that (3.21) can be rewritten as

$$\mathcal{T}^{(2)}(u) |\Phi_{m_1}\rangle = \Lambda^{(2)}(u) \prod_{j=1}^{m_1} f_2(u - u_j^{(1)}) |\Phi_{m_1}\rangle + \sum_{j=1}^{m_1} \Lambda^{(2)}(u_j^{(1)}) \tilde{\Lambda}'_j |\Phi_{m_1}^j(u)\rangle. \quad (3.24)$$

The cancellation of unwanted terms between equations (3.20) and (3.24) therefore leads to a first set of Bethe equations,

$$\Lambda^{(2)}(u_j^{(1)}) \tilde{\Lambda}'_j = -\Lambda'_j, \quad j = 1, \dots, m_1, \quad (3.25)$$

whereas the eigenvalue Λ_1 can be fully reexpressed in terms of $\Lambda^{(2)}$.

One is therefore left with the auxilliary eigenvalue problem

$$\tilde{T}^{(2)}(u) F^{(1)} = \Lambda^{(2)}(u) F^{(1)}, \quad (3.26)$$

which is in turn solved by a similar procedure, introducing a set of m_2 auxilliary Bethe roots $u_1^{(2)}, \dots, u_{m_2}^{(2)}$, etc... The program is complete after $n - 2$ of such steps, the last of which reducing simply to the usual algebraic Bethe ansatz presented earlier. The eigenvalues of the transfer matrix $T(u)$ are written in terms of $n - 1$ levels of Bethe roots sets, $u_1^{(k)}, \dots, u_{m_k}^{(k)}$, subject to a set of nested Bethe ansatz equations, which we will now be giving without an explicit derivation for the different models of interest (all can be found in [99]).

3.2 Continuum limit of the $a_2^{(2)}$ model

In this whole section, we consider the (twisted) periodic, homogeneous, $a_2^{(2)}$ (Izergin–Korepin) row-to-row transfer matrix

$$T(u) = \text{Tr}_a \left(\check{R}_{a1}(u) \dots \check{R}_{aL}(u) e^{i\varphi S_a^{(z)}} \right), \quad (3.27)$$

where each space carries the fundamental, three-dimensional representation of $U_q(sl_3^{(2)})$ which can also be interpreted as the spin one representation of an underlying $U_q(sl_2)$ subalgebra ($\mathfrak{q} = q^{\frac{1}{2}}$), the \check{R} matrix is (up to some proportionnality factor) that written explicitly in (2.84), and the boundary twist factor $e^{i\varphi S_a^{(z)}}$ acts on the auxilliary space (the model is invariant under $\varphi \rightarrow -\varphi$, so we will restrict ourselves to positive values of this

parameter). We recall the notations $q = e^{i\gamma}$, and $x = e^{iu}$. The transfer matrix commutes with the total magnetization

$$m = \sum_{i=1}^L S_i^{(z)}, \quad (3.28)$$

and its eigenvalues can therefore be classified according to the value of m , with a $m \rightarrow -m$ symmetry allowing us to restrict our study to $m \geq 0$. These are characterized by a set of

$$m_1 = L - m \quad (3.29)$$

roots λ_j (related to the usual u_j by $\lambda_j = \frac{i}{2}u_j$), solution of the Bethe ansatz equations [78, 99]

$$\left(\frac{\sinh(\lambda_j - i\frac{\gamma}{2})}{\sinh(\lambda_j + i\frac{\gamma}{2})} \right)^L = e^{i\varphi} \prod_{i(\neq j)} \frac{\sinh(\lambda_j - \lambda_i - i\gamma) \cosh(\lambda_j - \lambda_i + i\frac{\gamma}{2})}{\sinh(\lambda_j - \lambda_i + i\gamma) \cosh(\lambda_j - \lambda_i - i\frac{\gamma}{2})}. \quad (3.30)$$

That these equations involve only one type of roots (instead of two, as we should expect from the rank of the algebra) can be related to the twisted nature of $a_2^{(2)}$. From this point of view, the Bethe equations for $a_2^{(2)}$ can be seen as a folding of those for $a_2^{(1)}$, obtained from the latter by a one-to-one identification of the two types of roots.

There are two isotropic values of the spectral parameter u , namely $u_{\pm} = \frac{3\gamma}{2} \pm \frac{\pi}{2}$, corresponding to local maxima of the transfer matrix eigenvalues, and which are described by a different physics in the sense that they are not dominated by the same transfer matrix eigenstates. From the Hamiltonian point of view, these correspond to opposite signs in the definition of the energy, namely

$$E_{\pm} = \pm \sum_{i=1}^m \frac{\sin \gamma}{\cosh 2\lambda_i - \cos \gamma}. \quad (3.31)$$

Varying the parameter γ through $[0, \pi]$ and considering both signs of the energy (or, equivalently, the two isotropic points u_{\pm}), one actually encounters three regimes corresponding to distinct structural properties of the Bethe Ansatz solution and fundamentally different critical behaviours :

- Regime I corresponds to the isotropic point $u = u_+$, or equivalently the sign $+$ in the energy (3.31)
- Regime II corresponds to the isotropic point $u = u_-$ (sign $-$ in (3.31)), and $\gamma \in [\frac{\pi}{3}, \pi]$
- Regime III corresponds to the isotropic point $u = u_-$ (sign $-$ in (3.31)), and $\gamma \in [0, \frac{\pi}{3}]$.

In [78], these three regimes were studied by means of numerical resolution of the BAE and powerful analytical methods. Whereas the latter yielded the respective central charges $c = 1$, $c = \frac{3}{2}$ and $c = 2$ at zero twist, numerical results in regime III showed an unusually poor convergence of the central charge and critical exponents, together with unusual effects related to the addition of a twist and which will be the object of paragraph 3.2.4.

Treating regimes I and II as a warmup, which will also allow for a first encounter with the numerical and analytical tools and concepts proper to the resolution of Bethe Ansatz equations, we shall here revisit the study of the continuum limit in regime III which will lead us to interpret the unusual observations of [78] as the sign for a non-compact boson.

3.2.1 Continuum limit in regimes I and II

Before entering the details of Bethe ansatz solutions, let us describe in a few lines the general procedure that we will be using for all regimes and all models of interest in this thesis.

Given a certain regime, namely a certain value of the model's parameters (γ, u here), the natural first step is to compute and diagonalize directly the corresponding Hamiltonian or transfer matrix for small system sizes, typically less than $L = 10$, and to identify the leading eigenstates (Hamiltonian's ground state and first excitations, leading transfer matrix eigenvalues). These eigenstates are associated with some definite sets of Bethe roots, whose location in the complex plane can be found in two ways :

- The first way is to directly solve the Bethe equations in the complex plane by some numerical, Newton–Raphson like method. Such methods proceed iteratively from given starting values of the unknown roots, and well-chosen or random starting points should in principle be able to yield any possible solution. Shuffling between different solutions and computing the corresponding Bethe eigenvalues, one should after some time end up with the set of roots recovering any eigenvalue of interest in the transfer matrix spectrum.
- The second, more systematic way, is to directly compute the Bethe roots as solutions of a set of linear equations. This method, which is often referred to as the *McCoy method* [104], uses the fact that the coefficients of the \check{R} matrix under consideration are all polynomials of degree 2 in the variable x up to some global rescaling, and that integrability of the system ensures that the considered eigenvector can be chosen independently of x . Once given its coordinates $(v)_i$ in some basis of the space of states for the L sites chain, chosen such that $(v)_1 \neq 0$, we can therefore write the corresponding (properly rescaled) eigenvalue as

$$\Lambda(x) = \frac{(T(x) \cdot v)_1}{(v)_1}, \quad (3.32)$$

which is a polynomial of degree $2L$ in x , that can be computed numerically from the knowledge of v . The task is then to rewrite the Bethe expression of $\Lambda(x)$ in a polynomial form, whose coefficients are expressed in terms of the Bethe roots. The term-by-term identification with the numerical expression (3.32) builds up a system of equations on the Bethe roots, which in the $a_2^{(2)}$ case is linear-triangular and can be solved easily ¹.

Using the above methods to compute the Bethe roots associated to one state of interest for a few small system sizes, it is usually quite straightforward to see patterns emerge, namely the roots can for instance spread on the real axis, gather in complex multiplets, etc... In any case, the understanding of these structures allows to turn the Bethe equations into a set of real equations, paving the way for a systematic resolution at large system sizes as well as for analytical results. For reference, we note that most of the numerical techniques associated with the resolution of Bethe ansatz equations were pioneered by the 1988 paper of Batchelor, Barber and Alcaraz [105]. Many important analytical developments are presented in the book by Korepin, Bogoliubov and Izergin [37].

¹In higher-rank cases involving more than one type of Bethe roots, the system is in general non-linear and requires to be solved numerically.

Regime I

We now get specific and turn to the regime I, where it is seen that the ground state is made of L roots λ_i with imaginary part $\frac{\pi}{2}$. Setting $\lambda_i = x_i + i\frac{\pi}{2}$, we can rewrite the Bethe equations as

$$\left(\frac{\cosh(x_j - i\frac{\gamma}{2})}{\cosh(x_j + i\frac{\gamma}{2})} \right)^L = e^{i\varphi} \prod_{i(\neq j)} \frac{\sinh(x_j - x_i - i\gamma) \cosh(x_j - x_i + i\frac{\gamma}{2})}{\sinh(x_j - x_i + i\gamma) \cosh(x_j - x_i - i\frac{\gamma}{2})}. \quad (3.33)$$

A real form of the BAE can be achieved by taking the logarithm of (3.33), and using the function

$$\psi(x, y) = \frac{i}{2} \ln \frac{\sinh(x - iy)}{\sinh(x + iy)} = \arctan(\tan y \coth x), \quad (3.34)$$

namely

$$\pi I_j = L \psi\left(x_j, \frac{\gamma}{2} - \frac{\pi}{2}\right) + \frac{\varphi}{2} - \sum_{i(\neq j)} \left[\psi(x_j - x_i, \gamma) + \psi\left(x_j - x_i, -\frac{\gamma}{2} - \frac{\pi}{2}\right) \right], \quad (3.35)$$

where the I_j are distinct (half)-integers ($I_j - \frac{L+1}{2} \in \mathbb{Z}$), the so-called *Bethe integers*, which can be interpreted to account for the fermionic statistics of the Bethe roots. These are found to be symmetrically packed around zero for the ground state, which we usually describe as a *Fermi sea*, and allow for a description of part of the spectrum of low-lying excitations, namely

- *hole* excitations, which are obtained by creating vacancies in the distribution of I_j , hence accessing sectors of nonzero magnetization m .
- *backscattering* excitations, which are obtained by shifting all Bethe integers by a finite amount w , hence creating states with momentum w .

Solving numerically the Bethe equations (3.35) for the various sets of integers I_j of interest allows access to the corresponding excitation spectrum. In practice, the equations are easily solved for L up to a few hundreds using a MathematicaTM script based on the Newton–Raphson method. We augment L iteratively by steps of 2, and use at size $L+2$ starting points for the roots close to the solution found at size L . As an alternative way, the density of roots over the real axis can directly be guessed in the continuum limit (see discussion below; in particular, the density of roots in the $L \rightarrow \infty$ limit can be obtained from the Fourier transform of equation (3.39) for $\rho_1^h = 0$), and can be used to derive good approximations of the distribution of the roots in finite size, hence providing efficient starting points for the numerical resolution of the Bethe equations. The corrections to the estimation of the conformal spectrum are of the order of $O(L^{-2})$, and we recover without any ambiguity the central charge

$$c = 1 - \frac{3\varphi^2}{\pi\gamma} \quad (3.36)$$

of [78] and the conformal weights

$$\Delta(\bar{\Delta}) = \frac{\gamma}{8\pi} \left(m \pm \frac{2\pi}{\gamma} w \right)^2, \quad (3.37)$$

which are those of a free bosonic field with a charge at infinity, as will be explained in the following.

Before doing so, let us depict how the spectrum (3.37) can be recovered analytically from the continuum limit of equations (3.35). As $L \rightarrow \infty$ the real parts x_j form a continuous distribution modeled by the density

$$\rho(x) = \frac{1}{L} \frac{dI_j}{dx_j}, \quad (3.38)$$

and we similarly introduce the density of holes $\rho_h(x)$ to account for vacancies in the distribution of the I_j 's. Differentiating equation (3.35) with respect to x_j and rewriting the result in Fourier space leads to

$$\rho + \rho_h = \frac{\sinh \frac{\omega\gamma}{2}}{\sinh \frac{\omega\pi}{2}} + \frac{\sinh \frac{\omega(\pi-\gamma)}{4} \cosh \frac{\omega(\pi-3\gamma)}{4}}{\sinh \frac{\omega\pi}{2}} \rho, \quad (3.39)$$

which has the general form

$$\rho + \rho_h = s + K \rho. \quad (3.40)$$

From there, one can obtain the density of roots for the ground state by letting $\rho_h = 0$, namely $\rho_0 = (1 - K)^{-1}s$ in Fourier space. Translating this expression back to the real space, we can use it to derive an integral expression for the free energy in the thermodynamic limit. In turn, ρ_0 can be used to choose appropriate starting values of the x_j 's in numerical resolutions, as advertised above. The conformal spectrum itself can be directly extracted from (3.40) by various analytical methods such as the resolution of a Wiener-Hopf equation [37], and we should here only remember the generic result,

$$\Delta + \bar{\Delta} = \frac{1 - K}{4} m^2 + \frac{1}{1 - K} w^2, \quad (3.41)$$

where for K the zero-frequency limit has to be taken, namely $K = 1 - \frac{\gamma}{\pi}$. Using the fact that $\Delta - \bar{\Delta}$ counts the conformal spin $\Delta - \bar{\Delta} = w m$ this recovers the compact boson spectrum (3.37).

The physical interpretation of the continuum limit of the $a_2^{(2)}$ model in regime I as a free bosonic field can easily be understood in the geometrical setup via the *Coulomb gas* formalism (see [35] for a review). In this framework, the oriented loops of the underlying $O(n)$ model are interpreted as the domain walls encircling the valleys or hills of a real compactified height variable $h(x)$ defined on each site of the dual square lattice², and which in the continuum limit becomes described by a smooth field $\Phi(x)$ (with $\Phi \equiv \Phi + 2\pi R$) (see figure 3.1) with action

$$S = \frac{g}{4\pi} \int d^2x (\partial_\mu \Phi)^2. \quad (3.42)$$

This action is that of a free compactified boson, whose radius R can be fixed to $R = 1$ and where the coupling g accounts for the rigidity of the height interface and is in this sense an increasing function of the loop fugacity n , namely

$$n = -2 \cos \pi g, \quad (3.43)$$

that is $g = \frac{2\gamma}{\pi}$. The central charge and conformal weights of the ‘bare’ (untwisted) theory

²The compactification arises from the fact that, on a torus, periodicity of the heights cannot be guaranteed.

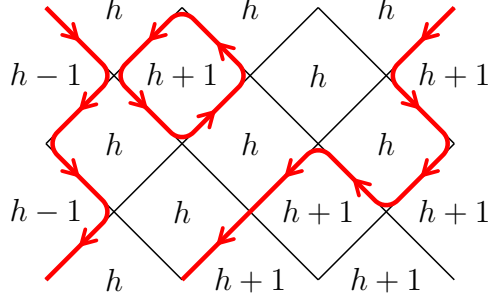


Figure 3.1: Mapping from an oriented configuration of $O(n)$ loops on the square lattice to a configuration of heights on the dual lattice.

read

$$\begin{aligned} c &= 1 \\ \Delta_{E,M} + \bar{\Delta}_{E,M} &= \frac{E^2}{2g} + g \frac{M^2}{2} \\ \Delta_{E,M} - \bar{\Delta}_{E,M} &= EM, \end{aligned} \quad (3.44)$$

where M and E are the so-called electric and magnetic charges. The effect of the twist parameter, which gives a weight $\tilde{n} = 2 \cos \varphi$ to non-contractible loops circling around the torus, is accounted for by the introduction of a *background charge*, namely an electric charge $e_0 = \frac{\varphi}{\pi}$ at infinity. The central charge is accordingly modified into

$$c = 1 - \frac{6e_0^2}{g}, \quad (3.45)$$

which recovers the Bethe ansatz result (3.36), and the electric charge in the expression of the conformal weights has to be shifted by an amount of e_0 . In order to obtain the conformal weights measured with respect to the screened central charge (3.45) these need to be further shifted by an amount $-\frac{e_0^2}{4g}$, hence leading to

$$\Delta_{E,M} + \bar{\Delta}_{E,M} = \frac{E(E - 2e_0)}{2g} + g \frac{M^2}{2}. \quad (3.46)$$

Relating E and M to the lattice excitations by $M = \frac{m}{2}$, $e = 2w$ then recovers at zero twist ($e_0 = 0$) the spectrum (3.37). Note that a continuum limit made of one free bosonic field is the same as what can be found for the integrable six-vertex model, introduced earlier. A Coulomb gas construction holds in that case too [40], the only difference being that there no lattice edges are left vacant. From this perspective, the presence of empty sites in the $a_2^{(2)}$ case does not modify the field content of the continuum limit in regime I, instead it amounts simply a renormalization of the coupling constant g .

Regime II

The L Bethe roots describing the ground state in regime II are this time organized as a set of $\frac{L}{2}$ complex conjugate pairs with imaginary parts slightly larger (in absolute value) than $\pm(\frac{\pi}{4} - \frac{\gamma}{4})$, the so-called *2-strings*. The existence of such complex solutions can be understood using the following standard argument : consider a solution of the Bethe

equations, where one root λ_j has a non trivial imaginary part δ (that is, not a multiple of $\frac{\pi}{2}$). From the equality (3.34), the left-hand side of (3.30) then has a modulus > 1 or < 1 (depending on the sign of δ), and therefore should either diverge or go to zero exponentially as the $L \rightarrow \infty$ limit is taken. Accordingly, the same singularity should be present on the right-hand side, or in other terms there should be another root λ'_j , such that $\lambda'_j - \lambda_j \simeq \pm i\gamma$, or $\lambda'_j - \lambda_j \simeq \pm i(\frac{\pi}{2} - \frac{\gamma}{2})$, where the \simeq indicates corrections decreasing exponentially with L . The same argument can in turn be applied to λ'_j , leading to another singularity which can itself be corrected by either another root λ''_j , or by λ_j itself. The structures emerging from this construction are the so-called *n-strings* (where n stands for the number of complex roots involved), and we should in all the following use two separate denominations, namely *n*-strings* and *n-strings*, for strings made of roots distant by $\simeq \pm i\gamma$ or $\simeq \pm i(\frac{\pi}{2} - \frac{\gamma}{2})$, respectively.

A real form of the Bethe equations is obtained for each 2-string $\lambda_j^{(\pm)} = x_j \pm i(\frac{\pi}{4} - \frac{\gamma}{4} + \epsilon)$ by combining the equations associated with $\lambda_j^{(+)}$ and $\lambda_j^{(-)}$, namely by considering the product and quotient of these two equations. Bethe integers can be associated with the former, hence equipping the centers x_j with fermionic statistics. Numerical resolution of the corresponding set of Bethe equations leads to

$$\begin{aligned} c &= \frac{3}{2} - \frac{3\varphi^2}{\pi(\pi - \gamma)} \\ \Delta(\bar{\Delta}) &= \frac{\pi - \gamma}{2\pi} \left(\frac{m}{2} \pm \frac{\pi}{2(\pi - \gamma)} w \right)^2, \end{aligned} \quad (3.47)$$

where now $\frac{m}{2}$ and w are the number of holes and backscattering index in the sea of 2-strings.

Similarly to what was done in regime I, this result can be recovered by looking at the Bethe equations for the densities of 2-string centers x_j , namely ³

$$\rho + \rho_h = \frac{2 \sinh \frac{\omega(\pi - \gamma)}{2} \cosh \frac{\omega(\pi - \gamma)}{4}}{\sinh \frac{\omega\pi}{2}} - \frac{\sinh \frac{\omega(\pi - 2\gamma)}{2} + \sinh \frac{\omega(2\pi - 3\gamma)}{2} + \sinh \frac{\omega\pi}{2}}{\sinh \frac{\omega\pi}{2}} \rho. \quad (3.48)$$

The corresponding kernel K is at zero frequency $K = \frac{4\gamma}{\pi} - 3$, recovering indeed (3.47). This spectrum has long been understood as that of a screened compact boson, supplemented by an Ising degree of freedom, giving respectively a contribution $1 - \frac{3\varphi^2}{\pi(\pi - \gamma)}$ and $\frac{1}{2}$ to the central charge [78]. This interpretation, which we will discuss further when considering the corresponding massive perturbations (see section 3.2.6), also bears a nice geometrical formulation similar to that presented in [106] (see also [107] for a comprehensive Coulomb gas description). Alternatively to the usual geometrical construction obtained by drawing oriented loop segments on edges occupied with ± 1 states, one can choose to put bonds on each edge carrying a 0 state as represented in figure 3.2 and forget about the remaining arrows, hence leaving one with the graphs of the low-temperature expansion of some Ising model on the dual square lattice. The Ising degree of freedom emerging from this construction, which did not contribute to the critical behaviour in regime I (it was then apparently massive), is therefore critical and fully decoupled in the continuum limit of regime II.

³In the limit $L \rightarrow \infty$, the corrections ϵ to imaginary parts become zero, and we are only left with equations over the centers of Bethe strings.

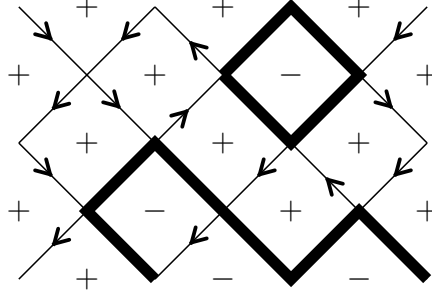


Figure 3.2: Configuration of graphs in the low-temperature expansion of the Ising model arising from configurations of the 19-vertex model on the square lattice.

3.2.2 First observations in regime III

Whereas the description of regimes I and II in terms of a compact boson and an Ising degree of freedom has been well known for quite a long time [78], a proper understanding of regime III has long been lacking. We will expose in this paragraph the reasons for the difficulties encountered in this case, mixing the early results of [78] together with our recent observations presented in [62].

As in regime II, the ground state of regime III is described by a set of $\frac{L}{2}$ 2-strings, whose imaginary part are however now slightly smaller (in absolute value) than $\frac{\pi}{4} - \frac{\gamma}{4}$. Due to analyticity properties of the kernels, the corresponding Bethe equations for densities in Fourier space have a different structure than those found in regime II, namely

$$\rho + \rho_h = \frac{2 \sinh \frac{\omega\gamma}{2} \cosh \omega \left(\frac{\pi+\gamma}{4} \right)}{\sinh \frac{\omega\pi}{2}} - \frac{\sinh \omega \left(\frac{\pi}{2} - \gamma \right) - \sinh \frac{3\omega\gamma}{2} + \sinh \frac{\omega\gamma}{2}}{\sinh \frac{\omega\pi}{2}} \rho. \quad (3.49)$$

At vanishing frequency $K = 1 - 4\frac{\gamma}{\pi}$, so from the now usual formula (3.41) we have

$$\Delta(\bar{\Delta}) = \frac{\gamma}{2\pi} \left(\frac{m}{2} \pm \frac{\pi}{2\gamma} w \right)^2, \quad (3.50)$$

while the central charge was found [78], after considerable analytical and numerical work, to be described by two different analytical formulae depending on the value of the twist parameter (see figure 3.3), namely

$$c = \begin{cases} 2 - \frac{3\varphi^2}{\pi\gamma} & \text{for } \varphi \leq \gamma, \\ -1 + \frac{3(\pi-\varphi)^2}{\pi(\pi-\gamma)} & \text{for } \gamma \leq \varphi. \end{cases} \quad (3.51)$$

Several observations are in order

- Looking at the numerical results of figure 3.3, one gets struck at the unusually large corrections to scaling in the $\varphi \leq \gamma$ region, whereas in most integrable systems study of the energy spectrum for system sizes of order $L = 10$ sites is usually enough to obtain the corresponding conformal content with good precision.
- The expression for the central charge for $\varphi \leq \gamma$ and the and conformal weights are quite reminiscent of what could be obtained from a one-component Coulomb gas (3.45), except for an extra +1 term contributing in the central charge and

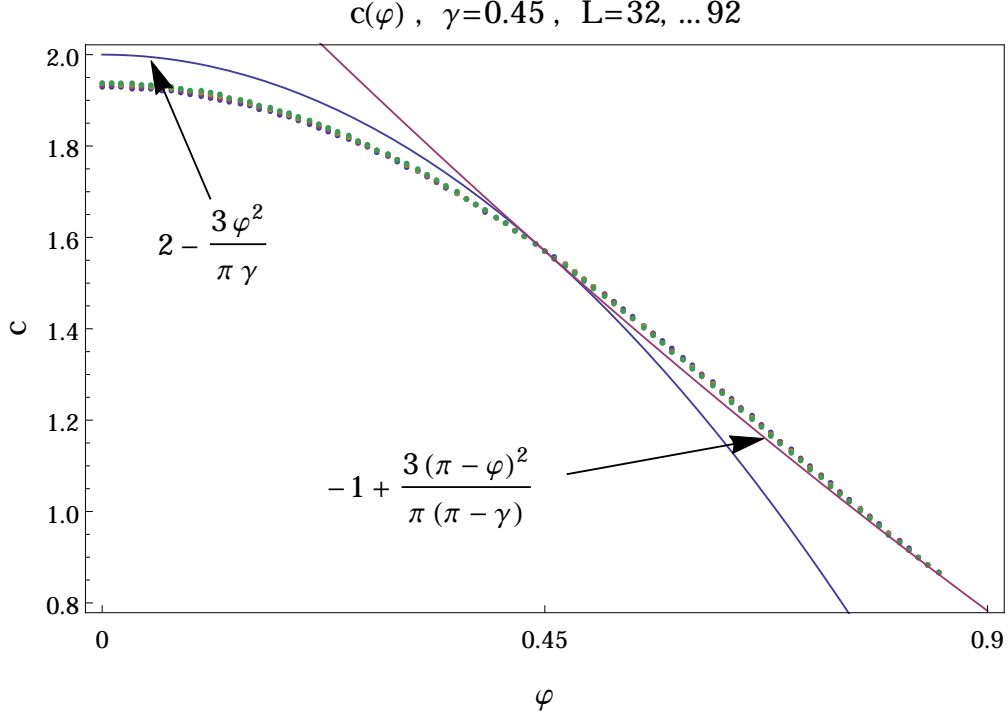


Figure 3.3: Central charge for the $a_2^{(2)}$ model, measured as a function of the twist parameter for system sizes ranging up to 92. The analytical predictions are plotted in comparison.

which remains to be elucidated. As for the $\varphi \geq \gamma$ expression of the central charge, it is manifestly different from anything one might expect from an usual free field construction.

- The single fact that the central charge (3.51) is described by another analytical formula for $\varphi \geq \gamma$, is itself quite extraordinary, as it has no counterpart in the finite lattice spectrum. Indeed, the two different analytical behaviours of the central charge are obtained from the *same* ground state followed continuously when varying the twist, and which in particular does not undergo any crossover, nor is degenerate at $\varphi = \gamma$.

As we will now see, these observations are of very profound origin. To gain understanding in the nature of the continuum limit in regime III, we turn to a meticulous analysis of the low-lying spectrum. As was previously stated, the ground state lies in the sector of zero magnetization and can be described by a set of $\frac{L}{2}$ 2-strings. It is observed that low-lying excitations with momentum zero and magnetization zero on top of this ground state can be formed by replacing an arbitrary number j of 2-strings by the same number of ‘*antistrings*’, namely pairs of roots with imaginary part $\frac{\pi}{2}$ (see figure 3.4). A similar construction holds in the sectors of non zero magnetization, allowing us to label all the low energy levels in regime III by three integers, (m, w, j) . For clarity we will from now on restrict to the states with no backscattering and will commonly use the notation $(m, j) \equiv (m, 0, j)$. The spectrum at finite size (and $w = 0$) therefore looks as follows :

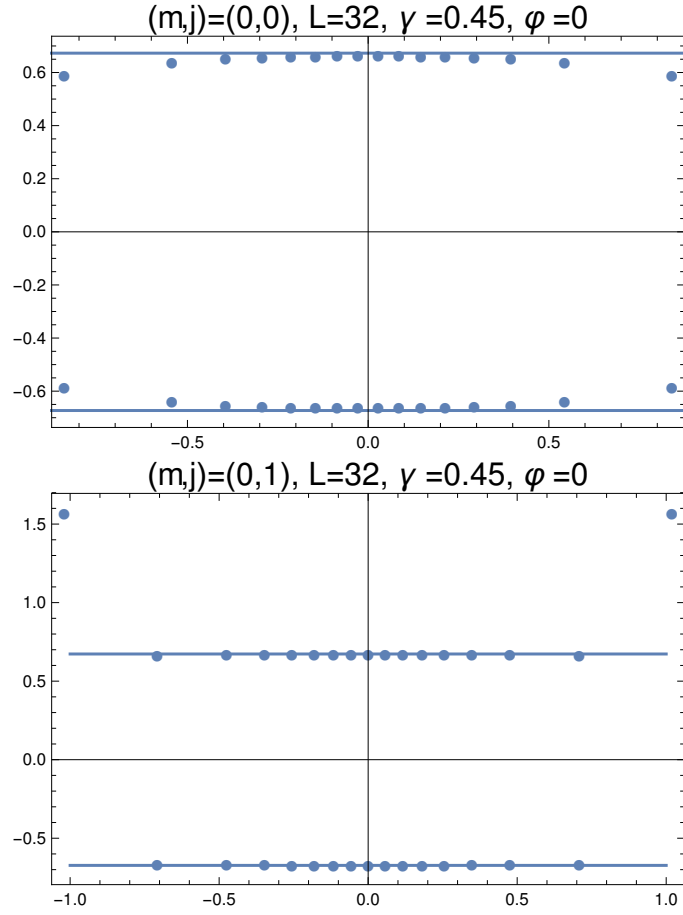
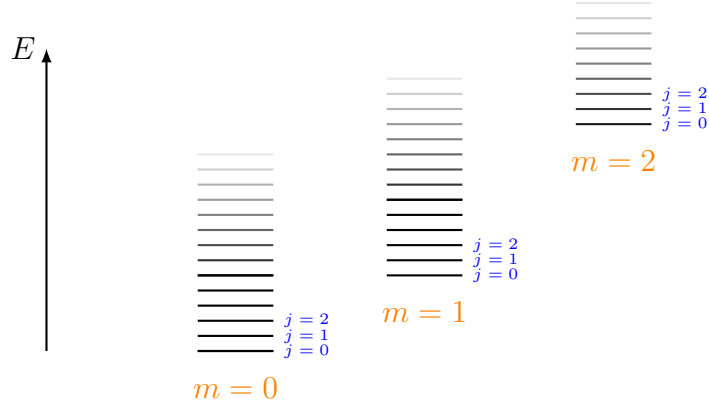


Figure 3.4: Bethe roots associated with the states $(m, j, w) = (0, 0, 0)$ (ground state) and $(m, j, w) = (0, 1, 0)$ in the regime III of the $a_3^{(2)}$ model, for $L = 32$, $\gamma = 0.45$, and at zero twist. For comparison we have plotted the lines of imaginary parts $\pm(\frac{\pi}{4} - \frac{\gamma}{4})$



For all the states (m, j) the Bethe equations can be solved at large sizes, leading, from the finite size scaling formulae (1.30) and (1.31) (or rather, equivalent formulae for the eigenenergies $E_{m,j}^{(L)}$), to finite size estimations of the conformal dimensions $x_{m,j} = \Delta_{m,j} + \bar{\Delta}_{m,j} = 2\Delta_{m,j}$ (since, in the $w = 0$ sector, $\Delta = \bar{\Delta}$) or associated effective central charges $c_{m,i} \equiv c - 12x_{m,i}$. After a considerable numerical analysis with system sizes ranging up to $L \sim 5000$ (this time using a C++ script), we end up with the following conjecture at zero twist :

$$-\frac{c_{m,j}}{12} = -\frac{2}{12} + m^2 \frac{\gamma}{4\pi} + (N_{m,j})^2 \frac{A(\gamma)}{[B_{m,j}(\gamma) + \log L]^2}, \quad (3.52)$$

where $N_{m,j} = \frac{3+(-1)^{m+1}}{2} + 2j = 1 + \text{number of Bethe roots } \lambda_i \text{ with } \Im \lambda_i = \frac{\pi}{2}$, and

$$A(\gamma) = \frac{5}{2} \frac{\gamma(\pi - \gamma)}{(\pi - 3\gamma)^2}, \quad (3.53)$$

whereas the functions $B_{m,j}(\gamma)$ (which extend to the more general family of functions $B_{m,j,w}$ when considering sectors of non zero momentum) could not be accessed numerically, but are believed to be indeed universal functions with no L dependence at this order (namely, the only further corrections to (3.75) come from the ‘usual’ terms of order $O(L^{-2})$).

Some conclusions can readily be drawn from these results

- The central charge (at zero twist) is of the form

$$c(L) = c_{0,0}(L) = 2 - \frac{12A(\gamma)}{[B + \log L]^2}, \quad (3.54)$$

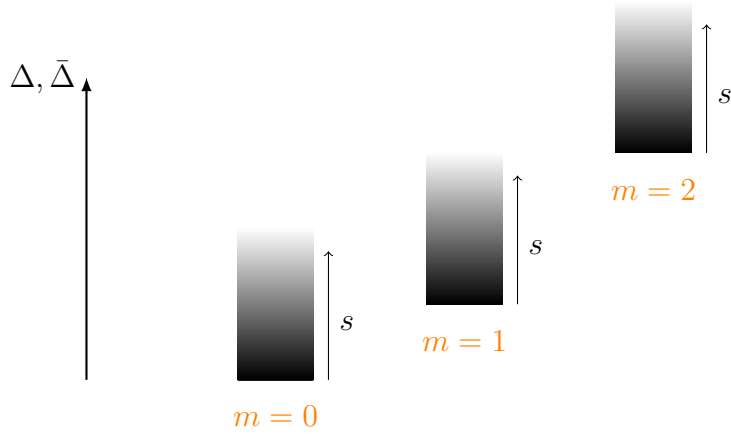
with logarithmic corrections accounting for the lack of convergence observed in the low twist regime.

- The magnetic dependence of the conformal weights is in agreement with the earlier formula (3.50), which we interpreted as the excitation spectrum of a compact bosonic degree of freedom.

Let us now look at the remaining part of the conformal weights, namely, that depending on j . As the continuum limit $L \rightarrow \infty$ is taken, we may replace the discrete index j by some *continuous* index $s = \sqrt{\frac{5}{2}} \frac{\pi - \gamma}{\pi - 3\gamma} \frac{(2j)}{B_j + \log L} \sim \frac{2j}{\log L}$ (the normalization is somewhat arbitrary at this stage), leading to conformal weights of the form

$$x_{m,s} = \frac{\gamma}{4\pi} m^2 + \frac{\gamma}{\pi - \gamma} s^2. \quad (3.55)$$

Qualitatively, the spectrum of conformal dimensions is therefore made of a continuous part and a discrete part:



which could very possibly be interpreted as the signature of a theory made of two bosonic fields, one compact and one *non compact*, namely, of infinite compactification radius. Going back to the Coulomb gas results presented in the analysis of regime I and fixing the coupling constant g rather than the radius R to some fixed normalization, it is indeed straightforwardly seen that taking the limit $R \rightarrow \infty$ results in a vanishing of the gaps associated to different values of the magnetic charge, analogously to what we are observing here.

3.2.3 The black hole CFT

So far, all our results in regime III are very reminiscent of those obtained in the case of the staggered six-vertex model [56, 57], whose continuum limit was identified [58] as the coset $SL(2, \mathbb{R})_k/U(1)$. This CFT was introduced by Witten in the context of two dimensional black holes in string theory [59], and will turn out to be of central importance for our work, so we shall now spend a little time reviewing how it comes about.

Strings in an empty flat, d -dimensional Minkowski space-time with metrics $G_{\mu,\nu} = \eta_{\mu,\nu}$ are described by the action

$$S_0 = -\frac{1}{4\pi\alpha'} \int d^2\sigma \sqrt{-h} h^{\alpha\beta} \partial_\alpha X^\mu \partial_\beta X^\nu G_{\mu\nu}, \quad (3.56)$$

where α' is the string coupling constant (small α' corresponds to the classical limit), the integration is over the world-sheet of the string with metric $h^{\alpha\beta}$, and the variables $X^\mu(\sigma)$, $\mu = 1, \dots, d$, are scalar fields embedding the string world-sheet into the space-time. The action is imposed to be conformally invariant with respect to fluctuations of the world-sheet metric $h_{\alpha,\beta}$, which, in more complicated cases of strings interacting with various backgrounds, imposes consistency conditions on the theory. One of the particularly important challenges of string theory as a candidate for describing quantum gravity is to give a correct review of the physics at very strong gravitational fields, for which the classical description of gravity fails. In particular, much effort has been put in the task of building up consistent string theories in presence of metrics $G_{\mu\nu}$ of the black hole type in two dimensions of space-time, which have proven an efficient laboratory for building up solvable toy-models. In [59], Witten considers the $SL(2, \mathbb{R})_k$ Wess-Zumino-Witten model with action of the form

$$\mathcal{S}_{\text{WZW}} = \frac{k}{8\pi} \int d^2\sigma \sqrt{-h} h^{\alpha\beta} \text{tr} (g^{-1} \partial_\alpha g g^{-1} \partial_\beta g) + ik\Gamma(g), \quad (3.57)$$

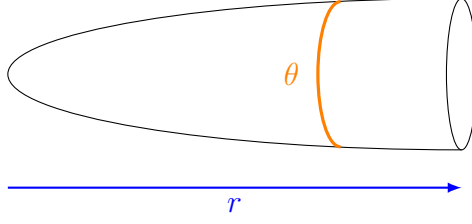


Figure 3.5: The half-infinite cigar shaped target space of the black hole CFT.

where g is some field taking values in $SL(2, \mathbb{R})$, and k some positive integer called the *level* of the theory, whereas the Wess-Zumino term $\Gamma(g)$ ensures the conformal invariance of the action. An abelian $U(1)$ symmetry can be gauged out, at the price of introducing some gauge field A . The gauge is fixed by parametrizing g in terms of two fluctuating fields, r and θ , as

$$g = \cosh r + \sinh r \begin{pmatrix} \cos \theta & \sin \theta \\ \sin \theta & -\cos \theta \end{pmatrix}, \quad (3.58)$$

and the gauge field can be integrated out, yielding the $SL(2, \mathbb{R})_k/U(1)$ model with action

$$\mathcal{S} = \frac{k}{4\pi} \int d^2\sigma \sqrt{-h} h^{\alpha\beta} (\partial_\alpha r \partial_\beta r + \tanh r \partial_\alpha \theta \partial_\beta \theta) + \dots \quad (3.59)$$

This corresponds, up to corrections which involve some *dilaton* field ensuring the conformal invariance of the model, to an action of the type (3.56) with a metric

$$ds^2 = G_{\mu\nu} dX^\mu dX^\nu = dr^2 + \tanh^2 r d\theta^2. \quad (3.60)$$

The metric (3.60) corresponds to the geometry of a semi-infinite cigar (see figure 3.5), and presents, in its Minkowski formulation ($\theta \rightarrow it$), all the required characteristics of a Schwarzschild black hole. In the limit $r \rightarrow \infty$ the cigar is asymptotic to $\mathbb{R} \times \mathcal{S}^1$, and the fields θ and r behave like two decoupled bosonic fields, compact and non compact respectively. For future reference, we point out that the action (3.59) can be rewritten in terms of the complex field $\Psi = \sinh r e^{i\theta}$ as

$$\mathcal{S} = \frac{k}{4\pi} \int d^2x \frac{\partial_\mu \Psi \partial_\mu \bar{\Psi}}{1 + |\Psi|^2} + \dots \quad (3.61)$$

The spectrum of string modes on the cigar background can be put in correspondence with the spectrum of primary fields of the $SL(2, \mathbb{R})/U(1)$ CFT, and we are led to look for eigenwavefunctions $\Psi(r, \theta)$ of the Hamiltonian associated to the action (3.59). These wavefunctions depend on the configurations of the fields r and θ at a given time on the string worldsheet, and some intuition can be gained by first looking at the *mini-superspace approximation* [108], where the spatial dependence of these fields is neglected (in other terms the strings become point-like). As already discussed in the introductory chapter (see section 1.1) the Hamiltonian becomes then a function on the target space itself, more precisely it corresponds to the Laplacian

$$\Delta = -\frac{2}{k} [\partial_r^2 + (\coth r + \tanh r) \partial_r + \coth^2 r \partial_\theta^2]. \quad (3.62)$$

The corresponding (δ function normalizable) eigenwavefunctions are parametrized by two quantum numbers, namely the momentum $J = -\frac{1}{2} + is$, $s \in \mathbb{R}$ along the axis of the cigar

and the angular momentum $n \in \mathbb{Z}$ of rotations around this axis. Going back to the full theory, one has to consider in addition strings that wind around the compact direction of the cigar, hence introducing a winding quantum number w . The conformal weights of the associated primaries therefore read

$$\Delta(\bar{\Delta}) = -\frac{J(J+1)}{k-2} + \frac{(n \pm kw)^2}{4k}. \quad (3.63)$$

Importantly, the true ground state of the Hamiltonian (identity field of the CFT, with central charge $c_{BH} = 2 + \frac{6}{k-2}$), with quantum numbers $J = n = w = 0$, corresponds to a non normalizable wavefunction and is therefore not expected to be observed in the spectrum⁴. Instead, the effective ground state has $J = -\frac{1}{2}$ ($s = 0$), leading to a central charge

$$c = c_{J=-\frac{1}{2}, n=0, w=0} = 2, \quad (3.64)$$

that is the central charge observed in the untwisted regime III $a_2^{(2)}$ model. With respect to this effective ground state, the conformal weights (3.63) get shifted, and we find in the sector $w = 0$

$$x_{n,s,w=0} = \Delta + \bar{\Delta} = \frac{n^2}{2k} + \frac{2s^2}{k-2}, \quad (3.65)$$

which is precisely the expression (3.55) found for the conformal weights in regime III after the identification $\gamma = \frac{2\pi}{k}$.

3.2.4 The density $\rho(s)$ and the discrete states

As it has been hinted from the comparison between (3.55) and (3.65), the conformal spectrum in the regime III with $\gamma = \frac{2\pi}{k}$ looks in many respects very much like that obtained for the $SL(2, \mathbb{R})_k/U(1)$ ‘black hole’ CFT. Remember, however, that in (3.55) an arbitrary normalization has been chosen for the definition of the continuous number s . In order to unambiguously identify the spectrum (3.55) with that of the black hole, one would actually need to compute the corresponding density of states $\rho(s)$, which is the main quantity allowing one to distinguish one theory with a non compact degree of freedom from another. The latter is defined from the relation introduced previously between the discrete quantum number j and the continuous quantum number s in a given magnetization sector, which we recast as

$$2j = \sqrt{\frac{2}{5}} \frac{\pi - 3\gamma}{\pi - \gamma} (B(s) + \log L) s, \quad (3.66)$$

leading to

$$\rho(s) \equiv \frac{\delta j}{\delta s} = \sqrt{\frac{2}{5}} \frac{\pi - 3\gamma}{\pi - \gamma} [\log L + \partial_s(sB(s))], \quad (3.67)$$

to be compared with the known expression of the density of states for the black hole [109],

$$\rho_{BH}(s) = \frac{1}{\pi} [\log \Lambda + \partial_s(sB_{BH}(s))] \quad (3.68)$$

$$B_{BH}(s) = \frac{1}{2s} \text{Im} \log \left[\Gamma \left(\frac{1-n+wk}{2} - is \right) \Gamma \left(\frac{1-n-wk}{2} - is \right) \right]. \quad (3.69)$$

⁴This issue will be put in a more general perspective in section 3.5.2

The different normalizations between (3.67) and (3.68) can of course be reabsorbed in the definition of B . More importantly, ρ_{BH} is made of a finite part and a cutoff Λ , which stems from the introduction of a *Liouville wall* in the cigar target space, and gets straightforwardly translated on the lattice as the finite system size L .

In the staggered six-vertex model, the function $B(s)$ (rather, an analog version thereof, differing from ours by normalization conventions) was estimated [58] in the large s , large m regime from the resolution of Wiener-Hopf equations derived from the Bethe ansatz equations, recovering the asymptotic behaviour of (3.69). This was pushed further in [110], where a set of non-linear integral equations (NLIE) were derived and solved numerically, leading to a perfect agreement between the resulting estimation of $B(s)$ and the black hole prediction. In the case of interest here, unfortunately, such a procedure seems much more difficult to achieve. This is due mostly to the nature of the Bethe roots, whose imaginary parts exhibit strong finite size corrections in regime III while for the staggered six-vertex model they are aligned on real lines. Building up the corresponding set of non-linear integral equations, though feasible, clearly looks like a considerable piece of work, and we here will, in order to identify the continuum limit in regime III as the black hole CFT, use instead an alternative strategy.

A crucial result of the black hole analysis is that on top of the continuous spectrum derived earlier, the latter also allows for *discrete states*, which can be considered as bound states localized near the tip of the cigar and do not show up in the minisuperspace analysis. As a matter of fact these are observed only in $w \neq 0$ sectors, and are associated with the quantum numbers [108, 109]

$$J \in \left[\frac{1-k}{2}, -\frac{1}{2} \right] \cap \left(\mathbb{N} - \frac{1}{2}|kw| + \frac{1}{2}|n| \right). \quad (3.70)$$

The question for us is therefore to check whether these discrete states appear also in the $a_2^{(2)}$ model. As it turns out, this issue is related to the appearance of the twist, which can be justified in the sigma model approach to fix the value of w to

$$w \equiv \frac{\varphi}{2\pi}. \quad (3.71)$$

Let us consider, to start with, the case $n = 0$, and focus on the upper bound of the interval in (3.70). Increasing the twist from $\varphi = 0$, we see that a new discrete state appears whenever there exists an integer $p \in \mathbb{N}$ such that

$$p - \frac{1}{2} \left\lfloor \frac{k\varphi}{2\pi} \right\rfloor \leq -\frac{1}{2}. \quad (3.72)$$

The associated conformal weight leads to the effective central charge

$$\begin{aligned} c_{2p+1} &\equiv c_{J=p-\frac{1}{2}\lfloor \frac{k\varphi}{2\pi} \rfloor, n=0, w=\frac{\varphi}{2\pi}} \\ &= c^* + \frac{6}{\pi^2(k-2)} \left[(2p+1)\pi - k\frac{\varphi}{2} \right]^2, \end{aligned} \quad (3.73)$$

where $c^* \equiv c_{J=-\frac{1}{2}, n=0, w=\frac{\varphi}{2\pi}} = 2 - 6k \left(\frac{\varphi}{\pi} \right)^2$ is the generalization of (3.64) to non zero values of the twist. Going back to the observed results in the $a_2^{(2)}$ case and in particular to equation (3.51) and figure 3.3, this is precisely what we observe : for small φ the state with $p = 0$ is not normalizable, and the lowest energy states of the lattice model are

instead the effective ground state with central charge c^* and the continuum above it. The former becomes normalizable at $\varphi = \frac{2\pi}{k} = \gamma$, where indeed the central charge of the lattice model is observed to ‘pop’ out on the continuum. We could not insist too much on the fact that these two regimes for the central charge are described by *the same eigenlevel* of the lattice model (namely that associated with $(m, j) = (0, 0)$), in particular there are no level crossings or degeneracies involved in the process⁵. The same process is observed for further values of p , namely the state $(m, j) = (0, p)$ becomes discrete, and described by the central charge c_p , for $\varphi \geq (2p + 1)\gamma$. Taking the lower bound of the interval (3.70) back into consideration, we actually see that the discrete level with central charge c_p should disappear when

$$\frac{\varphi}{2\pi} \geq 1 + \frac{2p - 1}{k}, \quad (3.74)$$

that is, precisely when it intersects the first ‘excited winding mode’ where in c^* , instead of taking just φ , we can take $\varphi \pm 2\pi w$, where $w = 1$ is the winding number (corresponding to the electric charge in the Coulomb gas analysis). This whole structure is summed up in figure 3.6, and generalizes easily to nonzero values of the magnetization (or n , in the black hole language), still in perfect agreement with the earlier observations of Nienhuis *et al* [78]. For future reference we write the effective central charges associated with the states (m, j) for $\varphi \leq \pi$, that is, forgetting about the excited winding modes, as

$$c_{m,j}(\varphi) = \begin{cases} c_m^* = 2 - 3\frac{\varphi^2}{\pi\gamma} - \frac{3\gamma m^2}{\pi} & \text{for } \varphi \leq (|m| + 2j + 1)\gamma \\ c_m^* + \frac{3}{\gamma(\pi - \gamma)} [\varphi - (|m| + 2j + 1)\gamma]^2 & \text{for } \varphi \geq (|m| + 2j + 1)\gamma. \end{cases} \quad (3.75)$$

3.2.5 The parafermions

Rather than from the (unachieved) identification of the continuum density of states $\rho(s)$, we have used the discrete states structure of the black hole $SL(2, \mathbb{R})/U(1)$ theory as the evidence for its identification as the continuum limit of the $a_2^{(2)}$ model in regime III. In finite size, the width L of the lattice serves as a cutoff for the sigma model, and the precise expression of the conformal weights (3.75) can be understood from a semi-classical analysis [62].

As we will now see, the discrete states originate for a complementary description of the continuum limit of regime III in terms of a whole different theory, this time related to a coset of the $SU(2)/U(1)$ type. The algebraic intuition for this can be traced back to a duality argument, which we will present in a more general context in section 3.4.1. For the moment, let us simply focus on the conformal spectrum associated with the discrete states for values of the twists where discrete states appear, namely $\varphi = (2p + 1)\gamma = (2p + 1)\frac{2\pi}{k}$, p integer. The lowest of these conformal weights corresponds to the state $(0, 0)$ at $\varphi = \gamma$, that is $p = 0$, and defines the so-called ‘central charge’

$$\tilde{c} \equiv c_{0,0} \left(\frac{\varphi}{2\pi} = \frac{1}{k} \right) = 2 - 3\frac{\gamma}{\pi} = 2 - \frac{6}{k}. \quad (3.76)$$

The other conformal weights, measured with respect to this central charge, are obtained at further values of p from the states $j = 0, \dots, p$, namely

$$\tilde{\Delta}_{2(p-j)}^{2p} \equiv -\frac{c_{0,j} \left(\frac{\varphi}{2\pi} = \frac{2p+1}{k} \right) - \tilde{c}}{24} = \frac{p(p+1)}{k} + \frac{(p-j)^2}{k-2}. \quad (3.77)$$

⁵This is in fact guaranteed by the Perron-Frobenius theorem, as, for instance in the loop representation, the transfer in the sector with zero through-lines is irreducible and has positive real entries.

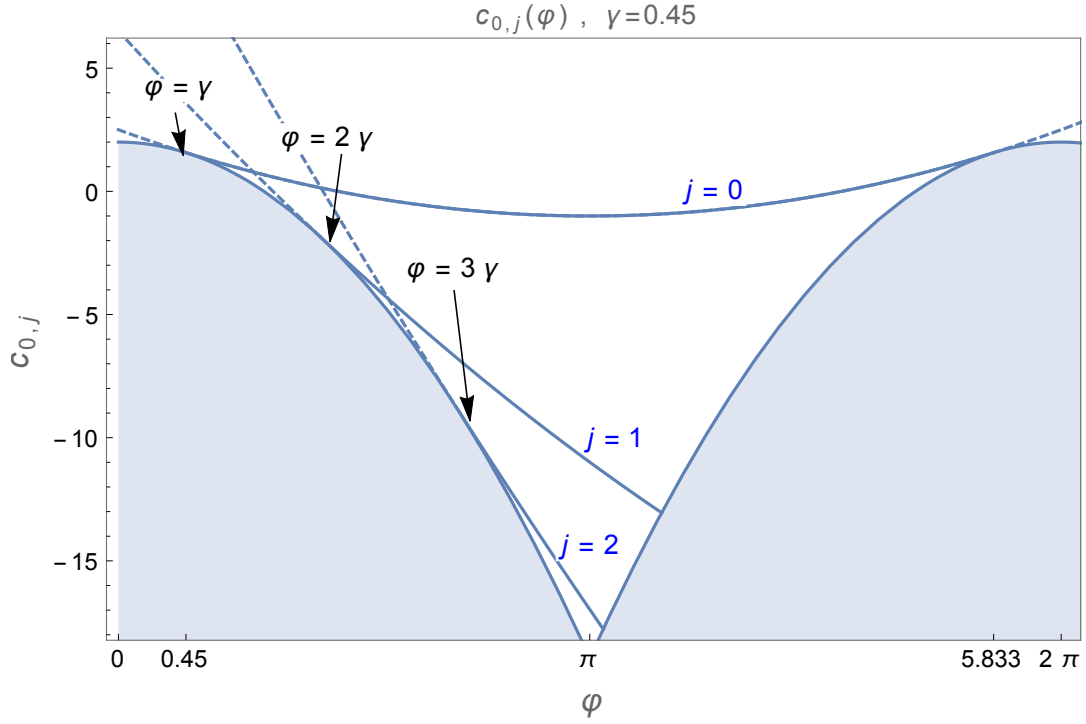


Figure 3.6: Discrete states structure observed in the sector of magnetization $m = 0$ of the $a_2^{(2)}$ model upon varying the twist. Shaded in blue is the continuum of states. The dashed lines correspond to non normalizable states, not present in the spectrum of the lattice model. As φ is increased, the states corresponding to increasing values of j 'pop' out of the continuum and become discrete. Increasing φ further these intersect the modes of excited electric charge and go back to the corresponding continuum.

For integer k , it is easy to recognize the central charge (3.76) and conformal weights (3.77) as those of the Z_{k-2} parafermionic theory [111], which can equivalently be described as the $SU(2)_{k-2}/U(1)$ coset CFT. In particular the exponents $\hat{\Delta}_0^{2p} = \frac{p(p+1)}{k}$ correspond to the so-called parafermionic *thermal fields*.

We therefore conclude from this analysis that the continuum limit of the $a_2^{(2)}$ model in regime III contains in some sense both the properties of the black hole and parafermionic CFTs, associated respectively to conformal cosets of the type $SL(2, \mathbb{R})/U(1)$ (non compact) and $SU(2)/U(1)$ (compact). Even though the precise connection between the two theories lacks a clear explanation, it is interesting to notice that these allow for closely related sigma model descriptions, with respective classical actions

$$\mathcal{S}_{\text{BH}} \propto \int d^2x \frac{\partial_\mu \Psi \partial_\mu \bar{\Psi}}{1 + |\Psi|^2}, \quad \mathcal{S}_{\text{PF}} \propto \int d^2x \frac{\partial_\mu \Psi \partial_\mu \bar{\Psi}}{1 - |\Psi|^2}, \quad (3.78)$$

(see equation (3.61) and reference [112] respectively; by ‘classical action’ we mean that in the black hole case the dilaton term is not included) or metrics

$$(ds^2)_{\text{BH}} \propto \frac{d\rho^2 + \rho^2 d\theta^2}{1 + \rho^2}, \quad (ds^2)_{\text{PF}} \propto \frac{d\rho^2 + \rho^2 d\theta^2}{1 - \rho^2}, \quad (3.79)$$

(see equation (3.60) and reference [113] respectively), where we have used the parametrization $\Psi = \rho e^{i\theta}$, so the correspondence with the black hole coordinates used in the previous section is $\rho = \sinh r$.

3.2.6 Conclusion: the continuum limit of the $a_2^{(2)}$ model

Let us recapitulate our results (recalling that the conclusions on both regimes I and II have been known for a long time [78]) :

- In regime I, the $a_2^{(2)}$ model is described by the conformal field theory of a free compact bosonic field, with a natural interpretation as emerging from the height model defined by the $O(n)$ loops on the square lattice.
- In regime II, this free boson gets supplemented by a decoupled critical Ising degree of freedom (Majorana fermion), interpreted geometrically as living on the empty edges of the square lattice.
- The continuum limit of the far more intriguing regime III is described by the black hole $SL(2, \mathbb{R})/U(1)$ CFT, which involves two coupled bosonic fields, respectively compact and non compact. Whereas it should be possible to relate the former to the one involved in the continuum limit of regimes I and II, the latter has a much more mysterious origin. The question of how to interpret this exotic degree of freedom geometrically will be addressed in a general perspective in section 3.5, and in more detail in the next chapter.

At the same time, we have observed that the continuum limit in regime III can be described in terms of a parafermionic, $SU(2)/U(1)$ CFT, whose precise connection with the former still lacks a precise explanation.

Needless to say, the emergence of a non compact continuum limit in a model where all that remained to be elucidated was mostly thought of in the community as technical

issues rather than fundamental ones comes out quite as a big surprise. As a matter of fact, this big surprise will be for us the beginning of a long story. In the further sections of this chapter, we will study a wealth of different integrable models where similar observations hold. Along with the fundamental importance of these results, we will also see how dramatic the practical consequences of non compact continuum limits can be regarding the experimental or numerical measures of critical exponents or correlation functions.

Going back to the $a_2^{(2)}$ case, there is yet more to the story than what we have presented so far. Indeed, integrable spin chains or vertex models whose continuum limit are identified as a certain CFT are only one particular case of a more general family of models which on the lattice are obtained by an *imaginary* staggering of the spectral parameters, and in the continuum limit correspond to integrable, massive perturbations around that CFT. One should therefore look at the staggered transfer matrices

$$T^{(L)}(u, i\alpha) = \text{diagram of an ellipse with four internal lines labeled } u, i\alpha, -i\alpha, i\alpha \text{ and two external lines labeled } i\alpha, -i\alpha \text{ on the right}, \quad (3.80)$$

(where we insist on the fact that imaginary spectral parameters do not bear the same geometrical interpretation as real ones), and try to understand, in each regime, the nature of the corresponding integrable field theory, that is find in each case an integrable action of the form

$$\mathcal{S} = \mathcal{S}_{\text{CFT}} + g \int d^2x [\Phi], \quad (3.81)$$

where \mathcal{S}_{CFT} can be seen as the UV limit of the perturbed action and $[\Phi]$ denotes an integrable perturbation by one or several relevant operators, whose associated coupling constant g shall ultimately be related to α . In each regime, the effect of an imaginary staggering is directly seen in the integral equations for the Bethe roots densities, where it amounts to a perturbation of the source term and can be related to the mass of the perturbed theory. The nature of the latter can in most cases further be guessed by looking at the scattering kernel involved in the Bethe equations and identifying it with the (derivatives of the) S -matrices of known integrable field theories. We refer to [62, 65] for details and simply present here the results obtained from this analysis.

Integrable perturbations in regime I

In regime I, the action of the perturbed theory is identified as that of the (imaginary) Bullough-Dodd model [114] with action

$$\mathcal{S}_I = \int d^2x (\partial_\mu \Phi)^2 + g \int d^2x (e^{-2i\beta\Phi} + e^{i\beta\Phi}), \quad (3.82)$$

where $\frac{\beta^2}{8\pi} = \frac{\gamma}{2\pi}$, and the coupling g is found to be related to the staggering α by $g \propto e^{-\frac{4}{3}\alpha}$ (the latter relation remains valid in the other regimes). Remember that the CFT part, namely the free bosonic action, is also obtained as the continuum limit of the integrable six-vertex model or the associated XXZ spin chain. We are now able to see where does lie the essential difference between the two models, namely that they correspond to different integrable perturbations around the same CFT (as was mentioned in the previous chapter, the continuum limit of the integrable six-vertex/XXZ/ $a_1^{(1)}$ model is described by the Sine-Gordon model, with action (2.29)).

For future reference, we note that the action (3.82) can also be identified as that of the (imaginary coupling) affine $a_2^{(2)}$ Toda theory [19].

Integrable perturbations in regime II

In regime II, the perturbed action is identified as

$$\mathcal{S}_{\text{II}} = \int d^2x (\partial_\mu \Phi)^2 + \int d^2x \bar{\psi} \gamma^\mu \partial_\mu \psi + g \int d^2x \left(\psi \bar{\psi} e^{-2i\beta' \Phi/2} + e^{i\beta' \Phi} \right), \quad (3.83)$$

where $\frac{(\beta')^2}{8\pi} = 2\frac{\pi-\gamma}{\pi}$. Φ is still a compact bosonic field, while $(\psi, \bar{\psi})$ is a Majorana fermion corresponding to the Ising degree of freedom. For future reference, we note that this identifies with the so-called (imaginary) $b(0, 1)^{(1)}$ Toda theory [115].

Integrable perturbations in regime III

The case of regime III is expectedly quite richer. Since the continuum limit of the lattice model in this regime was shown to present both the features of the $SL(2, \mathbb{R})/U(1)$ black hole and of the $SU(2)/U(1)$ parafermions, we naturally expect that its integrable deformations should bear an interpretation as integrable deformations of both cosets. Meanwhile, the staggered six-vertex model studied in [56, 57, 58] is also described, in the continuum limit, by these two theories. Once again, the two models are therefore expected to correspond to different integrable deformations of these CFTs.

Starting with the parafermionic description, the staggered six-vertex model and the $a_2^{(2)}$ model in regime III are observed [55, 62] to correspond respectively to deformations of the $SU(2)_{k-2}/U(1)$ coset by its first and second thermal operators, of respective dimensions $\tilde{\Delta}_0^2 = \frac{2}{k}$ and $\tilde{\Delta}_0^4 = \frac{6}{k}$. In the sigma model description, these are known from [112] and [V. Fateev, private communication] to be described respectively by the first and second version of the *complex sine-Gordon* model, with actions [116]

$$\mathcal{S}_{\text{CSG}_0} = \int d^2x \left[\frac{\partial_\mu \Psi \partial_\mu \bar{\Psi}}{1 - |\Psi|^2} - m^2 |\Psi|^2 \right], \quad (3.84)$$

$$\mathcal{S}_{\text{CSG}_1} = \int d^2x \left[\frac{\partial_\mu \Psi \partial_\mu \bar{\Psi}}{1 - |\Psi|^2} - m^2 (|\Psi|^2 - |\Psi|^4) \right]. \quad (3.85)$$

Interestingly, the similarity between the $SU(2)/U(1)$ and $SL(2, \mathbb{R})/U(1)$ sigma model descriptions, which are formally mapped onto one another by the transformation $|\Psi|^2 \rightarrow -|\Psi|^2$, extends to the integrable deformations of these cosets. There are indeed two known integrable deformations of the black hole CFT [117], associated respectively with the first and second *complex sinh-Gordon* models with actions

$$\mathcal{S}_{\text{CShG}_0} = \int d^2x \left[\frac{\partial_\mu \Psi \partial_\mu \bar{\Psi}}{1 + |\Psi|^2} + m^2 |\Psi|^2 \right], \quad (3.86)$$

$$\mathcal{S}_{\text{CShG}_1} = \int d^2x \left[\frac{\partial_\mu \Psi \partial_\mu \bar{\Psi}}{1 + |\Psi|^2} + m^2 (|\Psi|^2 + |\Psi|^4) \right], \quad (3.87)$$

and we therefore find natural to associate these two perturbations with the staggered six-vertex model and the $a_2^{(2)}$ model in regime III, respectively. This conjecture is strengthened by the observation that the CShG_0 model has local conserved quantities at all grades, both odd and even, a fact deeply related with the underlying symmetry of the

Z_2 staggered 6-vertex model, whereas CShG₁ has only local conserved quantities at odd grades, in agreement with the fact that there is no extra symmetry to distinguish regime III from the other regimes.

Next, we would be interested in finding a free field formulation of the perturbed action in regime III, as we did in regimes I and II. This can most easily be done starting from the parafermions, which are well known [118] to allow for a Coulomb gas formulation in terms of two bosonic fields Φ and ϕ , respectively compact and non compact. Note that such a free field formulation of the black hole also exists [119], whose precise relationship with the original, cigar-shaped target space is however not perfectly clear (naively, a free field theory made of one compact boson and one non compact boson amounts to a target space $\simeq \mathbb{R} \times \mathcal{S}^1$, and should therefore be supplemented by particular rules satisfied by the fields in order to recover the tip of the cigar). Back to parafermions, it is actually possible [V. Fateev, private communication] to write the $SU(2)/U(1)$ action perturbed by the p^{th} thermal operator as

$$\mathcal{S} = \int d^2x (\partial_\mu \Phi)^2 + \int d^2x (\partial_\mu \phi)^2 + g \int d^2x \left((\partial_\mu \phi)^2 e^{-i\beta''\Phi/2} + e^{ip\beta''\Phi} \right), \quad (3.88)$$

so in particular the bosonized form of the perturbation corresponding to the $a_2^{(2)}$ model in regime III simply reads

$$\mathcal{S}_{\text{III}} = \int d^2x (\partial_\mu \Phi)^2 + \int d^2x (\partial_\mu \phi)^2 + g \int d^2x \left((\partial_\mu \phi)^2 e^{-i\beta''\Phi/2} + e^{i2\beta''\Phi} \right), \quad (3.89)$$

where $\frac{(\beta'')^2}{8\pi} = \frac{2\gamma}{\pi} = \frac{4}{k}$.

3.3 Continuum limit of the $a_3^{(2)}$ model

We now move on to the case of the $a_3^{(2)}$ model, which was shown in section 2.4 to be related to a model of fully-packed loops of two colours on the square lattice. As explained in [92, 64] and reviewed in section 2.4.4, this loop model can in turn be seen as emerging from the geometrical reformulation of a problem of two $Q = n^2$ -states Potts models coupled by the product of their energy operators. Some of the corresponding critical properties have been previously studied in [92], yet leaving behind many unexplained aspects. Similarly to the $a_2^{(2)}$ case the Bethe ansatz analysis which we present in this section (see also [64]) will associate these unexplained features with the exotic, non compact nature of the corresponding continuum limit.

The $a_3^{(2)}$ transfer matrix acts on the tensor product of four-dimensional $U_q(sl_4^{(2)})$ evaluation representations, which may be interpreted as the product of two $U_q(sl_2)$ spin- $\frac{1}{2}$ associated to the two colours of loops. We therefore introduce on each site of the quantum space, as well as on the auxilliary space, two sets of spin- $\frac{1}{2}$ generators $S_{i,(1)}^{(x,y,z)}$, $S_{i,(2)}^{(x,y,z)}$, and write the transfer matrix as

$$T(u) = \text{Tr}_a \left(\check{R}_{a1}(u) \dots \check{R}_{aL}(u) e^{i(2\varphi_1 S_{a,(1)}^{(z)} + 2\varphi_2 S_{a,(2)}^{(z)})} \right), \quad (3.90)$$

where the \check{R} matrix (2.119) is given in its vertex formulation in reference [64], and we have introduced two independent twist parameters φ_1 , φ_2 associated respectively with the two colours (the model is invariant under $\varphi_1 \rightarrow -\varphi_1$, or $\varphi_2 \rightarrow -\varphi_2$, so we will restrict to

positive values of these twists). For further reference we point out that the \check{R} matrix has a symmetry $U_q(c_2) = U_q(sp(4))$, which is a subalgebra of $U_q(a_3^{(2)})$. The transfer matrix (3.90) commutes independently with the two magnetizations

$$\begin{aligned} m^{(1)} &= \sum_{i=1}^L S_{i,(1)}^{(z)} \\ m^{(2)} &= \sum_{i=1}^L S_{i,(2)}^{(z)}, \end{aligned} \quad (3.91)$$

(with two symmetries $m^{(1)} \rightarrow -m^{(1)}$, $m^{(2)} \rightarrow -m^{(2)}$, allowing us once again to restrict ourselves to $m^{(1)} \geq 0$, $m^{(2)} \geq 0$) and its eigenvalues in the sector $(m^{(1)}, m^{(2)})$ are described a set of roots of two types $\{\lambda_j^{(1)}, \lambda_k^{(2)}\}_{j=1,\dots,m_1; k=1,\dots,m_2}$, whose numbers m_1, m_2 are related to the magnetizations through

$$\begin{aligned} m^{(1)} &= \frac{L}{2} - m_1 + m_2 \\ m^{(2)} &= \frac{L}{2} - m_2, \end{aligned} \quad (3.92)$$

and which are solution of a set of nested Bethe ansatz equations

$$\begin{aligned} e^{2i\varphi_1} \left(\frac{\sinh(\lambda_i^{(1)} - i\frac{\gamma}{2})}{\sinh(\lambda_i^{(1)} + i\frac{\gamma}{2})} \right)^L &= \prod_{j=1, j \neq i}^{m_1} \frac{\sinh(\lambda_i^{(1)} - \lambda_j^{(1)} - i\gamma)}{\sinh(\lambda_i^{(1)} - \lambda_j^{(1)} + i\gamma)} \prod_{k=1}^{m_2} \frac{\sinh(2(\lambda_i^{(1)} - \lambda_k^{(2)} + i\frac{\gamma}{2}))}{\sinh(2(\lambda_i^{(1)} - \lambda_k^{(2)} - i\frac{\gamma}{2}))} \\ e^{2i(\varphi_1 - \varphi_2)} \prod_{j=1}^{m_1} \frac{\sinh(2(\lambda_k^{(2)} - \lambda_j^{(1)} - i\frac{\gamma}{2}))}{\sinh(2(\lambda_k^{(2)} - \lambda_j^{(1)} + i\frac{\gamma}{2}))} &= \prod_{l=1, l \neq k}^{m_2} \frac{\sinh(2(\lambda_k^{(2)} - \lambda_l^{(2)} - i\gamma))}{\sinh(2(\lambda_k^{(2)} - \lambda_l^{(2)} + i\gamma))}. \end{aligned} \quad (3.93)$$

The corresponding energies read

$$E = \pm \sum_{i=1}^{m_1} \frac{2 \sin \gamma}{2 \cosh 2\lambda_i^{(1)} - \cos \gamma}. \quad (3.94)$$

Similarly as what was observed for the $a_2^{(2)}$ model, there are once again two isotropic values of the spectral parameter $u_{\pm} = 2\gamma \mp \frac{\pi}{2}$ corresponding to local maxima of the Bethe ansatz eigenvalues and which we expect to be described by a different physics. We however have here an extra symmetry, as equations (3.93) and (3.94) are invariant under the simultaneous change $\gamma \rightarrow \pi - \gamma$ and shift of the roots $\{\lambda_j^{(1)}\}$ by $i\frac{\pi}{2}$, together with a change of the global sign in front of (3.94). This restricts the range of values of γ to be studied to $[0, \frac{\pi}{2}]$ together with the two signs of the energy (or the two isotropic values of u), and it turns out that as in $a_2^{(2)}$ three regimes have to be considered

- Regime I corresponds to the isotropic point $u = u_+$, or equivalently the sign $+$ in the energy (3.94)
- Regime II corresponds to the isotropic point $u = u_-$ (sign $-$ in (3.94)), and $\gamma \in [\frac{\pi}{4}, \frac{\pi}{2}]$
- Regime III corresponds to the isotropic point $u = u_-$ (sign $-$ in (3.94)), and $\gamma \in [0, \frac{\pi}{4}]$.

These three regimes can be studied in the same fashion as what we did in the $a_2^{(2)}$ case, and will be presented here with less emphasis on the technical details.

3.3.1 Continuum limit in regimes I and II

Regime I

The ground state in regime I lies in the zero magnetization sector, and is described by a set of L roots $\lambda^{(1)}$ on the axis of imaginary part $\frac{\pi}{2}$ and $\frac{L}{2}$ roots $\lambda^{(2)}$ on the axis of imaginary part $\frac{\pi}{4}$. The scattering equations for the corresponding densities of real parts read

$$\begin{pmatrix} \rho^{(1)} + \rho_h^{(1)} \\ \rho^{(2)} + \rho_h^{(2)} \end{pmatrix} = \begin{pmatrix} s^{(1)} \\ s^{(2)} \end{pmatrix} + K \begin{pmatrix} \rho^{(1)} \\ \rho^{(2)} \end{pmatrix}, \quad (3.95)$$

where in the zero frequency limit

$$1 - K = \frac{2\gamma}{\pi} \begin{pmatrix} 1 & -1 \\ -1 & 2 \end{pmatrix}, \quad (3.96)$$

which is proportional to the Cartan matrix of $c_2 = sp(4)$. From numerical study and analysis of (3.95), we get the central charge

$$c = 2 - \frac{6(\varphi_1^2 + \varphi_2^2)}{\pi\gamma} \quad (3.97)$$

and conformal weights

$$\Delta + \bar{\Delta} = \frac{\pi}{2\gamma} [(w_1 + w_2)^2 + w_1^2] + \frac{\gamma}{2\pi} [(n_1 - n_2)^2 + n_2^2], \quad (3.98)$$

where $n_1 = m^{(1)} + m^{(2)}$ and $n_2 = m^{(2)}$ are the changes in the number of roots $\lambda^{(1)}$ and $\lambda^{(2)}$ and w_1, w_2 are the corresponding backscatterings with respect to the ground state distribution. Therefore we can rewrite

$$\Delta + \bar{\Delta} = \frac{\pi}{2\gamma} ((m^{(1)})^2 + (m^{(2)})^2) + \frac{\gamma}{2\pi} ((w^{(1)})^2 + (w^{(2)})^2), \quad (3.99)$$

so the conformal spectrum in regime I is simply that of two decoupled free compact bosons with the same radius. These bear a simple geometrical interpretation as emerging from the two Coulomb gas constructions associated with the two colours of fully packed loops.

Turning to the massive deformations obtained by switching on an imaginary staggering $\pm i\alpha$ further identifies the corresponding perturbed field theory as the $a_3^{(2)}$ Toda field theory [19], which is a theory of two compact bosonic fields Φ_1, Φ_2 with action

$$\mathcal{S}_I = \int d^2x (\partial_\mu \Phi_1)^2 + \int d^2x (\partial_\mu \Phi_2)^2 + g \int d^2x \left(e^{-i\beta\sqrt{2}\Phi_1} + e^{i\beta\sqrt{2}(\Phi_1+\Phi_2)} + e^{i\beta\sqrt{2}\Phi_2} \right), \quad (3.100)$$

where $\frac{\beta^2}{8\pi} = \frac{\gamma}{2\pi}$, and $g \propto e^{-\frac{4}{3}\alpha}$ (same relation as in $a_2^{(2)}$).

Regime II

In regime II, the ground state is now described by a set of $\frac{L}{2}$ two-strings of roots $\lambda^{(1)}$ with imaginary parts close to (slightly smaller in absolute value than) $\pm(\frac{\pi}{4} - \frac{\gamma}{2})$ and $\frac{L}{2}$ roots $\lambda^{(2)}$ on the axis of imaginary part $\frac{\pi}{4}$. We write $\lambda_j^{(1)} = x_j \pm i(\frac{\pi}{4} - \frac{\gamma}{2} + \epsilon_\pm)$, with ϵ_\pm decreasing exponentially with L , and $\lambda_k^{(2)} = y_k + i\frac{\pi}{4}$. The second set of Bethe ansatz

equations (3.93) shows that $\epsilon_+ = \epsilon_-$, which allows to simplify in the large L limit the product of conjugate equations of the first set into

$$e^{4i\varphi_1} \left(\frac{\sinh\left(\lambda_i^{(1)} + i\left(\frac{\pi}{4} - \gamma\right)\right) \sinh\left(\lambda_i^{(1)} - i\frac{\pi}{4}\right)}{\sinh\left(\lambda_i^{(1)} - i\left(\frac{\pi}{4} - \gamma\right)\right) \sinh\left(\lambda_i^{(1)} + i\frac{\pi}{4}\right)} \right)^L = \prod_{j=1, j \neq i}^{m_1} \frac{\cosh(\lambda_i^{(1)} - \lambda_j^{(1)} - i\gamma) \cosh(\lambda_i^{(1)} - \lambda_j^{(1)} + 2i\gamma) \sinh(\lambda_i^{(1)} - \lambda_j^{(1)} + i\gamma)}{\cosh(\lambda_i^{(1)} - \lambda_j^{(1)} + i\gamma) \cosh(\lambda_i^{(1)} - \lambda_j^{(1)} - 2i\gamma) \sinh(\lambda_i^{(1)} - \lambda_j^{(1)} - i\gamma)} \quad (3.101)$$

We are therefore left in the continuum limit with a scalar equation over the density $\rho^{(1)}$ of 2-strings centers, namely

$$\rho^{(1)} + \rho_h^{(1)} = s + K \rho^{(1)}, \quad (3.102)$$

where in the zero frequency limit $K = \frac{4\gamma}{\pi} - 3$, hence the conformal spectrum

$$\Delta + \bar{\Delta} = \left(1 - \frac{\gamma}{\pi}\right) n_1^2 + \frac{1}{4\left(1 - \frac{\gamma}{\pi}\right)} w_1^2, \quad (3.103)$$

where n_1 and w_1 respectively count the number of holes and backscatterings of the sea of 2-strings. In particular, n_1 holes means $2n_1$ holes of $\lambda^{(1)}$ roots and n_1 holes of $\lambda^{(2)}$ roots, so we expect $m^{(1)} = m^{(2)} = n_1$. Since on the other hand the model is symmetric under the exchange of two colours ($m^{(1)} \leftrightarrow m^{(2)}$), and using a similar reasoning for the backscattering part, we therefore expect

$$\Delta + \bar{\Delta} = \frac{\pi - \gamma}{2\pi} ((m^{(1)})^2 + (m^{(2)})^2) + \frac{\pi}{2(\pi - \gamma)} ((w^{(1)})^2 + (w^{(2)})^2). \quad (3.104)$$

Meanwhile, the central charge is given by

$$c = 2 - \frac{6(\varphi_1^2 + \varphi_2^2)}{\pi(\pi - \gamma)}, \quad (3.105)$$

so this is simply the analytic continuation of regime I through $\gamma \rightarrow 1 - \gamma$, and we similarly expect that the same conclusions can be made about the corresponding massive deformations.

3.3.2 Continuum limit in regime III

Parallely to what was observed in the $a_2^{(2)}$ model, the Bethe roots structure describing regime III is analogue to that describing regime II, except for the sign of the two-strings imaginary parts deviations, with important consequences on the analyticity properties of the Bethe equations kernels. The discussion on the scattering equations is similar as that in regime II, and the scattering kernel now has a zero frequency limit $K = 1 - \frac{4\gamma}{\pi}$, hence the conformal spectrum

$$\Delta + \bar{\Delta} = \frac{\gamma}{\pi} n_1^2 + \frac{\pi}{4\gamma} w_1^2, \quad (3.106)$$

which can be rewritten in terms of the two colours quantum numbers as

$$\Delta + \bar{\Delta} = \frac{\gamma}{2\pi} ((m^{(1)})^2 + (m^{(2)})^2) + \frac{\pi}{2\gamma} ((w^{(1)})^2 + (w^{(2)})^2). \quad (3.107)$$

While the conformal weights (3.107) have once again the form of those of a theory of two compact bosons, the central charge in regime III is found to be at zero twist $c = 3$, hence leaving room for another, unidentified, degree of freedom.

As in the $a_2^{(2)}$ case, we search for an interpretation of this missing part in the analysis of the low-lying excitations, and the story turns out to look very much the same: in each (m_1, m_2) sector excited states can be formed by replacing 2-strings of $\lambda^{(1)}$ roots by ‘antistrings’, namely pairs of $\lambda^{(1)}$ roots with imaginary part $\frac{\pi}{2}$. Restricting to the sector with $w_1 = w_2 = 0$ we therefore label the low-lying eigenstates by three integers $(m^{(1)}, m^{(2)}, j)$, and find from numerical resolution of the Bethe equations the following spectrum of effective central charges at zero twist

$$-\frac{c_{m^{(1)}, m^{(2)}, j}}{12} = -\frac{3}{12} + \frac{\gamma}{2\pi} (m^{(1)} + m^{(2)})^2 + (N_{m^{(1)}, m^{(2)}, j})^2 \frac{A(\gamma)}{[B_{m^{(1)}, m^{(2)}, j}(\gamma) + \log L]^2}, \quad (3.108)$$

with quite strong numerical support for the following conjectures:

$$A(\gamma) = 10 \frac{\gamma(\pi - \gamma)}{(\pi - 4\gamma)^2}, \quad (3.109)$$

$$N_{m^{(1)}, m^{(2)}, j} = 1 + [\text{number of } \lambda^{(1)}\text{-roots with imaginary part } \frac{\pi}{2}]. \quad (3.110)$$

The numerical support for the functional dependence of $A(\gamma)$ on γ is very strong, whereas the determination of the proportionality factor 10 is slightly more hazardous, and as in the $a_2^{(2)}$ case precise determination of the $B_{n_1, n_2, j}(\gamma)$ functions is beyond the scope of our numerical accuracy. The conformal spectrum in the $L \rightarrow \infty$ limit is therefore made of two discrete and one continuous components, and should then expectedly described by some field theory involving two compact and one non compact bosonic fields. Following the lines of what was done in the $a_2^{(2)}$ case, it should be guessed at this stage that a lot of insight can now be gained by investigating the effect of turning on the twists on the conformal weights.

For simplicity let us first look at the ground state, namely the state with $(m^{(1)}, m^{(2)}, j) = (0, 0, 0)$. Investigating numerically the central charge, we find the following result

$$c = c_{0,0,0} = \begin{cases} 3 - 6 \frac{(\varphi_1)^2 + (\varphi_2)^2}{\pi\gamma} + o(1) & \text{for } \varphi_1 + \varphi_2 \leq \gamma, \\ 3 - 6 \frac{(\varphi_1)^2 + (\varphi_2)^2}{\pi\gamma} + 3 \frac{(\varphi_1 + \varphi_2 - (2j+1)\gamma)^2}{\gamma(\pi - \gamma)} & \text{for } \varphi_1 + \varphi_2 \geq \gamma, \end{cases} \quad (3.111)$$

where $o(1)$ indicates for the logarithmic corrections explicited in (3.108), and which disappear in the $\varphi_1 + \varphi_2 \geq \gamma$ regime. Needless to say, this is highly similar to what was observed in $a_2^{(2)}$ case. Extending this study to the full low-lying spectrum yields

$$c_{m^{(1)}, m^{(2)}, j} = \begin{cases} c_{m^{(1)}, m^{(2)}}^* + o(1) = 3 - 6 \frac{((m^{(1)})^2 + (m^{(2)})^2)\gamma}{\pi} - 6 \frac{(\varphi_1)^2 + (\varphi_2)^2}{\pi\gamma} + o(1) & \text{for } \varphi_1 + \varphi_2 \leq (m^{(1)} + m^{(2)} + 2j + 1)\gamma, \\ c_{m^{(1)}, m^{(2)}}^* + 3 \frac{(\varphi_1 + \varphi_2 - (m^{(1)} + m^{(2)} + 2j + 1)\gamma)^2}{\gamma(\pi - \gamma)} & \text{for } \varphi_1 + \varphi_2 \geq (m^{(1)} + m^{(2)} + 2j + 1)\gamma. \end{cases}$$

This spectrum can be conveniently interpreted by setting $m_{\pm} \equiv m^{(1)} \pm m^{(2)}$, $\varphi_{\pm} \equiv \varphi_1 \pm \varphi_2$, such that we can write $c_{m^{(1)}, m^{(2)}, j} = c_{m_-} + c_{m_+, j}$, where

$$c_{m_-}(\varphi_-) = 1 - 3 \frac{(\varphi_-)^2}{\pi\gamma} - 3 \frac{\gamma(m_-)^2}{\pi}, \quad (3.112)$$

which is straightforwardly associated with the contribution from a free compact boson, and

$$c_{m_+}(\varphi_+) = \begin{cases} c_{m_+}^* + o(1) = 2 - 3\frac{(\varphi_+)^2}{\pi\gamma} - 3\frac{\gamma(m_+)^2}{\pi} + o(1) & \text{for } \varphi_+ \leq (m_+ + 2j + 1)\gamma \\ c_{m_+}^* + 3\frac{(\varphi_+ - (m_+ + 2j + 1)\gamma)^2}{\pi(\pi - \gamma)} & \text{for } \varphi_+ \geq (m_+ + 2j + 1)\gamma, \end{cases} \quad (3.113)$$

which has exactly the structure of the discrete levels found for the black hole CFT in the continuum limit of the $a_2^{(2)}$ model in regime III, see equation (3.75).

As a conclusion, the continuum limit of the $a_3^{(2)}$ model in regime III is therefore the association of one $SL(2, \mathbb{R})/U(1)$ black hole, and one decoupled compact boson. Note that the dependence of the effective central charges in the quantum numbers m_- and m_+ is the same, which means that the two compact bosons (that involved in the black hole, and the decoupled one) have moreover the *same radius*. We can now go further and look for a free field action associated with integrable massive deformations of this model, labeling the compact fields Φ_+ and Φ_- and the non compact one ϕ_+ , in a natural way. Analysis of the Bethe ansatz equations suggests that the perturbed action should be of the form

$$\mathcal{S}_{\text{III}} = \int d^2x (\partial_\mu \Phi_-)^2 + \int d^2x (\partial_\mu \Phi_+)^2 + \int d^2x (\partial_\mu \phi_+)^2 \quad (3.114)$$

$$+ g \int d^2x \left((1, 1)e^{-i\beta''\Phi_+} + (1, 1)e^{i\beta''\Phi_-} + e^{i\beta''(\Phi_+ - \Phi_-)} \right), \quad (3.115)$$

where $\frac{(\beta'')^2}{4\pi} = \frac{\gamma}{\pi}$, and each $(1, 1)$ denotes for a field of dimensions $(\Delta, \bar{\Delta}) = (1, 1)$ with a non vanishing two point function. It should be possible to write such fields as combinations of the derivatives of the fields Φ_\pm , ϕ_+ , the precise form of which is fixed by imposing perturbatively the integrability of the theory. We will, however, not go any deeper into this matter here.

3.4 General solution of the $a_n^{(2)}$ chains

The $a_2^{(2)}$ and $a_3^{(2)}$ models are part of the more general series of $a_n^{(2)}$ integrable models, which we want to introduce now.

For this sake, we look back at the Birman–Wenzl–Murakami (BWM) algebra introduced in section 2.4.4, and in particular at the integrable trigonometric \check{R} matrices that can be built out of the $SO(N)$ BWM generators, (2.118). Using the level-rank duality there are actually two of them, which we write in terms of the multiplicative spectral parameter $x \equiv e^{iu}$ as

$$\begin{aligned} \check{R}^{(1)} &\propto 1 + \frac{x-1}{x+1} \frac{q^{N-2} + x}{q^{N-2} - x} E + \frac{x-1}{x+1} \frac{1}{q - q^{-1}} (B + B^{-1}) \\ \check{R}^{(2)} &\propto 1 + \frac{x-1}{x+1} \frac{q^N - x}{q^N + x} E + \frac{x-1}{x+1} \frac{1}{q - q^{-1}} (B + B^{-1}). \end{aligned} \quad (3.116)$$

We can consider these \check{R} matrices as acting on the product of the fundamental, N -dimensional representations of $SO(N)$. The cases N even and N odd then have to be distinguished :

- for $N = 2n$ even, both \check{R} matrices commute with the action of the quantum group $U_q(c_n) = U_q(sp(2n))$
 - $\check{R}^{(1)}$ is associated with the integrable $c_n^{(1)}$ model
 - $\check{R}^{(2)}$ is associated with the integrable $a_{2n-1}^{(2)}$ model (we recall that $U_q(c_n)$ is the maximal finite dimensional subalgebra of $U_q(a_{2n-1}^{(2)})$)
- for $N = 2n + 1$ even, both \check{R} matrices commute with the action of the quantum group $U_q(b_n) = U_q(so(2n + 1))$
 - $\check{R}^{(1)}$ is associated with the integrable $b_n^{(1)}$ model
 - $\check{R}^{(2)}$ is associated with the integrable $a_{2n}^{(2)}$ model (we recall that $U_q(b_n)$ is the maximal finite dimensional subalgebra of $U_q(a_{2n}^{(2)})$)

We here consider the series of $a_{N-1}^{(2)}$ models, inspired by our earlier observations on the $N = 3$ and $N = 4$ cases. The Bethe equations for the $a_{2n-1}^{(2)}$ and $a_{2n}^{(2)}$ models involve n families of roots, $\{\lambda_{i_1}^{(1)}, \dots, \lambda_{i_n}^{(n)}\}$, and the associated eigenvalues take the form

$$E_{\pm} = \pm \sum_{i_1} \frac{\sin \gamma}{\cosh 2\lambda_{i_1}^{(1)} - \cos \gamma}. \quad (3.117)$$

As in the $a_3^{(2)}$ case, in all the $a_{2n-1}^{(2)}$ models a transformation $\gamma \rightarrow \pi - \gamma$ combined with a global shift of the $\lambda_{i_1}^{(1)}$ roots by $i\frac{\pi}{2}$ is equivalent to a change the sign in front of the energy (3.117), hence restricting the range of values of γ to study to $[0, \frac{\pi}{2}]$, together with the two possible signs of the Hamiltonian. In contrast, no such symmetry is present in the $a_{2n}^{(2)}$ models, where we instead have to consider $\gamma \in [0, \pi]$ together with the two possible signs of the Hamiltonian.

In each case, we will get to consider three regimes, whose definition generalizes those of the $a_2^{(2)}$ and $a_3^{(2)}$ models: for $a_{N-1}^{(2)}$ with $N = 2n$ even,

- Regime I corresponds to a plus sign in the energy (3.117), and $\gamma \in [0, \frac{\pi}{2}]$.
- Regime II corresponds to a minus sign in the energy, and $\gamma \in [\frac{\pi}{N}, \frac{\pi}{2}]$.
- Regime III corresponds to a minus sign in the energy, and $\gamma \in [0, \frac{\pi}{N}]$,

while for $a_{N-1}^{(2)}$ with $N = 2n + 1$ odd,

- Regime I corresponds to a plus sign in the energy, and $\gamma \in [0, \pi]$.
- Regime II corresponds to a minus sign in the energy, and $\gamma \in [\frac{\pi}{N}, \pi]$.
- Regime III corresponds to a minus sign in the energy, and $\gamma \in [0, \frac{\pi}{N}]$.

The analysis of the Bethe equations similar to that presented in the $N = 3$ and $N = 4$ cases in the previous sections has been extended to $N = 5$ and $N = 6$, and we refer to [65] for details. Before presenting the resulting conjectures in each regime, a few general observations can be made.

3.4.1 Duality arguments for a non compact regime

Setting $q = e^{i\frac{\pi}{N+\tilde{N}-2}}$, N, \tilde{N} integers, the level-rank duality allows for a mapping between the \check{R} matrices built respectively from the $SO(N)$ and $SO(\tilde{N})$ algebras, namely

$$\check{R}^{(2)}, SO(N), x \longleftrightarrow \check{R}^{(1)}, SO(\tilde{N}), x^{-1}. \quad (3.118)$$

This mapping is only algebraic, as the two models for $N \neq \tilde{N}$ do not involve the same representations of the BWM generators, and therefore do not act on the same space of states. Moreover the \check{R} matrices correspond to a very particular choice of ‘gauge’ in the Yang–Baxter equation, which should result in a particular choice of the twist angle when considering the periodic integrable models built out of them. As it turns out, and as we will check explicitly in the $N = 3$ case, the equivalence can however be made rigorous by shifting to the quantum group restricted, solid-on-solid (RSOS) formulations of the corresponding models (see for instance [41]). These are built using the underlying quantum group structure by attaching *heights* encoding the quantum group representations to faces of the square lattice (or sites of the dual square lattice), so that the global choice of heights around each face of the dual lattice is coherent with the quantum group fusion rules and the corresponding face weights are obtained by a quantum analog of the 6j symbols [120]. In the $a_2^{(2)}$ case for instance we use the fact that each edge carries a spin one representation of the $U_q(sl_2)$ subalgebra ($q^2 = q$), and rephrase the decomposition of the \check{R} matrix over projectors over the representations of spin 0, 1 and 2 in the height language. Because of the peculiar features of the $U_q(sl_2)$ representation theory at q root of unity [32], the set of possible heights on each site for $q^2 = e^{i\frac{\pi}{N+\tilde{N}-2}} = e^{i\frac{\pi}{\tilde{N}+1}}$ is restricted to the set of (half-) integers ranging between 0 and \tilde{N} . Note that this algebraic construction differs from the geometrical one proposed in [129]. There, the loops of the equivalent $O(n)$ model are oriented and heights are assigned to the faces of the square lattice such that the heights of faces separated by a loop segment differ by ± 1 , according to the orientation of the latter. Whereas the algebraic and geometric constructions are equivalent in the spin- $\frac{1}{2}$ (fully packed loops) case, they differ in more general cases. The latter actually requires a loop weight $n = 2\cos(\pi/p)$, where $p = 3, 4, \dots$ is an integer, so in particular $n \geq 1$, which is clearly not the case in the regime III of $a_2^{(2)}$ (where we recall that $n = -2\cos 2\gamma < 1$). In particular, we insist on the fact that the weight of the algebraic RSOS constructoin for the $a_2^{(2)}$ model in regime III are all *positive*.

In the general case we will simply assume that a similar algebraic construction holds, and that the corresponding subset of eigenvalues does not lie too deep in the spectrum of the vertex model. All in all, we will use the RSOS equivalence (3.118) mainly as a hint for the vertex models’ continuum limit.

As it turns out, the quantum group restricted models associated with $\check{R}^{(1)}$, that is, the $SO(\tilde{N})^{(1)}$ models for $q = e^{i\frac{\pi}{N+\tilde{N}-2}}$, are believed to be described in the continuum limit by the diagonal conformal cosets

$$\frac{SO(\tilde{N})_1 \times SO(\tilde{N})_{N-1}}{SO(\tilde{N})_N}, \quad (3.119)$$

with central charge

$$c = \frac{\tilde{N}}{2} \frac{(N-1)(N+2\tilde{N}-4)}{(N+\tilde{N}-2)(N+\tilde{N}-3)} \quad (3.120)$$

We therefore conjecture that, in some regime, the (quantum group restricted) $a_{N-1}^{(2)}$ models should also be described by such cosets. Since for all this to make sense we need $\tilde{N} \geq 2$, it is natural to believe that the regime in question should actually correspond to $\gamma \in [0, \frac{\pi}{N}]$, which seems to identify with the regimes III observed previously in the $N = 3$ and $N = 4$ cases.

The $N = 3$ case: $a_2^{(2)}$ and parafermions

Before going any further, let us check all this guesswork against numerical investigation of the $N = 3$ case. The $a_2^{(2)}$ transfer matrix is implemented in its RSOS formulation numerically, and diagonalized for sizes ranging up to $L = 14$, for $\mathbf{q} = e^{i\frac{\pi}{k}}$, $k = 6, 7, 8, 9, 10$. Without any numerical ambiguity, we find in the region corresponding to regime III the central charge

$$c = 2 - \frac{6}{k}, \quad (3.121)$$

which is the central charge of the Z_{k-2} parafermionic theories and coincides with the case $N = 3$ of (3.120) once made the identification $k = 2(\tilde{N} + 1)$. Although the duality argument only applies to \tilde{N} integer, so k even, it is natural to expect that there is nothing special with parafermionic theories with even index, which is indeed confirmed numerically. The equivalence with parafermions is actually made complete by checking that the low-lying levels of the RSOS model indeed reproduce all the parafermionic conformal dimensions. These levels can alternatively be obtained as a subset of the vertex model eigenlevels for specific values of the twist, more precisely we observe that these coincide with the discrete levels ($m = 0, j = 0, \dots, p$) for twists of the form $\varphi = (2p + 1)\frac{2\pi}{k}$ (p integer), which we showed in section 3.2.5 that they indeed reproduce the parafermionic conformal spectrum.

The $N = 4$ case: $a_3^{(2)}$ and the $\frac{SU(2) \times SU(2)}{SU(2)}$ coset

A RSOS formulation can similarly be built for the $a_3^{(2)}$ model, and we expect that its conformal spectrum should similarly be described by the coset

$$\frac{SO(\tilde{N})_1 \times SO(\tilde{N})_3}{SO(\tilde{N})_4}, \quad (3.122)$$

which, anticipating on next paragraph's general discussion, we can reformulate as the coset

$$\frac{SO(4)_{\tilde{N}}}{SO(3)_{\tilde{N}}} = \frac{SU(2)_{\tilde{N}} \times SU(2)_{\tilde{N}}}{SU(2)_{2\tilde{N}}}, \quad (3.123)$$

whose central charge and conformal weights are given in [130]. The relation between the $a_3^{(2)}$ model (in its loop formulation) and the cosets (3.123) was already pointed out in [92]. Rather than studying the details of the RSOS model, let us simply use our Bethe ansatz analysis of the conformal spectrum, and study, to start with, the effective central charge resulting from the (discrete) state ($m^{(1)} = 0, m^{(2)} = 0, j = 0$) for twists $\varphi_1 = \varphi_2 = \gamma$. Recalling the parametrization $q = e^{i\frac{\pi}{\tilde{N}+2}}$ the latter reads from (3.112)

$$\tilde{c} = c_{0,0,0}(\varphi_1 = \varphi_2 = \gamma) = \frac{3\tilde{N}^2}{(\tilde{N} + 1)(\tilde{N} + 2)}, \quad (3.124)$$

which is precisely the central charge of the (3.123) coset, also obtained from (3.120). Going further, all the conformal weights of this coset, given by [130]

$$h_{r,s} = \frac{\left[2r(\tilde{N}+1) - r(\tilde{N}+2)\right]^2 - \tilde{N}^2}{8\tilde{N}(\tilde{N}+1)(\tilde{N}+2)} + \frac{t(\tilde{N}-t)}{2\tilde{N}(\tilde{N}+2)}, \quad \begin{cases} 1 \leq r \leq \tilde{N}+1 \\ 1 \leq s \leq 2\tilde{N}+1 \\ t = |(r-s) \bmod 2|, 0 \leq t \leq \tilde{N} \end{cases}, \quad (3.125)$$

can be obtained from the appropriately twisted discrete states of the $a_3^{(2)}$ model, measured with respect to the central charge (3.124), namely we find

$$h_{r,s} = \begin{cases} \Delta_{r,r-s+1,r-s} & \text{for } s \leq r \\ \Delta_{r,s-r+1,0} & \text{for } s \geq r \end{cases}, \quad (3.126)$$

where $\Delta_{p_1,p_2,j} \equiv -\frac{1}{24}(c_{0,0,j}(\varphi_1 = p_1\gamma, \varphi_2 = p_2\gamma) - \tilde{c})$. That this particular set of states for this very set of particular indeed constitutes the spectrum of the $a_3^{(2)}$ model in its RSOS formulation, although not checked explicitly, leaves very little doubt.

The general case: conformal duality, and Coulomb-gas description

Having checked the duality of quantum restricted models in the $N = 3$ case (and more superficially in the $N = 4$ case), we can now move back to the general case and assume this equivalence still holds. As it is usually the case, it is natural to look for representations of the corresponding continuum limits in terms of a set of free bosonic and/or fermionic fields. Such a Coulomb gas description, which we already have described in detail in the $N = 3$ and $N = 4$ cases (involving one non compact boson and respectively one and two compact bosons), should also transpire in the continuum limit of the restricted models and may therefore be partly guessed at this stage. The little knowledge we need for the moment can be stated as follows :

The Coulomb gas description of conformal field theories based on an algebra of rank p usually involves p bosons

(see the review by Fateev and Lukyanov [126]; explicit construction of Coulomb gases for $p = 2$ and $p = 3$ can be found in [127] and [107] respectively). Following this rule, whereas Coulomb gas descriptions of the coset (3.119) are expected to involve a \tilde{N} -dependent number of fields, a fact which is not only unpleasant since it would involve a γ -dependent field content for the $a_N^{(2)}$, but for which there is also no numerical evidence (see later discussions), we can profitably use the conformal duality

$$\frac{SO(\tilde{N})_1 \times SO(\tilde{N})_{N-1}}{SO(\tilde{N})_N} \longleftrightarrow \frac{SO(N)_{\tilde{N}}}{SO(N-1)_{\tilde{N}}}, \quad (3.127)$$

which is seen clearly from the equality of the central charges. For $N = 2n$ (resp. $2n+1$) $SO(N)$ has rank n and corresponds to n bosons, whereas dividing by $SO(N-1)$ of rank $n-1$ (resp. n) corresponds to subtracting the contributions of $n-1$ (resp. n) bosons to the conformal weights. More precisely the conformal weights are expected to bear the form

$$\Delta = \frac{\mathcal{C}_{SO(N)}}{N + \tilde{N} - 2} - \frac{\mathcal{C}_{SO(N-1)}}{N + \tilde{N} - 2}, \quad (3.128)$$

where $\mathcal{C}_{SO(N)}$ and $\mathcal{C}_{SO(N-1)}$ are the values of the Casimir of $SO(N)$ and $SO(N-1)$ in the corresponding representations. To interpret these contributions, note that in the theory

of a free bosonic field φ the scaling operators are the so-called *vertex operator*

$$V_\alpha \equiv : e^{i\alpha\phi} :, \quad (3.129)$$

with conformal weights $\Delta = \alpha^2$. In compactified theories $\phi \equiv \phi + 2\pi R$ such operators are properly defined only for real values of α . In non compact theories, however, nothing forbids purely imaginary values of α , hence negative conformal weights. From this very heuristic argument, we deduce that the bosons contributing negatively to the conformal weights (3.128) should be *non compact ones*. Once again this can be seen more concretely in the $N = 3$ case, where two Coulomb gas descriptions of the Z_{k-2} parafermions are known, one [128] involving a k - (hence γ -) dependent number of fields, and the other [118] involving independently of k two bosonic fields, respectively compact and non compact.

The conclusion of this long chain of arguments therefore generalizes our observations of sections 3.2 and 3.3 to any value of N , namely for each $a_{N-1}^{(2)}$ model we expect a ‘regime III’ corresponding to $\gamma \in [0, \frac{\pi}{N}]$, whose continuum limit should be described for $N = 2n + 1$ (resp. $N = 2n$) in terms of n compact bosons and n (resp. $n - 1$) non compact bosons.

3.4.2 The regimes I and II

The $a_{2n-1}^{(2)}$ models in regimes I and II

From our analysis of the Bethe ansatz equations, we conjecture that the continuum limit of the $a_{2n-1}^{(2)}$ model in regime I is described by a set of n compact bosons Φ_1, \dots, Φ_n , leading to a central charge $c = n$ in the purely periodic case. Further, the integrable massive deformations associated with imaginary staggering of the spectral parameter are conjectured to be described by the (imaginary) $a_{2n-1}^{(2)}$ Toda field theory, with action

$$\begin{aligned} \mathcal{S}_I = & \sum_{\alpha=1}^n \int d^2x (\partial_\mu \Phi_\alpha)^2 \\ & + g \int d^2x \left(e^{-2i\beta\Phi_1} + 2 \sum_{\alpha=1}^{n-2} e^{i\beta(\Phi_\alpha - \Phi_{\alpha+1})} + e^{i\beta(\Phi_{n-1} - \Phi_n)} + e^{i\beta(\Phi_{n-1} + \Phi_n)} \right) \end{aligned} \quad (3.130)$$

where the coupling β is related to γ by $\frac{\beta^2}{4\pi} = \frac{\gamma}{\pi}$.

Analogously to what we have observed in the particular $a_3^{(2)}$ case, the conjecture is that such a theory also governs the continuum limit of the $a_{2n-1}^{(2)}$ model in regime II, where the relation between β and γ has to be changed to $\frac{\beta^2}{4\pi} = \frac{\pi - \gamma}{\pi}$.

The $a_{2n}^{(2)}$ models in regimes I and II

The continuum limit of the $a_{2n}^{(2)}$ model in regime I is similarly described by a set of n compact bosons Φ_1, \dots, Φ_n , leading to a central charge $c = n$ in the purely periodic case, and the integrable perturbations are associated with the (imaginary) $a_{2n}^{(2)}$ Toda field theory, with action

$$\begin{aligned} \mathcal{S}_I = & \sum_{\alpha=1}^n \int d^2x (\partial_\mu \Phi_\alpha)^2 \\ & + g \int d^2x \left(e^{-2i\beta\Phi_1} + 2 \sum_{\alpha=1}^{n-1} e^{i\beta(\Phi_\alpha - \Phi_{\alpha+1})} + 2e^{i\beta\Phi_n} \right), \end{aligned} \quad (3.131)$$

where the relation between coupling β and γ is the same as in the regime I of $a_{2n-1}^{(2)}$ models, namely $\frac{\beta^2}{8\pi} = \frac{\gamma}{2\pi}$.

In contrast to the $a_{2n-1}^{(2)}$ case, the n bosons get coupled in the regime II of $a_{2n}^{(2)}$ to one Majorana fermion $(\psi, \bar{\psi})$, and the corresponding action is conjectured to be that of the so-called $b(0, n)^{(1)}$ Toda theory (see [115] for conventions), namely

$$\begin{aligned} \mathcal{S}_{\text{II}} = & \sum_{\alpha=1}^n \int d^2x (\partial_\mu \Phi_\alpha)^2 + \int d^2x \bar{\psi} \gamma^\mu \partial_\mu \psi \\ & + g \int d^2x \left(e^{-2i\beta' \Phi_1} + 2 \sum_{\alpha=1}^{n-1} e^{i\beta'(\Phi_\alpha - \Phi_{\alpha+1})} + \bar{\psi} \psi e^{i\beta' \Phi_n} \right), \end{aligned} \quad (3.132)$$

where, as in the $a_2^{(2)}$ case (3.83), $\frac{(\beta')^2}{8\pi} = 2\frac{\pi-\gamma}{\gamma}$. Although not entirely clear from a field-theoretical point of view, the appearance of a fermionic degree of freedom in the $a_{2n}^{(2)}$ models and not in the $a_{2n-1}^{(2)}$ ones can most likely be traced back to the fact that the former deal with odd-dimensional representations on each site of the lattice, for which states of ‘zero’ spin can be defined. As in the $a_2^{(2)}$ case, the edges carrying such states can be thought of as the domain walls of some Ising degree of freedom, which we therefore conjecture to become critical in the regime II of every $a_{2n-1}^{(2)}$ model.

3.4.3 The regimes III

We now turn to the regimes III of either $a_{N-1}^{(2)} = a_{2n-1}^{(2)}$ or $a_{2n}^{(2)}$ models, which we have argued from duality that they should be described by a set of n compact and $n-1$ (resp. n) non compact bosons, with a resulting central charge $c = N-1$ in the purely periodic case.

In order to investigate the nature of the corresponding integrable perturbations, we use the conjectured equivalence of the $a_{N-1}^{(2)}$ models in their regime III, for $q = e^{i\frac{\pi}{N+N-2}}$, with the diagonal conformal cosets $\frac{SO(\tilde{N})_1 \times SO(\tilde{N})_{N-1}}{SO(\tilde{N})_N}$ (see section 3.4.1), and the well-established fact [131] that imaginary staggering of the spectral parameter in integrable spin chains based on a group G whose continuum limit is the diagonal coset $\frac{G_k \times G_l}{G_{k+l}}$ leads to an adjoint perturbation with conformal weight

$$\Delta = 1 - \frac{h^*}{k + l + h^*}, \quad (3.133)$$

where h^* is the dual Coxeter number for the group G . In our case $G = SO(\tilde{N})$, $h^* = \tilde{N}-2$, and we find

$$\Delta = 1 - \frac{\tilde{N}-2}{N + \tilde{N} - 2} = \frac{N}{N + \tilde{N} - 2}. \quad (3.134)$$

Because of the conformal duality, the latter can as well be considered as a perturbation of the coset $\frac{SO(N)_{\tilde{N}}}{SO(N-1)_{\tilde{N}}}$. In the $N=3$ case corresponding to the $a_2^{(2)}$ model, we recover, setting $q = e^{i\frac{2\pi}{k}}$ (so $k = 2\tilde{N} + 2$) the conformal weight $\Delta = \frac{6}{k}$ associated with the second thermal operator of Z_{k-2} parafermions, in agreement with the conclusions of section 3.2. From there, two remarks can be made :

- As in the other regimes, we expect that the integrable perturbation corresponding to (3.134) may be written in a free field formulation in terms of the compact and non

compact bosonic fields $\Phi_1, \dots, \Phi_n, \phi_1, \dots, \phi_{n-1}, (\phi_n)$. The corresponding perturbed action was written explicitly in the $N = 3$ ($a_2^{(2)}$) case, see equation (3.89), and in a partly achieved form in the $N = 4$ ($a_3^{(2)}$) case (3.115). A general form of the perturbed action of the $a_{N-1}^{(2)}$ models in regime III, if tractable, would request a considerable amount of work.

- In the $a_2^{(2)}$ case, we were lead to consider two different perturbations of the coset $\frac{SU(2)}{U(1)} \simeq \frac{SO(3)}{SO(2)}$, associated respectively with the first and second thermal operators of the parafermionic theory. As it turns out, the existence of two integrable perturbations is generic to any N , and can be traced back to the so-called ‘*Pohlmeyer reduction*’ [132, 133], which relates the equations of motion for the fields on some sigma model to the conserved quantities associated with the integrable perturbation of a different, ‘reduced’ sigma model action. The first historical example of such a construction is that of the $O(3)$ sigma model, whose equations of motion were shown in [132] to map onto the conservation laws for the local charges of the sine-Gordon model. In the case of interest here, it is seen [133] that the $\frac{SO(N+1)}{SO(N)}$ and $\frac{SU(N+1)}{SO(N+1)}$ sigma models lead respectively to two different integrable perturbations of the coset $\frac{SO(N)}{SO(N-1)}$, each associated with a different set of conserved charges. For $N = 3$ these correspond to perturbations of the $\frac{SO(3)}{SO(2)}$ parafermions by the first and second thermal operators respectively, which we write as

$$\frac{SO(4)_{\tilde{N}}}{SO(3)_{\tilde{N}}} \longrightarrow \frac{SO(3)_{\tilde{N}}}{SO(2)_{\tilde{N}}} + \left(\Delta = \frac{1}{\tilde{N} + 1} \right) \quad (3.135)$$

$$\frac{SU(4)_{\tilde{N}}}{SO(4)_{\tilde{N}}} \longrightarrow \frac{SO(3)_{\tilde{N}}}{SO(2)_{\tilde{N}}} + \left(\Delta = \frac{3}{\tilde{N} + 1} \right). \quad (3.136)$$

For general N , we similarly expect to identify the two different Pohlmeyer reductions as perturbations of the $\frac{SO(N)_{\tilde{N}}}{SO(N-1)_{\tilde{N}}}$ coset by operators associated with given representations of $SO(N)$, for which the conformal weights read generically

$$\Delta = \frac{\mathcal{C}_{SO(N)}}{N + \tilde{N} - 2}. \quad (3.137)$$

Comparison with the case $N = 3$ and close examination of the case $N = 4$ suggests that for both N odd and even, the perturbations generalizing (3.135, 3.136) should be associated respectively with the vector representation for which $\mathcal{C}_{SO(N)} = \frac{N-1}{2}$, and the representation corresponding to $\mathcal{C}_{SO(N)} = N$. In the latter case this is in agreement with the independent conjecture (3.134), and we therefore write in summary

$$\frac{SO(N+1)_{\tilde{N}}}{SO(N)_{\tilde{N}}} \longrightarrow \frac{SO(N)_{\tilde{N}}}{SO(N-1)_{\tilde{N}}} + \left(\Delta = \frac{N-1}{2(N + \tilde{N} - 2)} \right) \quad (3.138)$$

$$\frac{SU(N+1)_{\tilde{N}}}{SO(N+1)_{\tilde{N}}} \longrightarrow \frac{SO(N)_{\tilde{N}}}{SO(N-1)_{\tilde{N}}} + \left(\Delta = \frac{N}{N + \tilde{N} - 2} \right), \quad (3.139)$$

where we recall that the *second* perturbation is the one we have associated to the continuum limit of the $a_{N-1}^{(2)}$ models in their regime III. The pending issue of which integrable lattice models could possibly correspond to the *first* perturbation will in fact reappear in chapter 5.

3.5 The non compact world

In the previous sections, we have derived without further comments the continuum limit of an infinite hierarchy of exactly solvable lattice models, which turns out to be, in a certain regime, of a non compact nature. Looking back at our discussion of section 1.5, this is now quite surprising: whereas the models found in the past to have a non compact continuum limit were characterized by several peculiar features such that supergroup symmetry or delicate staggering of the spectral parameters, the ones we have been dealing with in this presentation seem to be instead rather generic, as the only common feature they share is non unitarity. For instance, in the $a_2^{(2)}$ case, the quantum Hamiltonian can be written in terms of the $U_q(sl_2)$ spin-1 generators $\vec{S}_j = (S_j^x, S_j^y, S_j^z)$ as

$$\begin{aligned} H = & \pm \sum_{i=1}^L \cos \frac{3\gamma}{2} \tau_j + \cos \frac{\gamma}{2} (\tau_j)^2 + 4 \sin^2 \frac{\gamma}{4} \sin \frac{\gamma}{2} \sin \gamma (\tau_j^\perp \tau_j^z - \tau_j^z \tau_j^\perp) \\ & - 4 \sin^2 \frac{\gamma}{4} \cos \frac{3\gamma}{2} (S_j^z)^2 + 2 \sin^3 \frac{\gamma}{2} \sin \gamma (\tau_j^z - (\tau_j^z)^2) \\ & + \frac{i}{4} \sin 2\gamma \left[\tau_j^\perp (S_{j+1}^z - S_j^z) + (S_{j+1}^z - S_j^z) \tau_j^\perp + 2 \cos \frac{\gamma}{2} \tau_j^z (S_{j+1}^z - S_j^z) \right] \end{aligned} \quad (3.140)$$

(where $\tau_j = \vec{S}_j \cdot \vec{S}_{j+1} = \tau_j^\perp + \tau_j^z$, and the boundary twist is encoded by $S_{L+1}^z = S_1^z$, $S_{L+1}^\pm = e^{\pm i\varphi} S_1^\pm$), which is clearly non hermitian because of the imaginary factor in the last group of terms. Whereas this is most likely crucial in order to obtain a non compact continuum limit, it does however not prevent our models from having a perfectly physical interpretation: again in the $a_2^{(2)}$ case, we have seen and will see again that the loop formulation leads to a statistical mechanics model with positive definite Boltzmann weights, suitable to the description of two-dimensional polymers with various interactions.

This raises a couple of questions. First, it is now legitimate to wonder how frequent such examples of *compact* spin chains or lattice models with a *non compact* continuum limit actually are, and how the emergence of non compact degrees of freedom can be understood fundamentally. Second, we have not yet investigated what a non compact continuum limit might change in practice, for instance in experiments or numerical simulations.

3.5.1 A look at the Bethe ansatz kernels

In the previously known cases of non compact continuum limits, the best understood of which is probably the staggered six-vertex model, the emergence of a continuum spectrum of exponents could be understood simply by looking at the integral form of the Bethe equations in the thermodynamic limit (although a good qualitative understanding of such spectra requires more complicated tools such as non linear integral equations [110, 61]). As was exposed for specific cases in earlier sections, these are generally written as

$$\rho + \rho_h = s + K \rho, \quad (3.141)$$

where in cases involving several species of roots s, ρ, ρ_h are column vectors and K is a square matrix. The generalization of (3.41) for conformal weights reads

$$\Delta + \bar{\Delta} = \frac{1}{4} m^\dagger (1 - K) m + w^\dagger (1 - K)^{-1} w, \quad (3.142)$$

where for $1 - K$ the zero-frequency limit has to be taken. In all cases [54, 55], the kernel K was found to be singular, namely $1 - K$ has one or several zero eigenvalues, resulting in conformal weights of the form

$$\Delta + \bar{\Delta} = 0 \times m^2 + \infty \times w^2 + \dots, \quad (3.143)$$

where the $0 \times m^2$ part can be interpreted as an infinite degeneracy of the gaps, or, equivalently, as the trace for a continuous spectrum of exponents.

The cases we have been studying here differ fundamentally, in that the emergence of continuous spectra cannot apparently be traced back to any singularity of the scattering kernels. Taking for instance the regime III of $a_2^{(2)}$, we have seen that the 'non compact', $j \neq 0$ levels were obtained by allowing roots with imaginary part $\frac{\pi}{2}$ and it seems therefore natural to augment the scattering equations (3.49) with a finite density σ of such roots, leading to

$$\rho = \frac{1}{2 \cosh \frac{\omega}{4}(\pi - 3\gamma)} - \frac{\sinh \frac{\omega\pi}{2}}{4 \sinh \frac{\omega\gamma}{2} \cosh \frac{\omega}{4}(\pi + \gamma) \cosh \frac{\omega}{4}(\pi - 3\gamma)} \rho_h + \frac{1}{2 \cosh \frac{\omega}{4}(\pi + \gamma)} \sigma, \quad (3.144)$$

and

$$\sigma + \sigma_h = \frac{1}{2 \cosh \frac{\omega}{4}(\pi + \gamma)} \rho_h + \frac{\cosh \frac{\omega}{4}(\pi - 3\gamma)}{\cosh \frac{\omega}{4}(\pi + \gamma)} \sigma. \quad (3.145)$$

These equations seem, at first sight, perfectly innocuous, and suggest that the range of possible mechanisms leading to the emergence of non compact degrees of freedom in compact spin chains may be much richer than initially expected.

A possible suggestion might be to augment the scattering equations (3.144, 3.145) by considering the small deviations of the 2-strings imaginary parts with respect to their asymptotic value. From there, some singular coupling between, say, these deviations and the density σ might be observed. How to treat these corrections precisely is however not clear for the moment, and might require anyway to move further to non linear integral equations. **[TODO: give it a try?]**

3.5.2 The search for non compact degrees of freedom

Looking back at our conclusions of section 3.2.6 on the continuum limit of the $a_2^{(2)}$ model, one blatant aspect is that we have not been able, so far, to give any physical interpretation to the continuous quantum number s or its lattice counterpart j . More precisely, just as the discrete quantum number m at each imaginary time step is the integral over the quantum space of the local magnetization $m = \frac{1}{L} \sum_{i=1}^L S_i^{(z)}$, we could legitimately hope to find a lattice local observable σ_i such that $j = \frac{1}{L} \sum_{i=1}^L \sigma_i$, or at least a local density $\sigma(x, t)$ in the continuum limit such that

$$s = \frac{1}{L} \int_0^L dx \sigma(x, t). \quad (3.146)$$

In the next chapter, we will use a detailed analysis of the polymer phase diagram around the Izergin–Korepin integrable points to convince ourselves that the compact degree of freedom of regime III is in some sense closely related to the dynamics of empty edges. However, this is enough to provide us with a clear interpretation of the nature of this quantum number. Several attempts in this direction can be made. For instance,

we can consider an extended integrable $O(n)$ model where the empty edges (carrying $S^{(z)} = 0$) are now represented as carrying white loops, which now have a dynamics of their own. Different magnetization (‘through-lines’) sectors can be defined for these loops, and the corresponding critical (‘watermelon’) exponents may be hoped to recover the scaling exponents associated with different values of the quantum number j . Unfortunately, this does not seem to be the case. Alternatively, we can follow the lines of [121], where the $a_2^{(1)}$ model is mapped onto a $O(n)$ model on the square lattice. The latter can in turn be interpreted in terms of a model of fully packed loops on the honeycomb lattice, and from this mapping stems an additional symmetry of the model, namely an additional conserved quantum number $Q = \frac{1}{L} \sum_{i=1}^L (-1)^i |S_i^{(z)}|$. m and Q together correspond to the two Cartan generators of $a_2^{(1)}$, and we could wonder whether Q , or some modification thereof, might be conserved in the $a_2^{(2)}$ model too. Neither these ideas however seem to provide satisfactory results.

After this series of unfortunate attempts, we now want to present some arguments which, hopefully, should convince the reader that finding an interpretation of the conserved charge s as the integral of some local density is in fact an impossible task.

(Non-)normalizable states and (non-)local operators

Let us first consider the simple case of the free compact boson theory, $\Phi \equiv \Phi + 2\pi$, namely a quantum field theory whose target space is the compact group $U(1)$. As was introduced previously in the Coulomb-gas formalism, the primary fields of the theory can be put in correspondence with the unitary representations of the group, namely the vertex operators $V_m =: e^{im\Phi} :$, $m \in \mathbb{Z}$, as can straightforwardly be seen in the mini-superspace analysis where the primary fields are the eigenfunctions of the Laplacian on $U(1)$. In radial quantization (which is not here meant to be proper to CFTs), inserting a vertex operator V_m at the origin yields the state $|m\rangle = V_m(0) |0\rangle$, and the locality of the former gets translated in the torus as the locality of the magnetization density.

A fundamental difference occurring in quantum field theories with a non compact target space symmetry (such as Lorentz invariant theories) is that non compact groups do *not* allow for non-trivial finite-dimensional unitary representations. This raises an apparent paradox, as the action for such theories is usually written in terms of physical variables (the position, angular momentum, energy momentum tensor, etc...) and fields (the electromagnetic potential, the Dirac spinor, etc...) all transforming as finite-dimensional, hence non-unitary representations, whereas the physical Hilbert space is expected to carry an unitary and thus infinite-dimensional representation of the group. The answer to this paradox is that the physical spinors or other local fields are typically written as

$$\Psi^\alpha(x) = \sum_\lambda \int dp u^\alpha(p, \lambda) e^{ipx} a(\vec{p}, \lambda), \quad (3.147)$$

where the $a(p, \lambda)$ operators, which transform under unitary, infinite-dimensional representations, make up the actual observable content of the theory. In particular, these include the primary fields of the theory, which contrary to the vertex operators of the free compact boson theory, are not necessarily local anymore.

In the context of CFTs, any state $|m\rangle$ in the physical Hilbert space spectrum can be formally associated with an operator $\mathcal{O}_m = |m\rangle \langle 0|$, and we can in the radial quantization setup run imaginary time backwards so that the operator is inserted at the origin, and thus necessarily local, which seems in contradiction with the previous observations. The

answer in this puzzle actually has to deal with normalizability, as it may very well be that some operators inserted at the origin actually lead to non-normalizable, hence non-observable states. More precisely, the reversed mapping from an operator \mathcal{O} back to a state of the Hilbert space is made by performing partial functional integration over a circle with an insertion of \mathcal{O} at the center, and we are here considering the case where this functional integral may diverge, hence leading to a non-normalizable wave function.

The conclusion of all this is therefore that local operators such as the fields $\Psi^\alpha(x)$ correspond to *non-normalizable states*, not observed in the physical Hilbert space of the theory. Conversely, the Hilbert state is made of normalizable states, which correspond to non-local operators, or in other terms do not allow for a nice interpretation in terms of the basic fields $\Psi^\alpha(x)$ of the theory.

Let us see how this applies to the Black-Hole theory, whose primaries can be interpreted as representations of the non-compact group $SL(2, \mathbb{R})$. For our purpose it is enough to work in the mini-superspace description, namely $r(x, t) \rightarrow r(t)$ and $\theta(x, t) \rightarrow \theta(t)$, therefore to forget about the additional discrete states introduced in section 3.2.4. As already explained in section 3.2 the natural local fields r and θ can be recast in terms of the complex field $\Psi = \sinh r e^{i\theta}$, in terms of which we recall that the classical action (that is, without the dilaton term) has the simple expression

$$\mathcal{S} = \frac{k}{4\pi} \int d^2x \frac{\partial_\mu \Psi \partial^\mu \bar{\Psi}}{1 + |\Psi|^2}, \quad (3.148)$$

and the mini-superspace eigenwavefunctions are parametrized by the momenta n and J in the angular and axial directions of the cigar, namely

$$\begin{aligned} \phi_n^J(r, \theta) &= -\frac{\Gamma^2(-J + \frac{|n|}{2})}{\Gamma(|n| + 1)\Gamma(-2J - 1)} e^{in\theta} \\ &\quad \sinh^{|n|} r F(J + 1 + \frac{|n|}{2}, -J + \frac{|n|}{2}, |n| + 1, -\sinh^2 r). \end{aligned} \quad (3.149)$$

One can now distinguish between different series of $SL(2, \mathbb{R})$ representations, namely

- The *principal (continuous) series* $J = -\frac{1}{2} + is$, $s \in \mathbb{R}$, which gives rise to the continuous spectrum observed as the continuum limit of the $a_2^{(2)}$ regime III. The corresponding wave-functions are (δ function-) normalizable, but can however *not* be associated with simple expressions of the field Ψ .
- The *discrete series* $J = \frac{1}{2}, 1, \dots$, for which the hypergeometric functions truncate. The corresponding wave-functions have therefore a polynomial expression in terms of Ψ , but are however non-normalizable⁶.

This is in perfect agreement with the general predictions above, we can finally conclude that it should not be possible to relate primaries of the continuous series to local operators acting on the Hilbert space, or in other terms that there actually no point in looking for a nice, local interpretation of the continuous quantum number s .

⁶In the same way that the sigma model classical actions for the $SL(2, \mathbb{R})/U(1)$ black hole and for the $SU(2)/U(1)$ parafermions are obtained from one another by formally mapping $|\Psi|^2 \rightarrow -|\Psi|^2$, the eigenwavefunctions for the parafermions are obtained from the non-normalizable black hole wavefunctions through the same mapping.

In spite of this conclusion, several interesting directions can still be investigated. In particular, it might be possible to describe instead the quantum number s by some *non-local*, or *quasi-local* densities on the Izergin–Korepin lattice or in the continuum limit. In this spirit we mention the recent works on the spin $\frac{1}{2}$ XXZ ($a_1^{(1)}$) chain [122, 123], where auxiliary spaces carrying complex-spin representations of $U_q(sl_2)$ were for a whole different purpose used to construct a continuous family of quasi-local conserved charges, additional to the set of local charges corresponding to the successive derivatives of the usual transfer matrix. Since the construction seems to rely essentially on the existence of an underlying quantum group structure, it looks like it could without too much difficulty be adapted to other models such as those studied in this chapter.

3.5.3 Non compact theories in practice

We now turn to the practical effects going along with a non compact continuum limit for a given spin chain or lattice model. This general overview will be supplemented by concrete examples in the next two chapters.

Measures of correlation functions

The observables measured experimentally can be usually traced back to various (fixed time or dynamical) correlation functions. In condensed matter physics, particularly detailed information is provided by *inelastic neutron scattering* experiments, where neutrons are sent over a sample and the resulting scattering cross section is measured, which can be shown to be proportional to a particular retarded correlation function in the sample, the so-called dynamical structure factor.

Let us consider for instance the fixed-time correlation function $\langle \mathcal{O}(x)\mathcal{O}(y) \rangle$ of some observable, either defined on the lattice or as some physical observable in the continuum limit. In the critical case, such \mathcal{O} never in practice corresponds exactly to one pure scaling field, but rather can be decomposed over an infinite sum of scaling fields. As a result, the correlation $\langle \mathcal{O}(x)\mathcal{O}(y) \rangle$ is usually written in ordinary CFT as

$$\langle \mathcal{O}(x)\mathcal{O}(y) \rangle = \left(\frac{\epsilon}{|x-y|} \right)^{2x_1} + C \left(\frac{\epsilon}{|x-y|} \right)^{2x'_1} + \dots, \quad (3.150)$$

with $x'_1 > x_1$, so that its large distance behaviour is governed, at leading order, by a power-law with exponent x_1 . Turning now to non compact theories, we expect the sum (3.150) to be replaced by an integral coming from a continuum of subleading exponents, namely

$$\langle \mathcal{O}(x)\mathcal{O}(y) \rangle = \int_{\chi > x_1} d\chi \frac{f(\chi)}{|x-y|^{2\chi}} + \dots \quad (3.151)$$

The function $f(\chi)$, which is typically the product of the density of conformal states $\rho(\chi)$ times some matrix element, is in general quite hard to know precisely (even once the density of states is known, the computation of form factors associated with the operators \mathcal{O} is in general a very complicated task, see for instance [134]), however it can be readily guessed that an expression of the form (3.151) should result in some asymptotic behaviour really different than the power-law expected in the discrete case. In Chapter 4, we will consider such an example by making some reasonable analytic assumptions on the function $f(s)$, and will see how the result can be used to explain the so far unresolved output of Monte Carlo simulations.

Critical exponents from transfer matrix diagonalization

As discussed in the early sections of this manuscript, precise estimations of critical exponents for various statistical mechanics models or spin chains can usually be obtained from the diagonalization of finite size transfer matrices or Hamiltonians. Let us focus here on the example of the $a_3^{(2)}$ model, whose regime III, as reviewed previously, describes a particular critical point of a problem of two Potts model coupled by the product of their energy operators, or equivalently of a geometrical model involving two colours of loops. In this formulation, the central charge and so-called *two-colour watermelon exponents* x_{ℓ_1, ℓ_2} were defined and estimated numerically by Jacobsen and Fendley [92]⁷. These are obtained as

$$x_{\ell_1, \ell_2} = \frac{c - c_{\ell_1, \ell_2}}{12}, \quad (3.152)$$

where $c = \frac{3k^2}{(k+1)(k+2)}$ is the central charge of the loop model (obtained from the ground state of the vertex model at twists $\varphi_1 = \varphi_2 = \gamma$, and we use the parametrization $\gamma = \frac{\pi}{k+2}$), and c_{ℓ_1, ℓ_2} is the effective central charge in the sector with (ℓ_1, ℓ_2) legs. Whereas c is described by a discrete state, the central charges c_{ℓ_1, ℓ_2} for both ℓ_1 and ℓ_2 non zero are obtained from the vertex model at $\varphi_1 = \varphi_2 = 0$ and therefore belong to the continuum of states. In particular, we expect in this case finite size corrections of the form

$$x_{\ell_1 \neq 0, \ell_2 \neq 0}(L) = x_{\ell_1, \ell_2}(\infty) + \frac{A}{(B + \log L)^2}, \quad (3.153)$$

where the $x_{\ell_1, \ell_2}(\infty) \equiv x_{\ell_1, \ell_2}$ are found from our Bethe ansatz analysis (see in particular equation 3.112) to be given by $x_{\ell_1, \ell_2} = \frac{1}{k+2} \left(\frac{\ell_1^2 + \ell_2^2}{8} - 1 \right) + \frac{1}{4(k+1)}$.

As an example, let us look at the exponent $x_{2,2}$ for $k = 3$, whose finite size estimates obtained from numerical resolution of the Bethe ansatz equations for $L \leq 90$ are displayed in figure 3.7. The values accessible from direct diagonalization, namely $L \leq 16$, are plotted in red and we reproduce the extrapolation used by the authors of [92] (obtained by fitting the last few points to a second order polynomial in $1/L$), yielding the estimate $x_{2,2} = 0.200(2)$. Taking larger sizes (blue points) in consideration however makes it evident that this extrapolation is incorrect, as the logarithmic corrections in (3.153) should be taken in account. As a matter of fact the exactly determined value of the exponent is in this case $x_{2,2} = \frac{1}{16}$, which highly differs from the earlier estimation. This may be recovered using numerical fits as follows: using three successive sizes ($L, L+2, L+4$) we first fit to the form $x_{2,2}(L) = x_{2,2}^{\text{ext}}(L) + \frac{A}{(B + \log L)^2}$ to obtain a series of extrapolants $x_{2,2}^{\text{ext}}(L)$. Plotting those against $1/L$ we observe a residual finite-size dependence which is almost linear for $L \geq 50$. Fitting therefore $x_{2,2}^{\text{ext}}(L) = x_{2,2} + C/L$ we obtain finally $x_{2,2} = 0.071(6)$, which is in moderately good agreement with the exact conjecture.

This spectacular discrepancy between 'naive' small-size fitting and exact asymptotics can be generalized to other exponents and other values of k , as summed up in table 3.1. It is important to point out that for all of the exponents reproduced here the estimations of [92] were given with a precision of three digits or more, which means that polynomial fits in $\frac{1}{L}$ might very well have given satisfactory, though highly mislead, results for small system sizes. This raises the question of whether other such cases of numerically misestimated critical exponents might be hidden in the literature.

⁷See the beginning of chapter 4 for a definition of the watermelon exponents for another model, which can however be straightforwardly generalized to any of the loop models under consideration in this thesis.

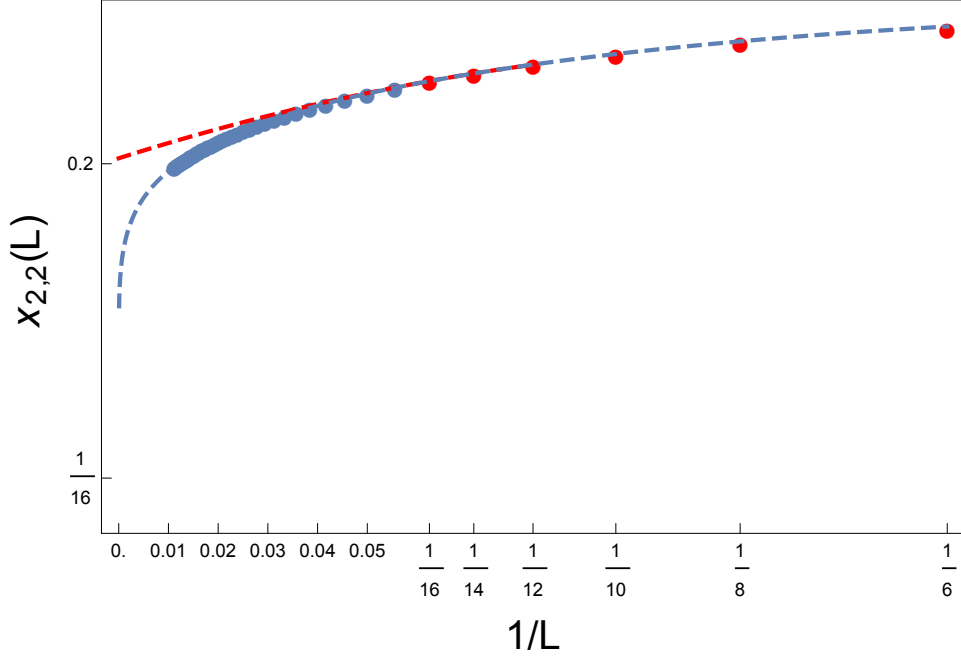


Figure 3.7: Finite-size estimates of the exponent $x_{2,2}$ of the $a_3^{(2)}$ model for $k = 3$, plotted against $1/L$. The red points are the data for $L \leq 16$ that were found in [92] by direct diagonalisation of the transfer matrix. The blue points, extending this to $L \leq 90$, were obtained here by numerical solution of the Bethe Ansatz equations. The extrapolation to $L \rightarrow \infty$ that led [92] to the erroneous value $x_{2,2} = 0.200(2)$ is shown as a red dashed curve. The extrapolation represented by a blue dashed curve takes into account logarithmic corrections to scaling and leads to $x_{2,2} = \frac{1}{16}$.

	$k = 3$		$k = 4$		$k = 5$	
$x_{2,2}$	0.200(2)	<i>0.0625</i>	0.130(2)	<i>0.05</i>	0.095(2)	<i>0.0417</i>
$x_{4,2}$	0.774(1)	<i>0.3625</i>	0.510(5)	<i>0.3</i>	0.392(4)	<i>0.2560</i>
$x_{4,4}$	0.926(4)	<i>0.6625</i>	0.677(2)	<i>0.55</i>	0.555(5)	<i>0.4702</i>
$x_{6,2}$	1.70(5)	<i>0.8625</i>	1.15(5)	<i>0.7167</i>	0.84(5)	<i>0.6131</i>
$x_{6,4}$	1.85(5)	<i>1.1625</i>	1.28(5)	<i>0.9667</i>	1.00(5)	<i>0.8274</i>
$x_{6,6}$	2.08(7)	<i>1.6625</i>	1.54(5)	<i>1.3833</i>	1.26(6)	<i>1.1845</i>

Table 3.1: Watermelon exponents x_{ℓ_1, ℓ_2} of the $a_3^{(2)}$ model for different values of $\gamma = \frac{\pi}{k+2}$. In each case two numerical values are given: first the numerical estimation of [92] (the error bar on the last quoted digit is given in parentheses), second, in italic, the exact value obtained from Bethe ansatz analysis.

Chapter 4

Polymer collapse and non compact degrees of freedom

In this whole chapter we shall focus on the vertex interacting self-avoiding walk (VISAW) introduced in section 2.3 for the description of two-dimensional polymers, and whose phase diagram contains in particular integrable points associated with the different regimes of the $a_2^{(2)}$ model. The aim of this study is twofold :

- First, the VISAW furnishes us with the first known example of a statistical mechanics model with positive Boltzmann weights and a non compact regime. Besides the fundamental importance of this observation, we would like to study more concretely the ‘experimental’ consequences of the non compact continuum limit, as advertized at the end of the last chapter.
- Second, we would like to investigate the nature of the polymers phase diagram around the regime III integrable point in order to understand better the physics associated with the non compact degree of freedom.

The plan of the presentation is the following. In section 4.1 we first introduce the VISAW phase diagram, and relate the integrable points found in section 2.3 to the universality classes of the different phases. In section 4.2 we specialize to the non compact point associated with the Izergin–Korepin model in regime III and investigate how the corresponding non compact continuum limit affects the observation of some physical properties. We then study numerically the (non integrable) perturbations around this point, and gain from there some understanding of the nature of the non compact degree of freedom (section 4.3). Besides these aspects, it comes rather as a by-product that our results can be applied to a better understanding of the two-dimensional collapse transition. In section 4.4, we present what we believe to be a close-to-complete answer to this long standing puzzle.

Preamble: polymer critical exponents from the transfer matrix

It has been shown previously in the framework of the six-vertex model how to relate the different sectors of a loop transfer matrix to the sectors of fixed magnetization of the corresponding twisted vertex transfer matrix.

In this short preamble, we define a set of interesting critical exponents, the *watermelon exponents*, that can be computed from the diagonalization of either of these transfer matrices, insisting on the fact that this procedure does not necessarily rely on integrability.

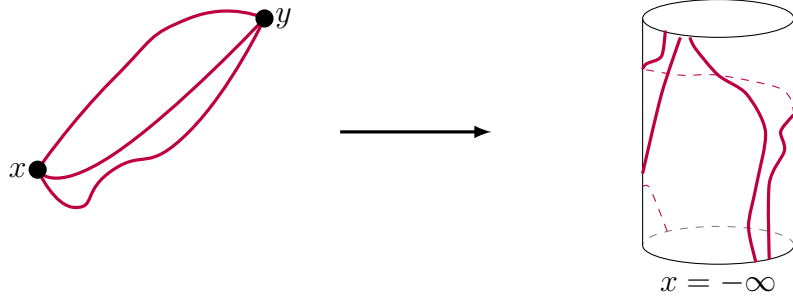


Figure 4.1: The ℓ -leg watermelon exponent is defined on the infinite plane from the correlation function $\langle \mathcal{O}_\ell(x) \mathcal{O}_{-\ell}(y) \rangle$ (left). By a conformal mapping, the plane is mapped on the cylinder, x is mapped to $t = -\infty$, and amounts to considering a transfer matrix acting on the sector with ℓ through-lines (right).

Let us temporarily assign an arbitrary orientation to each polymer in the model, destined to be summed over to eventually recover the original model. The ℓ -legs *watermelon* (or *fuseau*) *exponent* x_ℓ are defined from the correlation function between the operator $\mathcal{O}_\ell(x)$ inserting ℓ oriented legs in the vicinity of a point x and the operator $\mathcal{O}_{-\ell}(y)$ that conversely acts as a sink for ℓ legs in the vicinity of another point y (see figure 4.1). The operators $\mathcal{O}_{\pm\ell}$ are expected to be described in the continuum limit by an infinite sum of scaling fields, and the corresponding correlation function should therefore be dominated at large distance by the most relevant term, namely

$$\langle \mathcal{O}_\ell(x) \mathcal{O}_{-\ell}(y) \rangle \propto |x - y|^{-2x_\ell} + \dots \quad (4.1)$$

(the precise form of the corrections, already evoked in the previous chapter, is of course of great importance, and will be the object of section 4.2; for the moment we however wish to stay generic).

As explained on the figure as well as in the introductory section 1.4, a conformal mapping from the infinite plane onto a cylinder of width L shows that the exponents x_ℓ correspond precisely to those describing the scaling of transfer matrix eigenvalues in the sector with ℓ through-lines with respect to those in the ground state sector (with no through-lines propagating). In the language of a twisted spin-1 vertex model such as the Izergin–Korepin model, where closed loops are given a weight $n = -2 \cos 2\gamma = 2 \cos(\pi - 2\gamma)$ ($=0$ for polymers), we therefore measure the watermelon exponents as

$$x_\ell = \Delta_\ell + \bar{\Delta}_\ell = -\frac{c_\ell(\varphi = 0) - c_0(\varphi = \pi - 2\gamma)}{12}, \quad (4.2)$$

where $c_\ell(\varphi)$ is the effective central charge in the sector of magnetization sector ℓ for a transfer matrix with twist parameter φ .

4.1 The VISAW phase diagram

We recall that the VISAW Boltzmann weights are obtained as products of the local weights K , p and τ , associated respectively to each edge (‘monomer’), each straight segment and each doubly visited site. These can be recombined in terms of the weights associated with local plaquettes for some $O(n = 0)$ model, which in turn can be generalized to

anisotropic, spectral parameter-dependent expressions¹. From there, the Yang–Baxter equations can be solved, leading, back to the isotropic case, to five integrable points (see section 2.3):

- The first one, usually labeled ‘branch 0’, corresponds to $p = 0$, $K = \frac{1}{2}$, $\tau = 2$. For reasons that should appear clear later, we will also call this point Θ_{DS} , referring to Duplantier–Saleur [140].

The four others are associated with the $n = 0$ points of the four integrable branches of the Izergin–Korepin model (2.83), namely

- The point in branch 1 corresponds to $\gamma = \frac{\pi}{4}$, $u = u_+$ (in the notations of section 3.2), namely $K = 1.00315\dots$, $p = 1.38704\dots$, $\tau = 0.783227\dots$. From our earlier study of the $a_2^{(2)}$ model it is known to be described by the so-called regime I, more precisely in the *dense* phase of the latter (to be defined shortly).
- The point in branch 2 corresponds to $\gamma = \frac{3\pi}{4}$, $u = u_+$, namely $K = 0.408391\dots$, $p = 0.785695\dots$, $\tau = 0.675577\dots$, and is described by another point in regime I, more precisely in the *dilute* phase of the latter (to be defined shortly).
- The point in branch 3 corresponds to $\gamma = \frac{\pi}{4}$, $u = u_-$, namely $K = 0.446933\dots$, $p = 0.275899\dots$, $\tau = 2.63099\dots$, and is described by the exotic regime III. We will also call this point Θ_{BN} , referring to Blöte–Nienhuis [75].
- The point in branch 4 corresponds to $\gamma = \frac{3\pi}{4}$, $u = u_-$, namely $K = 15.4476\dots$, $p = 1.17588\dots$, $\tau = 0.0897902\dots$, and is described by the regime II.

The phase diagram of the VISAW in the p, K, τ space is depicted in figure 4.2, and we start discussing it for small values of the interaction parameter τ .

Weakly interacting case (small τ): the dilute and dense phases

For small values of the interaction parameter τ , the physics is essentially the same as for usual (non interacting) SAWs: for small values of the fugacity K the polymer is in a massive phase and remains of finite total length as the size of the system is sent to infinity, whereas for high values of K the polymer is in a critical, *dense* phase where it covers a finite fraction of the lattice edges in the thermodynamic limit; the two phases are separated at intermediate K by a different, *dilute* critical phase (represented by a red surface on the figure).

From the CFT point of view, the dense and dilute phases can be understood as the ‘dense’ and ‘dilute’ branches of the free compact boson theory, in the universality classes described by the respective branches 1 and 2 of the integrable regime I. In the Coulomb gas formulation of section 3.2.1 these correspond respectively to $g = \frac{1}{2}$ and $g = \frac{3}{2}$, and the corresponding central charges, obtained by giving non contractible loops the same weight as contractible ones, hence choosing a twist $\varphi = \pi - 2\gamma$ (so $e_0 = 1 - g$), are given by

$$c = 1 - \frac{6(1 - g)^2}{g}, \quad (4.3)$$

¹In all this presentation we will restrict to the $n = 0$ case which is the one relevant for the description of polymers, but most of the discussion of the phase diagram can be generalized to other values $-2 \leq n \leq 2$. As a matter of fact, we will sometimes use the denominations Θ_{DS} and Θ_{BN} in a looser sense, namely extended to the respective branches 0 and 3 for different values of n .

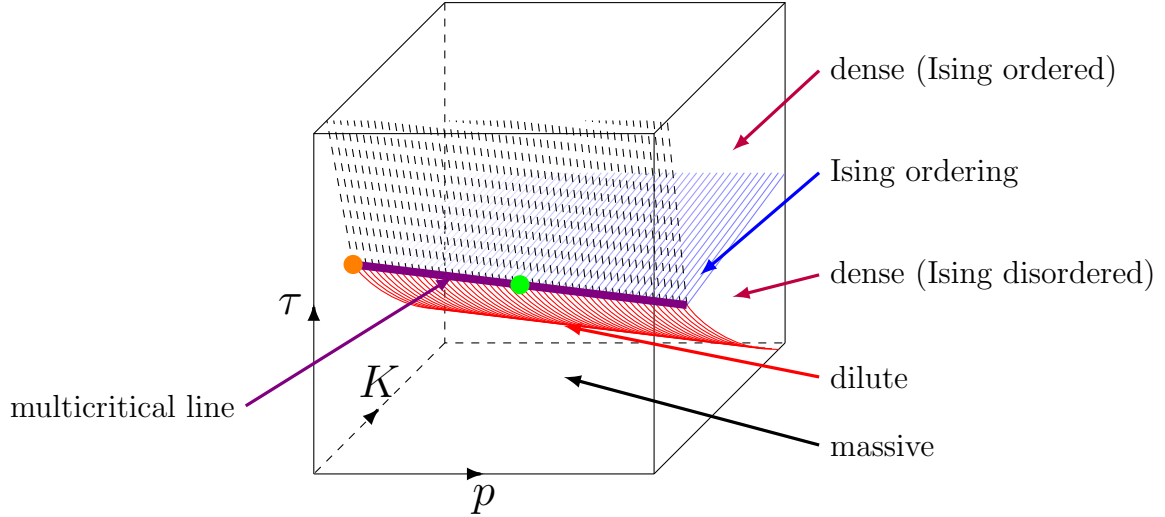


Figure 4.2: Phase diagram of the two-dimensional VISAW. The nature of the different phases and transitions between them is explained in the main text. The two candidates for the theta point universality class are represented by orange (DS) and green (BN) dots.

that is $c = -2$ in the dense phase and $c = 0$ in the dilute phase. The watermelon exponents are similarly obtained as magnetic exponents of the Coulomb gas, or alternatively by applying (4.2) to our Bethe ansatz results of section 3.2.1. We find respectively

$$x_\ell = \frac{\ell^2}{16} - \frac{1}{4} \quad (4.4)$$

in the dense phase, and

$$x_\ell = \frac{3\ell^2}{16} - \frac{1}{12} \quad (4.5)$$

in the dilute phase.

Increasing τ : the Ising ordering transition

In order to investigate the effect of larger values of τ , it is instructive to consider back the Ising degrees of freedom introduced in section 3.2.1 (see also figure 3.2), that is Ising living on the faces of the square lattice, such that two spins on adjacent faces share the same orientation iff they are separated by a polymer bit. Whereas this Ising degree of freedom is disordered in the usual SAW dense phase, it is clearly ordered in the ‘fully packed’ limit of large K , nonzero τ , and therefore some critical Ising surface should be expected in the phase diagram (in blue on the figure). Unsurprisingly, the universality class of this critical surface is precisely described by the integrable point of branch 4, namely the regime II of the $a_2^{(2)}$ model, which we know since our analysis of section 3.2.1 that it is described by a the dense branch of the free boson supplemented by a free Majorana fermion, with a total central charge

$$c = -2 + \frac{1}{2} = -\frac{3}{2}, \quad (4.6)$$

while the watermelon exponents keep the same value as in the rest of the dense phase, namely (4.4). Note however that whereas the Ising-ordered and Ising-disordered dense

phases are described by the same conformal field theory, they slightly differ on the lattice, namely the odd (resp. even) magnetization sectors (sectors with an odd (resp. even) number of through-lines) for lattices with an even (resp. odd) number of sites are massive in the ordered phase, while critical in the disordered phase. In the latter, the corresponding critical exponents reproduce precisely the dense spectrum (4.4).

Above the Ising critical surface, the transition between the massive and dense (ordered) phases is now of first order, represented by a dashed surface on the figure.

The multicritical line

Whereas all the phases described so far are by now well understood, it is not the case of the multicritical line joining the dilute, Ising critical, and first order surfaces, represented in violet on the figure.

On this line lie the two remaining integrable points, Θ_{DS} and Θ_{BN} , represented respectively by orange and green dots. As introduced in section 2.3, the physics at Θ_{DS} , and more generally in the whole branch 0, is conveniently described through a mapping of the dilute loop model at loop weight n onto a model of completely packed loops with weight $n' = n + 1$. The latter is critical for $-2 \leq n < 2$, and described by a compact free boson theory. Parametrizing $n' = -2 \cos \pi g$, the central charge and critical exponents are obtained from the now usual Coulomb-gas analysis (see section 3.2.1), in particular choosing the twist $e_0 = 1 - g$ (in the language of equation (3.45)) such as to give non contractible loops the same weights as to contractible ones, we find

$$\begin{aligned} c &= 1 - 6 \frac{(1-g)^2}{g} \\ x_{e_0, M} &= -\frac{(1-g)^2}{2g} + \frac{gM^2}{2}, \end{aligned} \quad (4.7)$$

which in particular yields at Θ_{DS} ($n = 0, n' = 1, g = \frac{2}{3}$) the central charge $c = 0$ and watermelon exponents

$$x_\ell = x_{e_0, \frac{\ell}{2}} = \frac{\ell^2 - 1}{12}, \quad (4.8)$$

as we have checked numerically from transfer matrix diagonalization. It should be pointed [75] that a subtlety occurs in this case, namely on a lattice of even size L only the dimensions corresponding to *even* values of ℓ are observed, as for instance one through-line in the dilute model implies the existence of a second through-line in its fully-packed reformulation.

Much differently, the point Θ_{BN} is described by the black hole CFT, of a non compact nature. The corresponding central charge is found by adjusting the twist in (3.51) to $\varphi = \pi - 2\gamma$, so $c = 0$ once again, while the watermelon exponents are computed, taking much care of the discrete states structure, as [63]

$$x_\ell = \frac{\ell^2}{16} - \frac{1}{6}. \quad (4.9)$$

Investigating the effects of such a non compact CFT on the physical quantities will be one of our important concerns in the course of this chapter. Another fundamental question will be for us to understand the nature of the critical theory along the multicritical line between Θ_{DS} and Θ_{BN} , and beyond.

4.2 Physical properties at the non compact point

In this section we focus on the point Θ_{BN} , where recent Monte-Carlo simulations by Bedini *et. al.* [135] yielded numerical estimations of some critical exponents disturbingly far-off the values derived from the Bethe ansatz solution.

These exponents are the correlation length exponent ν and the partition function exponent γ , both introduced in section 1.2, and which can be obtained from the watermelon exponents using the well known set of scaling relations [140],

$$\eta = 2x_1, \quad \nu = \frac{1}{2 - x_2}, \quad \frac{\gamma}{\nu} = 2 - \eta, \quad (4.10)$$

namely, using (4.9),

$$\nu = \frac{12}{23} \simeq 0.522, \quad \gamma = \frac{53}{46} \simeq 1.152, \quad (4.11)$$

as already computed by Nienhuis *et. al.* [78], whereas the simulations of [135] yielded

$$\nu \simeq 0.576(6), \quad \gamma \simeq 1.045(5). \quad (4.12)$$

The discrepancy between (4.11) and (4.12) is something essentially unheard of in the field of exactly solvable models and conformal field theory, where, usually, theory and ‘experiment’ match almost perfectly. One could legitimately argue that the simulations of [135] involve a canonical ensemble of polymers with fixed lengths whereas the (integrable) models we have been considered throughout this thesis involve a grand canonical ensemble of walks with fluctuating lengths, however this point is usually easily taken care of by considerations of Legendre transform, and has never, in all the other cases studied so far, led to any particular difficulty.

As we will see now, these mysterious features can be traced back to the peculiar, non compact nature of the continuum limit at Θ_{BN} . Rather than the canonical simulations of [135] we will here focus on grand canonical Monte-Carlo estimations of the exponent η , from which we will be able to deduce qualitative predictions about the discrepancies in ν and γ .

4.2.1 Grand-canonical Monte-Carlo simulations

Throughout this whole section we focus on the $n = 0$ version of the spin-spin correlation function, namely the correlation function

$$G_1(e, e') = \sum_{\text{VISA W: } e \rightarrow e'} K^{\# \text{ monomers}} \tau^{\# \text{ doubly visited sites}} p^{\# \text{ straight segments}}, \quad (4.13)$$

between two lattice edges e, e' which, in the continuum limit, becomes precisely the watermelon correlation function $\langle \mathcal{O}_1(r) \mathcal{O}_{-1}(r') \rangle$.

The polymer configurations are sampled on square lattices of sizes $L \times L$ with periodic boundary conditions in both directions, with one polymer end fixed at the center. The second end evolves according to an improved version of the so-called ‘backbite algorithm’ [136] (see also the extensive review on Monte Carlo simulations for polymers, [137]) such that it properly takes in account the Boltzmann weight of doubly visited sites and straight segments. The trivial, empty configuration which is just represented as a point-like polymer at the center of the $L \times L$ lattice is assigned the winding numbers $w_x = 0, w_y = 0$. Whenever the polymer crosses one vertical or horizontal boundary the corresponding winding number is increased by ± 1 . We proceed as follows

1. start from the trivial, point-like configuration
2. run $500 \times L \times L$ time steps to decorrelate from this initial configuration
3. then run $10^7 \times L \times L$ time steps, and sample the configurations with $w_x = w_y = 0$, measuring the end-to-end distance r between the two ends of the polymer.

This produces an histogram of r^2 of the form

$$H(r) = \sum_{|e' - 0|^2 = r^2} G_1(0, e') + \dots, \quad (4.14)$$

where the dots indicate for finite size corrections related to the fact that the polymer interacts with itself if part of it goes around the torus in either direction. In practice we produce for each size several of such histograms (between 10 or 20 depending on the size), and compute the corresponding average and error bars. The function $G_1(0, e')$ can be extracted from $H(r)$ by either some binning procedure, or for each integer value of r^2 by dividing the $H(r)$ by the number of different possible e' such that $|e' - 0|^2 = r^2$, eliminating those for which no such e' exist (for instance $r^2 = 3$ cannot be obtained on the lattice; more generally we are in presence of one application of Jacobi's two-squares theorem, a simple proof of which can be given in [138]). After normalizing $G_1(\text{one lattice spacing}) = 1$ the function we eventually consider is $G_1(r)$ measured for r given by a fixed ratio of L , $r = \alpha L$ with $\alpha \ll 1$. In practice $\alpha = 0.25$ will turn out convenient. This ensures that with respect to the total size of the lattice the polymer is almost closing on itself, and therefore that the corrections coming from walks going around the torus and back should scale as L^{-2x_2} , where the two-legs watermelon exponent x_2 is positive all the critical phases of interest.

We will in particular look at the points Θ_{BN} and Θ_{DS} . The latter, which is described by a compact CFT, will serve us as a check of the efficiency of our algorithm and as a comparison for the odd results obtained in the former.

Compact case: the point Θ_{DS}

The point Θ_{DS} is described by an ordinary, compact CFT, and we typically expect that $G_1(r)$ should be given by an expression of the form

$$G_1(r) \propto \left(\frac{\epsilon}{r_{IJ}} \right)^{2x_1} + C \left(\frac{\epsilon}{r_{IJ}} \right)^{2x'_1} + \dots, \quad (4.15)$$

where $x'_1 > x_1$. This guarantees that the contributions of the various terms to G_1 can be well separated at large distance, and that the asymptotic behavior is fully determined at leading order by x_1 , which is here known from (4.8) to be equal to $\frac{1}{4}$. From there, we expect that the measure of $G_1(\alpha L)$ as a function of L should behave as

$$\log G_1(\alpha L) = -2x_1 \log L + A + C \left(\frac{\epsilon}{\alpha L} \right)^{2x'_1} + \dots \quad (4.16)$$

As shown in figure 4.3 (where it turns out sufficient to simplify the corrections in (4.16) by setting $x'_1 = 1$, and where we further note $\frac{C\epsilon}{\alpha} \equiv B$), these expectations are nicely corroborated by our results, and yield an estimation $x_1 \simeq 0.245$ which is close to the expected $x_1 = \frac{1}{4}$. Note that this does not correspond to the $\ell = 1$ case in the previously given equation (4.8), but rather to $\ell = 2$, as stems from the previously mentioned argument that imposing one path between two sites on the square lattice with straight lines forbidden ($p = 0$) is actually equivalent to imposing two of them.

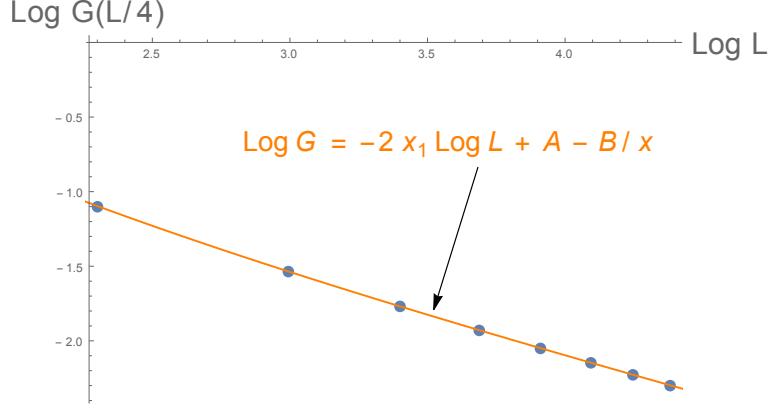


Figure 4.3: Fit of $\log G_1(0.25L)$ against $\log L$ measured from Monte-Carlo sampling at the point Θ_{DS} for $L = 10, \dots, 100$ (the error bars are also plotted, yet relatively small). A fit of the form (4.16) seems in good agreement with the numerical data, and yields $x_1 \simeq 0.245$.

Non compact case: the point Θ_{BN}

Things are different in the non compact case, where we expect that the operators $\mathcal{O}_{\pm 1}$ should be described by the whole continuum of exponents contributing to the $\ell = 1$ sectors, parametrized by an exponent of the form (3.55)

$$x_{1,s} = x_1 + \kappa s^2. \quad (4.17)$$

We therefore expect that $G_1(r)$ should have the form

$$G_1(r) \approx \int_0^\infty ds \frac{f_1(s)}{r^{2(x_1 + \kappa s^2)}}, \quad (4.18)$$

where the amplitude $f_1(s)$ is determined by several factors, including the matrix elements between the lattice spin observable and the eigenstates with quantum numbers $(m = 1, j = 0, 1, \dots)$ as defined in section 3.2 and the (properly defined) density of states of the corresponding continuum. Even though the theory is non unitary, we expect the function f_1 to be positive, as was checked on cylinders of sizes $L = 4, 6, 8, 10$, where we explicitly computed the matrix elements $\langle 1, j | \sum_{i=1}^L S_i^{(+)} | 0, 0 \rangle$.

The practical point of an expression such as (4.18) is that the term going as r^{-2x_1} , which is the only one identified by the naive determination of the 1-leg operator, determines the leading behavior of the correlation function at extremely large r only. It is difficult to say much more without having a better idea of the function f_1 , but it is nonetheless clear to start, that any match of an expression such as (4.18) to a pure power law r^{-2x} should lead to an effective exponent $x > x_1$. Let us try to go a bit further, by noting that writing

$$G_1(r) = r^{-2x_1} \int_0^\infty ds f_1(s) e^{-2a_1 s^2 \ln r}, \quad (4.19)$$

there are known techniques [139] to extract an asymptotic expansion for G_1 based on the analyticity properties of f_1 near the origin. We will restrict ourselves to the leading term here, and simply observe that, if

$$f_1(s) = s^z [b_0 + sb_1 + \dots], \quad s \rightarrow 0, \quad (4.20)$$

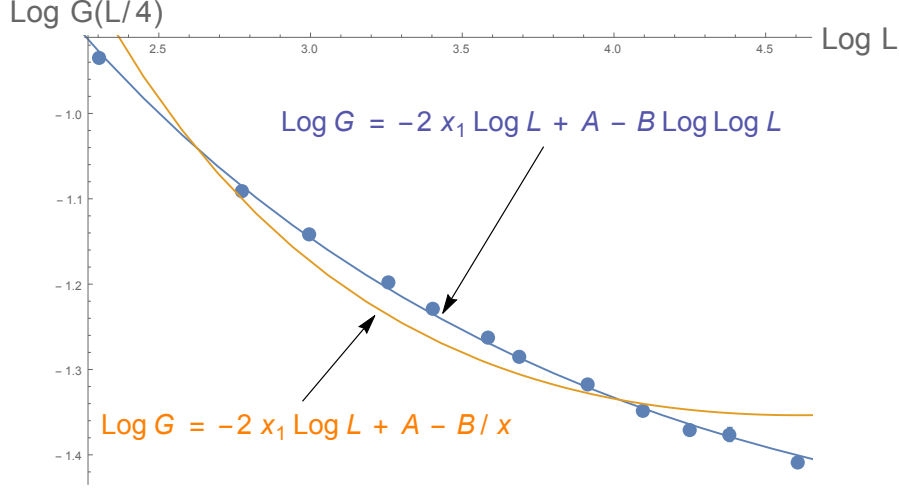


Figure 4.4: Fit of $\log G_1(0.25L)$ against $\log L$ measured from Monte-Carlo sampling at the point Θ_{BN} for $L = 10, \dots, 100$ (the error bars are also plotted, yet relatively small). In this case a fit of the form (4.16) is clearly not appropriate (orange curve), and we find much better agreement with (4.22) (blue curve).

we will have

$$G_1(r) = r^{-2x_1} (\ln r)^{-(1+z)/2} \left[c_0 + \frac{c_1}{\sqrt{\ln r}} + \dots \right], \quad (4.21)$$

so that the measure of $G_1(\alpha L)$ as a function of L should behave as

$$\log G_1(\alpha L) = -2x_1 \log L + A - \frac{1+z}{2} \log \log L + \frac{c_1}{\sqrt{\log L}} + \dots \quad (4.22)$$

Looking at our numerical results (see figure 4.4), the least we can say is that these seem much better accounted for by formula (4.22) than by the one we used in the compact case. The blue curve in the figure is obtained by keeping only the three first terms in the right-hand side of (4.22), and plugging at hand the known value of $x_1 = -\frac{5}{48}$. This yields the estimation $z \simeq 1.7$, which is however very sensitive to the presence of higher corrections in the fit, and shall therefore not be trusted too quantitatively.

Even though the numerical results presented in this section seem rather satisfactory, it could be of course that f_1 has some very different behavior: at this stage, very little is unfortunately known about this problem. It is in any case quite striking that, even though $x_1 < 0$ (and therefore at very large distances the function $G_1(r)$ should be an increasing function of r), at the distances that could be achieved here $G_1(r)$ is a decreasing function of r , hence an effective $x_1 > 0$ at intermediate distances.

4.2.2 The ν and γ exponents

We now come back to the canonical case, which the object of most of the lattice Monte Carlo simulations presented in the litterature [135]. Instead of the correlation function $G_1(e, e')$ (4.13), the quantity usually studied is rather the fixed length partition function,

$$Z_1(e, e') = \sum_{\text{VISAW}: e \rightarrow e'} \tau^{\# \text{ doubly visited sites}} p^{\# \text{ straight segments}}, \quad (4.23)$$

so even if the function $f_1(s)$ was known, going from $G_1(e, e')$ to $Z_1(e, e')$ would require making hypotheses on the scaling form of the correlation function in the vicinity of the critical point $K \neq K_{\text{BN}}$, and inverting the corresponding expressions of G_1 considered as a Laplace transform of Z_1 .

Although there seems little point in speculating about what may happen until more detail is available for the function f_1 , we can use a short cut to the estimations of the exponents ν and γ the set of scaling relations (4.10). Indeed, the canonical function Z_1 and its two-legs analog Z_2 should be expected to involve, as do their grand-canonical counterparts, a continuous mix of exponents resulting in effective values of x_1 and x_2 larger than their exact expectations (corresponding to the bottoms of the continua), and we therefore set $x_1 = -\frac{5}{48} + \epsilon$, $x_2 = \frac{1}{12} + \epsilon$. To first order in ϵ we thus find $\gamma = \frac{53}{46} - \frac{234}{529}\epsilon < \frac{53}{46}$ and $\nu = \frac{12}{23} + \frac{144}{329}\epsilon > \frac{12}{23}$, so namely the measured ν and γ should be respectively larger and smaller than their ‘true’ values, which is indeed the case in the simulations of [135], where we recall that $\gamma = 1.045 < \frac{53}{46}$ and $\nu = 0.576 > \frac{12}{23}$.

As far as the γ and ν exponents are concerned, the strange discrepancy observed between the numerics of [135] and exact results from integrability is therefore compatible with our scenario.

4.2.3 Discrete states and polymer attraction

We now turn to further observations relating the discrete states structure at the Θ_{BN} point to unusual physical properties. For this sake, let us recall the expression of the central charge of the regime III Izergin–Korepin at $\gamma = \frac{\pi}{4}$, namely, from (3.51),

$$c(\varphi) = \begin{cases} 2 - \frac{12\varphi^2}{\pi^2} & \text{for } \varphi \leq \frac{\pi}{4}, \\ -1 + \frac{4}{\pi^2}(\pi - \varphi)^2 & \text{for } \varphi \geq \frac{\pi}{4}, \end{cases} \quad (4.24)$$

which is related to the scaling of the leading transfer matrix eigenvalue $\Lambda_0^{(L)}$ by

$$-\frac{\log \Lambda_0^{(L)}}{L} = f_\infty - \frac{\pi c(\varphi)}{6L^2} + o(L^{-2}). \quad (4.25)$$

As discussed earlier, the point Θ_{BN} is recovered by taking $\varphi = \frac{\pi}{2}$, which leads to $c = 0$. It is now interesting to consider what happens near $\varphi = \frac{\pi}{2}$, and we set $\varphi = \frac{\pi}{2} - \frac{\epsilon}{2}$ so that non-contractible loops are now allowed, with a weight $\tilde{n} = \epsilon + O(\epsilon^3)$. Setting $f_\infty = 0$ in (4.25), which is the natural normalization where the partition function at $n = \tilde{n} = 0$ is unity (the only contributing configuration is the empty one, with weight 1), we can expand the central charge at this order, and thus

$$\log \Lambda_0^{(L)} = \frac{1}{L} \left(\frac{\tilde{n}}{3} + \frac{\tilde{n}^2}{6\pi} \right) \quad (4.26)$$

Imagine now taking a long cylinder of length L' : as explained in section 1.4, the partition function to leading order in L' is given by

$$\ln Z \approx L' \log \Lambda_0^{(L)} \approx \frac{L'}{L} \left(\frac{\tilde{n}}{3} + \frac{\tilde{n}^2}{6\pi} \right) \quad (4.27)$$

At the same time, this partition function can be expanded in powers of \tilde{n} as

$$Z = 1 + \tilde{n}z_1 + \tilde{n}^2z_2 + \dots \quad (4.28)$$

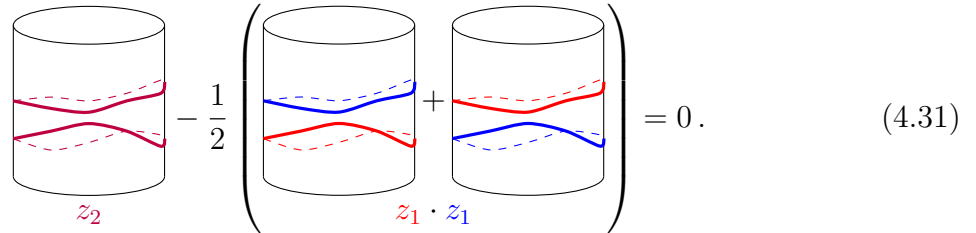
where z_1 is the partition function with one non contractible loop anywhere on the cylinder, z_2 the one with two such loops, etc... From this it results

$$\ln Z = \tilde{n} z_1 + \tilde{n}^2 \left(z_2 - \frac{1}{2} z_1^2 \right) + \dots, \quad (4.29)$$

and comparing (4.27) and (4.29), we find

$$z_2 - \frac{1}{2} z_1^2 = \frac{L'}{L} \frac{1}{6\pi}. \quad (4.30)$$

Clearly, the positive sign of the right-hand side of (4.27) has to do with the positive curvature of the second expression in (4.24), and is therefore intimately related with the discrete state structure, whereas for ‘usual’ critical phases for polymers the central charge is generally a quadratic function of the twist with negative curvature, resulting in a negative value of (4.27). Let us now see what this means physically. The terms in z_2 and $\frac{1}{2} z_1^2$ corresponding to pairs of non contractible loops distant from each other clearly cancel, as shown by the following diagram,



$$z_2 - \frac{1}{2} \left(z_1 \cdot z_1 \right) = 0. \quad (4.31)$$

On the contrary terms in z_1^2 where the two non contractible loops intersect each other are not allowed in z_2 , and are therefore responsible for negative contributions to $z_2 - \frac{1}{2} z_1^2$. In the case where polymers attract one another (that is, typically, $\tau > 1$), we however expect that this effect should be at least partially compensated by the mutual attraction energy between pairs of non contractible loops coming close to each other, which should increase the contributions of terms in z_2 without affecting those in z_1^2 . Whereas this countereffect is expected to remain rather small in usual cases such as the Θ_{DS} or the dense phase, it is noticeable that in the Θ_{BN} case the attraction seems strong enough to make those a priori small contributions in fact dominant.

4.3 Probing the non compact degrees of freedom

Having investigated in detail the physical properties at the peculiar point Θ_{BN} , we now wish to investigate the phase diagram in the vicinity of this point. As we will see, this will help us consolidate the intuition that the non compact degree of freedom s is closely related to the dynamics of empty lattice edges.

4.3.1 Relationship between the black hole and dense phase

We start with the simple but crucial observation that the radius (or, in the conventions of equation 3.46, the coupling constant g) of the compact boson in regime III is the *same*, for a given value of γ (that is, for a given values of the loop weight n), as that of the compact boson describing the corresponding dense phase. Specializing to the polymer

case ($n = 0$), we see for instance that the watermelon exponents in the dense phase (4.4) and at Θ_{BN} (4.9) are related by

$$x_m^{\text{D}} = x_m^{\text{BN}} - \frac{1}{12}, \quad (4.32)$$

which can be easily interpreted as the identical m^2 term arises from the fact that both theories involve the same compact boson, whereas the shift of $-\frac{1}{12}$ is associated with a shift of the central charge coming from the non compact boson. More precisely, we can ‘undo the twist’ and rewrite the scaling of the transfer matrix eigenvalues in both cases,

$$\begin{aligned} -\frac{\log \Lambda_{\ell, \text{BN}}^{(L)}}{L} &= f_{\infty} + \frac{2\pi}{L^2} \left(\frac{\ell^2}{16} - \frac{1+1}{12} \right), \\ -\frac{\log \Lambda_{\ell, \text{D}}^{(L)}}{L} &= f_{\infty} + \frac{2\pi}{L^2} \left(\frac{\ell^2}{16} - \frac{1}{12} \right), \end{aligned} \quad (4.33)$$

which shows that taking the leading eigenvalues in the ℓ -legs sectors at the Θ_{BN} point and making the non-compact boson massive, hence replacing the (untwisted) central charge $c = 1 + 1$ by $c = 1$, should recover the scaling behaviour of the dense phase.

Switching back to the twisted case, we expect that making the non compact boson massive while leaving the compact one untouched should make the discrete level disappear, letting the central charge be determined by the first expression of (4.24) at twist $\varphi = \pi - 2\gamma = \frac{\pi}{2}$ (that is $c = -1$), *minus* the $c = 1$ central charge of the free compact boson, so all in all $c = -2$, which is precisely the central charge of the dense polymers.

These observations made at $n = 0$ ($\gamma = \frac{\pi}{4}$) can be easily generalized, so the point Θ_{BN} , and more generally the critical point in regime III, therefore look in many respects like a dense polymer supplemented by a non compact degree of freedom. To illustrate this point, we refer to figure 4.5, where we study the evolution of the levels ($m = 0, j$) as we perturb the monomer fugacity K away from its value at Θ_{BN} . From there it is apparent that the non compact ($j \neq 0$) levels with become massive on both $K < K_{\text{BN}}$ and $K > K_{\text{BN}}$ sides, corresponding respectively to the massive and dense phases.

4.3.2 Probing degrees of freedom

We now turn more particularly to the study the average density of monomers $-\frac{\partial f_0}{\partial K}$ evaluated numerically from the ground state free energy $f_0 = -\frac{1}{L} \log \Lambda_0$ as a function of the monomer fugacity K . Both in the twisted and untwisted cases we find very clearly that there is a *first order phase transition*, with a discontinuity in monomer density. Whereas in the massive $K < K_{\text{BN}}$ phase the average density of monomers is simply equal to zero in the thermodynamic limit, in the dense $K > K_{\text{BN}}$ phase it assumes a finite value with non critical fluctuations, namely the physics of the model is simply the one of the six-vertex model or ordinary fully packed loops.

These observations strongly suggest that the non compact degree of freedom is associated with fluctuations of monomer density, as these fluctuations become non critical precisely when the non compact degree of freedom disappears. Since the total number of edges on the lattice is of course constant, the number of empty edges and the monomer density are directly related, and we therefore propose that the empty edges of the loop model (or, the edges carrying a state 0 in the vertex model) have a dynamics described in the continuum limit by a non compact boson, in a similar way as they do, at the point associated with regime II, have a dynamics described by a critical Ising degree of freedom.

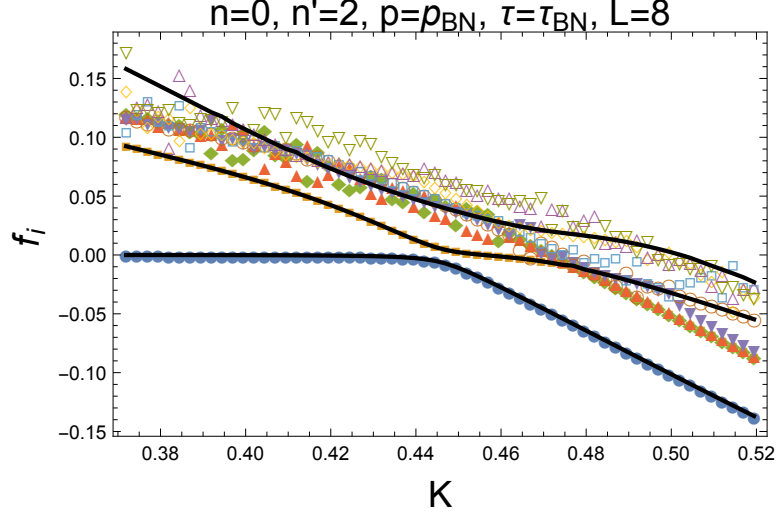


Figure 4.5: Eigenlevels $f_i = -\frac{1}{L} \log \Lambda_i$ in the sector $\ell = 0$, measured for $L = 8$ as a function of the monomer fugacity K around the point Θ_{BN} , in the 'untwisted' case where non contractible loops are assigned a weight $\tilde{n} = 2$. Overlined in black are the levels $(0, j)$ ($j = 0, 1, 2$ from bottom to top). For $j \neq 0$, these levels become massive away from $K = K_{\text{BN}}$. Similar results are observed in other magnetization sectors and for other values of the weight \tilde{n} of non contractible loops.

4.3.3 A model for $K \approx K_{\text{BN}}$

In order to refine the connection between the non compact boson and the dynamics of empty edges (or alternatively, the fluctuations of the monomer density), we now search for the operator content driving the transition from the black hole CFT to that of the dense compact boson. Namely, we look for a perturbation of the black hole action (3.61) of the form

$$\mathcal{S} = \frac{k}{4\pi} \int d^2x \frac{|\partial_\mu \Psi|^2}{1 + |\Psi|^2} + (K - K_{\text{BN}}) \int d^2x [\Phi] \quad (4.34)$$

which, contrary to the perturbations (3.81) associated with imaginary staggerings of the spectral parameter, is this time not integrable. Resulting from a perturbation of the form (4.34), we expect on dimensional grounds that the divergence of the correlation length as $K \rightarrow K_{\text{BN}}$ should be described by an exponent $\nu = \frac{1}{2-x}$, where x is the dimension of the most relevant operator Φ ². Numerically, we obtain the latter by studying the ratios $\frac{\Lambda_i^{(L)}}{\Lambda_0^{(L)}}$ between of the leading and some given excited transfer matrix eigenvalues at various system sizes L and looking for the value of ν for which the data at various sizes satisfy a collapse of the form

$$\log \frac{\Lambda_i^{(L)}}{\Lambda_0^{(L)}} = -\frac{2\pi}{L} F \left((K - K_{\text{BN}}) L^{\frac{1}{\nu}} \right). \quad (4.35)$$

As discussed in the previous chapter the black hole theory allows for operators as-

²There is not much experience in statistical mechanics dealing with theories with a non normalizable ground state, as it is the case for the black hole. As a consequence, it is not clear whether the exponents x entering the definition of ν should be measured with respect to the true $c = 2 + \frac{6}{k-2}$ central charge or the effective central charge $c = 2$.

sociated with both normalizable and non normalizable states, and the operator(s) $[\Phi]$ coupled to $K - K_{\text{BN}}$ may be of either nature. The former correspond to the non unitary series of $SL(2, \mathbb{R})$, with negative conformal weights both over the true $c = 2 + \frac{6}{k-2}$ and effective $c = 2$ central charges, and therefore would lead to exponents $\nu < \frac{1}{2}$. This case is easily discarded from the numerical estimation of ν , as we find at various twists and values of γ numerical estimations of ν which, although not very precise, are all definitely larger than $\frac{1}{2}$. This means that the operator coupled to $K - K_{\text{BN}}$ must be normalizable, hence belongs to the continuous, principal series $j = -\frac{1}{2} + i\mathbb{R}$, whose exponents we recall to be of the form

$$\Delta(\bar{\Delta}) = -\frac{j(j+1)}{k-2} + \frac{(n \pm kw)^2}{4k}. \quad (4.36)$$

It is reasonable, in the absence of other indications, to consider the bottoms of the continua given by $j = -\frac{1}{2}$. Since monomer pieces involve moreover two links, the most conservative operators one can think of are associated to $j = -\frac{1}{2}, n = 0$ and $j = -\frac{1}{2}, n = 2$, with respective dimensions $\Delta(\bar{\Delta}) = \frac{1}{4(k-2)}$ and $\Delta(\bar{\Delta}) = \frac{1}{4(k-2)} + \frac{1}{k}$ with respect to the true central charge of the model, and therefore of effective dimensions $\Delta(\bar{\Delta}) = 0$ and $\Delta(\bar{\Delta}) = \frac{1}{k}$ with respect to the effective central charge $c = 2$. (we see in particular that operators with $w \neq 0$ have too large a dimension to be relevant). The perturbation we consider is therefore written as a linear combination of these two operators, whose corresponding wavefunctions in the mini-superspace approximation are obtained from the formula (3.149), so in the action (4.34) we have to use

$$[\Phi] = \alpha F(1/2, 1/2; 1, -|\Psi|^2) + \beta(\Psi^2 + \bar{\Psi}^2)F(3/2, 3/2; 3, -|\Psi|^2) \quad (4.37)$$

We refer to [63] for a detailed analysis of the perturbation (4.37), where it is shown in particular that $\alpha = 0$ would lead to both fields r and θ becoming massive on both sides of the transition. Since this is clearly not the case we have $\alpha \neq 0$, so the action is dominated by the corresponding term, which is the most relevant, and we can simplify our analysis by taking $\beta = 0$. In this case the hypergeometric function is monotonically decreasing from $F = 1$ for $z = 0$ to $F \sim \frac{1}{|z|}$ when $|z| \rightarrow \infty$, so we are lead to the following conclusions.

- For $K < K_{\text{BN}}$, the action is minimized when F is at its maximum, so $|\Psi| = 0$. This corresponds to a massive theory, with no critical degrees of freedom left.
- For $K > K_{\text{BN}}$, the action is minimized when F is as small as possible, so $|\Psi| \rightarrow \infty$, or $r \rightarrow \infty$. This corresponds precisely to the cylinder limit of the cigar, and the only remaining fluctuating field is θ , namely the free compact bosonic part of the black hole, which we have besides identified as describing precisely the dense phase.

Note that this mechanism also nicely explains the first order transition observed in the previous section: for $K < K_{\text{BN}}$, $\Psi = 0$ yields an action $\mathcal{S} \approx \mathcal{S}_{\text{CFT}} + \int d^2x (K - K_{\text{BN}})\alpha$, while for $K > K_{\text{BN}}$ we find $\mathcal{S} \approx \mathcal{S}_{\text{CFT}} + 0$, hence a discontinuity in the derivative of the action, that is, a first order transition.

We point out a nice possible physical interpretation of $K > K_{\text{BN}}$ phase as a broken symmetry phase, and of the compact boson describing the dense phase as a *Goldstone boson*. Note that one has to be careful with the Coleman Mermin Wagner theorem, stating that *there is no long range order for a system with a broken continuous symmetry in two dimensions or less, at any non zero temperature*, but which stops being valid in the unitary case we are dealing with here. In fact, the phenomenology we propose is similar

in spirit to the first order phase transition occurring in systems described by a complex boson, with action

$$\mathcal{S} = \int d^2x |\partial_\mu \Psi|^2 + (K - K_{\text{BN}}) |\Psi|^2 (1 - |\Psi|^2) \quad (4.38)$$

a model known to describe the superfluid transition.

Partial conclusion

This is probably enough to convince us that indeed the transition when K crosses K_{BN} is driven by the field $j = -\frac{1}{2}, n = 0$, of dimension 0 with respect to the effective central charge $c_{\text{eff}} = 2$, and $\Delta = \frac{1}{4(k-2)}$ with respect to the true central charge of the theory, even though neither of these expressions could be securely observed from numerical estimations of the exponent ν . Turning now to the loop model, it is generally believed – and we have checked this numerically – that the ground state energy of the theory (or the free energy per site in the 2d statistical point of view) is independent of the boundary conditions. This means that the scaling should be described by the operator with weight $\Delta = \frac{1}{4(k-2)}$ again, unless – as happens in the case of the 6 vertex model and its loop formulation for instance – the change of boundary conditions leads to the cancellation of some terms, and another, related but different, scaling dimension. In our case however, the corresponding value

$$\nu = \frac{2(k-2)}{4k-9} \quad (4.39)$$

seems to fit numerics reasonably well, and is moreover definitely the correct value for $k = 8, n = 0$, as in this case one can directly identify the operator coupled with $K - K_{\text{BN}}$ with the two-leg operator \mathcal{O}_2 of dimension $\Delta = \frac{1}{24}$ at this point.

4.4 The collapse transition

We now turn back to the study of the collapse transition, or *theta point*. As introduced in section (1.2), this point is of a tricritical nature [18], and much effort has been put forward during the past 25 years to identify the corresponding exponents. In their 1987 paper [140], Duplantier and Saleur (DS) have studied a model proposed originally by Coniglio *et. al.* [141], where the polymer is represented by a SAW on the honeycomb lattice, the faces of which are absent with a probability p . The phase configurations are annealed, and result in a self-attraction of the polymer leading to a tricritical point at the percolation threshold $p = \frac{1}{2}$. The percolation clusters (the perimeters of the absent faces) form a gas of loops with weight $n = 1$ and monomer fugacity $K = 1$, and the approach of [140] uses the fact that the SAW describing the polymer can be considered on the same footing as the those loops, although of a different origin. As a result, the critical properties of the annealed SAW can be described in terms of a $O(n)$ model in its dense phase, for which the central charge and conformal exponents we have already studied in equations (4.7) and (4.8), and are therefore in the same universality class as the branch 0 in the VISAW phase diagram, explaining a posteriori the Θ_{DS} denomination. From there, Duplantier and Saleur yield the exponents

$$\nu_{\text{DS}} = \frac{4}{7}, \quad \gamma_{\text{DS}} = \frac{8}{7}, \quad (4.40)$$

which were then shown [142] to be stable against the addition of further interactions, as well as against a change of the lattice. The equivalence with the universality class of the Θ_{DS} point in the VISAW phase diagram was established further from numerical investigation in [143] through a mapping onto kinetic growth walks on the Manhattan lattice. It is worth noting that, although in the same universality class, the branch 0 yields $\nu_0 = \frac{4}{7}$, $\gamma_0 = \frac{6}{7}$, as results from the already explained fact that for the corresponding square lattice model the exponent x_1 is constrained to take the same value as x_2 , namely $x_1 = \frac{1}{4}$.

In spite of this promising results, a severe objection can be formulated to the claimed universality of the Θ_{DS} point. Indeed the latter is a point of particular ‘ $p = 0$ ’-related symmetry, which is otherwise broken whenever $p \neq 0$. Labeling by $1, \dots, L$ the sites of the loop row-to-row transfer matrix it is indeed easily seen that for $p = 0$ the action of the latter sends each loop segment occupying an odd (even) site on an even (odd) site, or alternatively contracts a pair of neighbouring segments or creates pairs on neighbouring sites, and therefore all in all anticommutes with the total $\tilde{m} = \sum_{i=1}^L (-1)^i |S_i^{(z)}|$ which counts a term ± 1 for each loop segment on a given row with a site parity-dependent sign. In each through-lines sector the transfer matrix therefore breaks into smaller sectors, which get mixed together as soon as $p \neq 0$. It can therefore reasonably argued, as it was in [75] the symmetry breaking at $p = 0$ might lead the system to another, more generic theta point describing the true nature of the collapse transition, whereas Θ_{DS} would then be of some higher multicritical nature. This observation lead Nienhuis and collaborators to naturally assume that the real theta point physics should correspond to the integrable Θ_{BN} point [75, 78], whose exponents ν and γ we recall to be given by

$$\nu_{\text{BN}} = \frac{12}{23} \simeq 0.522, \quad \gamma_{\text{BN}} = \frac{53}{46} \simeq 1.152. \quad (4.41)$$

Contrary to these expectations, evidence has been gathered over the last several years [144, 145] that the exponents (4.40) of the DS model are indeed those of the generic theta point. This however still did not complete the answer to the puzzle of understanding the full VISAW phase diagram, as it remained to be solved the fundamental question of which kind of physics did the Θ_{BN} point describe, if not the $O(n = 0)$ φ^6 theory expected for the tricritical theta point (see equation (1.12)). As we have reviewed at length throughout this manuscript the answer to this question is at the least quite surprising, as the Θ_{BN} point is in fact described by a CFT of a non compact nature, namely the $SL(2, \mathbb{R})_k/U(1)$ black hole, with $k = 8$ at the polymer point. That this CFT has obviously nothing to do with some $O(n = 0)$ φ^6 field theory arguably rules it out as a candidate for the description of the theta point, and we have moreover been able in the previous sections to relate the odd outcome of numerical experiments at this point to the continuous features of the corresponding CFT spectrum.

In order to make the picture complete, we now would like to understand the nature of the renormalization group flow along the multicritical line joining Θ_{DS} to Θ_{BN} , and beyond. Indeed, the conclusion that the former does correspond to *the* generic theta point suggests that it might be stable in the K, p, τ plane despite its apparent peculiar symmetry, and therefore that there should be a flow $\Theta_{\text{BN}} \rightarrow \Theta_{\text{DS}}$ in both directions of the multicritical line. This conjecture moreover agrees with Zamolodchikov’s c -theorem, stating that the central charge decreases along the renormalization group flow³, however checking it numerically is a very difficult task, as in particular the precise location of

³Note that the c -theorem only applies to unitary theories, and therefore not to the twisted Θ_{BN}

the multicritical line away from the points Θ_{BN} and Θ_{DS} is unknown, and numerical estimations of critical exponents slightly off it are badly plagued by the flow towards the dense or massive phases as well as the proximity with the Ising or dilute critical surfaces. We can, however, make interesting observations by investigating what happens of the non compact boson when following continuously the levels (m, j) from Θ_{BN} to Θ_{DS} . Whereas perturbations of the former point in the direction of the dense or dilute phases was shown to result in making the non compact boson massive (see for instance figure 4.5), we observe that the levels $j \neq 0$ appear to remain critical at Θ_{DS} , and therefore most likely on the whole multicritical line. From the study of the first few of these levels in the sectors of zero magnetization, it seems further these become degenerate with the magnetic excitations of the compact boson at Θ_{DS} , namely

$$x_{0,j}^{DS} = g \frac{j^2}{2}, \quad (4.42)$$

to be compared with (4.7).

To conclude, the conjecture we therefore make is that the critical behaviour on the multicritical line, except at the Θ_{BN} point, is described by the physics of the Θ_{DS} point, namely a free compact boson CFT with exponents given by (4.8), while the non compact levels of Θ_{BN} become exactly degenerate with the corresponding magnetic spectrum.

theory, which allows for negative conformal weights. However, it is natural to expect that the RG flow between twisted theories should be the same as the flow between their untwisted versions. In the latter case the theories can be considered as unitary provided one restricts to the normalizable states, and the c -theorem predicts a flow from the theory with $c = 2$ to the theory with $c = 1$, that is, from the Θ_{BN} black hole to the Θ_{DS} compact boson.

Chapter 5

Application to the Integer Quantum Hall Effect

In this final chapter we come back to what we initially gave as one of the main motivations for studying non compact CFTs, namely, the quest for an exact solution Integer Quantum Hall Effect plateau transition. In chapter 2 we have, following the work of Ikhlef *et. al.* [39], devised a truncated exactly solvable model for the computation of transport observables at the transition, the so-called $b_2^{(1)}$ model, and left pending the issue of whether such a truncation might or might not recover the untruncated universality class. Regarding the results of chapter 3, where several compact statistical mechanics models were shown to allow for an unsuspected non compact continuum limit, the more general question, to which a negative answer would have commonly been given until recently, of whether such a truncation might at all have for continuum limit a non compact field theory is now to be considered with some respect. After a review of the results by Ikhlef *et. al.* [39] in section 5.1, we will present in section 5.2 a complete solution of the $b_n^{(1)}$ model, borrowing heavily from our earlier analysis of the cousin $a_3^{(2)}$ model. It will not come as much surprise anymore that once again, the result is a CFT of a non compact nature, hence giving the latter question a positive answer. This will allow us to correct some of the results in [39], and to reconsider the former question of whether this CFT truly describes the plateau transition. Even though this may not be precisely the case, we will present in section 5.3 an appealing qualitative understanding of how the operator content of the IQHE transition might partly understood from its truncated counterpart.

5.1 Review of the results by Ikhlef *et. al.*

The construction of Ikhlef *et. al.* of an integrable model for the truncated geometrical description of transport observables at the Quantum Hall transition was presented in detail in section 2.4.

We will here review some of the results of [39] for this model, recast in the notations of the $b_2^{(1)}$ model. Namely, we rewrite the integrable weights (2.120) in terms of the quantum group anisotropy γ and the spectral parameter u , related to θ and φ by

$$\gamma = 2\pi - 2\theta, \quad u = \varphi, \quad (5.1)$$

so that in particular the loop weight is $n = -2 \cos 2\theta = -2 \cos \gamma$. The (loop) transfer matrix is 2π -periodic as a function of γ , and the study of its different regimes can be

restricted to the study of $\gamma \in [0, \pi]$ and the two isotropic values of the spectral parameter $u_{\pm} = \frac{3\gamma}{2} (+\pi)$. The different regimes identified in [39] are then

- Regime I, for $u = u_+$ and $\gamma \in [0, \frac{2\pi}{3}]$. The central charge of the loop model is found numerically to be of the form,

$$c = 2 \left[1 - \frac{6\gamma^2}{\pi(\pi - \gamma)} \right] + \frac{1}{2}, \quad (5.2)$$

and the physics of the model is identified as that of two decoupled compact bosons associated with the two colours of loops, plus some additional Ising degree of freedom which we presume to have the same origin as that appearing in the regime II of the $a_2^{(2)}$ model.

- Regime II, for $u = u_+$ and $\gamma \in [\frac{2\pi}{3}, \pi]$. The central charge of the loop model is

$$c = 2 \left[1 - \frac{6(\pi - \gamma)^2}{\pi\gamma} \right], \quad (5.3)$$

so this regime is described simply by the two decoupled bosons, without an additional degree of freedom.

- Regime III, for $u = u_-$ and $\gamma \in [\frac{2\pi}{3}, \pi]$. The central charge is of the form

$$c = \frac{3(\pi - 2\gamma)^2}{\pi\gamma} + \frac{1}{2}, \quad (5.4)$$

and the physics is presumably that of the regime IV, which will be studied in detail in the following, supplemented by a critical Ising degree of freedom.

- Regime IV, for $u = u_-$ and $\gamma \in [0, \frac{2\pi}{3}]$, with a central charge of the puzzling form.

$$c = \frac{3(\pi - 2\gamma)^2}{\pi(\pi - \gamma)}. \quad (5.5)$$

There are two points corresponding to $n = 0$, namely $\gamma = \frac{\pi}{2}$, which can be considered as candidates for recovering the universality class of the non integrable critical truncation (2.106). Among these two, the point in regime I is immediately discarded: first the two colours are trivially decoupled, which we would not expect from the strong coupling resulting from the averaging over random phases, second we have at this point $c = -\frac{7}{2}$, which is clearly not in agreement with the $c = 0$ value expected in the case of disordered systems, as can be seen from the trivial partition function $Z = 1$ or by numerical study of the non integrable truncation. In contrast, the point in regime IV seems to show a non trivially coupled physics and yields indeed $c = 0$, so gives presumably a good description of the original critical truncation. This motivates us to study regime IV further.

Parametrizing $\gamma = \frac{\pi}{k+2}$, the central charge in this regime reads

$$c = \frac{3k^2}{(k+1)(k+2)}, \quad (5.6)$$

and is for integer values of k identified with that of the coset

$$\frac{SU(2)_k \times SU(2)_k}{SU(2)_{2k}} = \frac{SO(4)_k}{SO(3)_k}, \quad (5.7)$$

Interestingly, this coset theory also appeared in the description of the $a_3^{(2)}$ model in regime III, see for instance equations (3.123) and following. Using the same parametrization of γ in that case and setting $\varphi_1 = \varphi_2 = \gamma$ such as to give non contractible loops the same weight n as contractible ones, we recover precisely the central charge (5.6) from the Bethe ansatz result (3.111), as was already observed by Fendley and Jacobsen in [92]. In this sense, the dilute model we are considering here and its fully packed counterpart in their respective regimes IV and III and for integer k can be considered as the ‘dilute’ and ‘dense’ branches of the same $\frac{SO(4)_k}{SO(3)_k}$ coset theory¹. This, however, is not enough of an answer for our purpose, as the coset description at integer k does not say anything about the nature of the CFT describing regime IV for continuous values of γ , and in particular in the $k = 0$ case of relevance in the Quantum Hall problem. Whereas it could be naturally believed that all critical exponents are given throughout the whole regime by an analytic continuation of their coset expressions, at it is the case for instance for the central charge, it is observed in [39] that in particular the thermal exponent x_t defined as the conformal dimension for the first excited state in the zero-leg sector deviates from the continued value $\frac{2k}{k+1}$ for $r \lesssim \frac{1}{2}$, a fact left unexplained by the authors of [39].

In order to fill these gaps, we therefore turn to a detailed analysis of the Bethe ansatz equation for the $b_n^{(1)}$ in the particular case of regime IV.

5.2 Continuum limit of the $b_n^{(1)}$ model

5.2.1 Bethe ansatz solution in regime IV

The $b_2^{(1)}$ transfer matrix acts on the tensor product of five-dimensional $U_q(so_5^{(1)})$ evaluation representations, to which we can assign the two colours interpretation by indexing the states as

$$\{\downarrow\downarrow, \uparrow\downarrow, 00, \downarrow\uparrow, \uparrow\uparrow\}, \quad (5.8)$$

and defining the two sets of spin *one* operators $S_{i,(1)}^{(z)}, S_{i,(2)}^{(z)}$, so that we write the transfer matrix as

$$T(u) = \text{Tr}_a \left(\check{R}_{a1}(u) \dots \check{R}_{aL}(u) e^{i(\varphi_1 S_{a,(1)}^{(z)} + \varphi_2 S_{a,(2)}^{(z)})} \right), \quad (5.9)$$

where the \check{R} matrix is given in its vertex formulation in [99], and as in the fully-packed, $a_3^{(2)}$ counterpart we have introduced two independent twist parameters φ_1 and φ_2 . The transfer matrix (5.9) commutes independently with the two magnetizations

$$\begin{aligned} m^{(1)} &= \frac{1}{2} \sum_{i=1}^L S_{i,(1)}^{(z)} \\ m^{(2)} &= \frac{1}{2} \sum_{i=1}^L S_{i,(2)}^{(z)}, \end{aligned} \quad (5.10)$$

(where the $\frac{1}{2}$ factors have been introduced to parallel the quantum numbers of $a_3^{(2)}$, where the eigenvalues of $S_{i,(1,2)}^{(z)}$ are $\pm\frac{1}{2}$ rather than $\pm 1, 0$) and its eigenvalues in the

¹One should however keep in mind that, whereas the regime IV of the dilute model is defined for $\gamma \in [0, \frac{2\pi}{3}]$, the regime III of the dense model is defined for $\gamma \in [0, \frac{\pi}{4}]$, so in particular does not contain the $n = 0$ point, at which the two colours are therefore decoupled.

sector $(m^{(1)}, m^{(2)})$ are described a set of roots of two types $\{\lambda_j^{(1)}, \lambda_k^{(2)}\}_{j=1, \dots, m_1; k=1, \dots, m_2}$, whose numbers m_1, m_2 are related to the magnetizations through

$$\begin{aligned} m^{(1)} &= \frac{L}{2} - \frac{m_1}{2} - \frac{m_2}{2} \\ m^{(2)} &= \frac{L}{2} - m_2, \end{aligned} \quad (5.11)$$

and which are solution of a set of nested Bethe ansatz equations [99]

$$\begin{aligned} e^{2i\varphi_1} \left(\frac{\sinh(\lambda_i^{(1)} - i\frac{\gamma}{2})}{\sinh(\lambda_i^{(1)} + i\frac{\gamma}{2})} \right)^L &= \prod_{j=1, j \neq i}^{m_1} \frac{\sinh(\lambda_i^{(1)} - \lambda_j^{(1)} - i\gamma)}{\sinh(\lambda_i^{(1)} - \lambda_j^{(1)} + i\gamma)} \prod_{k=1}^{m_2} \frac{\sinh(\lambda_i^{(1)} - \lambda_k^{(2)} + i\frac{\gamma}{2})}{\sinh(\lambda_i^{(1)} - \lambda_k^{(2)} - i\frac{\gamma}{2})} \\ e^{i(\varphi_1 - \varphi_2)} \prod_{j=1}^{m_1} \frac{\sinh(\lambda_k^{(2)} - \lambda_j^{(1)} - i\frac{\gamma}{2})}{\sinh(\lambda_k^{(2)} - \lambda_j^{(1)} + i\frac{\gamma}{2})} &= \prod_{l=1, l \neq k}^{m_2} \frac{\sinh(\lambda_k^{(2)} - \lambda_l^{(2)} - i\frac{\gamma}{2})}{\sinh(\lambda_k^{(2)} - \lambda_l^{(2)} + i\frac{\gamma}{2})}. \end{aligned} \quad (5.12)$$

The corresponding energies read

$$E = \pm \sum_{i=1}^{m_1} \frac{2 \sin \gamma}{2 \cosh 2\lambda_i^{(1)} - \cos \gamma}, \quad (5.13)$$

whose two signs can be related, as for the previously studied models, to the two choices u_{\pm} of the spectral parameter. In particular the regime IV corresponds to a minus sign and $\gamma \in [0, \frac{2\pi}{3}]$. There, the ground state is seen to be described by $\frac{L}{2}$ 2-strings of $\lambda^{(1)}$ roots with imaginary part slightly smaller than $\pm (\frac{\pi}{2} - \frac{\gamma}{4})$. and $\frac{L}{2}$ 2-strings of $\lambda^{(2)}$ roots with imaginary part slightly bigger than $\pm (\frac{\pi}{2} - \frac{\gamma}{4})^2$. The scattering equations for the corresponding densities read

$$\begin{aligned} \rho_1 + \rho_1^h &= \frac{\sinh \frac{\omega\gamma}{4} + \sinh \omega \frac{3\gamma}{4}}{\sinh \frac{\omega\pi}{2}} + \rho_1 \frac{\sinh \omega (\frac{\pi}{2} - \frac{3\gamma}{2}) + \sinh \omega (\frac{\pi}{2} - \frac{\gamma}{2}) + 2 \sinh \omega (\frac{\pi}{2} - \gamma)}{\sinh \frac{\omega\pi}{2}} \\ &+ \rho_2 \frac{-2 \sinh \omega (\frac{\pi}{2} - \frac{\gamma}{2}) - \sinh \omega (\frac{\pi}{2} - \gamma)}{\sinh \frac{\omega\pi}{2}} \end{aligned} \quad (5.14)$$

$$\begin{aligned} 0 &= \rho_1 \frac{-2 \sinh \omega (\frac{\pi}{2} - \frac{\gamma}{2}) - \sinh \omega (\frac{\pi}{2} - \gamma)}{\sinh \frac{\omega\pi}{2}} \\ &+ \rho_2 \frac{2 \sinh \omega (\frac{\pi}{2} - \frac{\gamma}{2}) + \sinh \omega (\frac{\pi}{2} - \gamma)}{\sinh \frac{\omega\pi}{2}}, \end{aligned} \quad (5.15)$$

that is $\rho_1 = \rho_2 \equiv \rho$, which is already apparent from the look of finite size solutions. The scattering equation for the density ρ is written in the now usual form (3.40), whose kernel at zero frequency reads $K = 1 - \frac{4\gamma}{\pi}$, so the conformal weights follow as

$$\Delta + \bar{\Delta} = \frac{\gamma}{\pi} n_1^2 + \frac{\pi}{4\gamma} w_1^2, \quad (5.16)$$

²A technical subtlety occurs with the latter for γ close to zero, as the imaginary parts $\pm (\frac{\pi}{2} - \frac{\gamma}{4} + \epsilon)$ reach $\pm \frac{\pi}{2}$ for finite values of γ , leading to singular roots configuration where the two roots of a 2-string are arbitrarily close to each other, since Bethe roots differing by shifts of $i\pi$ are identified. When this happens, the merged 2-string gets replaced by a pair of roots close to each other on the axis of imaginary part $\frac{\pi}{2}$. Here we will not need to bother about this difficulty, and considering γ far enough from zero will be enough for a general purpose.

where n_1 and w_1 are respectively the number of holes and backscatterings of the of 2-strings in the ground state distribution, so in particular each hole corresponds to 2 holes of $\lambda^{(1)}$ roots and 2 holes of $\lambda^{(2)}$ roots. Using similar arguments as in the regimes II and III of the $a_3^{(2)}$ model, this can be rewritten into

$$\Delta + \bar{\Delta} = \frac{\gamma}{2\pi} ((m^{(1)})^2 + (m^{(2)})^2) + \frac{\pi}{2\gamma} ((w^{(1)})^2 + (w^{(2)})^2), \quad (5.17)$$

which is precisely the same as the conformal weights (3.107) obtained for the regime III of the $a_3^{(2)}$ model, while the central charge is found numerically to be $c = 3$ at zero twist. As in the $a_3^{(2)}$ case only two compact bosons appear in the conformal spectrum (5.17), and we look for the missing part by a detailed analysis of the excitations in each $(m^{(1)}, m^{(2)})$ sector. These can once again be indexed by some integer j , and correspond to removing simultaneously j 2-strings of $\lambda^{(1)}$ roots and j 2-string of $\lambda^{(2)}$ roots, to be replaced respectively by j pairs of anticonjugate $\lambda^{(1)}$ (resp. $\lambda^{(2)}$) roots with imaginary parts $\frac{\pi}{2}$ (resp. on the real axis). Numerical resolution of the Bethe equations up to sizes $L \sim 100$, gives rather solid confidence the following spectrum of effective central charges at zero twist

$$-\frac{c_{m^{(1)}, m^{(2)}, j}}{12} = -\frac{3}{12} + \frac{\gamma}{2\pi} (m^{(1)} + m^{(2)})^2 + (N_{m^{(1)}, m^{(2)}, j})^2 \frac{A(\gamma)}{[B_{m^{(1)}, m^{(2)}, j}(\gamma) + \log L]^2}, \quad (5.18)$$

where this time none of the functions $A(\gamma)$ and $B_{m^{(1)}, m^{(2)}, j}(\gamma)$ could however be measured with suitable precision. Extending our study to non zero values of the twist, we observe that the effective central charge are described by the same exact same expressions as in the $a_3^{(2)}$ case, namely by equation (3.112). In particular the central charge reads

$$c = c_{0,0,0} = \begin{cases} 3 - 6 \frac{(\varphi_1)^2 + (\varphi_2)^2}{\pi\gamma} + o(1) & \text{for } \varphi_1 + \varphi_2 \leq \gamma, \\ 3 - 6 \frac{(\varphi_1)^2 + (\varphi_2)^2}{\pi\gamma} + 3 \frac{(\varphi_1 + \varphi_2 - (2j+1)\gamma)^2}{\gamma(\pi - \gamma)} & \text{for } \varphi_1 + \varphi_2 \geq \gamma, \end{cases} \quad (5.19)$$

so taking the values $\varphi_1 = \varphi_2 = \pi - \gamma$ which gives non contractible loops the same weight $n = -2\cos\gamma$ as contractible ones, we recover the expression (5.5). The watermelon operators x_{ℓ_1, ℓ_2} , which can be defined in the same fashion as they were for the one-colour model in the beginning of the previous chapter, are obtained from the scaling of the leading transfer matrix eigenvalues on the sector of magnetizations $(m^{(1)}, m^{(2)}) = (\frac{\ell_1}{2}, \frac{\ell_2}{2})$, so in particular for both ℓ_1 and ℓ_2 non zero we expect

$$x_{\ell_1, \ell_2} = -\frac{c_{2\ell_1, 2\ell_2, 0}(\varphi_1 = \varphi_2 = 0) - c_{0,0,0}(\varphi_1 = \varphi_2 = \pi - \gamma)}{12}, \quad (5.20)$$

that is,

$$\begin{aligned} x_{\ell_1, \ell_2} &= \left(\frac{(\ell_1)^2 + (\ell_2)^2}{8} - 1 \right) \frac{\gamma}{\pi} + \frac{\gamma}{4(\pi - \gamma)} \\ &= \left(\frac{(\ell_1)^2 + (\ell_2)^2}{8} - 1 \right) \frac{1}{k+2} + \frac{1}{4(k+1)}, \end{aligned} \quad (5.21)$$

(for either ℓ_1 or ℓ_2 equal to zero subtelties occur due to crossovers between levels; these occur analogously in the $a_3^{(2)}$ case and are analyzed in detail in [64], however such watermelon sectors will not be of any use for applications to the IQHE and we will not discuss them here).

From our analysis, we conclude that the regime IV of the $b_2^{(1)}$ model is described by the exact same CFT as the regime III of the $a_3^{(2)}$ model, namely a theory involving two compact and one non compact boson, or more precisely the product of the $SL(2, \mathbb{R})/U(1)$ black hole and one decoupled compact boson, which can alternatively related to a coset CFT of the type $SO(4)/SO(3)$. A particularly important point is that this geometrical truncation of the plateau transition has *itself* a non compact continuum limit, and therefore, if not equivalent to the original IQHE universality class, may at least share several important features of the latter.

Before looking in this direction, we would like to give a deeper field-theoretical interpretation to the equivalence between the continuum limits of the $a_3^{(2)}$ and $b_2^{(1)}$ models in their respective regimes III and IV.

5.2.2 $b_2^{(1)}$, $a_3^{(2)}$, and Pohlmeyer reduction

Let us first note that the similarity between the continuum limits of the $a_3^{(2)}$ and $b_2^{(1)}$ models had already been hinted from the duality of the associated Dynkin diagrams in the end of chapter 2. In general, the algebras $a_{2n-1}^{(2)}$ and $b_n^{(1)}$ are dual to each other, while the algebra $a_{2n}^{(2)}$ is self-dual. Let us also recall our conjecture from chapter 3, equations (3.138-3.139), namely that two integrable perturbations can be built from the $\frac{SO(N)_{\tilde{N}}}{SO(N-1)_{\tilde{N}}}$ coset, the latter of which (associated with the Pohlmeyer reduction of the $\frac{SU(N+1)}{SO(N+1)}$ coset) was identified in section 3.4 as the continuum limit of the $a_{N-1}^{(2)}$ model in regime III.

Gathering these two observations together with the results of the previous section, it seems reasonable to conjecture that the continuum limit of the $b_2^{(1)}$ model in regime IV corresponds precisely to the deformation of the $\frac{SO(4)}{SO(3)}$ coset resulting from the Pohlmeyer reduction of $\frac{SO(5)}{SO(4)}$, namely to a perturbation by an operator of dimension $\Delta = \frac{2}{\tilde{N}+2}$ (where $\tilde{N} = k$ in the notations of the previous sections). More generally, we conjecture that all the $b_n^{(1)}$ models have four different regimes, and that their continuum limit in regime IV can be related to the integrable perturbation (3.138) of the coset $\frac{SO(N)}{SO(N-1)}$, where $N = 2n$. In conclusion,

- For $N = 2n$ even, the two deformations of the coset $\frac{SO(N)}{SO(N-1)}$ are associated respectively with the $b_n^{(1)}$ model in regime IV and with the $a_{2n-1}^{(2)}$ model in regime III.
- For $N = 2n + 1$ odd, the deformation of the coset $\frac{SO(N)}{SO(N-1)}$ corresponding to the Pohlmeyer reduction of $\frac{SU(N+1)}{SO(N+1)}$ is associated with the $a_{2n}^{(2)}$ model in regime III. The remaining integrable deformation was related in the particular $N = 3$ case to the continuum limit of the staggered six-vertex model [55], but a possible generalization to higher values of N is left as an open problem.

We now leave these general considerations aside, and specialize to the case of the $b_2^{(1)}$ model in the regime IV of interest, for which we now have at hand a complete exact solution. In the next paragraph, we revisit some of the puzzling results presented in [39], and find in particular the exact expression of several interesting critical exponents. Recalling the discussion of section 3.5.3, it should not be a surprise for us that some of these expressions may show appreciable differences with the numerical estimations of [39]. This motivates the urge to seriously put back in question the main conclusion of

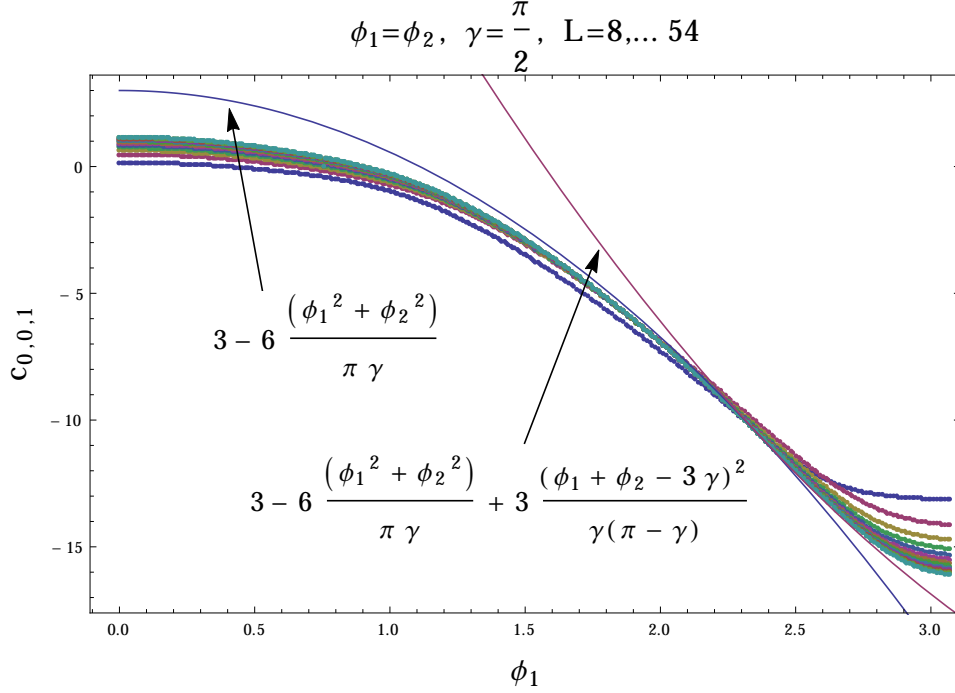


Figure 5.1: Effective central charge $c_{0,0,1}(\varphi_1, \varphi_2 = \varphi_1)$ as a function of φ_1 at $\gamma = \frac{\pi}{2}$, obtained from numerical resolution of the Bethe ansatz equations for sizes up to $L = 58$. For $\varphi_1 + \varphi_2 < 3\gamma$ (left part of the curve), the corresponding state lies in the continuum, and the convergence is logarithmic. For $\varphi_1 + \varphi_2 > 3\gamma$ the state is a discrete, and no logarithmic corrections to the central charge are expected. The reason for the bad convergence towards the expected result (purple curve) is that at $\varphi_1 = \pi$ the level jumps to an excited electric mode, hence a cusp in the central charge which is badly accommodated in finite size.

the latter work, namely that the geometrical truncation does *not* recover the universality class of the IQHE plateau transition.

5.2.3 Critical exponents of the truncated model

The thermal exponent of the truncated, model which we already mentioned in the end of section 5.1 is the conformal weight associated with the first excited state in the sector with no legs, that is, with the state $(m^{(1)}, m^{(2)}, j) = (0, 0, 1)$. From the results of the previous section we expect the central charge for this state is

$$c_{0,0,1} = \begin{cases} 3 - 6 \frac{(\varphi_1)^2 + (\varphi_2)^2}{\pi \gamma} + o(1) & \text{for } \varphi_1 + \varphi_2 \leq 3\gamma, \\ 3 - 6 \frac{(\varphi_1)^2 + (\varphi_2)^2}{\pi \gamma} + 3 \frac{(\varphi_1 + \varphi_2 - 3\gamma)^2}{\gamma(\pi - \gamma)} & \text{for } \varphi_1 + \varphi_2 \geq 3\gamma. \end{cases} \quad (5.22)$$

(see figure 5.1), so taking $\varphi_1 = \varphi_2 = \pi - \gamma$ we see that the relevant expression is the first one for $\frac{2\pi}{5} \leq \gamma \leq \pi$ and the second one for $0 \leq \gamma \leq \frac{2\pi}{5}$, yielding

$$x_t = -\frac{c_{0,0,1}(\pi - \gamma, \pi - \gamma) - c_{0,0,0}(\pi - \gamma, \pi - \gamma)}{12} = \begin{cases} k + \frac{1}{4} \frac{1}{1+k} & \text{for } k \leq \frac{1}{2}, \\ \frac{2k}{1+k} & \text{for } k \geq \frac{1}{2}, \end{cases} \quad (5.23)$$

which explains the change of regime observed in [39]. In particular, the $\frac{SU(2)_k \times SU(2)_k}{SU(2)_{2k}}$ thermal exponent $x_t = \frac{2k}{k+1}$ is obtained in the branch where $(0, 0, 1)$ corresponds to a discrete state, and does not account for the issues of normalizability occurring at low twist in the non compact CFT. On the contrary, the point $k = 0$ of interest for applications to the IQHE lies in the region where $(0, 0, j)$ is part of a continuum, and we expect at this point

$$x_t = \frac{1}{4}, \quad (5.24)$$

which is quite far from the numerical estimation of [39], hence giving another example of how unsuspected non compact CFTs can give rise to strongly misestimated critical exponents. As already noted in [39], the exponent (5.24) coincides at $k = 0$ with the watermelon $x_{2,2}$ (5.21), which means that as in the case of dilute polymers it is associated with a perturbation of the monomer fugacity.

We now turn to the correlation length exponent ν (1.18), which describes the power-law divergence of the correlation length when perturbing the energy level E away from the center of Landau bands E_c , and which is expected from various numerical experiments to lie somewhere between 2.3 and 2.6 at the IQHE transition (see the discussion in section 1.3). On the CC lattice, this perturbation is reproduced by introducing a staggering of the spectral parameter between the even and odd sublattices, which is *not* the same as the usual staggering between the vertical spaces in the row-to-row transfer matrix, and in particular does not preserve integrability, if any. Turning to the integrable truncated model, the latter remains exactly solvable under such a perturbation at the particular point $\gamma = \frac{\pi}{3}$, where it is mapped [39] onto a theory of a free Majorana fermion with a mass scale going like the *squared* magnitude of the staggering perturbation, which leads using scaling arguments to the relation

$$\nu = \frac{2}{2 - x_t} \quad (5.25)$$

differing from the usual formula (see, for instance, section 4.3.3) by a factor 2. The authors of [39] further assume that this relation should hold throughout the whole regime IV, which would yield, using our now exact value of the operator x_t ,

$$\nu = \frac{8}{7}. \quad (5.26)$$

The latter assumption may be criticized in several ways. First, it is possible that the relation (5.25) between ν and x_t , which is exact at $k = 1$, remains valid only in the ‘discrete state regime’ $k \geq \frac{1}{2}$. In the $k \leq \frac{1}{2}$ regime, the perturbation of the conformal action associated with the shift $|E - E_c|$ may indeed be described by a continuum of fields rather than by a single one, which would presumably result in a different expression for the exponent ν . Second, it is by no means guaranteed that the operator coupled to $|E - E_c|$ is truly what we identified as $(0, 0, j)$.

In the absence of any solid alternative proposition we therefore rely on the numerical estimations of ν by data collapse, which lead Ikhlef *et. al.* to $\nu \simeq 1.1$. The rather good agreement with (5.26) may be considered as an indication that despite the above criticism equation (5.25) or a closely related version thereof might hold at the $n = 0$ point, and we therefore reproduce the main conclusion of [39], namely, that *the truncated model is not in the universality class of the original IQHE plateau transition*. However, while it is concluded in [39] that the truncation should be considered as the first of a series of

models whose limit (corresponding to the untruncated case) should eventually recover the IQHE universality class, we claim here that it is, *by itself*, a lot more interesting than initially thought. Namely, we now want to convince the reader that several highly non trivial features of the plateau transition can be interpreted in the light of our analysis of the $b_2^{(1)}$ truncation.

5.3 Continuous exponents at the IQHE transitions

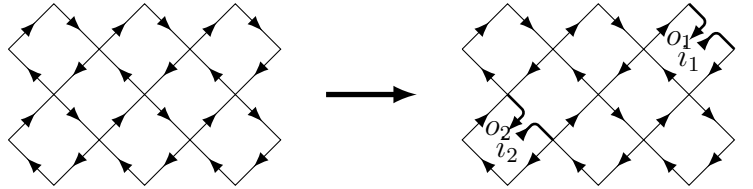
In section 2.4.2, we have sketched, following [82], the description of the Chalker–Coddington model in terms of a supersymmetric vertex with $GL(2|2)$ symmetry. These algebraic considerations were beautifully put to profit in the respective papers [82] and [147], in a way we shall now briefly review and try to interpret geometrically.

5.3.1 $GL(2|2)$ interpretation of point-contact conductances

To proceed, we recall our discussion of section 2.4.2, where it was explained, following [82], how the computation of disorder-averaged transport observables on the Chalker–Coddington network can be reexpressed in terms of a vertex model for supermatrix fields Z and \bar{Z} , symmetric under the naturally induced action of the $GL(2|2)$ Lie supergroup. Without going into too much detail, we shall only recall [86] that the latter includes the action of the a $SU(1, 1) \times SU(2)$ bosonic subgroup, whose property of being non compact will be essential for the following. In particular, we distinguish between the (infinite-dimensional) unitary irreducible representations of $SU(1, 1)$ the (positive and negative) *discrete series* labeled by a spin $j = -\frac{k}{2}, k \in \mathbb{N}$ and the *continuous series*, labeled by a spin $j = -\frac{1}{2} + i s, s > 0$. The corresponding quadratic Casimir has the same form as that of $SU(2)$, namely

$$\mathcal{C}_2 = j(j + 1). \quad (5.27)$$

In [82], this framework is used to study the moments of the point-contact conductance, defined in section 2.4.2, where it served as a setup for the definition of the now familiar two-colour loop model. On the Chalker–Coddington network, a subset of edges (e_1, e_2) is opened by introducing a on *each* a source and a drain, namely



The moments of the PCC, written in terms of the discrete time Green's function (2.91) as

$$\overline{g^q} = \overline{|\mathcal{G}(o_2, i_1, 1)|^{2q}}, \quad (5.28)$$

can be reformulated in the $GL(2|2)$ vertex model as

$$\overline{g^q} = \langle v_q(o_2) v_0^*(i_2) \times v_0(o_1) v_{-q}^*(i_1) \rangle, \quad (5.29)$$

where the operators v (resp. v^*) transform under the irreducible $GL(2|2)$ representations V, V^* already introduced in section 2.4.2. Importantly, the action of the subgroup

$SU(1, 1) \times SU(2)$ on these representations is unitary, and these are seen in [82] to belong to the (respectively positive and negative) $SU(1, 1)$ discrete series. The fact that the tensor product $V \otimes V^*$ decomposes over the continuous series of $SU(1, 1)$ representations is then used to write

$$\begin{aligned} v_q(o_2)v_0^*(i_2) &= \int_0^\infty ds \mu(s) \langle V, q \times V^*, 0|s, q \rangle \varphi_{s,q}(e_2) \\ v_0(o_1)v_{-q}^*(i_1) &= \int_0^\infty ds' \mu(s') \langle V, 0 \times V^*, -q|s', q \rangle \varphi_{s',-q}(e_1), \end{aligned} \quad (5.30)$$

where in the continuum limit the functions $\varphi_{s,\pm q}$ are described by sum of scaling fields, whose most relevant we denote by its dimension Δ_s . From $GL(2|2)$ invariance the correlation functions $\langle \varphi_{s,q} \varphi_{s',-q} \rangle$ are independent of q , and are non zero iff the product $\varphi_{s,q} \varphi_{s',-q}$ contains in its decomposition the trivial, singlet $GL(2|2)$ representation, namely iff $s = s'$. In other terms [82],

$$\langle \varphi_{s,q}(r) \varphi_{s',-q}(r') \rangle = \frac{\delta(s - s')}{\mu(s)} |r - r'|^{-2\Delta_s}, + \dots \quad (5.31)$$

which leads to

$$\bar{g}^q = \int_0^\infty \mu(s) ds \langle V, q \times V^*, 0|s, q \rangle \langle V, 0 \times V^*, -q|s, q \rangle |r - r'|^{-2\Delta_s} + \dots, \quad (5.32)$$

where the exponents Δ_s are then conjectured to be exactly quadratic, namely [82]

$$\Delta_s = \frac{X_t}{8}(s^2 + 1), \quad X_t = 0.613 \pm 0.012. \quad (5.33)$$

Such a form of the conformal weights owes to the fact that the CFT primaries should correspond to representations of the $GL(2|2)$ symmetry group, and that the conformal weights should have $GL(2|2)$ -invariant expressions, the simplest of which is given by the quadratic Casimir (5.27). A refined analysis [147] of the scaling exponents has shown recently that corrections to this parabolic dependence should be included, which one can interpret as coming from higher power terms such as $(\mathcal{C}_2)^4$ or the quartic Casimir invariant \mathcal{C}_4 .

5.3.2 Loop interpretation

The appearance of a continuous spectrum of critical exponents is, of course, related to the plateau transition CFT being non compact. More specifically, the expression (5.32) involving such a continuum is nothing else than another example of the generic formula for correlation functions in non compact CFTs, (3.151).

Let us now consider, as in as in section 2.4.2, the loop formulation of the $q = 1$ PCC moment between two edges e_1, e_2 , namely $\bar{g}(e_1, e_2)$, which we recall to be given as a the sum over disorder-averaged configurations of pairs of weighted paths joining the source i_1 to the drain o_2 in the above figure. In the continuum limit this is simply described as a correlation function

$$\bar{g}(r, r') = \langle \mathcal{O}_{1,1}(r) \mathcal{O}_{-1,-1}(r') \rangle, \quad (5.34)$$

where the operators $\mathcal{O}_{\ell_1, \ell_2}$ are the two-colour equivalent of the watermelon operators defined earlier for polymers, see figure 4.1. Specializing to the truncated model, we

expect that such operators should correspond to *continuous* sums of conformal fields corresponding to the continua in the (ℓ_1, ℓ_2) sectors. The exponent associated to the bottom of the continua in the $\ell_1 = \ell_2 = 1$ sectors reads from (5.21) as $x_{1,1} = -\frac{1}{8}$, and we therefore write for the truncated case, following the lines of section 4.2,

$$\bar{g}(r, r') = \int_0^\infty ds \frac{f_{1,1}(s)}{|r - r'|^{-\frac{1}{4} + \kappa s^2}}, \quad (5.35)$$

where, as in the case of polymers, $f_1(s)$ is expected to be some complicated function multiplying the black hole density $\rho(s)$ (3.68) by form factors of the watermelon operators. However, it is noticeable that the qualitative form (5.32) expected for the PCC at the quantum Hall transition can be recovered by the very first of the corresponding geometrical truncations (in particular, the expressions (5.32) involve the contribution from only one continuous quantum number s , as does (5.35)). A better understanding of this correspondence is certainly needed. In particular, the density $\mu(s)$ introduced by Janssen, Metzler and Zirnbauer is found to be

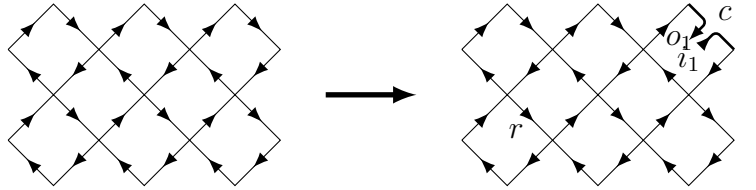
$$\mu(s) = \frac{s}{2} \tanh \frac{\pi s}{2}, \quad (5.36)$$

and obviously does not coincide with (3.68). In this sense the role of further truncations, if not to add other non compact directions to the theory, might be thought as correcting the density of states and the precise s, ℓ_1, ℓ_2 dependence of conformal exponents.

Leaving here this very speculative considerations, we now turn to an interesting conclusion that can be drawn for the more recent work of Bondesan and Zirnbauer, [147].

5.3.3 Pure scaling observables

There, inspired by the more general work [148], the authors construct correlation functions on the lattice which are argued to be described in the continuum limit this time not by a continuum of scaling fields, but rather by a pure power law. We will here consider the simplest of such functions, namely open only one edge $e_1 \equiv c$ on the CC lattice, and consider an *observation region* on some untouched edge $e_2 \equiv r$,



As for the computation of the PCC current is injected through i_1 at the rate of one unit of probability flux per discrete time unit, and after a sufficient amount of time the system has reached a stationary state $|\psi_k\rangle$ where the equivalent amount of probability flux exits through o_1 . Following [147], we then consider the moments of the probability amplitude at the observation points r , namely $|\psi_c(r)|^{2q}$, which in the supersymmetric vertex model should be written as a correlation function of the form

$$\overline{|\psi_c(r)|^{2q}} = \langle \Phi_q(r) \times v_o(o_1) v_{-q}^*(i_1) \rangle. \quad (5.37)$$

While $v_o(o_1) v_{-q}^*(i_1)$ has the same interpretation as for the computation of the PCC moments and therefore decomposes as a continuous sum over $SU(1, 1)$ representations (5.30),

$\Phi_q(r)$ is argued to be a *highest-weight* under the action of the latter group (actually for the whole $GL(2|2)$ action), and therefore to correspond, in the continuum limit, to a *pure scaling* conformal field. As a simple consequence of the orthogonality principle for two-point functions of conformal fields with different dimensions only one term of the continuous sum (5.30) contributes to the correlation function (5.37), which is therefore seen to decay with a pure power law, namely [147]

$$\overline{|\psi_c(r)|^{2q}} \sim |c - r|^{-2\Delta_q}, \quad (5.38)$$

where

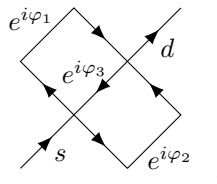
$$\Delta_q \equiv q(1 - q) \quad (5.39)$$

As in the PCC case, we look for an interpretation of this fact from the loop model perspective by restricting to $q = 1$, which is however quite a particular case in the sense that (5.39) yields $\Delta = 0$. More precisely the function $|\Psi_c(r)|^2$ is shown to be exactly = 1 for any r [R. Bondesan, private communication], a fact which will however not prevent us from making a few interesting observations³. In the loop language, it is easy to recognize $|\Psi_c(r)|^2$ as the sum over path configurations going from i_1 to o_1 and passing through the edge r (see figure 5.2) which we expect that they might be described in the continuum limit by a correlation function of the type

$$\overline{|\psi_c(r)|^2} = \left\langle \mathcal{O}_{2,2}(c) \tilde{\mathcal{O}}_2(r) \right\rangle. \quad (5.41)$$

While the operator $\mathcal{O}_{2,2}(c)$ is of the same nature as the watermelon operators $\mathcal{O}_{\pm\ell_1, \pm\ell_2}(c)$ considered in the computation of the PCC, we are tempted not to give the same interpretation to the operator $\tilde{\mathcal{O}}_2(r)$. In terms of paths summations the two indeed differ slightly in that the former opens edges which loops are therefore forbidden to go through, whereas the other does not. While in the continuum limit such a difference is irrelevant and the

³In particular, there is no combinatorial argument enforcing the function $|\Psi_c(r)|^2$ to be trivial. We note in passing that a trivial observable is obtained from the computation of a ‘conductance’ on a lattice with only one source and one drain, as can be interpreted from a probability conservation. This can be seen for instance by considering the following simple lattice



(where φ_1, φ_2 , are random phases φ_3). Introduce two ‘cuts’ ω_1 and ω_2 on edges with phases φ_1 and φ_2 , and label the different paths connecting s to d by the sequence of their crossings ω_1 and ω_2 . We then write $\mathcal{G}(s, d, 1) = \mathcal{G}_1 + \mathcal{G}_2$, where $\mathcal{G}_1 = \omega_1(1 + \omega_1 + (\omega_1)^2 + \dots)(1 + \tilde{\omega}_2 + (\tilde{\omega}_2)^2 + \dots)$, $\tilde{\omega}_2 = \omega_2(1 + \omega_1 + (\omega_1)^2 + \dots)$, and similarly for \mathcal{G}_2 with $1 \leftrightarrow 2$. It is then easy to see that

$$\mathcal{G}_1 = \frac{t^2 e^{i\varphi_1}}{1 - r^2 e^{i(\varphi_1 + \varphi_3)}} \left[1 - \frac{r^2 \left(1 - \frac{t^2 e^{i(\varphi_1 + \varphi_3)}}{1 - r^2 e^{i(\varphi_2 + \varphi_3)}} \right) e^{i(\varphi_2 + \varphi_3)}}{1 - t^2 \left(\frac{1}{1 - r^2 e^{i(\varphi_1 + \varphi_3)}} \right) e^{i(\varphi_2 + \varphi_3)}} \right], \quad (5.40)$$

and similarly for \mathcal{G}_2 with $r \leftrightarrow t$, $\varphi_1 \leftrightarrow \varphi_2$. The sum $\mathcal{G}_1 + \mathcal{G}_2$ can be simplified, and is seen to be of modulus one for any realization of the disorder.

In [39], it is stated that such a property can be related with the fact that a zero watermelon exponent $x_{1,1}$ should be expected in the vertex model. In contrast, we find for the truncated model $x_{1,1} = -\frac{1}{8}$, hence giving a meaning to the latter as a measure for the ‘quality’ of the truncation.

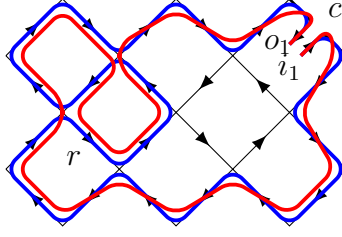


Figure 5.2: Loop configuration contributing to the pure scaling function $|\overline{\psi_c(r)}|^2$ at the IQHE transition.

,

watermelon operators can be defined without any particular precaution, it could be here that the operator $\tilde{\mathcal{O}}_2(r)$ ‘cuts’ the continuum of exponents in the $\ell_1 = \ell_2 = 2$ sector, hence accounting for the pure scaling behaviour of the correlation function $|\overline{\psi_c(r)}|^2$. Needless to say, this proposition would deserve to be extended to observables other than the trivial $|\overline{\psi_c(r)}|^2$ in order to gain any sort of credit, and at present it is not clear whether or how the the $q \neq 1$ moments $|\overline{\psi_c(r)}|^{2q}$ could be interpreted in the loop model formulation. In parallel, it would be interesting to look for the field content of the operators $\mathcal{O}_{\ell_1, \ell_2}$ and $\tilde{\mathcal{O}}_{\ell_1, \ell_2}$ without any reference to particular correlation function. For instance, a greatly satisfactory result would be that the former involve the whole continua of fields in the (ℓ_1, ℓ_2) sectors, while the latter only select the bottom of these continua. Investigating this direction however still requires quite a lot of progress and sends us back to the general problem of giving a clear meaning to the non compact degrees of freedom, starting with the simpler case of the $a_2^{(2)}$ model (see section 3.5.2).

Conclusion

TODO

Conclude
Perspectives

- One of the most intriguing questions opened by the models studied in this thesis is probably the understanding of the nature of their non compact degrees of freedom. As explained in section 3.5.2, we believe that these cannot be interpreted in terms of *local* operators, however much hope is put in the recent approach of [122, 123] (although derived in a whole different perspective), which construct *semi-local* conserved quantities for the spin- $\frac{1}{2}$ XXZ chain and seem like they may be generalized to other integrable models.
- Noticeable in all this work has been the major role played the black hole CFT. While this fascinating theory was already know to describe the continuum limit of the staggered 6v model [56, 58, 58](and further, of a larger phase in the phase diagram of the $U_q(sl(2|1))$ integrable model [60]), we have seen in this thesis that it is also obtained as the continuum limit of the $a_2^{(2)}$ model, and plays a fundamental role in that of the $a_3^{(2)}$ and $b_2^{(1)}$ models.

To my knowledge, not many non compact CFTs are as well known as the black hole, and it seems like an appealing perspective that we now could be able to gain knowledge in this field from a lattice approach. In particular, it would be interesting to understand better *what* are the non compact CFTs that we have identified as the continuum limit of further $a_n^{(2)}$ models. Series of integrable models associated with the other perturbation of the $SO(N)/SO(N-1)$ coset ?

It is also quite surprising that despite all of these results no compact lattice model is known to give rise in the continuum limit to the Liouville field theory. This seems definitely like an interesting direction to look to.

- Of course, the rich physics unveiled for the truncated model of the IQHE plateau transition brings on many interesting perspectives. As we have explained in section 5.3, several highly non trivial properties of the plateau transition might be understandable from the identified CFT of the first truncation. This definitely requires to be clarified algebraically, and also motivates the study of further truncations, even though this appears to be a difficult task. Big problems difficult numerically, no integrable solution.

Another key point in the study of this model is indecomposability. Measure b explain. Easier now that we have exact critical exponents cite work Romain.

Mapping to SQHE, flow in the space of different LCFTs.

Further, extend this to other symmetry classes of Anderson transitions. Work in progress with R Bondesan. For all class network formulation, for which we can build a loop model.

- paper de Moore sur polymers et IQHE 0104033. A lire. Connection ?

Bibliography

- [1] A. M. Polyakov, *Conformal symmetry of critical fluctuations*, JETP Lett. **12**, 381 (1970).
- [2] A. Belavin, A. Polyakov and A. Zamolodchikov, *Infinite conformal symmetry in two-dimensional quantum field theory*, Nuclear Physics B **241**(2), 333 (1984).
- [3] D. Friedan, Z. Qiu, and S. Shenker, *Conformal Invariance, Unitarity, and Critical Exponents in Two Dimensions*, Phys. Rev. Lett. **52**, 1575 (1984).
- [4] H. Saleur, *Conformal invariance for polymers and percolation*, J. Phys. A: Math. Gen. **20**(2), 455 (1987).
- [5] J. Cardy, *Logarithmic correlations in quenched random magnets and polymers* (1999) [arXiv:cond-mat/9911024].
- [6] D. Bernard and A. LeClair, *A classification of 2D random Dirac fermions*, J. Phys. A: Math. Gen. **35**, 2555 (2002), [arXiv:cond-mat/0109552].
- [7] K. v. Klitzing, G. Dorda and M. Pepper, *New method for high-accuracy determination of the fine-structure constant based on quantized Hall resistance*, Phys. Rev. Lett. **45**, 494–497 (1980).
- [8] A. M. Gainutdinov, J. L. Jacobsen, N. Read, H. Saleur and R. Vasseur, *Logarithmic Conformal Field Theory: a Lattice Approach* J. Phys. A: Math. Theor. **46**, 494012 (2013) [arXiv:1303.2082].
- [9] R. Vasseur, *Indecomposability in field theory and applications to disordered systems and geometrical problems*, PhD thesis, Université Paris 6 (2013).
- [10] C. Candu and H. Saleur, *A lattice approach to the conformal $OSp(2S + 2|2S)$ supercoset sigma model. Part II: The boundary spectrum*, Nucl.Phys.B **808**, 487–524 (2009) [arXiv:0801.0444].
- [11] J. Teschner, *Liouville theory revisited*, : Class. Quant. Grav. **18**, R153-R222 (2001) [arXiv:hep-th/0104158].
- [12] P. Flory, *Principles of Polymer Chemistry*, Cornell University Press, Ithaca, N. Y. (1971).
- [13] P.-G. de Gennes, *Scaling Concepts in Polymer Physics* Cornell University Press, Ithaca, N. Y. (1979).
- [14] H. E. Stanley, *Dependence of Critical Properties on Dimensionality of Spins* Phys. Rev. Lett. **20**, 589 (1989).

- [15] P.-G. de Gennes, *Exponents for the excluded volume problem as derived by the Wilson method*, Phys. Lett. A **38A** (5), 339–340 (1972).
- [16] J. Des Cloizeaux, *The Lagrangian theory of polymer solutions at intermediate concentrations*, Journal de Physique **36** (4), 281–291 (1975).
- [17] M. Müller, *Repliement d’hétéropolymères*, PhD thesis, Université Paris 11 (2003).
- [18] P.-G. de Gennes, *Collapse of a polymer chain in poor solvents* Journal de Physique Lettres **36** (3), 55–57 (1975).
- [19] G. Mussardo, *Statistical Field Theory: An Introduction to Exactly Solved Models in Statistical Physics*. Oxford Graduate Texts (OUP Oxford, 2010), ISBN 9780199547586.
- [20] http://www.nobelprize.org/nobel_prizes/physics/laureates/1998/press.html
- [21] B. Kramer, T. Ohtsuki and S. Kettemann, *Random network models and quantum phase transitions in two dimensions*, Phys. Rep. **417** (5-6), 211–342 (2005) [arXiv:cond-mat/0409625].
- [22] R. Bondesan, *Edge states and supersymmetric sigma models*, PhD thesis, Université Paris 6 (2012).
- [23] B. Huckestein, *Scaling Theory of the Integer Quantum Hall Effect*, Rev. Mod. Phys. **67**, 357 (1995) [arXiv:cond-mat/9501106].
- [24] Wanli Li, G. A. Csthy, D. C. Tsui, L. N. Pfeiffer and K. W. West, *Scaling and Universality of Integer Quantum Hall Plateau-to-Plateau Transitions*, Phys. Rev. Lett. **94**, 206807 (2005).
- [25] H. Obuse, I. A. Gruzberg and F. Evers, *Finite Size Effects and Irrelevant Corrections to Scaling near the Integer Quantum Hall Transition*, Phys. Rev. Lett. **109**, 206804 (2012) [arXiv:1205.2763].
- [26] A. Altland and M. R. Zirnbauer, *Nonstandard symmetry classes in mesoscopic normal-superconducting hybrid structures*, Phys. Rev. B **55**, 1142 (1997).
- [27] A. M. M. Pruisken, *On localization in the theory of the quantized Hall effect: a two-dimensional realization of the θ -vacuum*, Nucl. Phys. B **235**, 277–298 (1984).
- [28] H.A. Weidenmüller, *Single electron in a random potential and a strong magnetic field*, Nucl. Phys. B **290**, 87–110 (1987).
- [29] E. Abrahams, P. W. Anderson, D. C. Licciardello, and T. V. Ramakrishnan, *Scaling Theory of Localization: Absence of Quantum Diffusion in Two Dimensions*, Phys. Rev. Lett. **42**, 673 (1979).
- [30] P. Fendley, *Critical Points in Two-Dimensional Replica Sigma Models*, New Theoretical Approaches to Strongly Correlated Systems, NATO Science Series Vol. **23**, 141–161 (2001) [arXiv:cond-mat/0006360].

- [31] K. Kytölä and D. Ridout, *On staggered indecomposable Virasoro modules*, J. Math. Phys. **50** (12), 123503 (2009).
- [32] V. Pasquier and H. Saleur, *Common structures between finite systems and conformal field theories through quantum groups*, Nucl. Phys. B **330** (2-3), 523-556 (1990).
- [33] N. Read and H. Saleur, *Enlarged symmetry algebras of spin chains, loop models, and S-matrices*, Nucl. Phys. B **777**, 263-315 (2007) [arXiv:cond-mat/0701259].
N. Read and H. Saleur, *Associative-algebraic approach to logarithmic conformal field theories*, Nucl. Phys. B **777** (3), 316–351 (2007) [arXiv:hep-th/0701117].
- [34] P. A. Pearce, J. Rasmussen and J.-B. Zuber. *Logarithmic minimal models*, J. Stat. Mech. **1106**, P11017 (2006) [arXiv:hep-th/0607232].
- [35] B. Nienhuis, *Coulomb gas formulations of two-dimensional phase transitions*, in C. Domb and J. L. Lebovitz (eds.), *Phase transitions and critical phenomena*, vol. 11, pp. 1-53, Academic Press, London, 1987.
- [36] R. J. Baxter, *Exactly solved models in statistical mechanics*, London: Academic Press Inc. (1982), ISBN 9780120831807.
- [37] V.E. Korepin, N.M. Bogoliubov and A.G. Izergin, *Quantum Inverse Scattering Method and Correlation Functions*, Cambridge University Press (1993).
- [38] J. Cardy, *Network Models in Class C on Arbitrary Graphs*, Commun. Math. Phys. **258**, 87–102 (2005) [arXiv:math-ph/0406044].
- [39] Y. Ikhlef, P. Fendley, and J. Cardy, *An integrable modification of the critical Chalker–Coddington network model*, Phys. Rev. B **84**, 144201 (2011) [arXiv:1103.3368].
- [40] J. L. Jacobsen, *Conformal Field Theory Applied to Loop Models*, in Polygons, polyominoes and polycubes, (Springer), pp. 347-427 (2009)
- [41] P. Fendley, *Loop models and their critical points* J. Phys. A **39**, 15445 (2006) [arXiv:cond-mat/0609435].
- [42] P. Fendley and E. Fradkin, *Realizing non-Abelian statistics*, Phys.Rev. B **72**, 024412 (2005) [arXiv:cond-mat/0502071].
- [43] P. Fendley, *Quantum loop models and the non-abelian toric code*, [arXiv:0711.0014].
- [44] U. Grimm and P. A. Pearce, *Multi-Colour Braid-Monoid Algebras*, J.Phys. A **26**, 7435–7460 (1993) [arXiv:hep-th/9303161].
- [45] A. Nahum, P. Serna, A. M. Somoza and M. Ortuño, *Loop with crossings*, Phys. Rev. B **87**, 184204 (2013) [arXiv:1303.2342].
- [46] J. L. Cardy, *Conformal invariance and universality in finite-size scaling*, J. Phys. A: Math. Gen. **17** L385 (1987).
- [47] A.V. Belitsky, S.E. Derchakov, G.P. Korchemsky and A.N. Manashov, J.Stat.Mech. **0701**, P01005 *Baxter Q-operator for graded $SL(2|1)$ spin chain*, (2007) [hep-th/0610332].

- [48] C. Itzykson and J.-M. Drouffe, *Statistical Field Theory: Volume 1, From Brownian Motion to Renormalization and Lattice Gauge Theory*, Cambridge University Press (1991), Chapter 1.
- [49] B. Duplantier and K.-W. Kwoon, Conformal Invariance and Intersections of Random Walks, Phys. Rev. Lett. **61** (22), 2514 (1988).
- [50] J. L. Jacobsen, N. Read and H. Saleur, *Dense loops, supersymmetry, and Goldstone phases in two dimensions*, Phys. Rev. Lett. **90** 090601 (2003) [arXiv:cond-mat/0205033].
- [51] M. J. Martins, B. Nienhuis, and R. Rietman, *Intersecting Loop Model as a Solvable Super Spin Chain*, Phys. Rev. Lett. **81**, 504 (1998) [arXiv:cond-mat/9709051].
- [52] H. Frahm and M. J. Martins, *Finite-size effects in the spectrum of the $OSp(3-2)$ superspin chain* [arXiv:1502.05305].
- [53] Y. Ikhlef, J. Jacobsen and H. Saleur, *Non-intersection exponents of fully packed trails on the square lattice*, J. Stat. Mech. **0507**, P05005 (2007) [arXiv:cond-mat/0612258].
- [54] F. Essler, H. Frahm and H. Saleur, *Continuum Limit of the Integrable $sl(2|1)$ $3-\bar{3}$ Superspin Chain* Nucl.Phys. B **712** 513 (2005) [arXiv:cond-mat/0501197].
- [55] J.L. Jacobsen and H. Saleur, *The antiferromagnetic transition for the square-lattice Potts model* Nucl. Phys. B **743**, 207 (2006) [arXiv:cond-mat/0512058].
- [56] Y. Ikhlef, J. Jacobsen and H. Saleur, *A staggered six-vertex model with non-compact continuum limit* Nucl. Phys. B **789**, 483 (2008) [arXiv:cond-mat/0612037].
- [57] Y. Ikhlef, J. Jacobsen and H. Saleur, *The Z_2 staggered vertex model and its applications*, J. Phys. A: Math. Theor. **43**, 225201 (2010) [arXiv:0911.3003].
- [58] Y. Ikhlef, J. Jacobsen and H. Saleur, *An integrable spin chain for the $SL(2,R)/U(1)$ black hole sigma model*, Phys. Rev. Lett. **108**, 081601 (2012) [arXiv:1109.1119].
- [59] E. Witten, *String theory and black holes*, Phys. Rev. D **44**, 314 (1991);
R. Dijkgraaf, H. Verlinde and E. Verlinde, *String propagation in a black hole geometry*, Nucl. Phys. B **371**, 269 (1992).
- [60] H. Frahm and M. J. Martins, *Phase Diagram of an Integrable Alternating $U_q[sl(2|1)]$ Superspin Chain*, Nucl. Phys. B **862**, 504-552 (2012) [arXiv:1202.4676].
- [61] H. Frahm and A. Seel, *The Staggered Six-Vertex Model: Conformal Invariance and Corrections to Scaling*, Nucl. Phys. B **879**, 382 (2014) [arXiv:1311.6911].
- [62] E. Vernier, J.L. Jacobsen and H. Saleur, *Non compact conformal field theory and the $a_2^{(2)}$ (Izergin–Korepin) model in regime III*, J. Phys. A: Math. Theor. **47** (28), 285202 (2014) [arXiv:1404.4497].
- [63] E. Vernier, J.L. Jacobsen and H. Saleur, *Collapse of two-dimensional polymers*, to appear.

- [64] E. Vernier, J.L. Jacobsen and H. Saleur, *Non compact continuum limit of two coupled Potts models*, J. Stat. Mech. P10003 (2014) [arXiv:1406.1353].
- [65] E. Vernier, J.L. Jacobsen and H. Saleur, *Continuum limit of the $a_n^{(2)}$ models*, to appear.
- [66] H. Saleur and J.-B. Zuber, *Integrable lattice models and quantum groups*, in Spring School on String Theory and Quantum Gravity, Trieste, Italy, April 23 - May 4 1990 (eds.: Green M., Et Al), World Scientific, 1991, pp. 1-53.
- [67] A. B. Zamolodchikov and A. B. Zamolodchikov, *Factorized S-matrices in two dimensions as the exact solutions of certain relativistic quantum field theory models*, Annals of Physics **120**(2), 253-291 (1979).
- [68] P. Dorey, *Exact S-matrices*, in Conformal Field Theories and Integrable Models, Lecture Notes in Physics **498**, Springer, pp. 85-125 (1997) [arXiv:hep-th/9810026].
- [69] J.-S. Caux and J. Mossel, *Remarks on the notion of quantum integrability*, J. Stat. Mech. **0211**, P02023 (2011) [arXiv:1012.3587].
- [70] P. Zinn-Justin, *Quelques applications de l'ansatz de Bethe*, PhD thesis (1998), in French.
- [71] G. W. Delius, M. D. Gould and Y.-Z. Zhang, *On the construction of trigonometric solutions of the Yang-Baxter equation*, Nucl. Phys. B **432**, 377 (1994) [arXiv:hep-th/9405030].
- [72] G. W. Delius, M. D. Gould and Y.-Z. Zhang, *Twisted quantum affine algebras and solutions to the Yang-Baxter equation*, Int. J. Mod. Phys. A **11**, 3415, (1996) [arXiv:q-alg/9508012].
- [73] P. Martin, *Potts models and related problems in statistical mechanics*, Series on advances in statistical mechanics, World Scientific Publishing Company, Inc. (1991), ISBN 9789810200756.
- [74] V. F. Jones, *A quotient of the affine Hecke algebra in the Brauer algebra*, Enseignement mathématique **40**, 313–313 (1994).
- [75] H. W. J. Blöte and B. Nienhuis, *Critical behaviour and conformal anomaly of the $O(n)$ model on the square lattice* J. Phys. A: Math. Gen. **22**, 1415 (1989).
- [76] B. Nienhuis, *Critical spin-1 vertex models and $O(n)$ vertex models*, Int. J. Mod. Phys. B **04**, 929 (1990).
- [77] M. T. Batchelor, *Exact results for the critical behaviour of a Nienhuis $O(n)$ model on the square lattice*, J. Phys. A: Math. Gen. **26** 3733, (1993).
- [78] S. O. Warnaar, M. T. Batchelor and B. Nienhuis, *Critical properties of the Izergin–Korepin and solvable $O(n)$ models and their related quantum spin chains*, J. Phys. A **25** 3077 (1992).
- [79] A. G. Izergin and V. E. Korepin, *A lattice model related to the nonlinear Schroedinger equation*, Doklady Akademii Nauk **259**, 76 (1981).

- [80] J. L. Cardy, *Critical Percolation in Finite Geometries*, J. Phys. A **25**, L201L206 (1992) [arXiv:hep-th/9111026].
- [81] J. T. Chalker and P. D. Coddington, *Percolation, quantum tunnelling and the integer Hall effect*, J. Phys. C: Solid State Phys. **21**, 14, 2665 (1988).
- [82] M. Janssen, M. Metzler, and M. R. Zirnbauer, *Point-Contact Conductances at the Quantum Hall Transition*, Phys. Rev. B **59**, 15836 (1999), [arXiv:cond-mat/9810319].
- [83] E. Bettelheim, I. A. Gruzberg, and A. W. W. Ludwig, *Quantum Hall transitions: an exact theory based on conformal restriction*, Phys. Rev. B **86**, 165324 (2012) [arXiv:1202.4573].
- [84] I. A. Gruzberg, N. Read and S. Sachdev, *Scaling and crossover functions for the conductance in the directed network model of edge states*, Phys. Rev. B **55**, 10593 (1997) [arXiv:cond-mat/9612038].
- [85] R. Howe, *Remarks on classical invariant theory*, Trans. Amer. Math. Soc. 313, 539570 (1989).
- [86] M. R. Zirnbauer, *Conformal field theory of the integer quantum Hall plateau transition*, ArXiv High Energy Physics - Theory e-prints (1999) [arXiv:hep-th/9905054].
- [87] M. R. Zirnbauer, *Towards a theory of the integer quantum Hall transition: From the nonlinear sigma model to superspin chains*, Annalen der Physik **506 (7-8)**, 513577 (1994) [arXiv:cond-mat/9410040].
- [88] J. Kondev and J. B. Marston, *Supersymmetry and Localization in the Quantum Hall Effect*, Nucl. Phys. B **497 (3)**, 639-657 (1997) [arXiv:cond-mat/9612223].
J. B. Marston and S.-W. Tsai, *The Chalker–Coddington Network Model is Quantum Critical*, Phys. Rev. Lett. **82**, 49064909 (1999) [arXiv:cond-mat/9812261].
- [89] Dung-Hai Lee, *Network models of quantum percolation and their field-theory representations*, Phys. Rev. B **50**, 10788 (1994) [arXiv:cond-mat/9404011].
- [90] B. Nienhuis, *Exact Critical Point and Critical Exponents of $O(n)$ Models in Two Dimensions* Phys. Rev. Lett. **49**, 1062 (1982).
- [91] B. Nienhuis, *Loop models*. Lectures given at the 2008 Les Houches Summer School, *Exact methods in low-dimensional physics and quantum computing*, <http://staff.science.uva.nl/b.nienhuis/loops.pdf>.
- [92] P. Fendley and J.L. Jacobsen, *Critical points in coupled Potts models and critical phases in coupled loop models* J. Phys. A: Math. Theor. **41**, 215001 (2008) [arXiv:0803.2618].
- [93] P. Fendley and N. Read, *Exact S-matrices for supersymmetric sigma models and the Potts model*, J. Phys. A **35**, 10675 (2002) [arXiv:arXiv:hep-th/0207176].

- [94] J. Murakami, *The Kauffman polynomial of links and representation theory* Osaka J. Math. **24**, 745 (1987).
J. Birman and H. Wenzl, *Braids, link polynomials and a new algebra* Trans. Amer. Math. Soc. **313**, 239 (1989).
- [95] P. P. Kulish, N. Manojlovic and Z. Nagy, *Symmetries of spin systems and Birman–Wenzl–Murakami algebra*, J. Math. Phys. **51**, 043516 (2010) [arXiv:0910.4036].
- [96] M. Wadati, T. Deguchi and Y. Akutsu, *Exactly solvable models and knot theory*, Phys. Rep. **180**, 247 (1989).
- [97] P. Fendley and V. Krushkal, *Tutte chromatic identities from the TemperleyLieb algebra* Geom. Topol. **13** 709–741 (2009), [arXiv:0711.0016].
- [98] U. Grimm, *Trigonometric R-matrices related to ‘Dilute’ Birman–Wenzl–Murakami Algebra*, Lett. Math. Phys. **32**, 183–188 (1994) [arXiv:hep-th/9402094].
- [99] W. Galleas and M. J. Martins, *R -matrices and Spectrum of Vertex Models based on Superalgebras*, Nucl. Phys. B **699**, 455 (2004) [arXiv:nlin/0406003].
- [100] W. Galleas and M. J. Martins, *New R-matrices from Representations of Braid-Monoid Algebras based on Superalgebras*, Nucl. Phys. B **732**, 444 (2006) [arXiv:nlin/0509014].
- [101] P. Di Francesco, P. Mathieu and D. Sénéchal, *Conformal Field Theory*, Springer (1997) ISBN 9781461222569.
- [102] S. Belliard and E. Ragoucy, *The nested Bethe ansatz for ‘all’ closed spin chains*, J. Phys. A: Math. Theor. **41**, 295202 (2008) [arXiv:0804.2822].
- [103] V. G. Drinfeld, *Quantum Groups*, in ‘Proc. Int. Congress Math., Berkeley, 1986’, AMS, Providence RI, 1987, pp. 798–820.
- [104] G. Albertini, S. Dasmahapatra and B.M. McCoy, *Spectrum and completeness of the integrable 3-state Potts model: a finite size study*, Int. J. Mod. Phys. A **7**, Suppl. **1A**, 1 (1992).
K. Fabricius and B.M. McCoy, *Bethe’s equation is incomplete for the XXZ model at roots of unity*, J. Stat. Phys. **103**, 647 (2001).
R.I. Nepomechie and F. Ravanini, *Completeness of the Bethe Ansatz solution of the open XXZ chain with nondiagonal boundary terms*, J. Phys. A **36**, 11391 (2003) [arXiv:hep-th/0307095].
- [105] F. C. Alcaraz, M. N. Barber and M. T. Batchelor, *Conformal Invariance, the XXZ Chain and the Operator Content of Two-Dimensional Critical Systems*, Ann. Phys. **182**, 280–343 (1988).
- [106] P. Di Francesco, H. Saleur and J.-B. Zuber, *Generalized Colom-b-gas formalism for two-dimensional critical models based on SU(2) coset construction*, Nucl. Phys. B **300** [FS22], 393–432 (1988).

- [107] J. L. Jacobsen and J. Kondev, *Transition from the compact to the dense phase of two-dimensional polymers*, J. Stat. Phys. **96**, 21–48 (1999) [arXiv:cond-mat/9811085].
- [108] S. Ribault, V. Schomerus, *Branes in the 2D black hole* JHEP **02** 019 (2004) [arXiv:hep-th/0310024].
- [109] A. Hanany, N. Prezas and J. Troost, *he partition function of the two-dimensional black hole conformal field theory* JHEP **04** 014 (2002) [arXiv:hep-th/0202129].
- [110] C. Candu and Y. Ikhlef, *Nonlinear integral equations for the $SL(2, \mathbb{R})/U(1)$ black hole sigma model*, J. Phys. A: Math. Theor. **46** 415401 (2013) [arXiv:1306.2646].
- [111] A.B. Zamolodchikov and V.A. Fateev, *Nonlocal (parafermion) currents in two-dimensional conformal quantum field theory and self-dual critical points in Z_N -symmetric statistical systems*, Zh. Eksp. Teor. Fiz. **89**, 380 (1985) [English translation: Sov. Phys. JETP **62**, 215 (1985)].
- [112] I. Bakas, *Conservation Laws and Geometry of Perturbed Coset Models*, Int. J. Mod. Phys. A **9**, 3443–3472 (1994) [arXiv:hep-th/9310122].
- [113] J. Maldacena, G. Moore and N. Seiberg, *Geometrical interpretation of D-branes in gauged WZW models*, Journal of High Energy Physics **07**, 046 (2001) [arXiv:hep-th/0105038].
- [114] R.K. Bullough and R.K. Dodd, *Polynomial Conserved Densities for the Sine-Gordon Equations* Proc. Roy. Soc. London A **352**, 481 (1977).
- [115] J. M. Evans and J. O. Madsen, *Dynkin diagrams and integrable models based on Lie superalgebras*, Nucl. Phys. B **503** (3), 715746 (1997) [arXiv:hep-th/9703065].
- [116] G. Bonneau and F. Delduc, *S-matrix properties versus renormalizability in two-dimensional $O(N)$ symmetric models*, Nucl. Phys. B **250**, 561–592 (1985).
- [117] J. Schiff, *The Nonlinear Schrödinger Equation and Conserved Quantities in the Deformed Parafermion and $SL(2, R)/U(1)$ Coset Models*, [arXiv:hep-th/9210029].
- [118] T. Jayaraman, K. S. Narain and M. H. Sarmadi, *$SU(2)_k$ WZW and Z_k parafermion models on the torus*, Nucl. Phys. B **343** 418 (1990).
- [119] M. Bershadsky and D. Kutasov, *Comment of gauged WZW theory*, Phys. Let. B **266** (3–4), 345–352 (1991).
- [120] V. Pasquier, *Etymology of IRF models*, Commun. Math. Phys. **118**, 355 (1988).
- [121] N. Y. Reshetikhin, *A new exactly solvable case of an $O(n)$ -model on a hexagonal lattice*, J. Phys. A: Math. Gen. **24**, 2387 (1991).
- [122] T. Prozen, *Quasilocal conservation laws in XXZ spin-1/2 chains: open, periodic and twisted boundary conditions*, Nucl. Phys. B **886**, 1177 (2014) [arXiv:1406.2258].
- [123] R. G. Pereira, V. Pasquier, J. Sirker and I. Affleck, *Exactly conserved quasilocal operators for the XXZ spin chain*, J. Stat. Mech., P09037 (2014) [arXiv:1406.2306].

- [124] A. B. Zamolodchikov and V. A. Fateev, *Sov. J. Nucl. Phys.* **32** 298 (1980).
- [125] H. de Vega, *J. Phys. A* **20** 6023 (1987).
- [126] V. A. Fateev and S. Lukyanov, *The models of two-dimensional conformal quantum field theory with Z_n symmetry*, *Int. J. Mod. Phys. A* **03**, 507 (1988).
- [127] J. Kondev, J. De Gier and B. Nienhuis, *Operator spectrum and exact exponents of the fully packed loop model*, *J. Phys. A: Math. Gen.* **29** (20), 6489 [arXiv:cond-mat/9603170] (1996).
- [128] A. Gerasimov, A. Marshakov and A. Morozov, *Nucl. Phys. B* **328** 664 (1989).
- [129] S. O. Warnaar, B. Nienhuis, and K. A. Seaton, *New construction of solvable lattice models including an Ising model in a field*, *Phys. Rev. Lett.* **69**, 710 (1992).
- [130] D. Kastor, E. Martinec and Z. Qiu, *Current algebra and conformal discrete series*, *Phys. Lett. B* **200** (4), 434-440, (1988).
- [131] C. Ahn, D. Bernard and A. LeClair, *Fractional supersymmetries in perturbed coset CFTs and integrable soliton theory* *Nucl. Phys. B* **346** (2-3), 409-439 (1990).
- [132] K. Pohlmeyer, *Integrable Hamiltonian Systems and Interactions through Quadratic Constraints*, *Commun. math. Phys.* **46**, 207-221 (1976).
- [133] R. D'Auria, T. Regge and S. Sciuto, *Group theoretical construction of two-dimensional models with infinite sets of conservation laws*, *Nucl. Phys. B* **171**, 167-188 (1980).
- [134] N. Kitanine, K. K. Kozłowski, J.-M. Maillet, N. A. Slavnov and V. Terras, *Algebraic Bethe ansatz approach to the asymptotic behavior of correlation functions*, *J. Stat. Mech.* **0409**, P04003 (2009) [arXiv:0808.0227].
- [135] A. Bedini, A. L. Owczarek and T. Prellberg, *Numerical simulation of a lattice polymer model at its integrable point*, *J. Phys. A: Math. Theor.* **46**, 265003 (2013) [arXiv:1211.0252].
- [136] R. Oberdorf, A. Ferguson, J. L. Jacobsen and J. Kondev, *Secondary structures in long compact polymers*, *Phys. Rev. E* **74**, 051801 (2006) [arXiv:cond-mat/0508094].
J.L. Jacobsen, *Demixing of compact polymers chains in three dimensions*, *Phys. Rev. Lett.* **100**, 118102 (2008) [arXiv:1005.3610].
- [137] A. D. Sokal, *Monte Carlo Methods for the Self-Avoiding Walk* (1994) [arXiv:hep-lat/9405016].
- [138] <http://web.maths.unsw.edu.au/~mikeh/webpapers/paper21.pdf>
- [139] A. Erdélyi, *Asymptotic expansions*, Dover (1956).
- [140] B. Duplantier and H. Saleur, *Exact Tricritical Exponents for Polymers at the Θ Point in Two Dimensions* *Phys. Rev. Lett.* **59**, 539 (1987).

- [141] A. Coniglio, N. Jan, I. Majid and H. E. Stanley, *Conformation of a polymer chain at the ‘theta’ point: Connection to the external perimeter of a percolation cluster*, Phys. Rev. B **35** 3617 (1987).
- [142] B. Duplantier and H. Saleur, *Stability of the Polymer Θ Point in Two Dimensions*, Phys. Rev. Lett. **62,12**, 1368 (1989).
- [143] T. Prellberg and A. L. Owczarek, *Manhattan lattice Θ -point exponents from kinetic growth walks and exact results from the Nienhuis $O(n)$ model*, J. Phys. A: Math. Gen. **27**, 1811–1826 (1994).
- [144] J.H. Lee, S-Y Kim and J. Lee, *Collapse transition of a square-lattice polymer with next nearest-neighbor interaction* J. Chem. Phys. **135** 204102 (2011).
- [145] M. Gherardi, *Theta-point polymers in the plane and Schramm-Loewner evolution* Phys. Rev. E **88**, 032128 (2013) [arXiv:1306.4993].
- [146] H. Ui, *Clebsch-Gordan formulas of the $SU(1,1)$ group*, Prog. Theor. Phys. **44**, 689 (1970).
N. J. Vilenkin and A. U. Klimyk, *Representations of Lie Groups and Special Functions*, Vol. 1, Kluwer Academic Publishers, Dordrecht (1991), §6.4.
- [147] R. Bondesan, D. Wieczorek and M. R. Zirnbauer, *Pure scaling operators at the integer quantum Hall plateau transition*, Phys. Rev. Lett. **112**, 186803 (2014) [arXiv:1312.6172].
- [148] I. A. Gruzberg, A. D. Mirlin and M. R. Zirnbauer and *Classification and symmetry properties of scaling dimensions at Anderson transitions* Phys. Rev. B **87**, 125144 (2013) [arXiv:1210.6726].